Geochemical monitoring of soil pollution from the MWS-5 gold tailings facility on the Farm Stilfontein

A Daniell

21859442

Dissertation submitted in fulfilment of the requirements for the degree *Magister Scientiae* in Environmental Sciences at the Potchefstroom Campus of the North-West University

Supervisor: Mr PW van Deventer

May 2015

It all starts here ™

NORTH-WEST UNIVERSITY ®
YUNIBESITI YA BOKONE-BOPHIRIMA
NOORDWES-UNIVERSITEIT

DISCLAIMER

Although all reasonable care was taken in preparing the report, graphs and plans, the Geology Department of the North-West University (NWU)/NRF/THRIP/Anglo Gold Ashanti and/or the author is not responsible for any changes with respect to variations in weather conditions, tailings deposition, irrigation water quality, or whatever biophysical changes that might have an influence on the soil and vegetation quality. The integrity of this report and the Geology Department of the NWU/NRF/THRIP/Anglo Gold Ashanti and/or author nevertheless does not give any warranty whatsoever that the report is free of any misinterpretations of National or Provincial Acts or Regulations with respect to environmental and/or social issues. The integrity of this communication and the Geology Department of the NWU/NRF/THRIP/Anglo Gold Ashanti and/or author does not give any warranty whatsoever that the report is free of damaging code, viruses, errors, interference or interpretations of any nature. The Geology Department of the NWU/NRF/THRIP/Anglo Gold Ashanti and/or the author do not make any warranties in this regard whatsoever and cannot be held liable for any loss or damages incurred by the recipient or anybody who will use it in any respect. Although all possible care has been taken in the production of the graphs, maps and plans, the Geology Department of the NWU/NRF/THRIP/Anglo Gold Ashanti and/or the author cannot take any liability for perceived inaccuracy or misinterpretation of the information shown on these graphs, plans and maps.

ABSTRACT

The rehabilitation and restoration of degraded landscapes adjacent to gold tailings disposal facilities (TDFs) that have suffered loss of efficiency through anthropogenic forces has become a primary concern to environmental sciences and management in recent decades. Due to the lack of environmental legislation and enforcement thereof, minimal surface rehabilitation took place on the Mine Waste Solutions (MWS) No. 5 TDF prior to 1992, a commonplace occurrence in South Africa at the time.

In 2000, MWS intervened and committed to the rehabilitation of the entire site with profits generated by the reprocessing (extraction of residual gold and uranium) of certain TDFs. However, the adjacent grazing land north of the MWS No. 5 TDF had already been subjected to pollution from the TDF which resulted in a pollution plume on the land.

Although it has been inactive since April 2011, the pollution plume can be seen from the north-eastern corner of MWS No. 5 TDF, with a north-eastern/south-western direction on the farm Stilfontein. During dry periods, significant amounts of sulphate salts accumulate on the soil surface on the farm Stilfontein over a distance of at least 3.5 km from the TDF. The presence of sulphate salts in association with gold TDFs is highly common but not particularly common, in the chert-poor dolomites of the Oaktree Formation itself, in which the presence of sulphate salts is a rarity.

The primary concern of this study was to determine both the quantitative and extent of the pollution observed on the farm Stilfontein over a period of 30 months via monthly monitoring of the different soil geochemical assessments across twelve fixed points, and quarterly interval assessments of three transect lines. In addition, the study was also concerned with the identification of potential linear structure anomalies associated with the pollution plume and weathered zones (fractures, joints and cavities) in the Oaktree Formation dolomites. These zones may be associated with, or may result in, the pollution extending over the area despite a topography as well as geological dip and strike that is adverse.

These features and weathered zones create pathways for groundwater to flow and it was anticipated that, if present, these anomalies and weathered zones may be primary contributing factors to the pollution plume forming in a north-easterly direction and extending over the farm Stilfontein. The MWS No. 5 TDF has a hydraulic pressure head of approximately 40 m; the elevations of the north-eastern corner of the TDF and fixed point (FP) 8 (the farthest FP from the

TDF) are 1368 m and 1360 m respectively, falling in close range of each other. It is anticipated that as the TDF material dries, the phreatic water level inside the TDF will lower; causing the pressure exerted by the hydraulic head of the TDF to lower over time, which will eventually end the pollution process on the soil.

This study discusses the results of a holistic approach towards the evaluation of soil, vegetation and water pollution by utilizing soil quality parameters and indicators, geohydrology, geophysical surveys, Landscape Function Analysis (LFA) and other means of vegetation assessments.

Salt accumulation on the soil surface was common in specific areas from 2010 – 2012. X ray diffraction (XRD) analyses confirmed that the salts originated from the No. 5 TDF due to the similarity in mineralogy.

The pH values from the start of the 30-month monitoring period remained neutral to slightly alkaline due to the neutralising effect of the dolomitic bedrock. The electrical conductivity (EC) values of the soil decreased significantly from 2010 to 2014; during dry seasons since 2012, no sulphate salts accumulated on the soil surface. Joints, fractures and cavities were found within the bedrock dolomites which created pathways for the polluted TDF water and groundwater to flow towards the study area.

It was also established that there were no adverse effects on the natural vegetation, other than encroachment by *Seriphium plumosum* which affected the grazing quality (overgrazed sites) of the area. It was therefore concluded that after the TDF became dormant in April 2011, the pollution plume in this area is decreasing in magnitude and severity due the lowering of the phreatic water level inside the TDF to significantly lower levels. Consequently, the decrease of the hydraulic pressure head of the TDF as well as rainwater infiltration and high percolation due to the presence of fractures, joints and cavities in the dolomites resulted in the leaching of the sulphate salts to a significant extent. It was also concluded that while there were no apparent adverse effects of the pollution on the functionality of the land, additional monitoring and maintenance would be required for at least the next five years in order to ensure the continuance of current conditions.

Keywords: pollution plume, gold tailings disposal facility, adjacent land, dolomites, long-term monitoring.

UITTREKSEL

In die laaste dekade het omgewingsstudies baie gefokus op die antropogeniese degradasie en die verlies van effektiwiteit van landskappe wat grens aan goud uitskothope. Minimale rehabilitasie en restorasie het plaasgevind by die Mine Waste Solutions (MWS) Nr. 5 uitskothoop voor 1992 as gevolg van swak wetgewing en uitvoer daarvan.

In 2000 het MWS begin met die rehabilitasie van die hele area deur gebruik te maak van winste wat gegenereer is deur die reserwe goud en uraan te ontgin vanaf sekere uitskothope. Die aangrensende landskap noord van die MWS Nr. 5 uitskothoop is egter toe alreeds blootgestel aan die besoedeling afkomstig van die uitskothoop.

Die MWS Nr. 5 uitskothoop is onaktief vanaf April 2011 en die besoedelde area kan gesien word vanaf die noord-oostelike hoek van die MWS Nr. 5 uitskothoop met ’n noord-oos/suid-westelike rigting op die plaas Stilfontein. Gedurende droë tye akkumuleer besonderse hoeveelhede sulfaatsoute op die grond oppervlak, oor ’n area van ten minste 3.5 km vanaf die uitskothoop. Die teenwoordigheid van die sulfaatsoute is baie algemeen wanneer geassosieer met goud uitskothope, maar nie baie algemeen in die chert-arme dolomiete van die Oaktree Formasie nie.

Die primêre doel van hierdie studie was om die kwantitatiewe en mate van besoedeling te bepaal. Die studie het oor 30 maande gestrek en is gemoniteer met behulp van maandelikse assessering van die verskillende grond geochemiese aanslae van die 12 vastepunte en drie-maandelikse interval assesserings van drie transeksie lyne. Die studie het ook gefokus op die identifikasie van potensiële liniêre struktuur afwykings wat met die besoedelingsarea geassosieer kan word, asook verweerde sones van die dolomiete in die Oaktree Formasie, wat geassosieer of verantwoordelik is vir die uitbreiding van die besoedeling oor die area, ten spyte van die topografie asook die helling en strekking van die geologie.

Hierdie eienskappe en verwering sones het paaie vir grondwater geskep om te vloei en dit word verwag dat indien dit teenwoordig is, sal hierdie verwering sones en afwykings ’n bydraende faktor wees vir die besoedelings area in ’n noord-oostelike rigting wat oor die plaas strek.

Die hidrouliese druk hoof van die MWS No. 5 uitskothoop is ongeveer 40 m en die elevasie van die noord-oostelike hoek en vastepunt (FP) 8 is 1368 m en 1360 m, onderskeidelik. Dit word verwag dat wanneer die materiaal van die uitskothoop droog word, sal die freatiese water vlak van die hoop verlaag. Hierdie verandering sal veroorsaak dat die druk wat die hidrouliese hoof

van die uitskothoop uitoefen, mettertyd verlaag, wat dan weer die besoedeling in die omliggende grond sal beëindig.

Die resultate word as ʼn geheel bespreek in terme van grond, plantegroei en water besoedeling. Die evaluering is gedoen deur gebruik te maak van grond kwaliteit parameters en indikators, geohidrologie, geofisiese opnames, Landskap Funksie Analiese (LFA) en ook ander plantegroei opnames.

Vanaf 2010 tot 2012 was sout akkumulasie op die grond oppervlak baie algemeen. X-straal diffraksie (XRD) analises het bevestig dat dit afkomstig was vanaf die Nr. 5 uitskothoop. Vanaf die begin van die 30-maande studie was die pH waardes neutraal tot effens alkalies. Hierdie verskynsel kan toegeskryf word aan die onderliggende dolomiete wat ʼn neutraliserende effek het. Die elektriese geleidings (EC) waardes van die grond het beduidend gedaal tydens 2010 tot 2014, en vanaf 2012 tydens die droë maande het geen sulfaatsoute op die oppervlak geakkumuleer nie. Nate, krake en holtes is gevind binne die onderliggende dolomite hierdie strukture vorm deurpaaie vir die besoedelde oppervlak-en grondwater van die Nr. 5 uitskothoop na die studie area.

Tydens die studie is daar gevind dat die besoedeling geen negatiewe effek op die natuurlike plantegroei gehad het nie, behalwe vir die indringing van *Seriphium plumosum*, wat die weiding kwaliteit van die area beïnvloed het. Die gevolgtrekking is gemaak dat die besoedeling area besig is om te verklein in omvang en erns. Dit kan toegeskryf word aan die verlaging van die freatiese water vlak na aansienlik laer vlakke nadat die uitskothoop dormant geword het in April 2011. Die verlaging van die hidroliese hoofdruk sowel as die infiltrasie van die reënwater en die hoë deursyfering (as gevolg van nate, krake en holtes) het die sulfate tot ʼn beduidende mate geloog.

Alhoewel daar geen negatiewe effek van die besoedeling op die landskap funksies gevind is nie, sal daar aanbeveel word dat deurlopende monitering en instandhouding gedoen word vir ten minste die volgende 5 jaar om die huidige toestande te handhaaf.

Sleutel woorde: besoedelde area, goud uitskothoop, aangrensende landskap, dolomiete, lang-termyn monitering

DECLARATION

The research was selected to be submitted in the normal dissertation format. The work outlined in this MSc dissertation was carried out in the School of Geo- and Spatial Sciences (Geology / Soil Science) at the North-West University (Potchefstroom Campus) during the period from August 2011 to November 2014 under the supervision of Mr PW van Deventer.

This dissertation is the outcome of my own work and may include results of work done in collaboration with this study by Dawid Malo and Melani van der Merwe in 2012; however this is stated in the text where applicable. Some of the material used in this study, e.g. results from 2012, was submitted for a B.Sc Honours degree at the North-West University (Potchefstroom Campus) in 2012.

No part of this dissertation has been, or is currently, submitted for any other degree or qualifications. Various assistances from some University students were used in the field work and data processing.

ACKNOWLEDGMENT

I would like to thank the NRF/THRIP, Mine Waste Solutions and AngloGold Ashanti for making this project possible by providing both the funding and support for this project, it was much appreciated. I wish to attribute my successes thus far to the Lord Jesus - His guidance has been a light without which I would not have succeeded.

I also wish to extend my warmest gratitude for much needed support, guidance and insight to my supervisor for this project, PW van Deventer.

I would like to thank Melt Marais from Mine Waste Solutions who sadly passed away in 2013, for the initiation of this project. He will be greatly missed.

I would like to thank AngloGold Ashanti (industrial partners), in particular John van Wyk and Etienne Grond, for granting me access to the farm Stilfontein, and Joël Malan for the borehole data and literature reports regarding my project site.

I also wish to acknowledge Terina Vermeulen, Yvonne Visagie and their co-workers at Eco-Analytica Laboratories for all of their assistance, as well as Belinda Venter for the XRD analysis, and finally the various assistants for their time, effort and hard work in helping me in the almost endless field work.

Last but not least I would like to thank Alida Slabbert for all her support and final review.

"Live as if you were to die tomorrow. Learn as if you were to live forever."

-Mahatma Gandhi

TABLE OF CONTENTS

CHAPTER 1: INTRODUCTION **1**

1.1 BACKGROUND 1

1.2 STUDY AREA 3

1.2.1 Site Locality *3*

1.2.2 Geology *5*

1.2.3 Soils *10*

1.2.4 Climate *11*

1.2.5 Vegetation *14*

1.2.6 Topography and Surface Draining *14*

1.3 PROBLEM STATEMENT AND SUBSTANTIATION 15

1.4 RESEARCH AIMS AND OBJECTIVES 18

1.4.1 General Aims *18*

1.4.2 Objectives *18*

1.5 BASIC HYPOTHESIS 19

1.6 LAYOUT OF THIS DISSERTATION 20

1.7 EXCLUSIONS 20

CHAPTER 2: LITERATURE REVIEW **21**

2.1 INTRODUCTION 21

2.2 THE IMPORTANCE OF SOIL QUALITY AND SUSTAINABILITY IN SOUTH AFRICA 21

2.3 MINING IN SOUTH AFRICA AND THE ENVIRONMENT 27

2.3.1 The Mine Life Cycle System *28*

2.3.2 Gold Mining and Tailings Material *30*

2.3.2.1 Gold Recovery 30

2.3.2.2 Gold Tailings Material 31

2.3.3 The Negative Impacts of Gold Mining and Tailings Disposal Facilities (TDFs) in South Africa *31*

2.3.3.1 Acid Mine Drainage (AMD) 32

2.3.3.2 Salinisation and Sodification 36

2.3.3.3 Toxic Trace Metal Elements 36

2.3.3.4 Dust Pollution 38

2.3.3.5 Radiation and Radioactivity 38

2.4 GROUNDWATER CHEMISTRY 38

2.4.1 Groundwater Recharge *39*
2.4.2 Chemical Weathering of Minerals and Parent Rock *40*
2.4.2.1 Silicate Weathering 40
2.4.2.2 Carbonate Weathering 41
2.4.3 Groundwater Contamination *42*
2.4.3.1 Mining Activities 42
2.5 LANDSCAPE FUNCTION ANALYSIS (LFA) 43
2.6 PREVIOUS STUDIES DONE ON THE MINE WASTE SOLUTIONS NO. 4 AND 5 TAILINGS DISPOSAL FACILITIES 44
CHAPTER 3: MATERIALS AND METHODS 47
3.1 SOIL SAMPLING 47
3.1.1 Baseline Assessment *47*
3.1.2 Sampling of the Fixed Monitoring Sites *47*
3.1.3 Sampling of the Three Transect Lines *49*
3.2 SOIL SAMPLE PREPARATION 49
3.3 CHEMICAL ANALYSES OF THE SOIL 51
3.3.1 pH *51*
3.3.2 Electrical Conductivity (EC) *51*
3.3.3 Exchangeable Cation Analysis *52*
3.3.4 Cation Exchange Capacity (CEC) Determination *52*
3.3.5 Anion Concentration Analysis *53*
3.3.6 Total Trace Metal Element Analysis of the Soil *54*
3.3.7 Soluble/Available Trace Metal Element Analysis of the Soil *56*
3.4 PARTICLE SIZE DISTRIBUTION ANALYSIS BY MEANS OF THE HYDROMETER METHOD 56
3.5 MINERAL PHASE IDENTIFICATION OF THE SOIL 58
3.5.1 X-ray Diffraction *58*
3.6 BOREHOLE WATER ANALYSIS 61
3.6.1 Accuracy of Chemical Analysis *63*
3.6.2 Data Evaluation *64*
3.6.2.1 Ternary Diagrams 64
3.6.2.2 Piper Diagrams 65
3.6.2.3 Stiff Diagrams 66
3.6.3 Water Sampling *67*
3.6.4 Water Analysis *69*

3.6.4.1 Total Alkalinity (TAL) Analysis 69
3.6.4.2 Major Ion Analysis 70
3.6.4.3 Trace Element Analysis 70
3.6.5 Down-hole Camera Survey 70
3.7 MAGNETIC SURVEY 72
3.7.1 Geo-magnetic Survey 73
3.8 VEGETATION 75
3.8.1 Vegetation Sampling 75
3.8.2 Plant Tissue Preparation 75
3.8.3 Plant Tissue Analysis 75
3.8.4 Landscape Function Analysis (LFA) 76
3.8.4.1 Field Procedure 76
3.8.5 Descending Point Method 87
CHAPTER 4: SOIL ANALYSES RESULTS AND DISCUSSION 88
4.1 BASELINE ASSESSMENT 88
4.2 pH 89
4.3 ELECTRICAL CONDUCTIVITY (EC) 89
4.4 EXCHANGEABLE CATION AND CATION EXCHANGE CAPACITY (CEC) 95
4.5 TOTAL MACRO ELEMENT CONCENTRATION 98
4.6 TOTAL ANION CONCENTRATIONS 107
4.7 TOTAL AND SOLUBLE/AVAILABLE TRACE METAL ELEMENTS IN THE SOIL 109
4.7.1 Total Trace Metal Elements in the Soil 110
4.7.2 Soluble/Available Trace Metal Elements in the Soil 117
4.8 PARTICLE SIZE DISTRIBUTION 120
4.9 MINERAL PHASE IDENTIFICATION 122
4.9.1 X-ray Diffraction 122
4.10 BASIC CONCLUSION 125
CHAPTER 5: WATER ANALYSES RESULTS AND DISCUSSION 126
5.1 TERNARY DIAGRAMS 126
5.2 PIPER DIAGRAMS 127
5.3 STIFF DIAGRAMS 127
5.4 BASIC CONCLUSION 128
CHAPTER 6: GEOPHYSICAL SURVEY, SURFACE OBSERVATIONS AND DOWN-HOLE CAMERA SURVEY RESULTS AND DISCUSSION 129

6.1 MAGNETOMETER SURVEY 129
6.2 SURFACE OBSERVATIONS AND DOWN-HOLE CAMERA SURVEY 132
6.2.1 Surface Observations 132
6.2.2 Aerial Examination of the Plume 133
6.2.3 Down-hole Camera Survey 133
6.3 BASIC CONCLUSION 134
CHAPTER 7: VEGETATION AND LANDSCAPE FUNCTION ANALYSIS (LFA) RESULTS AND DISCUSSION 135
7.1 VEGETATION CHEMICAL ANALYSES 135
7.2 TRACE METAL ELEMENTS CONCENTRATIONS IN THE VEGETATION 142
7.3 DESCENDING POINT METHOD ANALYSES 149
7.4 LANDSCAPE FUNCTION ANALYSIS (LFA) 154
7.4.1 Patch/Inter-patch Description 154
7.4.2 LFA Values 156
7.4.3 Landscape Function Analysis (LFA) Data Comparison 159
7.5 SITE COMPARISON 161
7.6 BASIC CONCLUSION 163
CHAPTER 8: FINAL CONCLUSION AND RECOMMENDATIONS 164
8.1 CONCLUSIONS 164
8.1.1 MONITORING THE QUANTITATIVE, QUALITATIVE AND AERIAL EXTENT OF THE POLLUTION PLUME 164
8.1.2 CONCLUSIONS OF THE MONITORING OF THE QUANTITATIVE, QUALITATIVE AND AERIAL EXTENT OF THE POLLUTION PLUME 165
8.1.2.1 Soil Monitoring 165
8.1.2.2 Water Monitoring 165
8.1.2.3 Surveys Conducted in the Area 166
8.1.2.4 Vegetation Monitoring 166
8.1.2.5 Final Conclusion 167
8.2 RECOMMENDATIONS 167
CHAPTER 9: REFERENCES 169
CHAPTER 10: APPENDICES DESCRIPTION 181
LIST OF APPENDICES 181

LIST OF ACRONYMS

AMD	Acid mine drainage
ARD	Acid rock drainage
CCA	Canonical Correspondence Analysis
CEC	Cation exchange capacity ($cmol^+/kg$)
DGP	Dense Grass Patch
DIN 19730	Deutsches Institut für Normung method 19730
DNHPD	Department of Health and Population Development
DP	Dung Patch
EC	Electrical conductivity (mS/m)
EPA method 3050B	Environmental Protection Agency method 3050B
EW	East-West transect
FbP	Forb Patch
FESLM	Framework for evaluating sustainable land management
FGP	Forb Grass Patch
FP	Fixed point
FSSA	Fertilizer Society of South Africa
GLP	Grass Litter Patch
GP	Grass Patch
ICP-MS	Inductively Coupled Plasma-Mass Spectrometry
IP	Inter-patch
IWG	International Work Group
K	Control site
LFA	Landscape Function Analysis
LOI	Landscape Organisation Index
LP	Litter Patch

MAT	Maximum Available Threshold
MSW	Mine Waste Solutions
NAPP	Net acid producing potential
NS	North-South transect
NWU	North-West University
RP	Rock Patch
SGP	Sparse Grass Patch
SLM `	Sustainable land management
SOM	Soil organic matter
SPP	*Seriphium plumosum* Patch
SSA	Soil Surface Assessment
TDF	Tailings disposal facility
TMT	Total Maximum Threshold
TPC	Threshold of Potential Concern
VCT	Ventersdorp Contact Reef
XRD	X-ray Diffraction

LIST OF FIGURES

FIGURE 1: AERIAL PHOTOGRAPH OF THE CHEMWES TAILINGS COMPLEX. MODIFIED (WITH PERMISSION) FROM VAN DEVENTER (2011A). 1

FIGURE 2: LOCALITY MAP OF THE STUDY AREA WITH ADJACENT TAILINGS AND FOOTPRINTS. RED LINE = STUDY AREA BOUNDARIES (GOOGLE EARTH, 2013). 4

FIGURE 3: REGIONAL GEOLOGY MAP OF THE STUDY AREA. [SPGRP = SUPERGROUP, FM = FORMATION] (GOOGLE EARTH, 2013). 7

FIGURE 4: A SCHEMATIC CROSS SECTION OF THE STUDY AREA, ILLUSTRATING THE TOPOGRAPHY AND GEOLOGY UNITS IN A NORTH-WESTERN (A) TO A SOUTH-EASTERN (B) DIRECTION. (SPGRP = SUPERGROUP, FM = FORMATION). 8

FIGURE 5: JOINTS AND FRACTURES PRESENT IN, AND ON THE SURFACE OF, THE OAKTREE FORMATION DOLOMITES. PHOTOGRAPH TAKEN BY DANIELL (2013). 9

FIGURE 6: EROSION SLUMP STRUCTURES ASSOCIATED WITH STROMATOLITIC IN CHERT (ARROW) IN THE MONTE CHRISTO FORMATION. PHOTOGRAPH TAKEN BY VAN DEVENTER (2008), WITH PERMISSION. 10

FIGURE 7: AVERAGE MINIMUM MONTHLY TEMPERATURES OF THE NEIGHBOURING FARM. DATA PROVIDED BY F VAN ZYL, 2014 (PERSONAL COMMUNICATION). 12

FIGURE 8: AVERAGE MAXIMUM MONTHLY TEMPERATURES OF THE NEIGHBOURING FARM. DATA PROVIDED BY F VAN ZYL, 2014 (PERSONAL COMMUNICATION). 13

FIGURE 9: AVERAGE MONTHLY PRECIPITATION OF THE NEIGHBOURING FARM. DATA PROVIDED BY F VAN ZYL, 2014 (PERSONAL COMMUNICATION). 13

FIGURE 10: MAP SHOWING THE POLLUTION PLUME AND ITS GENERAL DIRECTION, AS WELL AS THE SURFACE TOPOGRAPHY AND DIP OF THE GEOLOGICAL FORMATIONS (GOOGLE EARTH, 2013). 17

FIGURE 11: INTERACTION DIAGRAM BETWEEN SUSTAINABLE LAND MANAGEMENT (SLM), SOIL QUALITY INDICATORS AND SOIL FUNCTIONS. 25

FIGURE 12: THE MINE LIFE CYCLE. MODIFIED FROM MÖHR-SWART *ET AL.* (2008); VAN ZYL (2008); VAN DEVENTER AND HATTINGH (2009). 29

FIGURE 13: ACID MINE DRAINAGE SOURCES, PATHWAYS AND RECEPTORS DIAGRAM. MODIFIED FROM INAP (2009). 34

FIGURE 14: ACID MINE DRAINAGE (AMD) EFFECTS ON WATER SYSTEMS DIAGRAM. MODIFIED FROM GRAY (1997). 35

FIGURE 15: GOLDICH (1938) WEATHERING SEQUENCE. 41

FIGURE 16: MAP SHOWING THE LOCATION OF THE 12 FIXED POINTS (FP 1-9 AND FP-K1-K3) AND THE THREE TRANSECT LINES NS1, EW1AND EW2. (GOOGLE EARTH, 2013). 48
FIGURE 17: PHOTOGRAPH SHOWING A SOIL AUGER. PHOTOGRAPH TAKEN BY DANIELL (2013). 49
FIGURE 18: PHOTOGRAPH ILLUSTRATING AIR-DRIED SOIL SAMPLES AT THE NORTH-WEST UNIVERSITY, POTCHEFSTROOM. PHOTOGRAPH TAKEN BY VAN DER MERWE (2012), WITH PERMISSION. 50
FIGURE 19: PHOTOGRAPH SHOWING THE FUMES GENERATED BY THE HNO_3 DIGESTING THE SOIL. PHOTOGRAPH TAKEN BY VAN DER MERWE (2012), WITH PERMISSION. 54
FIGURE 20: A SCHEMATIC REPRESENTATION OF AN ICP TORCH (WOLF, 2005). 55
FIGURE 21: GEOMETRY OF X-RAY DIFFRACTION FROM EQUALLY SPACED PLANES IN A CRYSTAL STRUCTURE WITH SPACING D BETWEEN THEM (CRAIN, 2001)..... 59
FIGURE 22: SCHEMATIC ILLUSTRATION OF THE ESSENTIAL COMPONENTS OF A POWDER X-RAY DIFFRACTOMETER. IN SUCH AN INSTRUMENT, THE SAMPLE HOLDER ROTATES AT Θº WHILE THE DETECTOR ROTATES 2Θº. (KLEIN AND DUTROW, 2008)..... 60
FIGURE 23: MAP SHOWING THE LOCATIONS OF THE BOREHOLES WHICH WERE SAMPLED. (GOOGLE EARTH, 2013). 62
FIGURE 24: TERNARY DIAGRAM SHOWING THE CHARACTERISATION OF THE INORGANIC WATER CHEMISTRY. 1 = CHEMICAL WEATHERING ZONE, 2 = CHEMICAL WEATHERING (≥ 50%) AND CL-SAL AND SO_4–CONT (≤ 50%), 3 = CHEMICAL WEATHERING (≤ 50%) AND CL-SAL AND SO_4–CONT (≥ 50%), 4 = CHLORIDE SALINISATION, 5 = SULPHATE CONTAMINATION. MODIFIED FROM HUIZENGA (2011)..... 65
FIGURE 25: PIPER DIAGRAM USED FOR BULK CHEMICAL COMPOSITION OF THE BOREHOLE SAMPLES. 66
FIGURE 26: ILLUSTRATION OF A STIFF DIAGRAM, SHOWING THE CONCENTRATIONS OF THE REPRESENTATIVE CATIONS AND ANIONS..... 67
FIGURE 27: PHOTOGRAPH ILLUSTRATING WATER BEING SAMPLED WITH AN ELECTRICAL UPGRADED WATER SAMPLER. PHOTOGRAPH TAKEN BY DANIELL (2014). 68
FIGURE 28: PHOTOGRAPH OF BOREHOLE WATER BEING FILTERED PRIOR TO STORAGE. PHOTOGRAPH TAKEN BY DANIELL (2014). 68
FIGURE 29: MAP SHOWING THE LOCATIONS OF THE BOREHOLES THAT WERE USED TO CONDUCT THE DOWN-HOLE CAMERA SURVEY (GOOGLE EARTH, 2013)..... 71
FIGURE 30: DOWN HOLE CAMERA FROM THE NWU USED TO CONDUCT THE DOWN-HOLE CAMERA SURVEY. PHOTOGRAPH TAKEN BY DANIELL (2014). 72

FIGURE 31: TRIPOD PLACED DIRECTLY OVER THE BOREHOLES FOR GUIDANCE AND SUPPORT OF THE CAMERA. PHOTOGRAPH TAKEN BY DANIELL (2014). 72
FIGURE 32: MAP SHOWING THE LOCATIONS OF THE MAGNETOMETER LINES (GOOGLE EARTH, 2013)..... 74
FIGURE 33: LANDSCAPE ORGANISATION SCHEMATIC TO ILLUSTRATE, A TRANSECT LAYOUT, IN THE DIRECTION OF RESOURCE FLOW AND THE VARIOUS MEASUREMENTS NECESSARY TO CONDUCT AN LFA. (TONGWAY AND HINDLEY, 2004; TONGWAY AND LUDWIG, 2011). 77
FIGURE 34: PHOTOGRAPH DISPLAYING A DENSE GRASS PATCH, WITH MEASUREMENTS WHICH INDICATE THE EXTENT OF THE PATCH. PHOTOGRAPH TAKEN BY MALO (2012), WITH PERMISSION. 78
FIGURE 35: PHOTOGRAPH SHOWING A SINGLE FORB PATCH WITH MEASUREMENTS WHICH INDICATE THE EXTENT OF THE PATCH. PHOTOGRAPH TAKEN BY DANIELL (2014). 78
FIGURE 36: PHOTOGRAPH SHOWS A SINGLE GRASS PATCH WITH MEASUREMENTS WHICH INDICATE THE EXTENT OF THE PATCH. PHOTOGRAPH TAKEN BY MALO (2012), WITH PERMISSION. 79
FIGURE 37: PHOTOGRAPH DISPLAYING A LITTER PATCH WITH MEASUREMENTS WHICH INDICATE THE EXTENT OF THE PATCH. PHOTOGRAPH TAKEN BY MALO (2012), WITH PERMISSION. 80
FIGURE 38: PHOTOGRAPH SHOWING A GRASS LITTER PATCH WITH MEASUREMENTS WHICH INDICATE THE EXTENT OF THE PATCH. PHOTOGRAPH TAKEN BY MALO (2012), WITH PERMISSION. 81
FIGURE 39: PHOTOGRAPH DISPLAYING A ROCK PATCH WITH MEASUREMENTS WHICH INDICATE THE EXTENT OF THE PATCH. PHOTOGRAPH TAKEN BY DANIELL (2014). 82
FIGURE 40: PHOTOGRAPH SHOWING AN INTER-PATCH WITH MEASUREMENTS WHICH INDICATE THE EXTENT OF THE PATCH. PHOTOGRAPH TAKEN BY MALO (2012), WITH PERMISSION. 82
FIGURE 41: PHOTOGRAPH SHOWING A DUNG PATCH WITH MEASUREMENTS WHICH INDICATE THE EXTENT OF THE PATCH. PHOTOGRAPH TAKEN BY DANIELL (2014). 83
FIGURE 42: PHOTOGRAPH SHOWING A *SERIPHIUM PLUMOSUM* PATCH WITH MEASUREMENTS WHICH INDICATE THE EXTENT OF THE PATCH. PHOTOGRAPH TAKEN BY DANIELL (2014). 84
FIGURE 43: PHOTOGRAPH SHOWING SPARSE GRASS PATCHES SCATTERED OVER THE AREA. PHOTOGRAPH TAKEN BY DANIELL (2014). 84
FIGURE 44: THE 11 SSA INDICATORS AND THE ALLOCATION OF THESE INDICATORS TO THE THREE LFA INDICES. (TONGWAY AND HINDLEY, 2004). 86
FIGURE 45: PHOTOGRAPH SHOWING A SHALE LENS WITHIN THE OAKTREE FORMATION DOLOMITES IN A BORROW PIT IN THE STUDY AREA. PHOTOGRAPH TAKEN BY BONESCHANS (2013), WITH PERMITION. 88

FIGURE 46: ELECTRICAL CONDUCTIVITY OF FP–1 AND -6 IN AUGUST 2010 (VAN DEVENTER, 2011B). 90
FIGURE 47: ELECTRICAL CONDUCTIVITY (EC) OF THE NINE FPS AND THREE CONTROL SITES IN AUGUST 2011, 2012 AND 2013. 91
FIGURE 48: ELECTRICAL CONDUCTIVITY OF THE NORTH-SOUTH TRANSECT LINE IN AUGUST 2011, 2012 AND 2013. 92
FIGURE 49: ELECTRICAL CONDUCTIVITY OF EAST-WEST 1 TRANSECT LINE IN AUGUST 2011, 2012 AND 2013. 93
FIGURE 50: ELECTRICAL CONDUCTIVITY OF THE EAST-WEST 2 TRANSECT LINE IN AUGUST 2011, 2012 AND 2013. 94
FIGURE 51: EXCHANGEABLE CATIONS AND CATION EXCHANGE CAPACITY (CEC) OF THE FIXED POINTS AND CONTROL SITES IN 2012. 96
FIGURE 52: EXCHANGEABLE CATIONS AND CATION EXCHANGE CAPACITY (CEC) OF THE FIXED POINTS AND CONTROL SITES IN 2013. 96
FIGURE 53: TOTAL MACRO ELEMENT CONCENTRATION FOR FP-1 (EPA 3050B, 1996). 99
FIGURE 54: TOTAL MACRO ELEMENT CONCENTRATION FOR FP-2 (EPA 3050B, 1996). 99
FIGURE 55: TOTAL MACRO ELEMENT CONCENTRATION FOR FP-3 (EPA 3050B, 1996). 100
FIGURE 56: TOTAL MACRO ELEMENT CONCENTRATION FOR FP-4 (EPA 3050B, 1996). 101
FIGURE 57: TOTAL MACRO ELEMENT CONCENTRATION FOR FP-5 (EPA 3050B, 1996). 101
FIGURE 58: TOTAL MACRO ELEMENT (MG^{2+} AND CA^{2+}) CONCENTRATION FOR FP-6 (EPA 3050B, 1996). 102
FIGURE 59: TOTAL MACRO ELEMENT (NA^{+}, P^{3-} AND K^{+}) CONCENTRATION FOR FP-6 (EPA 3050B, 1996). 103
FIGURE 60: TOTAL MACRO ELEMENT CONCENTRATION FOR FP-7 (EPA 3050B, 1996). 103
FIGURE 61: TOTAL MACRO ELEMENT CONCENTRATION FOR FP-8 (EPA 3050B, 1996). 104
FIGURE 62: TOTAL MACRO ELEMENT CONCENTRATION FOR FP-9 (EPA 3050B, 1996). 104
FIGURE 63: TOTAL MACRO ELEMENT CONCENTRATION FOR FP-K1 (EPA 3050B, 1996). 105
FIGURE 64: TOTAL MACRO ELEMENT CONCENTRATION FOR FP-K2 (EPA 3050B, 1996). 106
FIGURE 65: TOTAL MACRO ELEMENT CONCENTRATION FOR FP-K3 (EPA 3050B, 1996). 106
FIGURE 66: CHLORIDE CONCENTRATION OF THE 12 FIXED POINTS IN AUGUST 2011 AND 2013. 108
FIGURE 67: NITRATE CONCENTRATION (MG/L) OF THE 12 FIXED POINTS IN AUGUST 2011 AND 2013. 108
FIGURE 68: SULPHATE CONCENTRATION (MG/L) OF THE 12 FIXED POINTS IN AUGUST 2011 AND 2013. 109

FIGURE 69: CADMIUM CONCENTRATION (MG/KG) OF THE 12 FIXED POINTS IN 2011 AND 2014. (EPA 3050B, 1996). 112
FIGURE 70: CHROMIUM CONCENTRATION (MG/KG) OF THE 12 FIXED POINTS IN 2011 AND 2014. (EPA 3050B, 1996). 113
FIGURE 71: COBALT CONCENTRATION (MG/KG) OF THE 12 FIXED POINTS IN 2011 AND 2014. (EPA 3050B, 1996). 113
FIGURE 72: NICKEL CONCENTRATION (MG/KG) OF THE 12 FIXED POINTS IN 2011 AND 2014. (EPA 3050B, 1996). 114
FIGURE 73: COPPER CONCENTRATION (MG/KG) OF THE 12 FIXED POINTS IN 2011 AND 2014. (EPA 3050B, 1996). 114
FIGURE 74: ZINC CONCENTRATION (MG/KG) OF THE 12 FIXED POINTS IN 2011 AND 2014. (EPA 3050B, 1996). 115
FIGURE 75: LEAD CONCENTRATION (MG/KG) OF THE 12 FIXED POINTS IN 2011 AND 2014. (EPA 3050B, 1996). 115
FIGURE 76: ARSENIC CONCENTRATION (MG/KG) OF THE 12 FIXED POINTS IN 2011 AND 2014. (EPA 3050B, 1996). 116
FIGURE 77: URANIUM CONCENTRATION (MG/KG) OF THE 12 FIXED POINTS IN 2011 AND 2014. (EPA 3050B, 1996). 116
FIGURE 78: PARTICLE SIZE DISTRIBUTION CURVES OF THE 12 FIXED POINT SAMPLES. 120
FIGURE 79: SOIL TEXTURAL TRIANGLE OF THE 12 FIXED POINT SOIL SAMPLES (CALCULATED FROM USDA-NRCS, 2014). 121
FIGURE 80: POTENTIAL DYKES FOUND AND MAGNETOMETER ANOMALIES FOUND IN THE STUDY AREA. (GOOGLE EARTH, 2013). 131
FIGURE 81: PHOTOGRAPHS SHOWING THE FRACTURES AND JOINTS PRESENT ON THE SURFACE DOLOMITES. PHOTOGRAPHS TAKEN BY DANIELL (2014). 132
FIGURE 82: PHOTOGRAPH SHOWING A SHALLOW HOLE PRESENT ON THE SURFACE OF THE OAKTREE FORMATION DOLOMITES IN THE STUDY AREA. PHOTOGRAPH TAKEN BY DANIELL (2014). 133
FIGURE 83: DOWN-HOLE CAMERA PHOTOGRAPHS. A: SHOWS A CAVITY. B: SHOWS A CAVITY. C: SHOWS A CAVITY. D: SHOWS FRACTURES. E: SHOWS JOINTS. F: SHOWS FRACTURES. ALL PRESENT WITHIN THE OAKTREE FORMATION DOLOMITES. 134
FIGURE 84: LANDSCAPE ORGANISATION INDEX FOR THE 12 FIXED POINTS OF THE 2012 AND 2014 SURVEYS. 159
FIGURE 85: MEAN VALUES OF THE LFA INDICES WITH TREND LINES INDICATING A DECREASE OR INCREASE IN LFA INDEX VALUES OF THE 2012 SURVEY. 160

FIGURE 86: MEAN VALUES OF THE LFA INDICES WITH TREND LINES INDICATING A DECREASE OR INCREASE IN LFA INDEX VALUES OF THE 2014 SURVEY. 160
FIGURE 87: SPECIES, ENVIRONMENTAL DATA AND LFA DATA TRI-PLOT FROM CANONICAL CORRESPONDENCE ANALYSIS (CANOCO) IN 2012 (MALO, 2012). 162
FIGURE 88: SPECIES, ENVIRONMENTAL DATA AND LFA DATA TRI-PLOT FROM CANONICAL CORRESPONDENCE ANALYSIS (CANOCO) IN 2014. 162

LIST OF TABLES

TABLE 1: SIMPLIFIED STRATIGRAPHIC UNITS OF THE KLERKSDORP GOLDFIELD (MCCARTHY, 2006). 6
TABLE 2: SIMPLIFIED STRATIGRAPHIC UNITS OF THE TRANSVAAL SUPERGROUP (ERIKSSON *ET AL.*, 2006)..... 6
TABLE 3: SUMMARY OF THE THREE SOIL INDICATORS UTILISED TO ASSES SOIL FUNCTION (KINYANGI, 2007). 23
TABLE 4: SUMMARY OF THE INTERACTION BETWEEN THE FRAMEWORK FOR EVALUATING SUSTAINABLE LAND MANAGEMENT (FESLM), THE THREE SOIL QUALITY INDICATORS AND SOIL FUNCTIONS. 26
TABLE 5: FARM STILFONTEIN BOREHOLE SITE DESCRIPTIONS. 63
TABLE 6: THE DATASET MODIFICATION..... 64
TABLE 7: SSA-11 INDICATORS AND THE MEASUREMENT OF THE OBJECTIVES FOR THE DIFFERENT SSA INDICATORS (TONGWAY AND HINDLEY, 2004; HAAGNER, 2008)..... 85
TABLE 8: PROPORTIONS OF CATIONS TO THE EFFECTIVE CATION EXCHANGE CAPACITY (CEC) AND CA:MG RATIO OF THE 12 FIXED POINTS IN 2012. 97
TABLE 9: PROPORTIONS OF CATIONS TO THE EFFECTIVE CATION EXCHANGE CAPACITY (CEC) AND CA:MG RATIO OF THE 12 FIXED POINTS IN 2013. 98
TABLE 10: TOTAL AND AVAILABLE (SOLUBLE) THRESHOLDS/GUIDELINES FOR SPECIFIC POTENTIALLY TOXIC TRACE METAL ELEMENTS..... 110
TABLE 11: SOLUBLE/AVAILABLE TRACE METAL ELEMENT CONCENTRATIONS (MG/KG) OF THE 12 FIXED POINTS IN 2011, 2013 AND 2014 (DIN 19730, 1997). 118
TABLE 12: SUMMARY OF THE TEXTURAL PROPERTIES OF 12 FIXED POINTS. 121
TABLE 13: XRD ANALYSIS OF FP-1 DONE IN 2010..... 123
TABLE 14: XRD ANALYSIS OF FP-6 DONE IN 2010..... 123
TABLE 15: XRD ANALYSIS OF FP-1 DONE IN 2013..... 123
TABLE 16: XRD ANALYSIS OF FP-6 DONE IN 2013..... 123
TABLE 17: RESULTS OF THE XRD ANALYSIS OF THE REMAINING 10 FIXED POINTS DONE IN 2013. 124
TABLE 18: SUMMATIVE REPRESENTATION OF THE TERNARY DIAGRAMS FOR THE BOREHOLE SITES WITH PLOTS GREATER THAN 0.7 HCO_3..... 126
TABLE 19: MAJOR MAGNETIC ANOMALIES FOUND IN THE STUDY AREA, DURING THE MAGNETOMETER SURVEY..... 130

TABLE 20: VEGETATION CHEMICAL ANALYSES OF SPECIES FOR MICRO- AND MACRO-NUTRIENT CONCENTRATION (MG/KG) IN 2012. 137
TABLE 21: VEGETATION CHEMICAL ANALYSES OF SPECIES FOR MICRO- AND MACRO-NUTRIENT CONCENTRATION (MG/KG) IN 2013. 138
TABLE 22: VEGETATION CHEMICAL ANALYSES OF SPECIES FOR MICRO- AND MACRO-NUTRIENT CONCENTRATION (MG/KG) IN 2014. 140
TABLE 23: TOTAL TRACE METAL ELEMENT CONCENTRATION (MG/KG) OF THE DIFFERENT GRASS SPECIES SAMPLES ON EACH SITE IN 2012 (EPA 3050B, 1996). 144
TABLE 24: TOTAL TRACE METAL ELEMENT CONCENTRATION (MG/KG) OF THE DIFFERENT GRASS SPECIES SAMPLES ON EACH SITE IN 2013 (EPA 3050B, 1996). 145
TABLE 25: TOTAL TRACE METAL ELEMENT CONCENTRATION (MG/KG) OF THE DIFFERENT GRASS SPECIES SAMPLES ON EACH SITE IN 2014 (EPA 3050B, 1996). 147
TABLE 26: AVERAGE RELATIVE FREQUENCY OF SPECIES ON THE THREE TRANSECTS PER SITE IN 2012. THE TABLE ALSO ILLUSTRATES THE SPECIES COMPOSITION AND ECOLOGICAL STATUS (MALO, 2012). 151
TABLE 27: AVERAGE RELATIVE FREQUENCY OF SPECIES ON THE THREE TRANSECTS PER SITE IN 2014. THE TABLE ALSO ILLUSTRATES THE SPECIES COMPOSITION AND ECOLOGICAL STATUS. 152
TABLE 28: THE MEAN PATCH AND INTER-PATCH CONTRIBUTION TO THE LANDSCAPE FUNCTION ANALYSIS (LFA) INDEX FUNCTION FOR THE 12 FIXED POINTS IN 2012 (MALO, 2012). 155
TABLE 29: THE MEAN PATCH AND INTER-PATCH CONTRIBUTION TO THE LANDSCAPE FUNCTION ANALYSIS (LFA) INDEX FUNCTION FOR THE 12 FIXED POINTS IN 2014. 155
TABLE 30: SUMMARY OF THE LANDSCAPE FUNCTION ANALYSIS (LFA) VARIABLES FOR THE 2012 SURVEY. 157
TABLE 31: SUMMARY OF THE LANDSCAPE FUNCTION ANALYSIS (LFA) VARIABLES FOR THE 2014 SURVEY. 158

LIST OF EQUATIONS

Eq. 1 14
Eq. 2 32
Eq. 3 32
Eq. 4 32
Eq. 5 33
Eq. 6 33
Eq. 7 41
Eq. 8 42
Eq. 9 42
Eq. 10 61
Eq. 11 61
Eq. 12 61
Eq. 13 63
Eq. 14 64
Eq. 15 64
Eq. 16 64
Eq. 17 69
Eq. 18 69
Eq. 19 69
Eq. 20 157

CHAPTER 1: INTRODUCTION

1.1 BACKGROUND

In 1887, gold was discovered in the conglomerates of the Klerksdorp/Stilfontein area as an isolated outcrop only a year after the discovery of gold on the Witwatersrand (Van Deventer and Marais, 2003; King *et al.,* 2007; Van Deventer, 2011a). After this discovery, the exploitation of gold in this area by numerous mining companies started during the next few years. The Stilfontein Gold Mines started in July 1952 after the two shafts (Margret and Charles) were sunk in 1949; peak mining activities occurred during 1970 to 1980 (Van Deventer and Marais, 2003; Marais *et al.,* 2006; Van Deventer, 2011a).

Underground mining in this area ceased in January 1992, with no ore hoisted since then (Van Deventer and Marais, 2003; King *et al.,* 2007; Van Deventer, 2011a). By this time, a total of 67.2 million metric tons of ore had been treated, which yielded an average of 10.316 g/t of gold (Van Deventer and Marais, 2003; Van Deventer, 2011a). The fine tailings were pumped to tailings disposal facilities (TDFs) as shown Figure 1. The waste rock was dumped on rock dumps and is utilized for crusher material in construction projects.

Figure 1: Aerial photograph of the Chemwes tailings complex. Modified (with permission) from Van Deventer (2011a).

According to Van Deventer and Marais (2003), the Stilfontein Gold Mine forms part of the greater Klerksdorp Goldfield of the Witwatersrand Supergroup; the majority of the mined ore was from the Vaal Reef (previously known as the Strathmore Reef), with minor ore originating from the Black Reef and the Ventersdorp Contact Reef (VCR).

In its 40 years of production, the Stilfontein Gold Mine produced roughly 693.5 tons of gold (Van Deventer, 2011a). Since 1992, certain structures were demolished, and shafts were plugged and capped; other shafts were kept operational for the service and maintenance of underground pumps (Van Deventer and Marais, 2003).

According to Van Deventer (2011a), the most common problem with the outlying gold TDFs is seepage towards adjacent lands and soil pollution, as well as groundwater pollution. In 2010, S van Rensburg, a farmer from a nearby farm north of the TDFs, suspected pollution on his farmland stemming from one of the adjacent Mine Waste Solutions (MWS) tailings dams (Van Deventer, 2012, personal communication).

In 2010, MWS requested that the Geology Department of the North-West University (NWU) conduct an investigation into the allegations of soil pollution on the site derived from the Chemwes No. 5 TDF (now known as MWS No. 5 TDF). Agreenco Environmental Projects and JM Hattingh were asked to review the report and findings (Van Deventer, 2012, personal communication).

The main conclusions drawn by Van Deventer (2011b), Steenekamp and Haagner (2010), were that the salt crusts on the farm Stilfontein are mineralogically related to the salt crusts at the toe of the MWS No. 5 TDF, and that the pollution plume was highly visible, running along a north-eastern/south-western (NE-SW) orientation from the NE corner of MWS No. 5 TDF, and extending for over 3.5 km onto the farm Stilfontein.

A discernable change was also noted in the vegetation covering the areas within the plume and those outside the plume.

Steenekamp and Haagner (2010) also stated that changes were apparent in plant structure due to the lack of utilization of affected areas, despite clear access of livestock to the affected areas as well as the presence of highly palatable and preferred species for grazing, such as *Themeda triandra*, *Digitaria eriantha*, *Anthephora pubescens* and *Brachiaria serrata*.

Therefore it was recommended that a more detailed site survey should be conducted over a larger area to the north and northeast of the MWS No. 5 TDF.

In May 2011, a monitoring program was proposed together with other features which could be related to the pollution plume. The proposal was accepted and a 30-month monitoring program was laid out. The soil monitoring was started in August 2011 by Van der Merwe (2012) and continued until December 2012.

The study was then resumed in January 2013 and continued until the end of the monitoring period in January 2014. The first vegetation assessment was completed by Malo in 2012, and the final one in 2014.

The project started in August 2011 with site identification and description; 12 fixed points (FPs) were selected, with nine of these localities displaying evidence of accumulated salts on the soil surface and the remaining three in the areas without accumulated salts on the soil surface, so as to serve as control sites to be sampled on a monthly basis.

Three transect lines were selected, one with a north-south orientation and two with an east-west orientation, over the extent of the pollution plume which were to be sampled on a three-monthly interval.

These localities were selected by PW van Deventer (NWU) from previous studies conducted on the site by the NWU, MWS and Agreenco.

1.2 STUDY AREA

1.2.1 Site Locality

The study area is located in North West Province in South Africa, roughly 160 km south-west of Johannesburg and 110 km north-west of the Free State Goldfields, approximately 30 km west-south-west of Potchefstroom and north of the N12 highway (as shown in Figure 2), and 8 km from Klerksdorp.

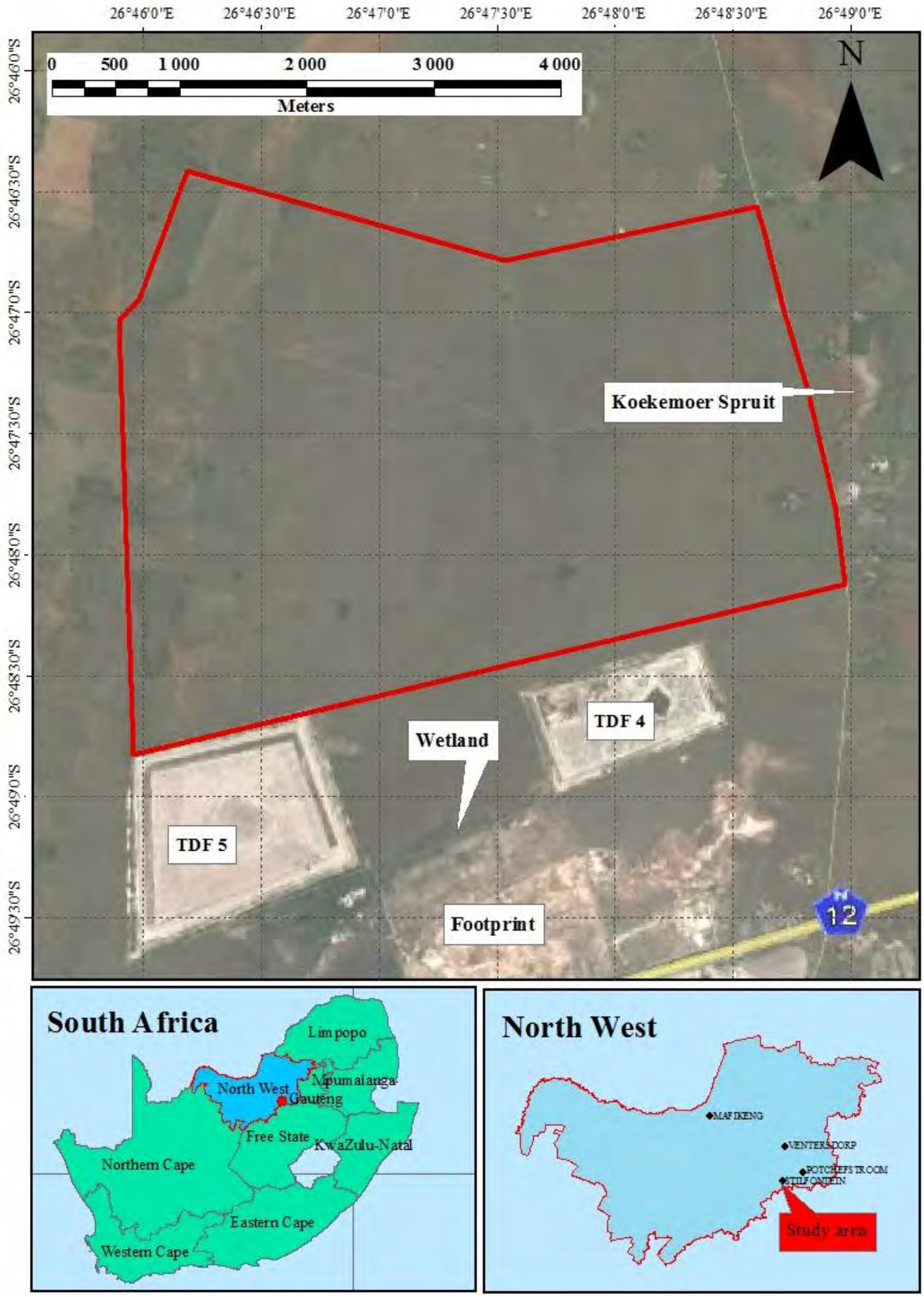

Figure 2: Locality map of the study area with adjacent tailings and footprints. Red line = study area boundaries (Google Earth, 2013).

1.2.2 Geology

The Vaal Reef, which was actively mined in the area, forms part of the greater Klerksdorp Goldfield of the Johannesburg Subgroup which falls within the Central Rand Group of the Witwatersrand Supergroup, as illustrated in Table 1 (McCarthy, 2006).

In the study area, the Witwatersrand Supergroup is overlain by Ventersdorp lava and Transvaal sedimentary rocks however only the Transvaal sedimentary rocks are visible in Figure 3.

The Black Reef Formation belongs to the Transvaal Supergroup, as shown Table 2. The Black Reef Formation lies directly above the Ventersdorp Supergroup lavas, as shown in Figure 4. The Black Reef Formation consists mainly of mature quartz arenites, lesser conglomerates and mudrock, as well as carbonaceous shale (Aucamp, 2003; Eriksson *et al.,* 2006; King *et al.,* 2007) it is associated with weakly defined beds of gold-bearing conglomerate (Nel *et al.,* 1939).

The Black Reef Formation underlies the Oaktree dolomites and outcrops on the far north-western corner of the farm (Figure 3).

The geology of the area is dominated by the dark-coloured, chert-poor dolomites of the Oaktree Formation, with only a small outcrop of the lightly-coloured chert-rich dolomites of the Monte Christo Formation in the south-east of No. 2 footprint and north of the N12 Highway, as illustrated in Figure 3.

Both Formations are subdivisions of the Malmani Subgroup of the Chuniespoort Group which belongs to the Transvaal Supergroup, as laid out in Table 2 (Aucamp, 2003; King *et al.,* 2007; Labuschagne, 2008; Van Deventer, 2011a).

The dolomites dip approximately 5-8° in a south-eastern direction (Van Deventer, 2011b) which might be due to post-Transvaal faulting, and according to Van Deventer and Bloem (2007), dips to the south-east at an angle of 3-12°, which gradually increases with depth and distance up to 35° as shown on the 1:250 000, 2626 West Rand Geological Plan from the Council for Geoscience published in 1986 (Map).

The Oaktree Formation consists of 10-200 m of stromatolitic dolomites, irregular shales and locally-developed quartzites (Eriksson *et al.,* 2006; King *et al.,* 2007; Van Deventer and Bloem, 2007). Massive chert bands are absent in the Oaktree Formation, with only thin and small chert bands occurring, and resulting in the Oaktree Formation being mainly chert-poor dolomites (King *et al.,* 2007; Van Deventer, 2011a).

Superficial deposits are thin and scattered in the area and are not shown in Figure 3.

Table 1: Simplified stratigraphic units of the Klerksdorp Goldfield (McCarthy, 2006).

Supergroup	Group	Subgroup	Formation	Klerksdorp	Rock types
Witwatersrand Supergroup	Central Rand Group	Johannesburg Subgroup	Booysens	Doornkop Member	Shale and quartzite
			Krugersdorp	**Vaal Reef**	Conglomerates and quartzite
			Luipaardsvlei	Livingstone Reef	Conglomerates and quartzite
			Randfontein	Commonage Reef	Quartzite
			Main	Commonage Reef	Conglomerates and quartzite
			Blyvooruitzicht	Ada May Reef	Conglomerates and quartzite

Table 2: Simplified stratigraphic units of the Transvaal Supergroup (Eriksson *et al.,* 2006).

Supergroup	Group	Subgroup	Formation
Transvaal Supergroup	Chuniespoort Group	Malmani Subgroup	Monte Christo
			Oaktree
			Black Reef

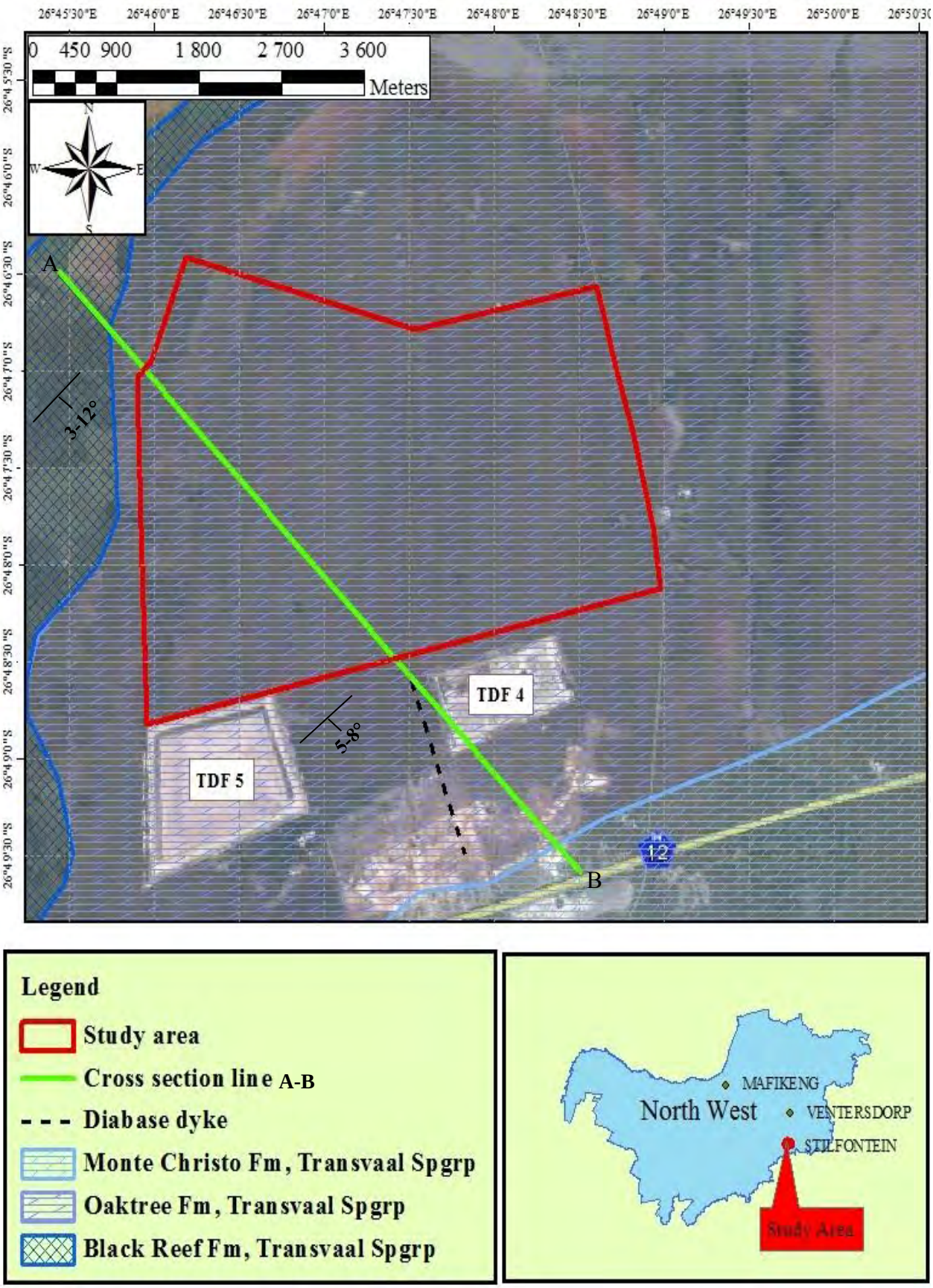

Figure 3: Regional geology map of the study area. [Spgrp = Supergroup, Fm = Formation] (Google Earth, 2013).

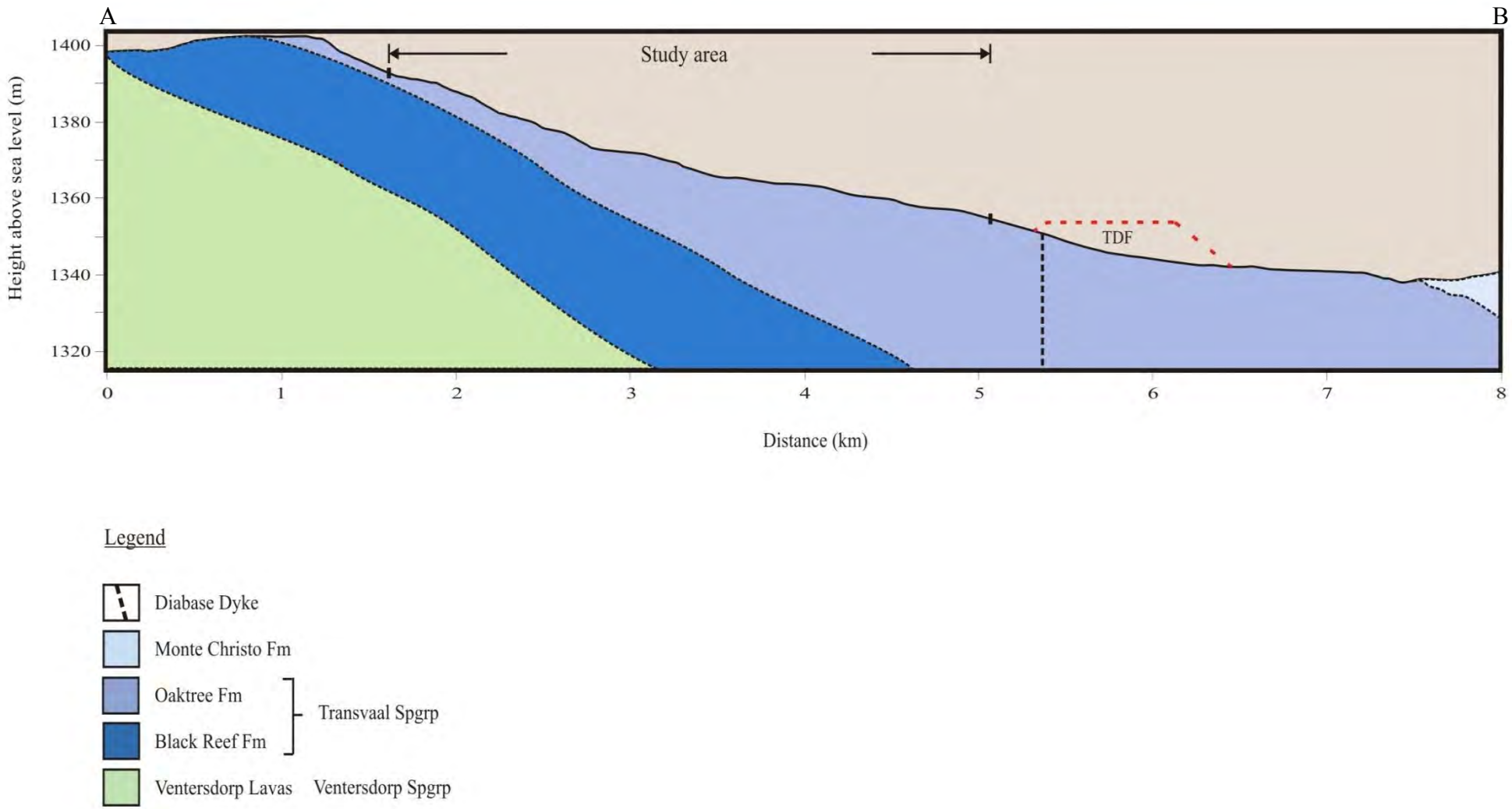

Figure 4: A schematic cross section of the study area, illustrating the topography and geology units in a north-western (A) to a south-eastern (B) direction. (Spgrp = Supergroup, Fm = Formation).

Figure 5 illustrates typical joints and fractures present on the surface of the dolomites of the Oaktree Formation in the study area.

The Monte Christo Formation is 300-500 m thick and starts with a breccia, extending with light-coloured chert-rich bands with stromatolitic and oolitic in the dolomites (Aucamp, 2003; Eriksson *et al.,* 2006; King *et al.,* 2007).

The Monte Christo Formation is dominated by weathered chert and erosion-slump structures which are pronounced in mined areas, as shown in Figure 6 (Van Deventer, 2011a).

The Monte Christo Formation does not show significant signs of joints and fractures such as those of the Oaktree Formation; however, it cannot be regarded as joint- and fracture-free.

Figure 5: Joints and fractures present in, and on the surface of, the Oaktree Formation dolomites. Photograph taken by Daniell (2013).

One major diabase dyke occurs in this area in a southern-northern direction between TDF No. 4 and 5, as shown in Figure 3 and on the 1:250 000, 2626 West Rand Geological Plan from the Council for Geoscience published in 1986.

This was confirmed in a magnetic study conducted in 2007 by GeoLab (Van Deventer and Bloem, 2007).

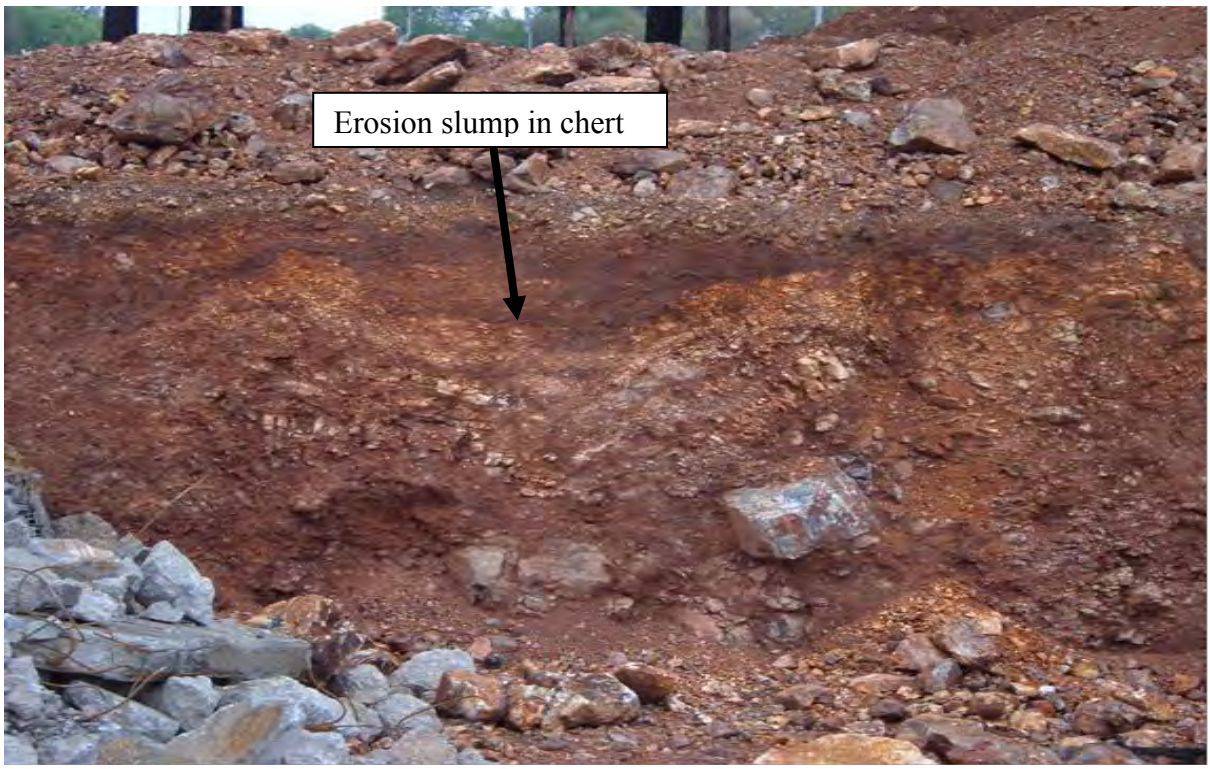

Figure 6: Erosion slump structures associated with stromatolitic in chert (arrow) in the Monte Christo Formation. Photograph taken by Van Deventer (2008), with permission.

No evidence of the diabase outcrop, vegetation anomaly or change in soil colour was observed, while the drilling conducted in 2008 (Labuschagne, 2008) correspondingly affirm no evidence of the diabase dyke.

The magnetic anomaly data confirmed the position of the dyke. There is a fair amount of speculation relating to other dykes in the area. This is more thoroughly discussed in Chapter 6 of this dissertation.

1.2.3 Soils

Most of the soils are thin on the dolomite outcrops (which barely exceed 20 cm) with the exception of the western areas where some agronomy activities occur (Van Deventer and Bloem, 2007). Mucina and Rutherford (2006) stated that more than 50% of the main soil types are relatively shallow and rocky. The soil forms in this area are dominated by Hutton, Glenrosa, Mispah (Haagner, 2008), Dresden and Lichtenberg soil forms (Fey, 2010).

The soils are dominated by manganese and iron oxides (oxisoils). Due to the fact that some natural zinc and nickel anomalies occur in the dolomites, the soils can contain high Zn and Ni

concentrations (Van Deventer, 2011a). The cover soils on the dolomites change colour from ~~–r~~eddish" to ~~–d~~ark brown" (5YR4/6 to 5YR2/2) which is due to the variation in iron and manganese in the soils (Van Deventer and Bloem, 2007). The manganocrete (superficial deposits) is mostly associated with the Dresden and Lichtenberg soil forms (Fey, 2010).

The colour of the soils on the shales is light grey (Van Deventer and Bloem, 2007). The soils on the Black Reef Formation are more severely weathered and more reddish in colour with lower pH levels than those of the dolomite formations (Van Deventer, 2011b).

1.2.4 Climate

The climate of this area is typically that of the South African Highveld, with warm to hot (average ~ 30°C) rainy summers and with cold, dry sunny winters (average ~ 18°C), with frost normally occurring between April and September (Mucina and Rutherford, 2006; Odendaal *et al.,* 2008).

Rainfall normally occurs as isolated spring and summer thunderstorms and showers, with an average rainfall of between 300-625 mm per year (Mucina and Rutherford, 2006; Odendaal *et al.,* 2008; Van Deventer, 2011a). The mean annual potential evaporation of this area is 2407 mm (Mucina and Rutherford, 2006).

During the study period (2011-2014), daily weather data were obtained from a neighbouring farmer (Van Zyl, 2014, personal communication) with the following coordinates: longitude 26°.48.631 E, latitude 26°.44.535 S. The mini-weather station installed in the area during December 2011 failed. Winds in this area are mainly from the northerly sector with north-west being dominant.

The minimum and maximum temperatures followed a steady decrease from January to July throughout the timespan of the study period (Van Zyl, 2014, personal communication). The temperatures peaked at approximately 30-33°C, with lowest temperatures around –2 to –5°C. The temperatures increased steadily from August to December throughout the study period, with the exception of 2013 where there was a sudden decrease in minimum and maximum temperatures from July to August, as illustrated in Figure 7 and Figure 8 (Van Zyl, 2014, personal communication). The mean annual temperature of 2011 was 16.8°C with an average minimum temperature of 7.5°C and an average maximum temperature of 26.2°C (Van Zyl, 2014, personal communication). The mean annual temperature of 2012 was 16.7°C, with an average

minimum temperature of 7.5°C and an average maximum temperature of 25.8°C (Van Zyl, 2014, personal communication). The mean annual temperature of 2013 was 16.4°C, with an average minimum temperature of 7.1°C and an average maximum temperature of 25.7°C (Van Zyl, 2014, personal communication). There were only slight variations in the mean annual temperatures over the different years, with no dramatic changes.

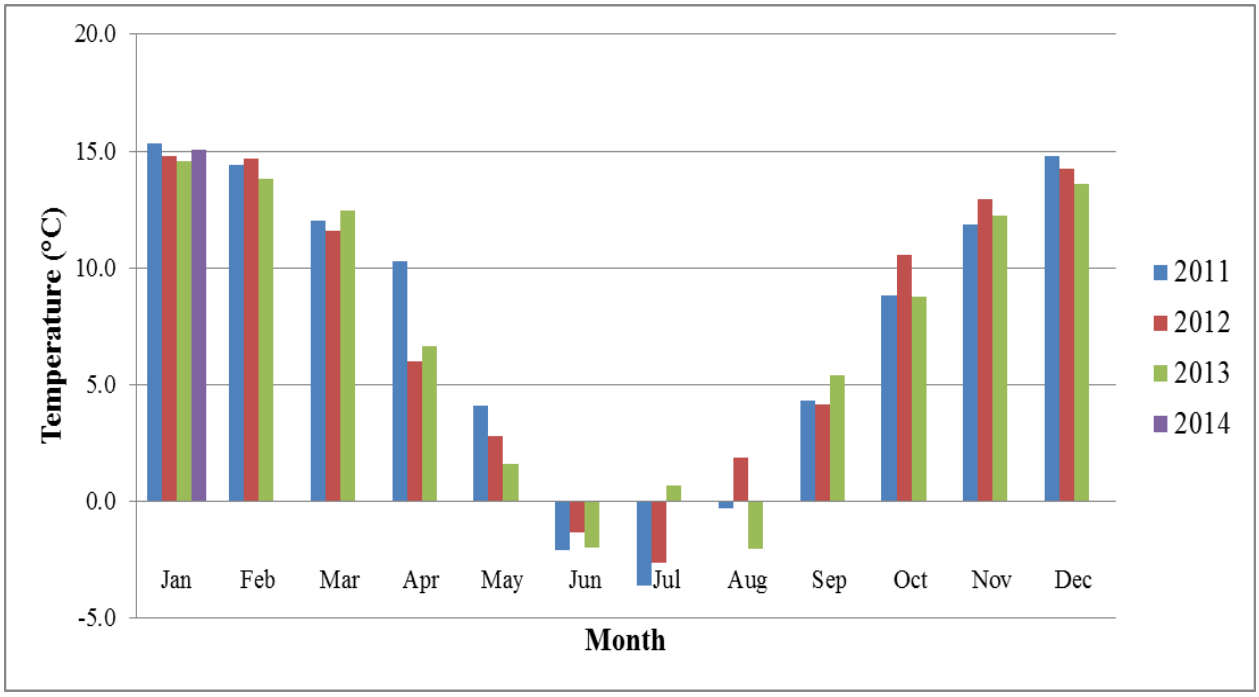

Figure 7: Average minimum monthly temperatures of the neighbouring farm. Data provided by F van Zyl, 2014 (personal communication).

Throughout the study period, the highest average precipitation occurred over the months of January, February and December, which is in accordance with the expected precipitation and weather patterns for the area, as displayed in Figure 9 (Van Zyl, 2014, personal communication).

The highest recorded precipitation occurred in January 2011 with 187.5 mm (Figure 9). Precipitation started to decrease slightly from March up to September (Figure 9) throughout the study period. In 2013, no precipitation occurred between June and September (Van Zyl, 2014, personal communication).

In December 2012, the precipitation exceeded 160 mm (Figure 9). As of the year to date, precipitation between January 2011 and December 2011 totalled 724.25 mm; between January 2012 and December 2012, precipitation totalled 628.5 mm; and between January 2013 and December 2013, precipitation totalled 439 mm [Figure 9] (Van Zyl, 2014, personal

communication). This indicates that there was a slight decrease in annual precipitation from 2011 to 2013 (Figure 9).

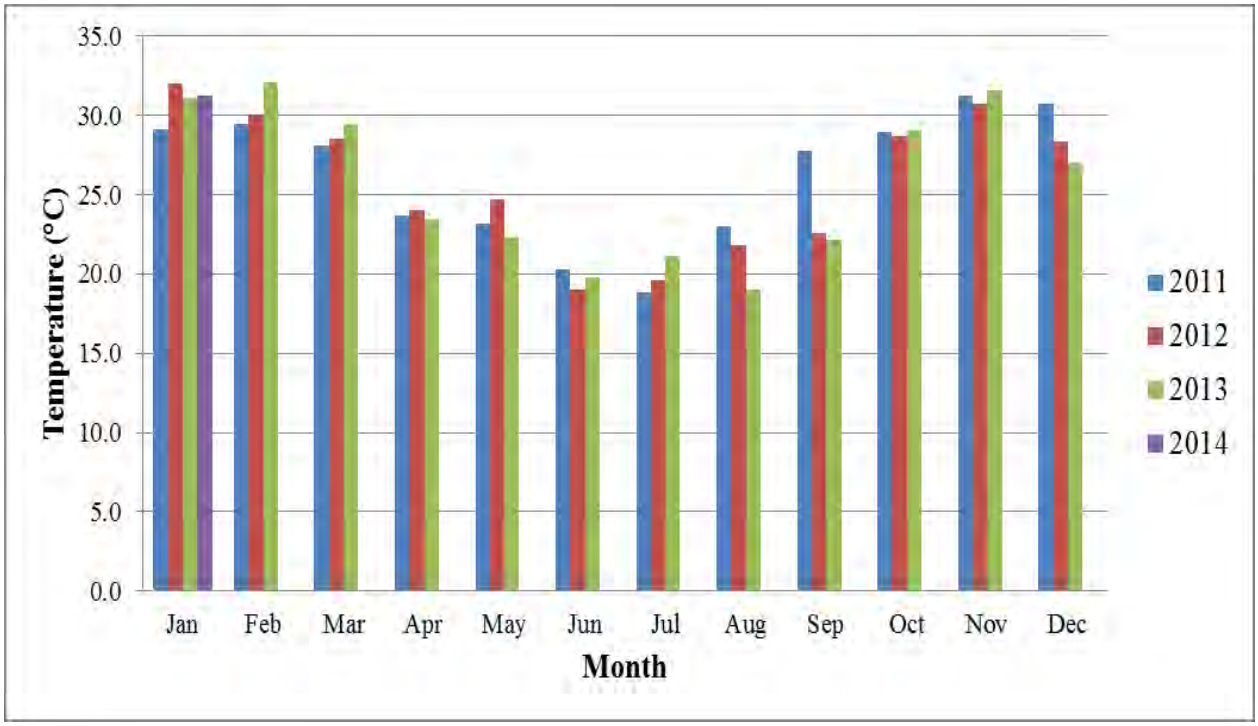

Figure 8: Average maximum monthly temperatures of the neighbouring farm. Data provided by F van Zyl, 2014 (personal communication).

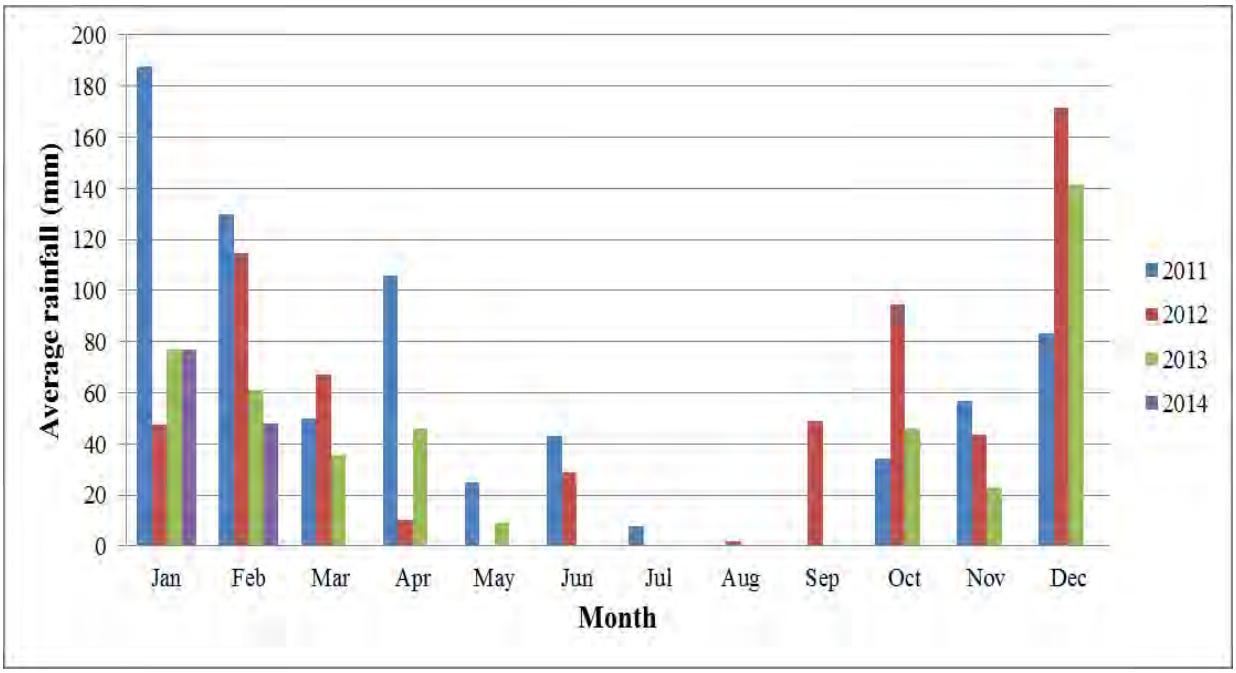

Figure 9: Average monthly precipitation of the neighbouring farm. Data provided by F van Zyl, 2014 (personal communication).

1.2.5 Vegetation

According Mucina and Rutherford (2006), the vegetation of this area belongs to the Gh 12 Vaal Reefs Dolomite Sinkhole Woodland vegetation type of the Dry Highveld Grassland unit. The woodland is the most distinctive vegetation feature occurring naturally in places of dolomite outcrops which clusters around sinkholes (Malo, 2012).

Although no sinkholes or paleo sinkholes are present in the Oaktree Formation, vegetation clusters are still found (Van Deventer and Bloem, 2007).

Natural grass species in this area include *Themeda triandra*, which is mostly unstable due to unpredictable rainfall and overgrazing; this led to the wide-scale changes in these grassland units (Haagner, 2008). Mucina and Rutherford (2006) stated that this normally results in the invasion of these areas by *Eragrostis curvula, Eragrostis plana, Cynodon dactylon, Sporobolus africanus,* and *Aristida junciformis.*

According to Tainton (1999, cited by Haagner, 2008) the exclusion of fire also caused changes in the grass species composition, and *Themeda triandra* was replaced by unpalatable, perennial grasses such as *Cymbopogon plurinoidis* and *Hyparrhenia hirta*.

The study conducted by Malo (2012) stated that the most common grass species in the study area include: *Eragrostis curvula*, *Eragrostis plana*, *Eragrostis chloromelas* and *Setaria sphacelata* var. *torta* (listed in sequence of decreased frequency).

1.2.6 Topography and Surface Draining

The overall topography of the study area is considered to be relatively flat with a very gentle slope to the south-east in the area and as calculated in Figure 4:

$$\frac{30\text{ m}}{3500\text{ m}} \quad 0.009 \text{ (topographical gradient)} \qquad \text{Eq. 1}$$

From this calculation it is clear that there is less than a 0.9% increase in slope.

The wetland south of the No. 4 and 5 TDF does not drain into the Koekemoer Spruit but rather into the shallow hole and pseudo sinkholes at the south-east corner of the No. 4 TDF.

The Koekemoer Spruit to the east of the study area flows from north to south, but does not fall within the study area. Pollution studies along the Koekemoer Spruit are currently in progress by Slabbert (2014), with the title: Surface impacts of gold mining activities on the Kromdraai/Koekemoerspruit: a situation analysis.

However, these studies on the Koekemoer Spruit focus on the pollution from other mining activities in the upper catchment area of the Koekemoer Spruit and Kromdraai Spruit.

According to the previous farm owner, the study area is categorised as a dry dolomite area which means that there is a significant deficiency of groundwater in this area (Van Deventer and Bloem, 2007).

1.3 PROBLEM STATEMENT AND SUBSTANTIATION

According to Cairns (1995), Cramer and Hobbs (2007) and Aronson *et al.* (2007) (cited by Haagner, 2008), restoring degraded landscapes that have suffered loss of efficiency through anthropogenic (man-made) or natural forces has become a primary concern for environmental sciences and management in recent decades.

Due to lack of environmental legislation and/or the enforcement thereof, very little surface rehabilitation took place on the MWS No. 5 TDF (previously known as the Chemwes No. 5 TDF) prior to 1992, a common occurrence in South Africa at the time (Haagner, 2008).

In 2000, MWS intervened and committed to the rehabilitation of the entire site, with profits generated by the reprocessing of specific TDFs for gold and uranium extraction (Haagner, 2008).

The pollution plume can be seen from the north-east corner of MWS No. 5 TDF and its general direction is to the north-east/south-west on the farm Stilfontein, as illustrated in Figure 10. During dry winter months, significant amounts of sulphate salts accumulate on the surface of the farm Stilfontein over a distance of up to 3.5 km from the TDF.

The presence of sulphate salts in association with gold TDFs is highly common, but not particularly common on dolomites. The pollution plume is not recognisable on an aerial photograph or from aerial observations, e.g. by aeroplane, but is definitely visible on a Google Earth Image taken in 2010 and 2011.

The primary purpose of this study is to determine the quantitative and aerial extent of the pollution observed on the farm Stilfontein over a period of 30 months via the monthly monitoring assessments across fixed points and quarterly interval assessments of the transect lines.

In addition, the purpose of this study also involves the identification of potential linear structure anomalies (dyke systems) associated with the polluted area (pollution plume), as well as weathered zones (fractures, joints and cavities) in the dolomites.

These zones may be associated with, or may result in, the pollution extending over the area despite its unfavourable surface topography and slope angle, as well as dip and strike of the geological formations.

These anomalies and weathered zones create pathways for groundwater to flow and it is anticipated that if present, these anomalies and weathered zones may be a primary contributing factor in the formation of the pollution plume in a north-eastern direction, which extends over the study area.

The MWS No. 5 TDF has a hydraulic pressure head of approximately 40 m, the elevation of the north-eastern corner of the TDF and FP 8 (the farthest FP from the TDF) are 1368 m and 1360 m, respectively, falling in close range of each other. It is also of the utmost importance to determine the effect of the pollution on nearby vegetation in this area via the employment of Landscape Function Analysis (LFA).

In order to investigate the pollution in the study area, the aims and objectives are set out below in paragraph 1.4.

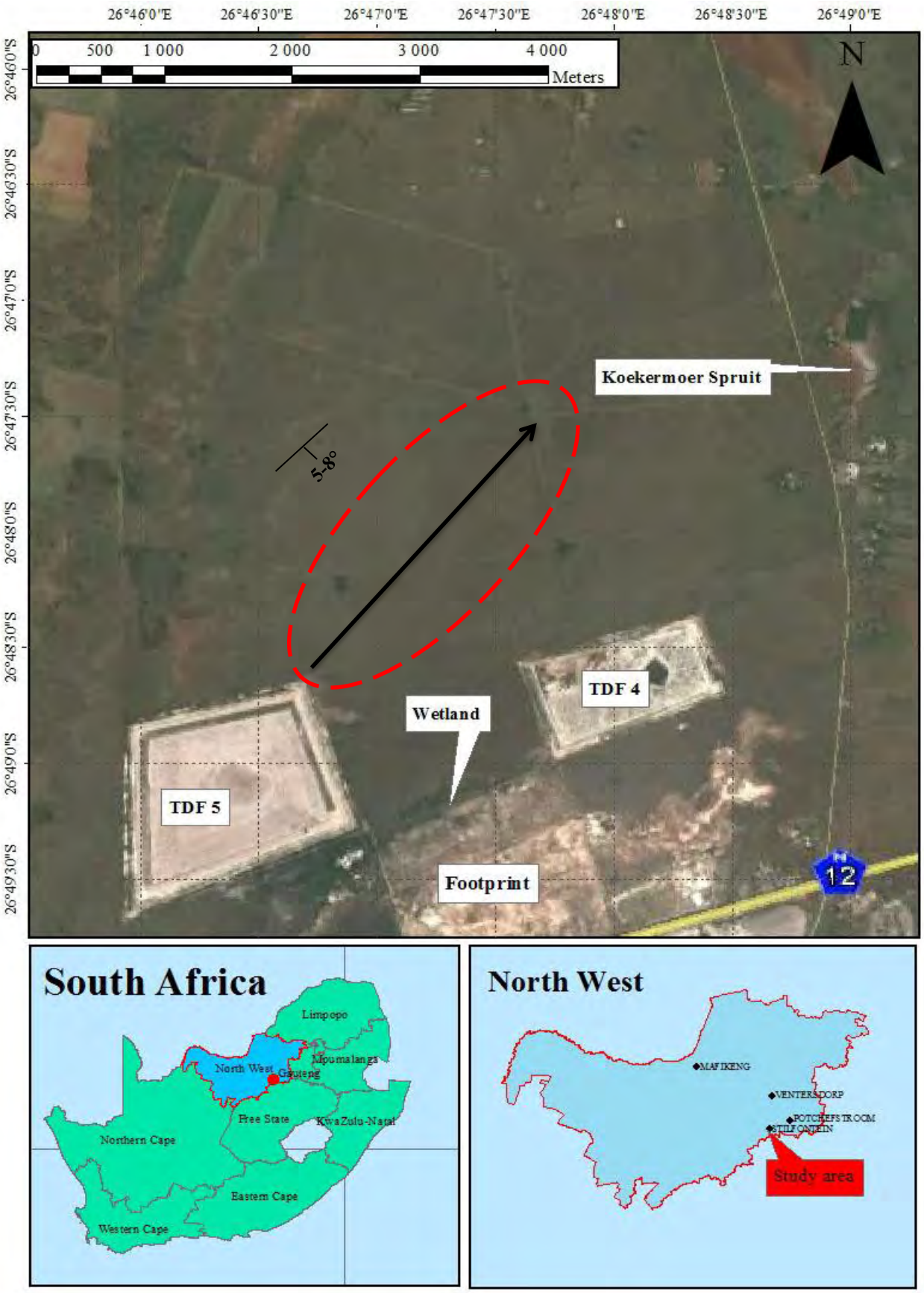

Figure 10: Map showing the pollution plume and its general direction, as well as the surface topography and dip of the geological formations (Google Earth, 2013).

1.4 RESEARCH AIMS AND OBJECTIVES

1.4.1 General Aims

The aims of this study were to monitor the extent and severity of a pollution plume observed in the study area, as well as to identify major fractures, joints, dykes and weathered zones within the dolomites which might be associated with or result in the pollution to extending over the area despite the contradictory slope angle, geology and topography of the area.

1.4.2 Objectives

To accomplish the above aims, the following project objectives were set:

1. Identify twelve fixed monitoring sites to monitor monthly: nine of these localities in areas with evidence of accumulated salts on the soil surface, and the remaining three localities in areas without accumulated salts on the soil surface in order to serve as control sites.
2. Sample these twelve sites monthly using a soil auger to produce composite soil samples on site.
3. Execute a base line soil chemical analysis of the twelve fixed monitoring sites at the beginning (August 2011) and end (January 2014) of the set period.
4. Identify three transect lines, one line with a north-south orientation and two lines with an east-west orientation over the extent of the potential pollution plume.
5. Sample these three lines over a quarterly interval.
6. Assess the electrical conductivity (EC) and pH of the soil samples collected on a monthly basis and the three transect line soil samples retrieved quarterly.
7. Conduct detailed pedochemical, particle-size distribution and mineralogical analysis on the soil from the twelve fixed monitoring sites.
8. Conduct trace metal element analysis on the samples at the beginning and end of the 30-month monitoring period.
9. Conduct trace metal element analysis on plant tissue material throughout the different sites and correlate this with soluble/available and total soil trace metal elements.

10. Conduct a detailed LFA on the 12 FPs monitoring sites at the beginning and end of the monitoring period.

11. Conduct water analyses on the monitoring boreholes twofold.

12. Conduct down-hole camera analysis on selected boreholes in the study site to identify fractures, joints or cavities.

13. Conduct a magnetic survey i.e. a magnetic assessment across the pollution plume to identify potential geological structures and pathways of the sulphates derived from the TDF.

14. Take an aerial photograph of the study area at the end of the monitoring period.

15. Create GIS maps to visually present the area of influence.

The results of this study will provide a solid basis for future research into the rehabilitation of natural environments which were subjected to pollution adjacent to mining land on dolomites.

1.5 BASIC HYPOTHESIS

The MWS No. 5 gold TDF is causing pollution on the farm Stilfontein; however the MWS No. 5 gold TDF has been inactive since April 2011 as the tailings were pumped to the new Kareerand TDF (mega dam).

It is anticipated that as the TDF material dries, the phreatic water level inside the TDF will lower; causing the pressure exerted by the hydraulic head of the TDF to lower over time, which will eventually end the pollution process on the soil.

Due to the relatively flat topography of the area and the very low runoff, it is anticipated that rainwater infiltration and percolation will leach the sulphate salts to such an extent that the pollution plume will diminish significantly.

It is also anticipated that there may be structural anomalies, e.g. dykes, in the area creating a division into different water compartments. The existence of cavities, fractures and joints in the dolomite creating pathways for the contaminated seepage water from the TDF to flow in a north-eastern direction towards the farm Stilfontein is also anticipated.

1.6 LAYOUT OF THIS DISSERTATION

Chapter 2 encompasses a literature review of the area relating to soil quality and sustainability in South Africa, and includes an overview of mining in South Africa including the mining life cycle with a particular emphasis on gold mining. Chapter 2 also discusses common environmental problems associated with mining such as acid mine drainage (AMD), also known as acid rock drainage (ARD). Groundwater chemistry is briefly discussed as well as recharge, weathering and contamination. An overview of LFA and an outline of previous studies completed on the MWS No. 5 TDF are included.

In Chapter 3, sampling and analytical materials and methods are explained. Sampling and analytical techniques are delineated and an overview as to how samples were prepared in relation to the methods discussed is given.

Chapter 4 comprises the study results and a discussion of the results relating to the soil analysis conducted.

The water monitoring results and discussion are laid out in Chapter 5.

Chapter 6 contains the geophysical work conducted in and around the study area as well as the discussion of the findings.

The vegetation analysis and LFA conducted on the site are discussed in Chapter 7.

The conclusion drawn from the study, as well as recommendations for future research in this particular study area has been included in Chapter 8.

The coordinates, supporting diffractograms and analytical data of the samples as well as calculations referred to in the text, but not directly involved in the discussions, are attached as appendices.

1.7 EXCLUSIONS

- No radiometric pollution was investigated.
- No quantitative geological structure study was done (only surface observations and down-hole photos of cavities were taken).
- Detailed groundwater studies with respect to flow, water levels and geochemistry were not conducted; only sufficient observations were made to confirm the hypothesis.

CHAPTER 2: LITERATURE REVIEW

2.1 INTRODUCTION

The focus of this chapter is to address the key issues relating to gold mine tailings pollution on adjacent landscapes and ecosystems in South Africa, along with highlighting the importance of protecting soils from pollution and degradation. This chapter also addresses certain negative aspects of gold mining and gold tailings in terms of environment pollution, referring to vectors arising from gold mining together with their immediate and long term effects, and with a particular focus applied to soil and water pollution as well as vegetation degradation.

2.2 THE IMPORTANCE OF SOIL QUALITY AND SUSTAINABILITY IN SOUTH AFRICA

According to Stenberg (2010), soil, air and water are fundamental natural resources without which life on earth would not be sustainable. One of the primary functions of soil is to serve as a medium for plant production, rendering soil and its future sustainability of pivotal concern for the longevity of life on earth (Stenberg, 2010; Huizenga, 2012).

Soil interacts closely with water and air; it serves as a filter for water, and as a medium for the degradation of waste and instantiation of gases via biological activities (Stenberg, 2010).

To protect soils which have been subject to pollution from outlying gold TDFs from further degradation, as well as to permit sustainable soil management, soil quality assessments and monitoring are of vital importance.

Soil degradation effectively occurs when there is an observed decrease in soil quality. Given the multitudinous aspects and purposes of soil, an assortment of definitions exists for soil quality, as illustrated in the literature:

Anderson and Gregorich (1984, cited by Crater *et al.,* 1997) stated that soil quality refers to "*the sustained capacity of a soil to accept, store and recycle water, nutrients and energy*". According to Gregorich and Acton (1995, cited by Crater *et al.,* 1997), soil quality can be defined as "*the soil's capacity or fitness to support crop growth without resulting in soil degradation or otherwise harming the environment*".

Larson and pierce (1991, cited by Crater *et al.,* 1997) explained soil quality as ~~"~~*the capacity of a soil to function within its ecosystem boundaries and interact positively with the environment external to that ecosystem*". Almost related to above mentioned definition, Doran *et al*. (1996, cited by Crater *et al.,* 1997) went a bit further and defined soil quality as ~~"~~*the capacity of a soil to function, within ecosystem and land use boundaries, to sustain biological productivity, maintain environmental quality, and promote plant, animal and human health*".

From these definitions it can be said that, from an environmental perspective, soil quality can be defined as a soil‘s ability to maintain or improve the soil‘s potential in the critical areas of biodiversity, water quality, nutrient cycling and biomass production, and thus to secure the health of plants, animals and ultimately humans.

Soil quality can be gauged by studying how effectively soils implement and sustain the above stated function, and is divided into two parts: inherent soil quality and dynamic soil quality.

According to Gregorich and Acton (1995), a soil‘s inherent or natural qualities are the properties that are subject to very little change, and are generally a result of how the soil has formed, such as climate, topography, parent material, biota and time.

Dynamic soil quality properties refer to the properties that are immediately affected by human management and environmental disturbances, and as such, dynamic properties are subject to more rapid change than inherent properties (Gregorich and Acton, 1995).

The measurement of how effectively a soil's inherent and dynamic properties function can be determined via the assessment of predefined soil quality indicators, which are in turn divided into three primary categories based on their effect on the soil‘s function, namely physical, chemical and biological, as shown in Table 3. Human activities, either directly or indirectly, frequently result in the degradation of soil quality.

Human-related pollutants such as overgrazing via the cultivation of livestock, contamination due to industrialization such as water leaching from landfills and mine waste dumps, and the destruction of natural vegetation via a multitude of vectors that ultimately results in increased soil erosion, are but a few of the soil degrading contributors within a vast catalogue (Huizenga, 2012).

Various delivery mechanisms exist for soil pollutants, such as: mobility through solution in soil water, volatilization in the soil and dust pollution (Huizenga, 2012). In order to maintain a soil‘s

quality, monitoring of the soil is often necessary on a regular basis to confirm whether the soil is degrading, and the rate of its degradation.

Monitoring is also required in order to establish the cause of degradation and to determine any potential mitigating measures which may be taken in consideration in order to prevent further degradation and land use losses.

Table 3: Summary of the three soil indicators utilised to asses soil function (Kinyangi, 2007).

Indicators	**Soil functions**
Physical: soil depth, available water capacity, soil aggregate stability, infiltration, bulk density, soil structure and texture etc.	Retention and transport of water and nutrients; a habitat for macro and micro fauna and flora (Bengtsson, 1998; Swift *et al*., 2004), potential for compaction and to support plant growth.
Chemical: pH, extractable soil nutrients, N-P-K, base cations, EC, toxic compounds, sodicity.	Soil biological and chemical thresholds; plant available nutrients and potential for N and P as well as loss of base cations (Doran and Jones, 1996; Drinkwater *et al.,* 1996). The salinity of the soil and pollution is also responsible for physical stability (dispersion)
Biological: microbial biomass, C, N; potentially mineralizable, and soil organic matter (SOM).	Microbial catalytic potential and depository for C and N; soil productivity and N-supplying potential of the soil (Doran *et al.,* 1996; Cadisch and Giller, 1997). Soil organic matter (SOM) assist in soil structure, stability of the soil, nutrient and water retention, water infiltration and soil erosion reduction (Carter, 2002).

Most of the soils in South Africa affected by pollution often require rehabilitation in order to restore the land to its original use or to redefine its previous land use in a manner which conforms to the precepts of sustainable land management (SLM).

To successfully and sustainably manage land within a given situation over a specific period of time, a framework for evaluating sustainable land management (FESLM) was developed by an International Work Group (IWG) which defined it as follows (Smyth and Dumansky, 1993):

"Sustainable land management combines technologies, policies and activities aimed at integrating socio-economic principles with environmental concerns so as to simultaneously address:

- *Productivity: maintain/enhance production requirements of the land.*
- *Security: the reduction of potential risk affecting the land's productivity.*
- *Protection: this involves the protection of natural resources and the prevention of soil and water degradation.*
- *Viability: the potential for the land to be economically viable.*
- *Acceptability: the acceptability of the development and use of the land in question".*
- And in order to make a success of the FESLM, management of the land is much needed (manageability).

With these six aspects, there are other factors to consider in order for FESLM to work, such as soil quality indicators and soil functions (Table 3). Figure 11 illustrates the interaction between sustainable land management (SLM), soil quality indicators and soil functions, and how they go hand in hand with the six aspects of the FESLM.

Table 4 summarizes how these six aspects, soil quality indicators and soil functions work together and interact with each other.

These factors and indicators should be carefully monitored on a regular basis in order for the FESLM framework to be implemented successfully.

For example, if the EC of a soil is high, the osmotic potential of the soil is low, which results in the uptake of toxic ions and may reduce the uptake of essential plant nutrients, disrupting the nutrient cycle and soil organic matter (SOM) of the soil.

This in turn leads to a decrease in plant material, productivity, security, protection, viability, acceptability and consequently the land becomes harder to manage.

These quality indicators can be used to explain the encroachment of *Seriphium plumosum* (*Afr*. Bankrotbos) as detailed in this study, given the increase of the soil EC resulting in a negative osmotic effect in the soil and therefore providing an environment in which *S. plumosum* thrives (due to its high tolerance for large amounts of salts).

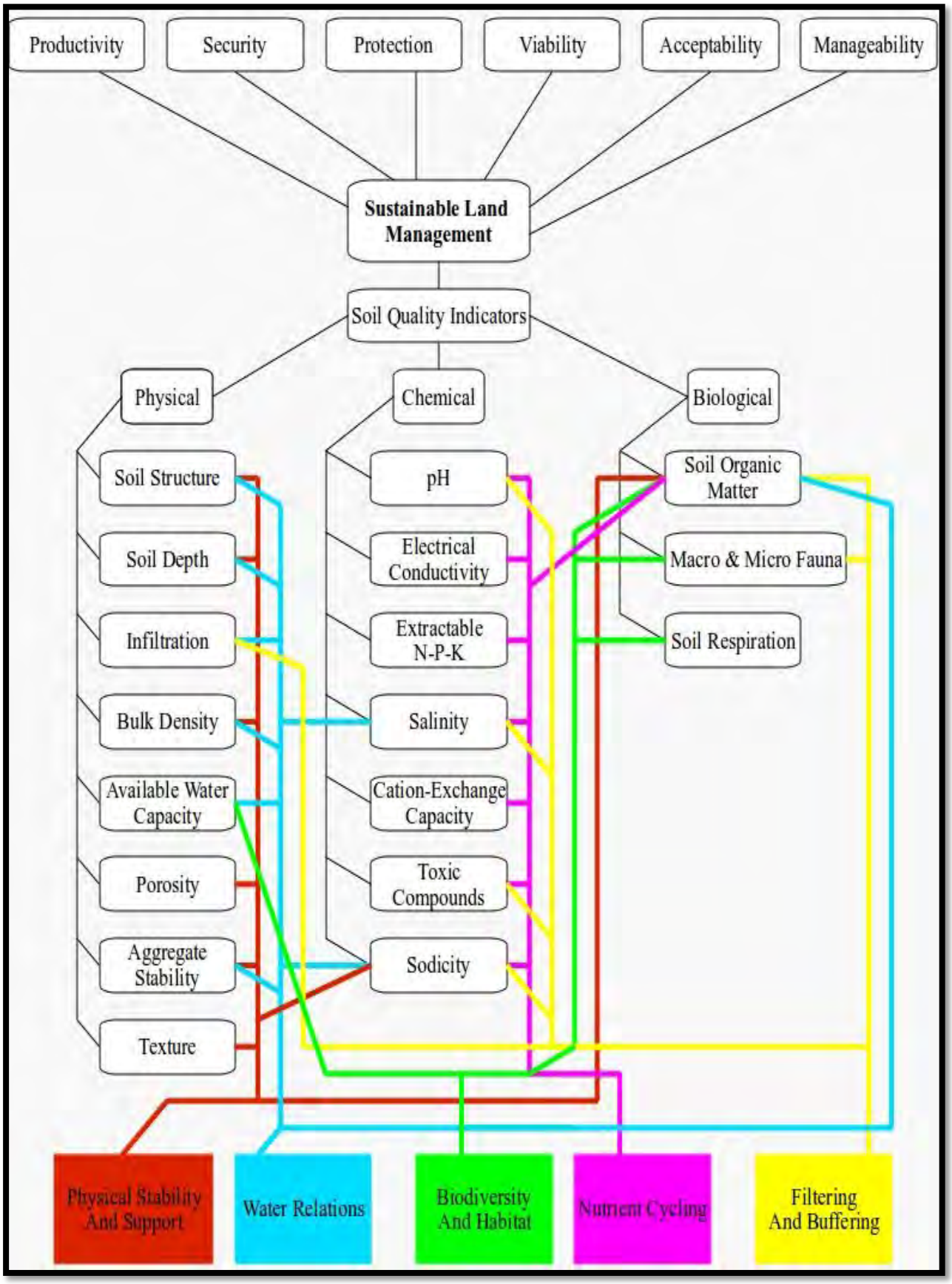

Figure 11: Interaction diagram between sustainable land management (SLM), soil quality indicators and soil functions.

Table 4: Summary of the interaction between the framework for evaluating sustainable land management (FESLM), the three soil quality indicators and soil functions.

	Physical stability and support	**Water relations**	**Biodiversity and habitat**	**Nutrient cycling**	**Filtering and buffering**
Physical	Soil- structure, texture, depth, bulk density, infiltration, available water capacity, aggregate stability and porosity	Soil- structure, depth, bulk density, infiltration, available water capacity and aggregate stability	Available water capacity	X	Infiltration
Chemical	Sodicity	Salinity and sodicity	X	pH, EC, CEC salinity, sodicity, toxic compounds and extractable N-P-K	pH, salinity, sodicity and toxic compounds
Biological	SOM	SOM	SOM, macro and micro fauna and flora and soil respiration	SOM	SOM and macro and micro fauna and flora
FESLM	Productivity, security and protection	Productivity, security, viability and protection	Productivity, security, viability, acceptability and protection	Productivity, security, viability, protection and acceptability	Productivity, security, viability and acceptability

2.3 MINING IN SOUTH AFRICA AND THE ENVIRONMENT

According to Fairbanks *et al*. (2000) and the DEAT (2006), approximately 200 000 ha of South Africa‘s land surface is directly affected by mining, with this figure increasing due to many new leases granted each year (Haagner, 2008). Tailings disposal facilities and waste rock dumps cover nearly 47 000 ha in South Africa alone (DEAT, 2006).

Mining changes land topography, results in pollution, destroys natural habitats and the aesthetic value of land, depletes surface and groundwater resources, and degrades soils (DEAT, 2006). However, the mining sector in South Africa plays a vital role in social and economic development, with gold mining specifically making a large contribution to South Africa‘s mineral exports (holistically). Nevertheless, thousands of hectares of terrestrial ecosystems are affected by mining in South Africa (Milton, 2001).

In the North-West Province alone, the mining sector contributes to the provincial economy, creating 42% of the Gross Geographic Product (GGP), which is an indicator of the overall contribution of an individual province's economy towards the Gross Domestic Product [GDP] (NWDACE, 2002) The North-West province's gold mines deliver 25% of the national production and employ 39% of the province's active labour force (NWDACE, 2002).

South Africa lays claim to 40% of the world‘s gold reserves, and contributes to a large percentage of the global gold supply (Stilwell *et al.,* 2000; Mabuza 2006; IBP, USA Staff, 2013). On a national scale, the South African mining industry was responsible for contributing between 22.5% and 9% to the country‘s GDP from 1980 up to 1990, and continues to contribute between 6.5% and 9% to the country‘s GDP since 1990 (Mabuza, 2006).

The South African gold mining sector, specifically, is directly responsible for the employment of approximately 150 000 people, contributing towards roughly 36% of the total employment provided by the South African mining industry (Mabuza, 2006).

Although South Africa is not at the top of the list of gold producers, the legacy of the old mining sites remains a reality. In terms of sustainable development from both social and environmental perspectives, the South African gold mining industry has in recent years begun to embrace social and environmental management programs in an effort to reduce their impact on surrounding communities and ecologies, with a view towards enhanced compliance with current legislation (Möhr-Swart *et al.,* 2008).

The South African mining industry, and the gold sector in particular, has also played a role in contributing towards research and development within both closely related and indirect fields, resulting in cleaner mining and rehabilitative initiatives, such as the development and implementation of sustainable environmental frameworks (Mabuza, 2006; Möhr-Swart *et al.,* 2008).

There is an underlying negative perception of the gold mining industry on a national level. Often, the gold mining industry is portrayed as both economically and environmentally irresponsible, especially when considering the severe socio-economic challenges it is currently faced with. However a paradigm shift towards both economically and environmentally sound practices within the gold mining industry and the South African mining industry holistically, cannot be denied.

2.3.1 The Mine Life Cycle System

Most mines will remain active for an average of 25 years (Weaver and Caldwell, 1999); however exceptions can occur where mines will close prematurely or extend well beyond the average age, such as with the Stilfontein Gold Mines which were active for 40 years as previously stated in Chapter 1.

The mine life cycle consists of all the activities involved in the mining process, from the prospecting and exploration phase to the post-closure phase [Figure 12] (DWAF, 2008b). The environmental impact of the mine life cycle will differ according to the particular phase within the cycle, the type of mining taking place, the specific mineral being extracted and the waste materials produced, as well as environmental factors and attributes such as climate, soils, groundwater, topography and geology.

It is necessary to incorporate sound environmental management practices throughout each of the phases within the mine life cycle in order to reduce the environmental impact of each of the relevant mine life cycle stages, as illustrated in Figure 12 (Weaver and Caldwell, 1999; Van Zyl, 2008; Van Deventer and Hattingh, 2009; Van Deventer *et al.,* 2009).

During the prospecting and exploration phase of the mine life cycle, a pre-site assessment should be conducted in order to identify the potential for ARD, seepage, release of toxic trace metal elements and other possible pollutant factors. The planning of potential waste management and

disposal facilities, such as probable locations for TDFs, should also be considered during the pre-site assessment (Marais *et al.,* 2006; Van Zyl, 2008).

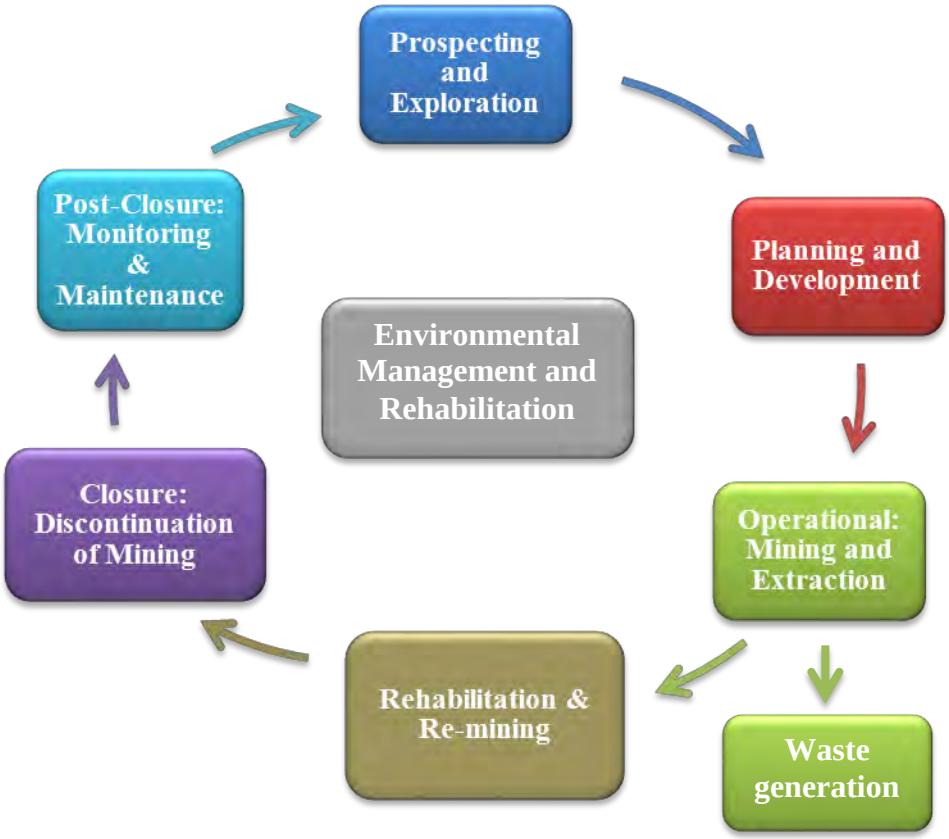

Figure 12: The Mine Life Cycle. Modified from Möhr-Swart *et al.* (2008); Van Zyl (2008); Van Deventer and Hattingh (2009).

As part of the planning and development phase of the mine life cycle, it is important to complete a detailed waste management assessment. The assessment should establish an optimal location for the TDF and evaluate waste disposal options (DWAF, 2008a).

The waste management design should be completed during this phase and the construction of waste management infrastructure should be initiated. Within the planning and development phase, rehabilitation considerations need to be made, such as the ideal method of rehabilitation, for example: rock cladding, vegetation, rock armory or a combination of these methods. Mine closure planning should also be considered and pre-existing closure plans updated (DWAF, 2007; DWAF, 2008a; Van Zyl, 2008).

Throughout the operational phase of the mine life cycle, waste facility performance evaluations should be conducted periodically. The mine closure plan should at this point be reflective of the

desired end land use objectives. Rehabilitation during the operational phase is a continual process in order to mitigate potential environmental and financial risks, with rehabilitation methods optimized to conform to waste characterization (Marais *et al.,* 2006; DWAF, 2008a; Van Zyl, 2008; Van Deventer and Hattingh, 2009).

The rehabilitation phase can be considered an appraisal of the total rehabilitative efforts conducted during the operational phase, and the evaluation and implementation of any additional rehabilitation measures prior to the initiation of the mine closure phase, with a view to ensure alignment with the expected outcomes outlined for the end land use (DWAF, 2008b; Van Deventer and Hattingh, 2009).

Upon conclusion of the operational phase, the closure phase of the mine life cycle is initiated. The closure phase encompasses the implementation of the measures required to minimize residual environmental impact, enhance aesthetic value, mitigate any potential safety or health hazards, and the qualification of rehabilitation measures in order to ensure compliance with FESLM and environmental legislature (DWAF, 2008b; Van Deventer and Hattingh, 2009).

The post-closure phase of the mine life cycle involves the continual monitoring of the rehabilitation measures implemented, and the execution of any required maintenance to ensure that the integrity and performance of the rehabilitation method remains aligned with the end land use objectives (Van Deventer and Hattingh, 2009).

2.3.2 Gold Mining and Tailings Material

2.3.2.1 Gold Recovery

The gold recovery process has certain environmental implications and potential consequences, the extent of which can be correlated with the manner of the extraction process and the mechanisms employed during separation (Naicker *et al.,* 2003; INAP, 2009; McCarthy, 2011; Huizenga, 2012; Sabah and Fouzul, 2012).

A common modern recovery technique involves the use of cyanide salts (cyanidation), which is effective due to gold‘s propensity to form strong complexes with certain soft ligands (Pinkney, 1956; Naicker *et al.,* 2003; Blom, 2011). In the presence of a cyanide salt such as KCN, gold will oxidize over time to form the soluble complex $K_2Au(CN)_4$ which is subsequently leached from the ore into a recoverable concentrate. The use of cyanide salts in the gold recovery process can

pose significant environmental risks, not only due to the high toxicity of the cyanide but also due to the potential for cyanide to form soluble complexes with other toxic metal elements which may be present in the ore. The toxic metal elements can include: zinc [Zn], copper [Cu], cadmium [Cd] and arsenic [As] (Naicker *et al.,* 2003; INAP, 2009; Blom, 2011; McCarthy, 2011; Huizenga, 2012; Sabah and Fouzul, 2012).

2.3.2.2 Gold Tailings Material

Tailings material can generally be defined as the waste output of mining activities, commonly from mineral processing or beneficiation (Bell, 1999; Van Deventer, 2011a). The physical and chemical characteristics of tailings materials will be directly influenced by the mineralogy and geochemical composition of the treated material, the processing techniques used, the particle size of the crushed ore and the nature of process chemicals employed (Naicker *et al.,* 2003; Lottermoser, 2010; Van Deventer *et al.,* 2009).

Gold tailings material mineralogy is predominantly quartz (70 – 90%); it contains approximately 3% pyrite and lesser oxide minerals such as uraninite (UO_2), brannerite ($UO_3Ti_2O_4$) and chromite ($FeCr_2O_4$), as well as a multitude of other sulphide minerals which include arsenopyrite (FeAsS), galena (PbS), gersdorffite (NiAsS), pyrrhotite (FeS) and cobaltite [CoAsS] (Naicker *et al.,* 2003; McCarthy and Rubidge, 2005; Blom, 2011; Ratlhogo, 2011; Sabah and Fouzul, 2012).

Gold tailings material will commonly consist of a platy structure and under certain conditions, may be predisposed to compaction and crusting, which can result in low infiltration rates (Van Deventer, 2012, personal communication).

2.3.3 The Negative Impacts of Gold Mining and Tailings Disposal Facilities (TDFs) in South Africa

The oxidation of pyrite (FeS_2) across the outer layers of gold tailings materials can yield significantly increased acidity to the extent where toxic and potentially radioactive metal elements are mobilized. Gold tailings materials also possess a variety of potentially impactful properties, such as high salinity and sodicity (dispersion) due to the presence of free salts, and the potential for dust pollution due to fine particle size. A detailed description of the potential pollutant types derived from gold tailings materials is provided below (McCarthy, 2011; Sabah and Fouzul, 2012).

2.3.3.1 Acid Mine Drainage (AMD)

Acid mine drainage is the result of a reaction that occurs between three primary reactants, namely water, oxygen and a sulphur-bearing mineral such as pyrite (FeS_2), to produce sulphuric acid (Gagliano and Brigham, 2006; Sabah and Fouzul, 2012). Pyrite minerals can be found in mine waste or rock (Bell and Donnelly, 2006). These wastes and rock are usually associated with coal and metal mining, such as gold (Bell, 1999; McCarthy, 2011).

The pH which usually accompanies AMD varies between 2 and 4, yet pH values as lower as 2 have been reported (Gagliano and Brigham, 2006; Van Deventer *et al.,* 2009). Neutral pH values associated with AMD are uncommon, with the exception of instances where underlying geology consists of carbonate rocks (Gagliano and Brigham, 2006) such as limestone ($CaCO_3$) or dolomite ($CaMg[CO_3\ _2$), the latter being the case in this particular study (Marais *et al.,* 2006; Van Deventer, 2011a; Van Deventer, 2011b).

- **Chemistry of Acid Mine Drainage**

Gagliano and Brigham (2006) summarize the complete reaction that takes place during the formation of acid as follows:

$$4FeS_2 \quad 14H_2O \quad 15O_2 \quad 4F \quad e(OH)_3 \quad 8H_2SO_4 \qquad \text{Eq. 2}$$

The fact of the matter is that the reaction taking place is far more complicated than this, and can thus be described as a two-stage process, where the pyrite first oxidizes to produce sulphuric acid and ferrous sulphate and oxidizes again to produce orange-red ferric hydroxide and more sulphuric acid (Van Deventer *et al.,* 2008; McCarthy, 2011), which can be illustrated by the following two reactions respectively (Gagliano and Brigham, 2006) [Eq. 3 and Eq. 4]:

$$2FeS_2 \quad 2H_2O \quad 7O_2 \quad 2F \quad e \quad 4(SO_4^2\ ) \quad 4H \qquad \text{Eq. 3}$$

$$4Fe^2 \quad O_2 \quad 4H \quad 4 \quad Fe^3 \quad 2H_2O \qquad \text{Eq. 4}$$

Reaction 2 (Eq. 4) takes place rapidly in the presence of oxygen at pH > 3. Microbes of the *Acidithiobacillus* genus assist the oxidation of ferrous iron (Fe^2) to ferric iron (Fe^3) in reaction 2 (Eq. 4) at pH < 3 (Gagliano and Brigham, 2006).

The ferric iron produced in reaction 2 now acts as an oxidant, thus promoting further pyrite oxidation or a hydrolysis reaction to produce goethite ($Fe(OH)_3$), and releases alternative acid protons (Eq. 5).

$$14Fe^{3} \quad FeS_2 \quad 8H_2O \quad 15 \quad Fe^{2} \quad 2(SO_4^{2}) \quad 16H \qquad \text{Eq. 5}$$

When the pyrite is oxidized by the ferric iron, the reaction takes place considerably faster and produces far more acid protons than the reaction with oxygen as illustrated by reaction 4 (Eq. 6).

$$Fe^{3} \quad 3H_2O \quad F \quad e(OH)_3 \quad 3H \qquad \text{Eq. 6}$$

Goethite is not the only mineral that precipitates; instead, the mineralogy depends on certain parameters such as pH values, and the metal and sulphur concentrations present. The other most common minerals include: ferrihydrite $[Fe_5(OH)_8.4H_2O$, schwertmannite $[Fe_8O_8(OH)_6SO_4$ and jarosite $[(H,K,Na)Fe_3(OH)_6(SO_4)_2$ (Gagliano and Brigham, 2006). Goethite will be produced over a wide range of pH values and is rather stable, whereas ferrihydrite is more commonly produced at pH > 6.5.

Schwertmannite can be found where pH values vary between 2.8 and 4.5, and where the sulphur concentration is moderate to high. Jarosite will be found in only the most extreme conditions where pH values are < 3, very high concentrations of sulphur exist and adequate amounts of K and Na are present (Gagliano and Brigham, 2006).

- **The Movement of Acid Mine Drainage in the Environment**

The movement of AMD in the environment mostly depends on the sources, pathways, and receptors involved (DWAF, 2007; Van Deventer *et al.,* 2008; INAP, 2009; Rashed, 2010). The source, pathway and end environment varies by product, soils, climate, the mine facility itself and the mine phase (DWAF, 2007; Van Deventer *et al.,* 2008; INAP, 2009; Rashed, 2010; Slabbert, 2014). Figure 13 summarizes the movement of AMD.

The sources contain reactive sulphide and potentially neutralizing minerals involved in the alleviation of acidity, and vary in commodity and ore-deposit type, type of mining, and waste-disposal strategy (DWAF, 2007; INAP, 2009; McCarthy, 2011; Sabah and Fouzul, 2012).

Variables that will tend to impact pathways and transport mechanisms may relate to the nature of the hydraulic processes specific to the mine or waste facility, which will influence the contact time between solid and solution (such as rapid preferential flow vs. a gradual matrix flow) or potentially, the ratio of flushed mine waste (DWAF, 2007; INAP, 2009).

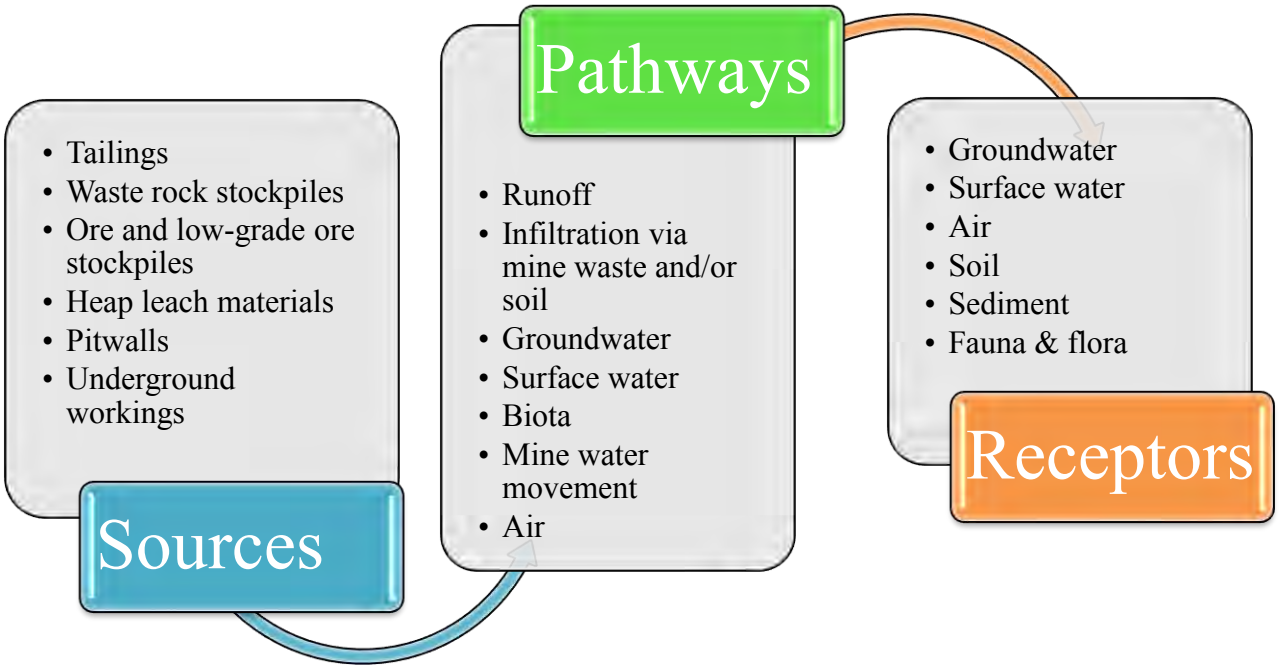

Figure 13: Acid mine drainage sources, pathways and receptors diagram. Modified from INAP (2009).

The climate and seasonal temperament of the area and its surrounds also has bearing on the mechanisms involved in drainage, given the effect it exacts on mine discharge in terms of concentration ratio and the rate of discharge (INAP, 2009).

Mine drainage will also be influenced by the traits of the receiving environment. Physical mixing, as well as chemical and biological reactions with the receptors have the potential to modify the mine discharge from its basic characteristics (DWAF, 2007; INAP, 2009; Sabah and Fouzul, 2012).

- **Acid Mine Drainage and the Environment**

AMD causes water pollution of surface and groundwater resources (DWAF, 2007; DWAF, 2008a; DWAF, 2008b) and can, if not controlled, lead to high levels of toxic trace metal elements (Sabah and Fouzul, 2012), salinity and sulphate within water, which will lead to the

deterioration of water quality, ultimately affecting the fauna and flora of the aquatic environment (Bell, 1999; DWAF, 2007; DWAF, 2008a; DWAF, 2008b; Van Deventer *et al.,* 2008; McCarthy, 2011; Sabah and Fouzul, 2012).

The impact of AMD is generally hard to predict due to the fact that discharge is often hard to quantify, and its composition can fluctuate seasonally (Gray, 1997; DWAF, 2007; DWAF, 2008a; DWAF, 2008b).

The effects of AMD can be categorized as physical, chemical, biological and ecological, for example elimination of species, abridging the food chains, and reduction in ecological stability of lotic systems, as shown in Figure 14 (Gray, 1997; Van Deventer *et al.,* 2008; McCarthy, 2011; Malo, 2012; Sabah and Fouzul, 2012).

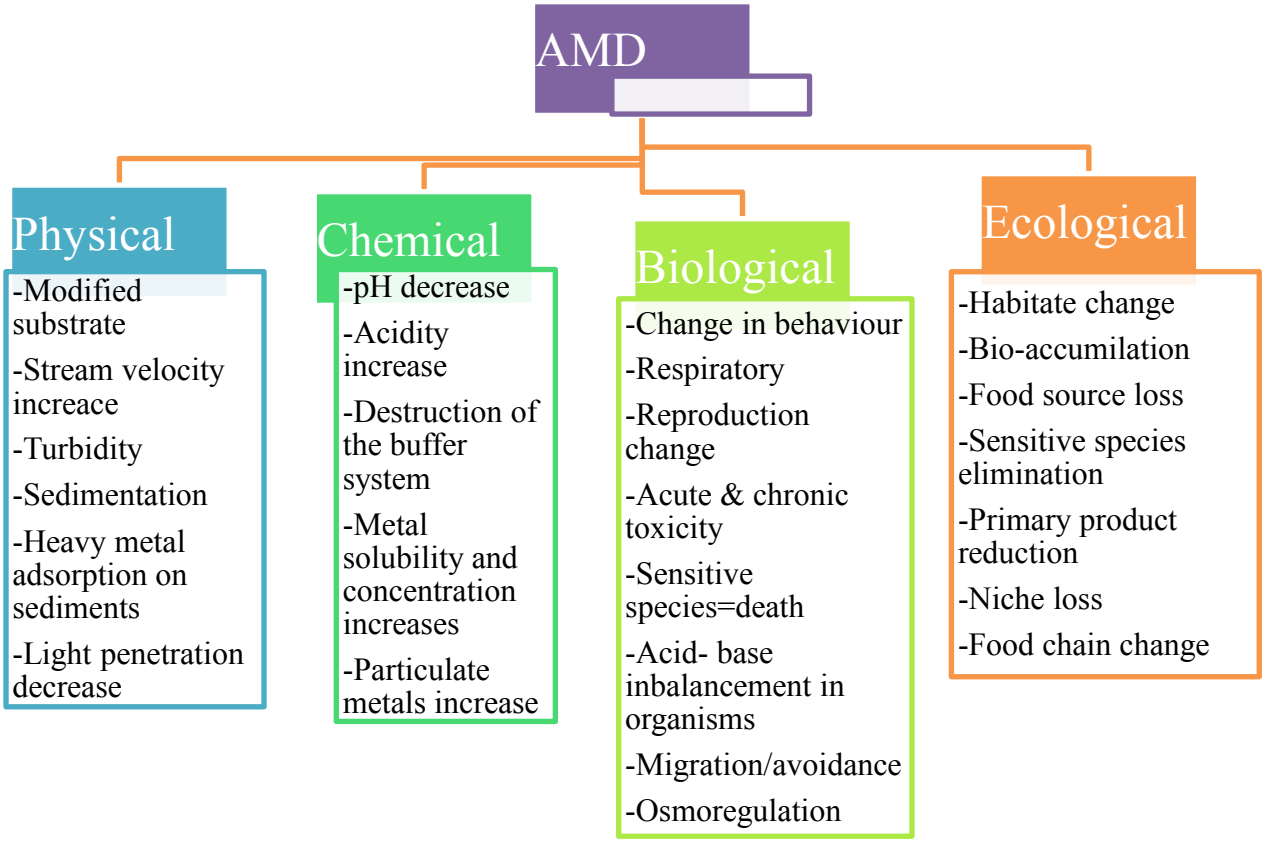

Figure 14: Acid mine drainage (AMD) effects on water systems diagram. Modified from Gray (1997).

2.3.3.2 Salinisation and Sodification

Soil salinity and sodicity are among the oldest soil pollution issues recognized (Van Deventer, 2011b). Accumulated salts can be present within moist soils via dissolution or as crystals within dry soil. Salinisation and sodification are two major factors that can potentially influence the water quality and residues on soil within a specific area.

According to Van Deventer (2011c) the ideal EC value for soils in South Africa should not exceed 360-400 mS/m. Should the EC be in excess of these levels, the presence of soluble salts and ions such as Cl^-, SO_4^{2-}, HCO_3^-, Na , Ca^2 , Mg^2 , NO_3^- and K may damage vegetation by reducing the osmotic potential, and may result in water deficiencies. High salinity and sodicity in the soil can also contribute to the decrease in water quality and increase the solubilisation of trace metal elements which can further have hostile effects on plant growth (Seiderer, 2011).

During handling, transportation and storage of gold TDF material, water evaporates and salt previously held in solution precipitates on the soil surface to form salt crusts (Haagner, 2008). This process results in the reduction of soil friability, soil structural integrity, and water and nutrient uptake by plants by increasing osmotic potential (Zhu, 2001; Malo, 2012), as well as changing the natural biotic communities.

Van Deventer (2011b) stated that the effects of salinity and sodicity on plant growth also may include:

- Direct toxicities such as of sodium.
- Deficiencies of micro-nutrients due to high pH conditions when carbonated species are dominant.

Naicker *et al.* (2003), Haagner (2008), McCarthy (2011) and Van Deventer (2011b) stated that these salts are highly mobile and can cause pollution far away from the mining and dump sites.

2.3.3.3 Toxic Trace Metal Elements

Trace metal element pollution, in which toxic metal element contaminants originate primarily from ore processing, tailings disposal and waste water, pose a significant and persistent threat to nearby ecosystems, habitats and ultimately surrounding communities (Ratlhogo, 2011; Sabah and Fouzul, 2012).

Trace metal element pollution arising from mining activities is of particular concern as toxic metal elements do not biodegrade over time, but accrue in sediments, soils and water resources via multiple pathways such as parent rock inheritance, waterways and atmosphere-borne emission deposits such as dust (Blom, 2011; Sabah and Fouzul, 2012; Koch, 2013; Slabbert, 2014).

Trace metal element pollution from gold tailings is considered a major contributing factor in vegetative stress across surrounding ecosystems due to metals such as As, which suppresses plant metabolic processes, and Cu, which impedes natural photosynthetic processes within plants (Sabah and Fouzul, 2012).

Trace metal element mobility within soil and tailings arising from the presence of toxic metal elements such as As, manganese [Mn], selenium [Se], Cd, Cu, cobalt [Co], Zn, nickel [Ni], lead [Pb] and uranium [U] are directly affected by multiple soil and tailings properties and processes (Herselman, 2007; Sabah and Fouzul, 2012). Trace metal element solubility is impacted by soil and tailings pH levels since solubility tends to increase as pH levels decrease (Herselman, 2007; Sabah and Fouzul, 2012).

Soil organic matter will affect trace metal element availability due to its propensity to adsorb metal cations and its negative charges resulting from the dissociation of organic acids (Herselman, 2007). This effect has no bearing on tailings materials due to its non-existent organic matter content.

Herselman (2007) stated that in soil specifically, clay particle content will also play a role in the reduction of toxic metal element availability due to the negative charge of clay particles leading to a high tendency for trace metal element adsorption.

Although tailings material particle sizes resemble those of clay particle sizes (> 0.002 mm), the capacity for trace element adsorption within tailings material particles is nullified, given that tailings material particles have no charge whatsoever.

Cation exchange capacity also influences trace metal element mobility as compositional changes may result in increased trace metal element availability due to ion exchange (Herselman, 2007).

2.3.3.4 Dust Pollution

According to Haagner (2008) and Sabah and Fouzul (2012), dust pollution is one of the most obvious environmental contaminations from gold mines and tailings material due to the fine-grained material which is easily airborne during windy conditions.

Dust accumulation from gold TDFs can be a severe health concern for surrounding communities and occurs more frequently and at higher volumes in the late, dry winter and early summer months when the TDF is dry and not covered by vegetation (Van Deventer *et al.,* 2009; Sabah and Fouzul, 2012). Dust may contain harmful particles and can be transported for kilometers.

2.3.3.5 Radiation and Radioactivity

Uranium is a naturally occurring radioactive material with an abundance of 2.7 g/t in the earth‘s crust (Wendel, 1998; Koch, 2013). It is commonly found within the Witwatersrand gold reefs as uranium oxides; in lower concentrations which are deemed not feasible for extraction, it will remain present in waste rock and tailings material, posing a significant threat to human health and the environment given its radioactive properties and equally toxic decay products (Van Deventer and Hattingh, 2009; Koch, 2013).

These uranium oxides are generally insoluble but uranyl (UO_2^2) has a high potential for solubility, and uranyl compounds can cause high concentrations of soluble uranium to occur in mine tailings and mine waters (Wendel, 1998; Koch, 2013).

2.4 GROUNDWATER CHEMISTRY

In general, the natural influence of groundwater chemistry is directly and indirectly affected by the weathering of minerals in parent rock – water relations, anthropogenic activities and biogeochemical processes (Appelo and Postma, 1994; Dennis *et al.,* 2008; INAP, 2009).

Appelo and Postma (1994) stated that groundwater composition changes through reactions with the environment and also may reveal information about the environment through which the water has flowed. Groundwater chemistry can also provide vital information due to the fact that chemical reactions are time and space-dependent (Appelo and Postma, 1994).

In South Africa, industries such as mining play a major role in the economy and have a negative effect on groundwater quality (Dennis *et al.,* 2008; Van Deventer *et al.,* 2009). The factors of importance in this study are further discussed below.

2.4.1 Groundwater Recharge

Groundwater recharge refers to the process whereby water infiltrates pores and fractures in the soil and rocks to reach the water table (Gotkowitz, 2010). Groundwater recharge can occur naturally as the net gain from precipitation or runoff, or artificially by injecting water into an aquifer through wells (Spangenberg, 2000; Knödel *et al.,* 2007).

Direct runoff into a collecting pond with a permeable bottom is another form of recharge (Lloyd, 1986; Knödel *et al.,* 2007). The recharge area or zone can be defined as the area where recharge occurs. Areas of several sizes are involved.

The recharge area is specifically vulnerable to any pollutants that may be present in the water (Spangenberg, 2000; Knödel *et al.,* 2007). Important factors that affect recharge include type of land cover, soil type, vegetation, and rainfall timing and intensity (Spangenberg, 2000). For example, infiltration rates are higher in sandy soil than in clayey soils or asphalt.

Based on the source of water and the pathway the water takes to enter the saturated zone, direct and indirect recharge can be classified as the two principal types of recharge (Simmers, 1998; Knödel *et al.,* 2007).

Lloyd (1986) and Simmers (1997, 1998) defined direct recharge as water added to the groundwater reservoir by direct infiltration of precipitation through the unsaturated zone. The main processes of groundwater recharge include infiltration and soil water seepage (Simmers, 1998). Direct recharge is also referred to as diffuse recharge which occurs over large areas, such as a watershed (Knödel *et al.,* 2007).

The amount of water that infiltrates depends on climate, vegetation cover, the slope of the surface, soil composition, depth of the water table and the presence or absence of confining beds, while groundwater recharge depends on vegetation cover and is promoted by flat topography, permeable soil, a deep water table and the absence of confining beds (Simmers, 1998; Knödel *et al.,* 2007).

According to Simmers (1998) and Knödel *et al.* (2007), indirect recharge occurs from natural depressions, ponds, channels and losing streams (influent streams), dry lakes, dry stream beds or by interflow, vertical leakage across aquitards and underflow from adjacent aquifers. Losing streams, dry stream beds and ponds play an important role in indirect recharge in arid and semi-arid areas (Knödel *et al.,* 2007).

Mountain front recharge takes place as unsaturated and saturated flow in fractured rocks and as infiltration along channels flowing across alluvial fans (Stephens, 1996; Simmers, 1998). Recharge from water mains, septic tanks, sewers and drainage ditches in urban areas can also account for indirect recharge (Simmers, 1998; Knödel *et al.,* 2007).

Local recharge occurs when water infiltrates from perennial and/or ephemeral channels and lakes, and irrigation can also contribute to groundwater recharge (Simmers, 1998; Knödel *et al.,* 2007). In arid and semi-arid climates as found in South Africa, precipitation occurs as intense summer thunderstorms and frontal showers in the winter and spring (Knödel *et al.,* 2007). Indirect methods are used to determine groundwater recharge, either in local (point) investigations and/or in areal investigations (Simmers, 1998; Knödel *et al.,* 2007).

Common methods to gauge groundwater recharge include: measurements with soil lysimeters, water balance estimation, evaluation of groundwater hydrographs, stream gauging, soil-water flow modelling, estimations using groundwater flow models and chemical methods (Knödel *et al.,* 2007).

2.4.2 Chemical Weathering of Minerals and Parent Rock

The weathering of minerals and parent rock normally plays a vital role in the chemistry of groundwater. The concentrations of ions found in water are usually a reflection of the ions that make up the rock composition.

The mineralogy is not the only factor that influences the chemistry and the rate of weathering. Minerals involved in chemical weathering may be silicates, carbonates or evaporated salts.

2.4.2.1 Silicate Weathering

The dissolution of carbonate minerals is directly displayed in the water chemistry; however, the weathering of silicate minerals (due to the slow dissolution reaction of silicate minerals) results in a less ostensible change in the chemistry of the water (Appelo and Postma, 1994).

Silicate weathering is one of the most important buffering mechanisms of soil- and groundwater against acidification in sediments free of carbonate minerals (Appelo and Postma, 1994).

The following equation (Eq. 7) illustrates the weathering of silicates (Huizenga, 2011):

Silicate Mineral H_2O CO_2 A l residue $(HCO_3)^-$ H_4SiO_4 ions Eq. 7

The amount of bicarbonate and the type of ions produced during the weathering is dependent on the type of minerals found in the rock. Mafic minerals such as olivine and pyroxene are more susceptible to weathering when compared to felsic minerals like quartz and feldspar, as illustrated by Goldich in 1938 (Figure 15).

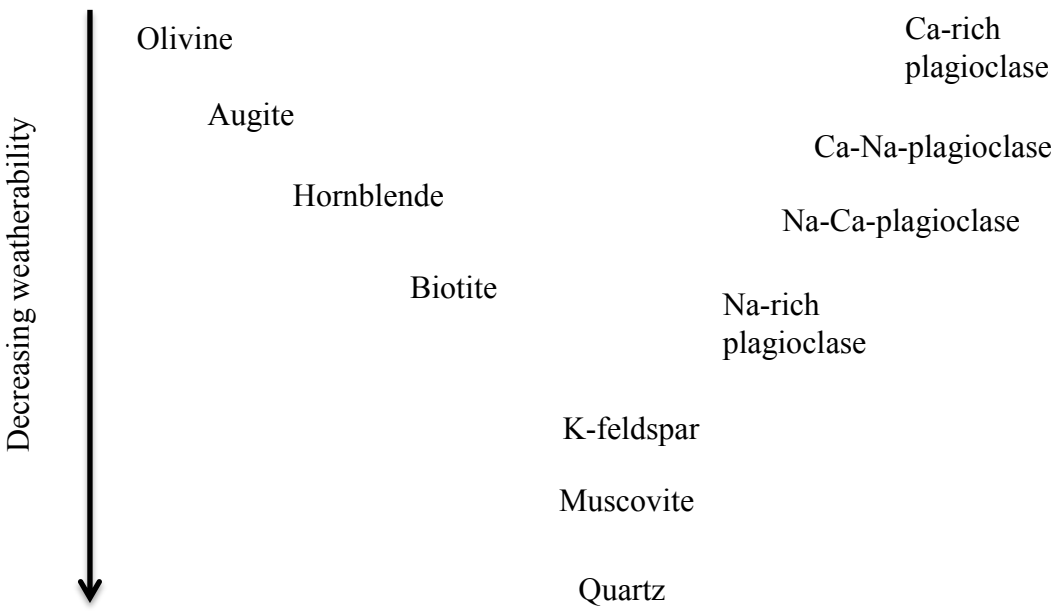

Figure 15: Goldich (1938) weathering sequence.

With an advanced degree of weathering, bicarbonate concentration increases, which in turn lead to an increase of the total dissolve solids (TDS) within water. Mafic rocks degenerate to form waters rich in $Mg^{2+}$and Ca^{2+}, while felsic rock waters are rich in Na^+ and K^+ (Huizenga, 2011).

2.4.2.2 Carbonate Weathering

Carbonate mineral/rock reactions play an important role in regulating groundwater composition; these carbonated rocks, such as limestone and dolomite, are normally associated with high-

efficiency aquifers and offer auspicious conditions for the extraction of groundwater (Appelo and Postma, 1994). The minerals such as dolomite ($CaMg(CO_3)_2$), calcite ($CaCO_3$) and aragonite ($CaCO_3$) are found in the composition of carbonate rocks. These minerals dissolve easily and give water its _hard‘ character (Appelo and Postma, 1994).

The dissolution is expressed in the following reactions [Eq. 8 and Eq. 9] (Appelo & Postma, 2005; Huizenga, 2011):

$$CaCO_3 \quad H_2O \quad CO_2 \quad Ca^{+} \quad 2(HCO_3)^{-} \qquad \text{Eq. 8}$$

$$CaMg(CO_3)_2 \quad 2H_2O \quad 2CO_2 \quad Ca^{+} \quad Mg^{+} \quad 4(HCO_3)^{-} \qquad \text{Eq. 9}$$

The weathering products are Ca^{2+}, or Ca^{2+} and Mg^{2+}, respectively, and a bicarbonate concentration that is equal to the concentration of the cations (Appelo and Postma, 1994; Huizenga, 2011).

In water affected by AMD, carbonate rocks act as a neutralising agent which may be beneficial. However, increased dissolution may result in the formation of underground cavities that cause subsidence of the surface.

2.4.3 Groundwater Contamination

Groundwater quality degradation can be caused by industrialization, mining, increased urbanization, deteriorating standards in waste management, agriculture, waste disposal, and inappropriate land use (DEAT, 2006). However mining activities are the only relevant contributors to groundwater contamination in this study.

2.4.3.1 Mining Activities

Groundwater management in South Africa fell under the Groundwater Division of the Geological survey up until 1977 (Dennis *et al.,* 2008). During this time, groundwater was regarded as a mineral; however, after the establishment of the Directorate for Geohydrology at DWAF, the main focus on groundwater changed to viewing it as a potential water resource (Dennis *et al.,* 2008).

A large portion of mining activities contribute to groundwater pollution in some form, from the operational stage of the mine life cycle to the post-closure phase. The severity and extent of groundwater pollution will, however, vary between these stages (DWAF, 2008a).

During the earlier stages of mining in the 20th century, little scrutiny was given to the release of mine tailings material, and commonly the closest waterway at hand was utilized for discard, ultimately resulting in a severe negative impact on surface water (Dennis *et al.,* 2008). The realizations of these negative impacts lead to the development of alternative methods of disposing of tailings materials. In the 1940s, TDF construction became a more common practice in the mining industry (Dennis *et al.,* 2008).

Tailings disposal facilities usually form recharge points for groundwater, and therefore groundwater pollution is considered a common trait. The nature and design of the TDF plays a vital role in the impact on the groundwater system. Mining activities can cause the pH of groundwater to lower due to AMD, as well as increase salinity, metal element content of the water and sediment load of the groundwater (DEAT, 2006; DWAF, 2007).

In short, acidification of water can mobilize trace metal elements such as Cd and Pb, which has adverse impacts on aquatic life and water users (DEAT, 2006; DWAF, 2007).

An increase in the salinity of the water can cause the salinization of irrigated soils, reduce crop production, and increase scale and corrosion in domestic and industrial water pipes; it may result in negative health effects, such as renal failure (DEAT, 2006; DWAF, 2007). An increase in water sediment load may result in an impact to aquatic organisms and their habitats (DEAT, 2006).

2.5 LANDSCAPE FUNCTION ANALYSIS (LFA)

Landscape Function Analysis is a procedure that monitors the developed soil surface indicators to evaluate the biogeochemical functions of landscapes, and how well the ecosystem works as a biophysical system (Tongway and Hindley, 2004). Haagner (2008) stated that these indicators mainly concentrate on the soil surface processes and not the absence or abundance of selected biota, which makes the information gathered, different from any former monitoring procedure.

According to Tongway and Hindley (2004), this approach examines the functionality of a landscape and is separate from the biological composition and structure which have typically

been the assessed characteristics. The LFA comprises four components, namely: conceptual framework, field methodology, data reduction and tabulation, and interpretational framework (Tongway and Hindley, 2004).

The conceptual framework suggests looking at vital resources and identifying potential enhanced losses and processes that maintain these resources (Tongway and Hindley, 2004; Haagner, 2008). The main purpose of the field methodology is to identify and describe the landscape units that accumulate resources, such as patches, and promote the loss of resources, such as inter-patches (Haagner, 2008). The field methodology data outputs include: the landscape organisation of the area at hillslope scale and the soil surface assessment of the patches and inter-patches which was identified in the landscape organisation step (Haagner 2008).

The field methodology was particularly designed to be utilised over time to perceive any trends that may be present as well as to see if the landscape management objectives were met (Haagner, 2008).

Tongway and Hindley (2004) and Haagner (2008) stated that the observations made during the soil surface assessment step are grouped into three indices, namely: stability, nutrient cycling and infiltration. Each one holds a unique significance for the functioning of the landscape as a biophysical system. A more detailed description of the LFA is given in Chapter 3.

2.6 PREVIOUS STUDIES DONE ON THE MINE WASTE SOLUTIONS NO. 4 AND 5 TAILINGS DISPOSAL FACILITIES

Haagner (2008) studied the role of vegetation in characterizing landscape function in the rehabilitation of gold tailings in 2008 by discussing the rehabilitation processes of the TDF in detail, with reference to the structure and chemical properties of the TDF's. His studies also assist in the remediation of the problem sites.

The results of Haagner's study in 2008 showed that the TDFs had a different composition of vegetation cover from that of the reference site, but did not show statistically significant differences in the composition across the remediating chronosequence. Haagner‘s (2008) study also found correlations between the age of the rehabilitation site and landscape function indices, thus suggesting improvement in terms of ecosystem development.

Within certain sites, there was a noticeable deterioration in substrate quality due to increased acidity and salinity, resulting in a decline in landscape function. Haagner (2008) concludes this deterioration was likely due to the oxidation of pyrite and the existence of free salts within the tailings material. This author goes on to conclude that sites which displayed enhanced landscape function were seemingly able to negate the observed negative chemical changes via temporary combative ecosystem processes; however, given the potential for acid formation within the tailings material and the potentially poor resilience of existing vegetative cover, Haagner (2008) proposed that an optimized monitoring framework be implemented across the target sites.

Ratlhogo (2011) studied the acid mine drainage potential of the MWS No. 5 TDF in 2011 and stated that there were two deposition stages on the TDF. During the first stage of deposition, pyrite was removed from the gold ore due to the economic value of pyrite. Therefore, the MWS No. 5 TDF presented no threat of generating AMD (Pinkney, 1956). The second stage of deposition included the waste from re-processed TDFs which resulted in the deposition of pyrite and SO_4^{2-} anions onto MWS No. 5 TDF. The deposition of pyrite on the TDF poses a potential threat of AMD generation.

Ratlhogo (2011) suggested that, should AMD be present in the second stage of deposited material, its products might be leached to the lowermost terraces and subsequently lead to the pollution of the environment adjacent to the TDF. This author found that the average pH of the TDF was 3.16, yet the lowest measured pH was 2.4. Thus the low pH levels on the TDF show that AMD is present. The XRD analysis revealed the presence of quartz and gypsum throughout the TDF, with numerous clay minerals also being present.

Ratlhogo (2011) also found that jarosite ($KFe_3(SO_4)_2(OH)_6$) was present on the surface of the TDF, this secondary mineral is usually the most common mineral in AMD conditions. Although no pyrite was detected in the XRD analysis (due to the lowest detection limit of XRD which is 1% in mixed materials), it was concluded that the presence of SO_4^{2-} ions is an indication of pyrite being present in the TDF.

Ratlhogo (2011) made use of a Flicklin plot to reveal the presence of AMD from the trace metal element analysis. The results showed that AMD is present even in the lowest terrace which was created during the first stage of deposition (which previously did not show any signs of AMD), which in turn indicates that the AMD is seeping towards the lower terrace. After calculating the

net acid producing potential (NAPP), values greater than 20 ppm indicate the presence of acid-generating materials.

The seepage water from the No. 5 TDF contained toxic trace elements, which may have the potential to pollute adjacent soils and underlying aquifers (Ratlhogo, 2011).

CHAPTER 3: MATERIALS AND METHODS

During this study, various techniques and methods were used to gain information about the samples taken on the farm Stilfontein in order to determine whether the soil is polluted by the MWS No. 5 TDF, as well as to establish whether the pollution in the area decreases over time as the TDF material dries out. This chapter details the methods of sample extraction and the various techniques employed in sample preparation and analysis.

3.1 SOIL SAMPLING

The soils were sampled for laboratory analyses. Methods are explained below.

3.1.1 Baseline Assessment

At the beginning (August 2011) and end (January 2014) of the monitoring period a baseline assessment was completed on the 12 fixed point samples as an indication that a composite sample around the monitoring FPs were representative for this study. Eleven samples were collected within a radius of ten meters around the FPs, approximately the same depth (30 cm). Each sample was placed in an individual plastic bag and marked according to the site and the number of the sample. For example: FP-1 sample no. 1, 2, etc. The pH and EC were measured for the individual samples and then a composite sample from the 11 samples was made, whereafter the pH and EC were measured. The averages of the 11 samples were calculated and compared with the pH and EC values of the composite sample. Results are explained in Chapter 4.

Data are shown in Appendix A.

3.1.2 Sampling of the Fixed Monitoring Sites

Twelve fixed point samples, FP-1-9 and FP-K1-3 (K = control sites), as identified in the Project Plan in 2011 by Mine Waste Solutions and PW van Deventer (as illustrated in Figure 16, with coordinates shown in Appendix A2), were collected each month over a 30-month period. The samples were taken utilizing a soil auger (Figure 17) within a ten meter radius around the FPs. Eleven holes (approximately the same size, 30 cm deep) were drilled around the FPs and

samples were thoroughly mixed together with a shovel, placed into a plastic bag and marked according to the site and date of collection, e.g. FP-06 (08/11/2011).

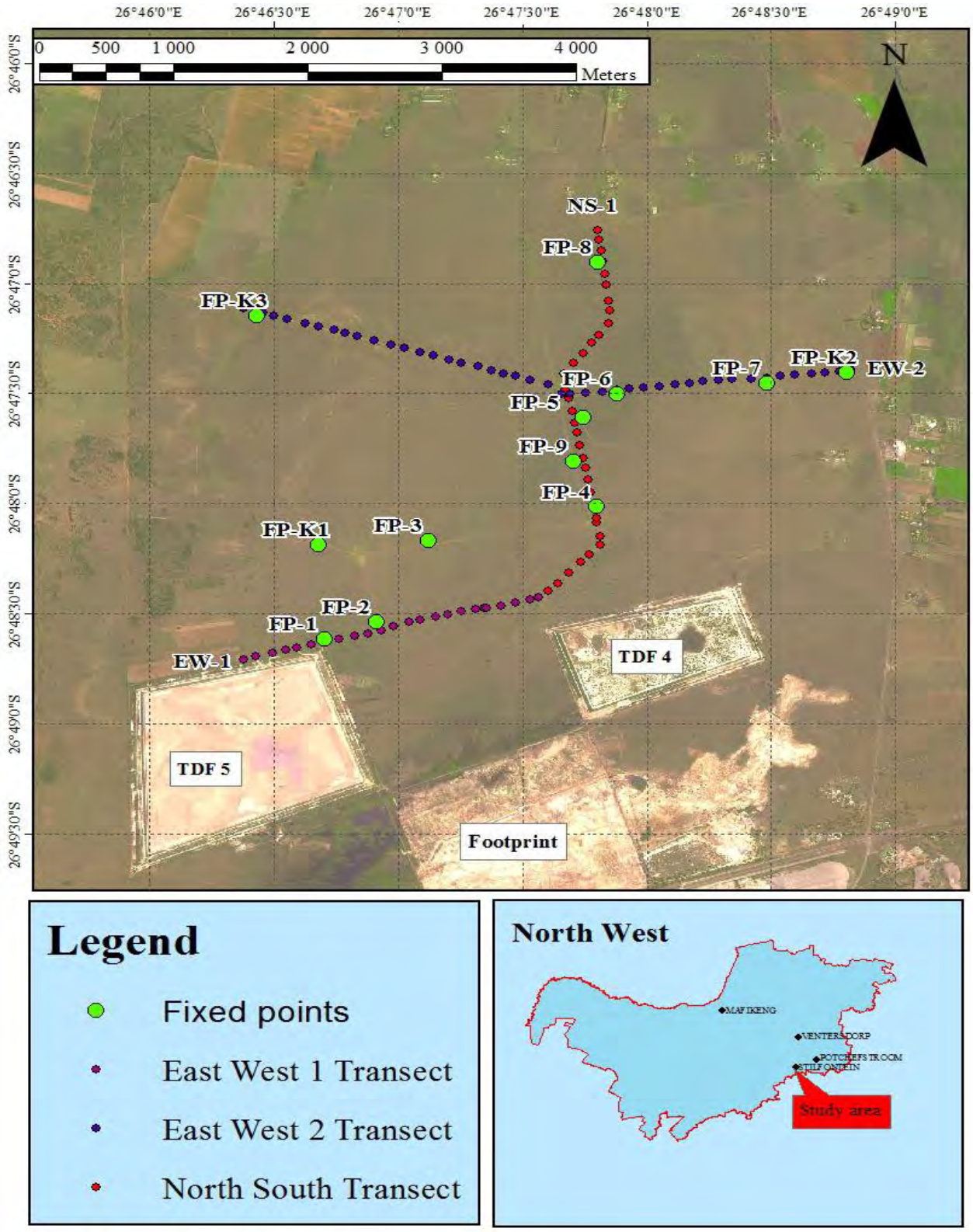

Figure 16: Map showing the location of the 12 fixed points (FP 1-9 and FP-K1-K3) and the three transect lines NS1, EW1and EW2. (Google Earth, 2013).

3.1.3 Sampling of the Three Transect Lines

The three transect lines (NS, EW-1 and EW-2) were sampled as identified in the Project Plan in 2011 (coordinates available in Appendix A3–A5), namely every third month at 100 m intervals between the sample sites.

The samples were taken by utilizing a soil auger (Figure 17), placed into a plastic bag and marked according to the line, sample number and date, e.g. NS-24 (09/11/2011) or EW2- 24 (09/11/2011).

The north-south line is represented by NS, EW-1 represents the east-west line closest to the TDF, and EW-2 represents the second east-west line (Figure 16).

Figure 17: Photograph showing a soil auger. Photograph taken by Daniell (2013).

3.2 SOIL SAMPLE PREPARATION

The research methods that were used to analyze the fixed points and the three transect line samples include: chemical analyses of pH, EC, exchangeable cations, exchangeable cation

capacity (CEC), total and soluble/available trace metal element concentrations of the soil, and anion concentrations (phosphates, sulfates, carbonates, bicarbonate, nitrates, chloride and total alkalinity). Particle size analyses and mineral identification by means of XRD were done only on the FP samples.

The soil samples were prepared according to the methods described by the Non–Affiliated Soil Analysis Work Committee (1990). The samples used for analysis must be dried either with an oven that does not exceed 40°C or air-dried in order to prevent fixation and release of compounds; samples need to be sheltered from direct sunlight. The samples for this study were air-dried, as illustrated in Figure 18.

Figure 18: Photograph illustrating air-dried soil samples at the North-West University, Potchefstroom. Photograph taken by Van der Merwe (2012), with permission.

The samples were crushed after drying to pass through a two mm stainless steel sieve, and thoroughly mixed; it should be noted that stones should not be crushed and if small soil masses (< five grams) or volume-based methods of analysis are to be used, soil should be ground to pass through a one mm sieve (Non–Affiliated Soil Analysis Work Committee, 1990). This soil preparation was a standard procedure for all the analyses conducted, and further preparation of the samples for individual analysis will be described separately.

3.3 CHEMICAL ANALYSES OF THE SOIL

These analyses were done at the soil laboratories of the NWU (Potchefstroom Campus) and Eco-Analytica, and were conducted in order to gain information about the chemical properties of the soil and the extent of the pollution plume from the MWS No. 5 tailings dam on the soils of the study area.

3.3.1 pH

All readings were done using a Hannah multi-meter, which was calibrated prior to taking the measurements. The calibration was done using pH buffer solutions of pH 4.01, 7.01 and 10.1. The lowering of the pH is mostly due to the presence of soluble cations with a greater affinity for adsorption onto the exchange site of the soil, which will displace the adsorbed H^+ ions from such sites (Non–Affiliated Soil Analysis Work Committee, 1990).

The pH was measured in distilled water in a ratio of 1:2.5 soil:solution according to the standard methods of the Non–Affiliated Soil Analysis Work Committee (1990).

3.3.2 Electrical Conductivity (EC)

The EC of a soil is a measurement of the amount of salts present in the soil solution and/or the ability of the soil to conduct or transmit electricity, and is normally expressed in units of MilliSiemens per meter (mS/m).

All readings were done using a Hannah multi-meter, which was calibrated prior to the measurements. The calibration for EC was done using an EC calibration solution of 12.88 mS/m.

The EC values are utilized to categorize the salt hazard of saline soils, and to estimate the leaching requirements of saline soils for reclamation purposes (Non–Affiliated Soil Analysis Work Committee, 1990) and the degree of saline pollution on the soils. It should be noted that EC values of certain samples may fluctuate as seasonal deviations occur.

The reason for this is simply due to the fact that in more rainy seasons, more leaching, percolation and dilution of salts occur than in dry, sunny seasons when the precipitation of salts are more likely to occur on the surface. The high risk EC value of soil is 360 mS/m.

The EC was measured on the saturated paste extract according to the standard method of the Non–Affiliated Soil Analysis Work Committee (1990). The saturated paste method provides an approximation of the total soluble salts present in the soil.

Graphical displays of the EC data are shown in Appendix B.

3.3.3 Exchangeable Cation Analysis

The 12 FP samples collected each month were sent to the Eco-Analytica laboratory (NWU, Potchefstroom) where they were tested for exchangeable cations, i.e. Ca^{2+}, Mg^{2+}, Na^{+} and K^{+}, via inductively coupled plasma-mass spectrometry (ICP-MS) according to the EPA 3050B (1996) method.

The extraction solution normally used for exchangeable cation testing is ammonium acetate (0.2 mol/dm). The ammonium ions displace the cations on the exchangeable position. The concentrations of the displaced cations are determined with a Varian SpectrAA 250 Plus AA (The Non-Affiliated Soil Analysis Work Committee, 1990).

This process is a function of temperature and thus should be conducted at a constant temperature of 20ºC, including the extract solution (Hesse, 1971). The samples were further prepared by first extracting five grams of sample material (> 2 mm) to be mixed with 50 ml of ammonium acetate within a Schott-bottle. The suspension was then shaken for 15 min on an oscillating shaker at 180 rpm. Two to three drops of superflok (1%) were added to the shaken suspension (The Non-Affiliated Soil Analysis Work Committee, 1990).

The top layer of the suspended liquid was then filtrated into a clean Schott-bottle, until clear. Ten ml of the filtrate was then placed into a 50 ml volumetric flask and 10 ml of lanthanum solution (500 dpm) was added to the filtrate, after which the flask was filled up to volume with the ammonium acetate. The cations are normally extracted with a sample to extraction ratio of 1:10 g/ml (The Non-Affiliated Soil Analysis Work Committee, 1990).

Data are shown in Appendix C.

3.3.4 Cation Exchange Capacity (CEC) Determination

The CEC of a soil is its capacity to adsorb cations on the clay particles. The same samples used for exchangeable cation analysis were used in the determination of CEC (done by Eco-Analytica

laboratory, NWU, Potchefstroom). In order to determine the CEC of the samples, five grams were mixed with 50 ml of sodium acetate within a Schott bottle. The suspension was shaken for an additional 15 min within an oscillating shaker at 180 rpm (The Non-Affiliated Soil Analysis Work Committee, 1990).

The suspension is filtered into leach tubes in order to separate the sodium acetate from the sample. The remaining solid sample, which contains excess sodium, is then washed out with 50 ml of ethanol:dH_2O (1:1), and this process is repeated five times. The sample is then washed three times with 30 ml of ammonium acetate in order to remove the sodium from the exchangeable position. The liquid is then placed into a 100 ml volumetric flask, which is filled to volume with ammonium acetate (The Non-Affiliated Soil Analysis Work Committee, 1990).

The solution is then diluted by an order of ten, by placing five ml of original solution in a 50 ml volumetric flask and filling the remainder to volume with ammonium acetate. The concentration of sodium is then measured with the Varian SpectrAA 250 Plus AA (The Non-Affiliated Soil Analysis Work Committee, 1990).

Data are shown in Appendix C.

3.3.5 Anion Concentration Analysis

The method used to analyse the anions present in the soil was the saturated paste method described in the handbook of standard soil testing methods for advisory purposes (Non-Affiliated Soil Analysis Work Committee, 1990). The 12 FP samples were sent to Eco-Analytica laboratory (NWU, Potchefstroom) where the samples were tested for the following anions: Cl^-, SO_4^{2-}, PO_4^{2-}, NO_2^-, NO_3^-.

First, 250 grams air-dried soil was weighed into a suitable container. De-ionised water was added to the dry soil and mixed with a spatula until the paste shone and flowed marginally as the container was being tilted; it did not cling to the spatula without any free water collecting when a small channel was drawn on the surface of the paste. The paste was left for an hour and then it was re-checked for the saturation properties listed above. The paste was filtered with a vacuum filtration utilizing a Buchner or Richards funnel fitted with a Whatman No. 50 filter paper with a 180 mm diameter. The collected filtrate was filtered until clear. The filtrate was then used to test for anions. Data are shown in Appendix D.

3.3.6 Total Trace Metal Element Analysis of the Soil

This analysis was done according to the EPA 3050B (1996) method. The 12 FP soil samples at approximately the beginning and end of the monitoring period were taken to Eco-Analytica laboratory (NWU, Potchefstroom). The total trace metal element concentration of the soil was conducted by means of acid digestion.

First, 25 grams of the soil was placed in a 150 ml beaker. Then 15 ml nitric acid was carefully added to the soil sample, immediately covered with a watch glass and placed within the sand bath which was set at a medium temperature of ± 95°C. The mixture was left to reflux for an hour. Fumes generated during the digestion processes are shown in Figure 19; therefore, this preparation was done in a fume cupboard. The watch glasses were removed when the fumes diminished, which was an indication that the sample was digested.

Figure 19: Photograph showing the fumes generated by the HNO_3 digesting the soil. Photograph taken by Van der Merwe (2012), with permission.

The acid was evaporated by heating the sample until the volume was reduced to ± five ml. The sample was cooled in order to add three ml hydrogen peroxide (H_2O_2). The sample was cooled down again and this was repeated three times. Ten ml of 3N HCl was added and covered again with a watch glass. The mixture was placed on the sand bath in the fume cupboard and was refluxed for about an hour. After the hour of reflux, the sample was cooled down to room

temperature. The mixture was filtered through a Whatman 40 filter paper into a 50 ml volumetric flask. The filter paper was washed with deionized water. The volumetric flask was filled with deionized water.

The samples were tested via ICP-MS according to the EPA 3050B (1996) method for total trace metal elements such as, vanadium [V], chromium [Cr], Co, Ni, Cu, Zn, As, Se, molybdenum [Mo], palladium [Pd], silver [Ag], Cd, barium [Ba], platinum [Pt], gold [Au], mercury [Hg], thallium [Tl], Pb, and U. The ICP-MS technique is used for chemical element determination and concentrations. The technique is the combination of a high-temperature ICP source with a mass spectrometer (Wolf, 2005).

Figure 20 illustrates the role of the ICP source as described in the following. The argon gas flows inside the concentric channels of the ICP torch. When power is supplied to the radio frequency RF load coil, oscillating electric and magnetic fields from the RF generator are established at the end of the torch. When a spark is applied to the flowing argon gas, electrons are stripped from the argon atoms, thus forming argon ions. When these ions are caught in the oscillating fields and collide with other argon atoms, argon plasma is then formed (Wolf, 2005).

The sample is usually presented to the ICP plasma as an aerosol, either by aspirating a liquid or dissolving a solid sample into a nebulizer, or by using a laser to directly convert solid samples into an aerosol (Wolf, 2005).

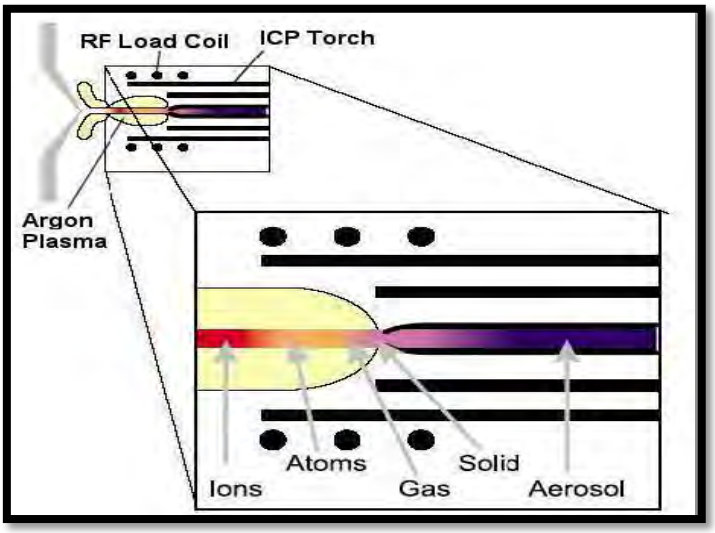

Figure 20: A schematic representation of an ICP torch (Wolf, 2005).

Once the sample aerosol is introduced into the ICP torch, the elements in the aerosol are converted first into gaseous atoms and then ionized towards the end of the plasma. Once the ions

enter the mass spectrometer, they are separated by their mass-to-charge ratio and information can then be gained (Wolf, 2005). The quadruple mass filter is the most generally used mass spectrometer with four rods which is roughly 1 cm in diameter and 15-20 cm long (Wolf, 2005).

Interchanging AC and DC voltages are applied in the mass filter to opposite pairs of these rods, these alternating voltages are regularly switched along with the RF-field which results in an electrostatic filter that only allows ions of a single mass-to-charge ratio to pass through the rods to the detector at a given instant in time (Wolf, 2005).

Data are shown in Appendix E.

3.3.7 Soluble/Available Trace Metal Element Analysis of the Soil

This analysis was done according to the DIN 19730 (1997) method. The 12 FP soil samples collected at approximately the beginning, middle and end of the monitoring period were taken to Eco-Analytica laboratory (NWU, Potchefstroom).

The soluble/extractable/available trace metal element concentration of the soil was determined by means of the ammonium nitrate (NH_4NO_3) solution method. Twenty grams of the air-dried soil was placed in a 100–150 ml shaking bottle; exactly 50 ml of the ammonium nitrate solution was added. The mixture was shaken for two hours at 20 rpm at room temperature.

The solid particles were allowed to settle for 15 min before the supernatant solution was filtered by making use of a 0.45 µm filter. The first five milliliters were disposed of. The solution that remained was collected in a 50 ml bottle for analysis. The samples were tested via ICP-MS according to the DIN 19730 (1997) method for soluble/available trace metal elements such as, V, Cr, Co, Ni, Cu, Zn, As, Se, Mo, Pd, Ag, Cd, Ba, Pt, Au, Hg, Tl, Pb, U etc.

Data are shown in Appendix E.

3.4 PARTICLE SIZE DISTRIBUTION ANALYSIS BY MEANS OF THE HYDROMETER METHOD

The particle size distribution of the soil was done according to the Hydrometer method of the Laboratory Testing Manual 2000 of the Central Materials Laboratory (2000).

The Hydrometer method covers the quantitative determination of a soil‘s particle size distribution from the coarse sand size to the clay size particles by means of sedimentation, which enables a continuous particle size distribution curve of a soil to be plotted from the coarsest particles down to the clay sizes; this analysis requires that the density of the soil sample is known (Central Materials Laboratory, 2000).

The 12 fixed point samples were sent to the Eco-Analytica laboratory (NWU, Potchefstroom) where they were analyzed to determine the particle size distribution of the soil samples. In order to do so, 100 g of dry soil was mixed with 100 ml dispersing agent, this mixture was shaken for five minutes to ensure that the soil was broken down into individual particles (Central Materials Laboratory, 2000).

The suspension from the flask was then transferred to the 75 µm sieve placed on a funnel, which was in turn placed on a measuring cylinder, and then washed with distilled water (Central Materials Laboratory, 2000). The soil material retained on the 75 µm sieve was oven-dried and then sieved through a series of sieves. The soils retained on each individual sieve were weighed (Central Materials Laboratory, 2000).

A control sample was prepared by utilizing 100 ml dispersing solution and distilled water (Central Materials Laboratory, 2000). The dispersing solution and distilled water were placed in a measuring cylinder up to the cylinder mark (Central Materials Laboratory, 2000).

The soil suspension in the cylinder was mixed by placing one palm on the open end of the cylinder and turning it vigorously end-over-end until there was no more soil at the bottom of the cylinder. The cylinder then was placed on the table and the timer was started (Central Materials Laboratory, 2000).

The Hydrometer was immersed and allowed to float freely; the readings were then taken at the upper ring of the meniscus for each cylinder in periods of e.g. 0.5 min, 1 min, 2 min and 5 min, 10 min, 15 min, 30 min, 60 min, 240 min, and 24 hours. The temperature was also recorded using the same time intervals as those for the hydrometer (Central Materials Laboratory, 2000).

Calculations were done according to the method described by Central Materials Laboratory (2000).Once the percentage of sand, silt and clay are known the soil texture can be assigned by making use of the USDA soil textural triangle.

Data are shown in Appendix F.

3.5 MINERAL PHASE IDENTIFICATION OF THE SOIL

3.5.1 X-ray Diffraction

The samples used for XRD analyses were finely powdered with the tungsten carbide ring mill. This finely powdered material (5 µm - 2.5 µm) was used to prepare the samples utilizing a back loading technique; the amount of samples used in grams varies from sample to sample due to the weight difference of the various samples. A PANalytical X'Pert Pro instrument at the Geo XRD & XRF Laboratory (NWU, Potchefstroom Campus) was employed in order to conduct a broad range identification of the materials present in the samples. The samples were loaded onto a spinner stage inside the XRD.

The samples were then scanned utilizing X-radiation generated by a Cu X-ray tube (operated at 40 kV, 45 mA). The samples were scanned from 4° to 100° 2θ, and the scanning tempo was 20.955° 2θ/s. An X'celerator detector was used to detect the different crystal structures of the minerals present in the samples, which resulted in a unique diffractogram for each of the samples.

The diffractogram displays the different phases (unique set of peak positions of each mineral in d-spacings) and the phase concentration (defined by peak heights of the peak sets compared to peak heights and concentrations of known standards) of the materials in the samples. The X'Pert Highscore Plus PW3212 and PDF 4+ software of the International Centre for Diffraction Data (ICDD), consisting of a database of more than 300 000 different crystalline phases, was used to identify the different minerals present in the samples.

Quantification by means of the Rietveld refinement technique was utilized to determine the weight percentage of the minerals present. Diffractograms of the samples are shown in Appendix G.

The generation of X-radiation was achieved by utilizing a high vacuum X-ray tube which consists of a fitted tungsten filament as a cathode that provides the source of electrons. The anode consists of a single metal element such as Mo, Cu, or iron [Fe] which acts as the target for the electrons.

When a current is supplied to the filament, it is heated and electrons are emitted that are accelerated toward the target anode by a high voltage applied across the tube. X-radiation is generated when the source electrons impact the target (Klein and Dutrow, 2008).

According to Klein and Dutrow (2008), the XRD technique applies to crystals as they consist of ordered three-dimensional structures with periodic atomic arrangements along crystallographic axes. When struck by an X-ray beam, electrons within the X-ray beam‘s path vibrate and form the initial point of the generation of secondary waves of equivalent frequency and wavelength as the original X-radiation.

Diffraction occurs when these secondary waves experience constructive interference, or support each other and produce waves that are in phase with each other. When constructive interference occurs we can say that Bragg‘s Law ($n\lambda=2d \sin\theta$) has been satisfied, where n is an integer, λ is the wavelength of the original X-rays, d is the given interplanar spacing within the atomic matrix, and θ is the angle between the original incident X-ray and the atomic plane of the crystal structure, as illustrated in Figure 21 (Klein and Dutrow, 2008).

These diffracted X-rays are then detected, processed and counted. Scanning the sample holder that rotates at θ^o which is not the case X‘Pert Pro instrument that was used, while the detector rotates $2\theta^o$ (as illustrated in Figure 22) is performed in order to ensure that all the different diffraction directions of the matrix are achieved due to the random orientation of the powdered material.

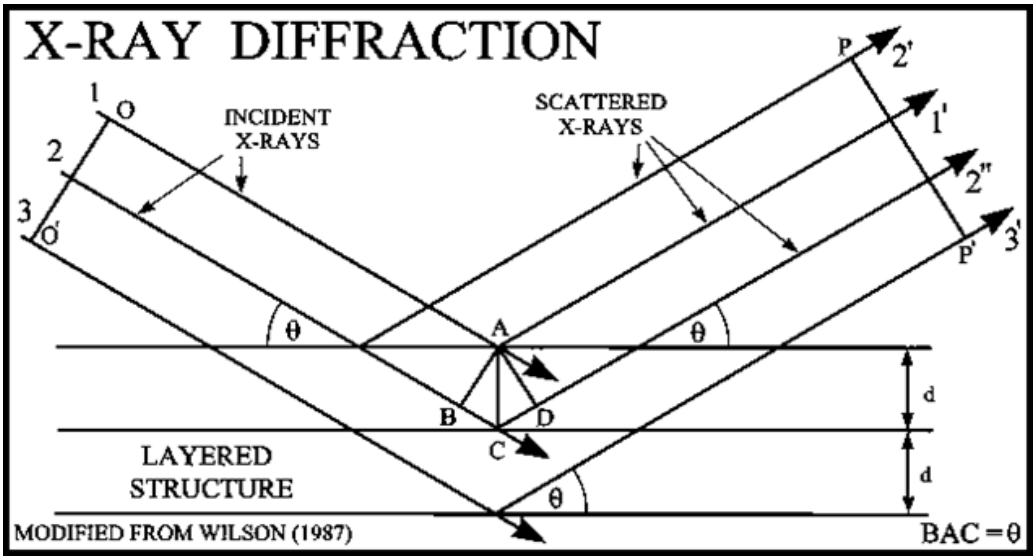

Figure 21: Geometry of X-ray diffraction from equally spaced planes in a crystal structure with spacing d between them (Crain, 2001).

The conversion of the diffraction peak positions (2θº) to d-spacing with Bragg‘s Law (mentioned above) will allow minerals to be identified due to each mineral consisting of a unique set of d-spacings, and together with the relative intensities (*I* with the strongest peak represented by 100 and all the other peaks scaled with respect to 100), the mineral identification process may then commence (Klein and Dutrow, 2008).

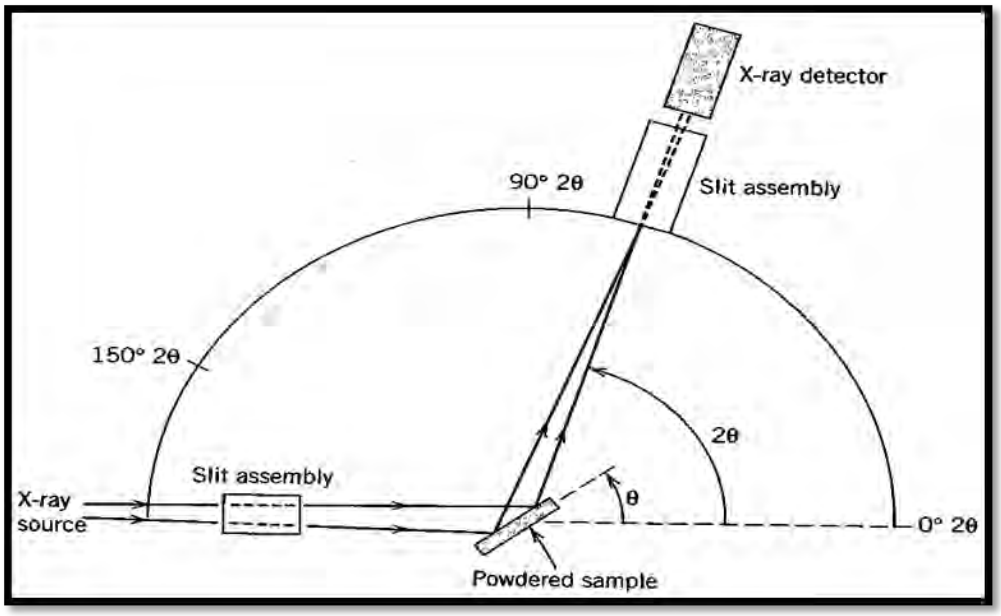

Figure 22: Schematic illustration of the essential components of a powder X-ray diffractometer. In such an instrument, the sample holder rotates at θº while the detector rotates 2θº. (Klein and Dutrow, 2008).

In order to contribute to the identification process, the International Centre for Diffraction Data (ICDD) has made a large volume of known X-ray powder diffraction patterns available, by releasing the Powder Diffraction File.

The powder diffraction file (PDF) includes upwards of 217 000 diffraction patterns for various crystalline materials.

The d-spacings and intensities retrieved from the analysis are then compared with d-spacings and intensities of the standard reference XRD patterns of the ICDD PDF, and minerals can thus be identified (Dutrow and Clark, 2012).

3.6 BOREHOLE WATER ANALYSIS

Water analysis was done in order to determine whether the pollution plume diminishes in size and over time as assumed in the hypothesis of the study. Various water data were obtained from AngloGold Ashanti and MWS.

Two monitoring boreholes from Department of Water Affairs (DWA) are situated on the study area (FS008 and FS009). Data was also obtained from the DWA for these two boreholes. BTRW and CW5-F water samples were obtained from previous studies conducted on MWS No. 5 TDF. A total of 12 boreholes on the study site were used for analysis, as shown in Figure 23 and Table 5.

The water analyses include pH, TDS, total alkalinity (TAL) as $CaCO_3$ in mg/ℓ, and the concentrations of major species such as: sodium (Na^+), potassium (K^+), calcium (Ca^{2+}), magnesium (Mg^{2+}), ammonium (NH^{4+}), fluoride (F^-), orthophosphate $(PO_4)^{3-}$, chloride (Cl^-), sulphate $(SO_4)^{2-}$, nitrate/nitrite $(NO_3)^-/(NO_2)^-$ and bicarbonate $(HCO_3)^-$ [all in mg/ℓ].

The pH and TAL were used to calculate the carbonate and bicarbonate concentrations with the following equations [Eq. 10 and Eq. 11] (Appelo and Postma, 2005; Huizenga, 2011):

$$[HCO_3^- = \frac{2\ TAL\ -10^{-14\ \ pH}}{1\ 2\quad K\ \ 10^{pH}} \qquad \text{Eq. 10}$$

$$[CO_3^2 \qquad \frac{K\quad HCO_3}{10^{\ pH}} \qquad \text{Eq. 11}$$

where $K = 10^{-10.3}$, and is the equilibrium constant for the reaction (Eq. 12):

$$HCO_3^- + H_2O \leftrightarrow CO_3^{2-} + H_3O \qquad \text{Eq. 12}$$

Microsoft Excel was used for the analysis of the data using the pH, TDS and concentrations of the following major elements: Na , Ca^2 , Mg^2 , Cl^-, SO_4^{2-} and HCO_3^-. *Rockworks15* was used to draw the Stiff diagrams. *Corel draw X3* was then used to redraw the diagrams; this was done for quality purposes only.

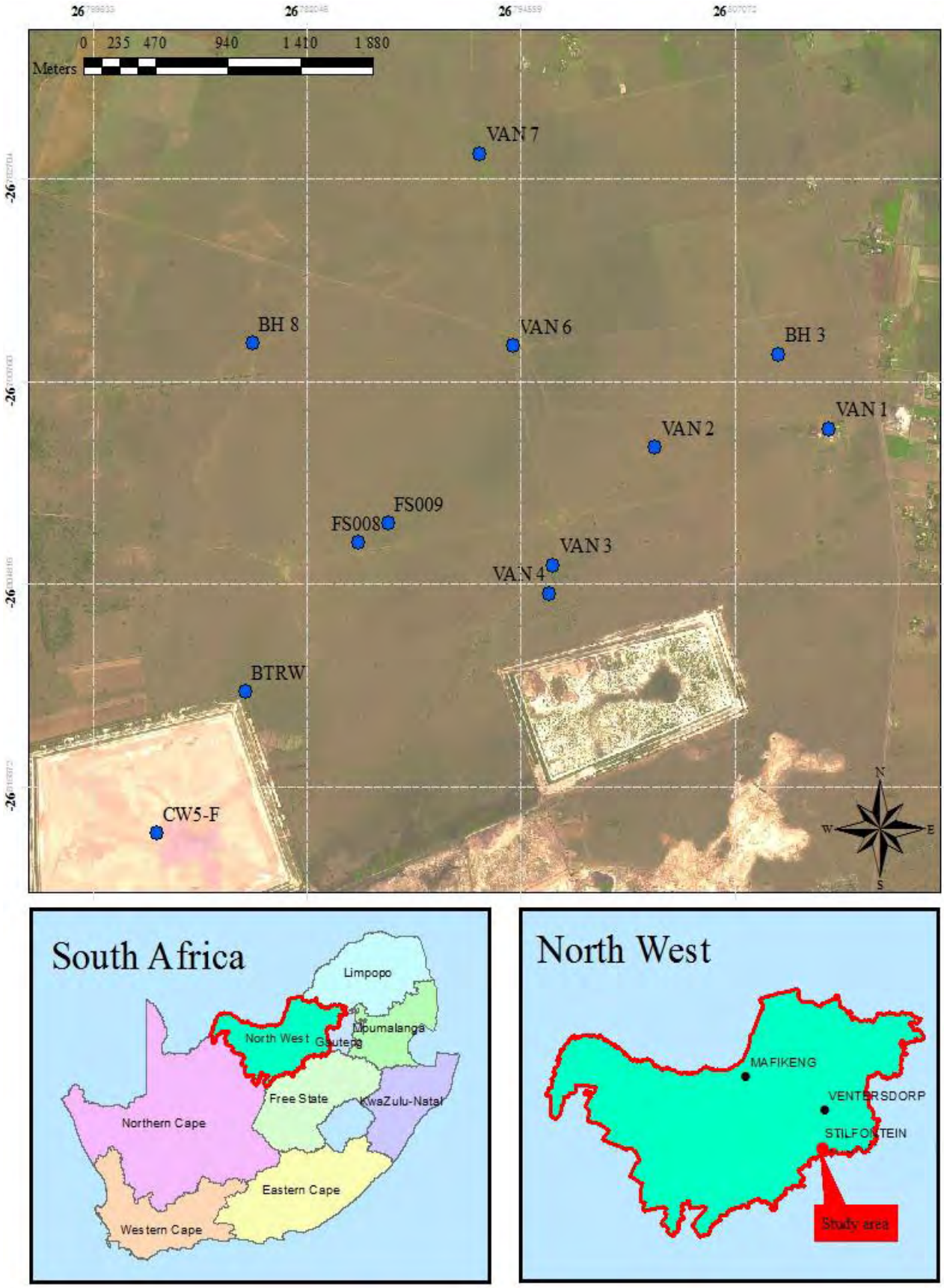

Figure 23: Map showing the locations of the boreholes which were sampled. (Google Earth, 2013).

Table 5: Farm Stilfontein borehole site descriptions.

Borehole number	Borehole ID	Coordinates		Number of samples
		Lat.	Long.	
1	VAN 1	-26.796361	26.812583	15
2	VAN 2	-26.797389	26.802389	12
3	VAN 3	-26.803806	26.796417	18
4	VAN 4	-26.805361	26.796194	19
5	VAN 6	-26.791861	26.794083	55
6	VAN 7	-26.781361	26.792167	11
7	BH 3	-26.792310	26.809610	3
8	BH 8	-26.791720	26.778880	3
9	FS008	-26.802590	26.785020	1
10	FS009	-26.801520	26.786820	1
11	CW5-F	-26.81845	26.77326	1
12	BTRW	-26.81073	26.77844	1

3.6.1 Accuracy of Chemical Analysis

There is no such thing as perfect chemical water analysis; errors do occur, and therefore the accuracy of the given and calculated data was screened using the calculated stoichiometric charge balance (SCB) equation to evaluate the data and to analyse data that are correct and relevant.

Errors are often caused by faulty procedures, interference during analysis or some ions that are not included in the chemical analysis (Appelo and Postma, 2005; Huizenga, 2011).

The charge balance equation is as follows [Eq. 13] (Appelo and Postma, 2005):

$$\text{SCB (\%)} \quad \frac{(\sum \text{Cations} \quad \sum \text{Anions})}{(\sum \text{Cations} \quad \sum \text{Anions})} \text{ X } 100 \qquad \text{Eq. 13}$$

The values used in the equation for the concentrations of cations and anions are expressed in meq/ℓ. Acceptable results (Table 6) within a ± 5% range were used for further calculations and the drawing of diagrams (Zhu and Andersen, 2002; Appelo and Postma, 2005).

Table 6: The dataset modification.

	Number of water samples	Percentage from raw data set
Raw data set before filtering	140	100 %
Useable dataset (charge balance error within ± 5%)	80	57 %

3.6.2 Data Evaluation

Various geochemical models were used to analyse and evaluate the data set. These models make use of ternary, Piper and Stiff diagrams.

3.6.2.1 Ternary Diagrams

Ternary diagrams (HCO_3^-, SO_4^{2-} and Cl^-) were developed to categorize the factors in water that control weathering (Huizenga, 2011). The diagram as shown in Figure 24 indicates whether the water chemistry is controlled by chemical rock weathering, sulphate contamination or chloride salination (Huizenga, 2011). For the construction of this diagram in *Microsoft Excel,* TRI-PLOT (Graham and Midgley, 2000) was used.

The calculated median values (50 percentile) for HCO_3^-, SO_4^{2-} and Cl^- were used for plotting normalised values in meq/ℓ. Where (Eq. 14, Eq. 15 and Eq. 16):

$$[HCO_3^-]_{norm} = 100 \frac{[HCO_3^-]}{[HCO_3^-] + 2[SO_4^{2-}] + [Cl^-]} \qquad \text{Eq. 14}$$

$$[SO_4^{2-}]_{norm} = 100 \frac{[SO_4^{2-}]}{[HCO_3^-] + 2[SO_4^{2-}] + [Cl^-]} \text{ and} \qquad \text{Eq. 15}$$

$$[Cl^-]_{norm} = 100 \frac{[Cl^-]}{[HCO_3^-] + 2[SO_4^{2-}] + [Cl^-]} \qquad \text{Eq. 16}$$

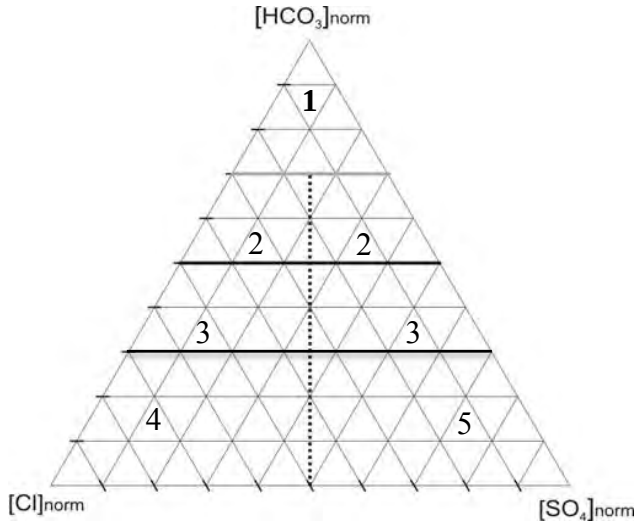

Figure 24: Ternary diagram showing the characterisation of the inorganic water chemistry. 1 = Chemical weathering Zone, 2 Chemical weathering (≥ 50%) and Cl-sal and SO_4–cont (≤ 50%), 3 Chemical weathering (≤ 50%) and Cl-sal and SO_4–cont (≥ 50%), 4 = Chloride salinisation, 5 = Sulphate contamination. Modified from Huizenga (2011).

3.6.2.2 Piper Diagrams

Piper diagrams, named after Piper (1944), plot the major ions such as Na , Ca^2 , Mg^2 , K , HCO_3^-, SO_4^{2-} and Cl^- as percentages of meq on two different triangles, one for the cations and one for the anions, as shown in Figure 25. The sum of the concentration of the four cations in meq/ℓ is recalculated to 100% and the relative compositions are plotted in the triangle (Appelo and Postma, 2005). The same procedure was used to plot the anions in the triangle.

The diamond shape diagram combines the composition of the cations and anions (Bucas, 2006), which are indicated as a single point on the diamond diagram. According to Appelo and Postma (2005), the descriptive terminology of the chemical composition of the groundwater is often determined by the diamond diagram.

The Piper diagrams were used to indicate the overall chemical composition for the borehole samples over the years.

The USGS Gw_Chart Calibration Plots: A Graphing tool for Model Analysis Vision 1.26.0.0 is a free plotting tool which was used to construct the Piper diagrams. This free tool can be obtained from the following website: http://water.usgs.gov/nrp/gwsoftware/GW_Chart/GW_Chart.html *Corel draw X3* was used to redraw the diagrams; this was done for quality purposes only.

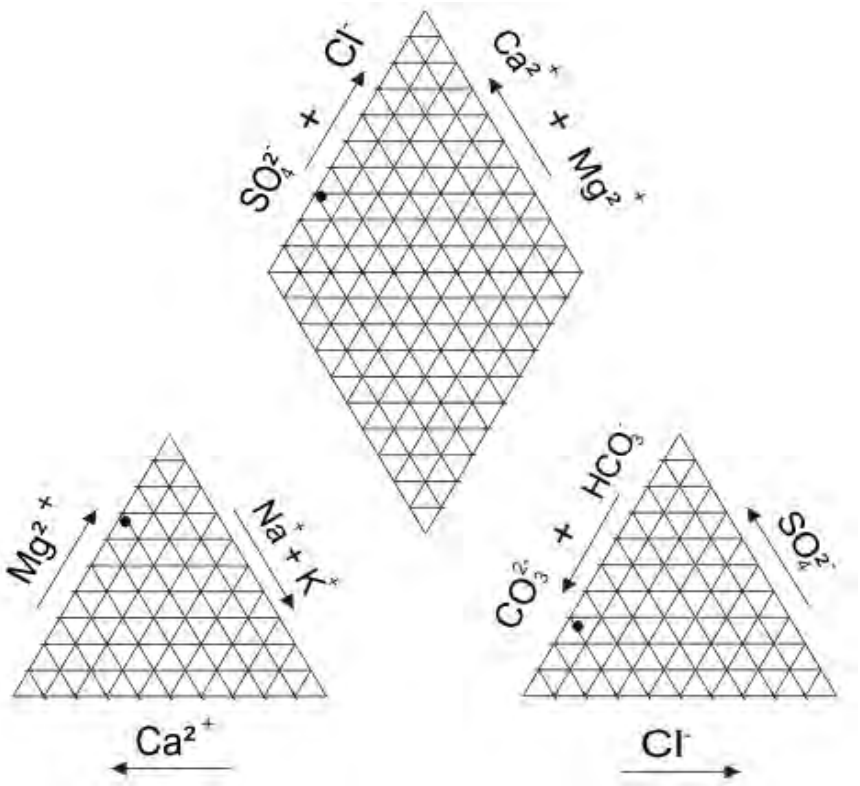

Figure 25: Piper diagram used for bulk chemical composition of the borehole samples.

3.6.2.3 Stiff Diagrams

Stiff diagrams, named after Stiff (1951), display the different patterns of cations and anions present in the groundwater, and are converted from mg/ℓ to meq/ℓ. Cations are plotted to the left and anions to the right, as illustrated in Figure 26 (Appelo and Postma, 2005).

After the concentrations are plotted, the values of each are connected with lines so that a typical shape surface is apparent (Appelo and Postma, 2005). The shape of the diagram will help identify borehole samples with the same composition and assist in determining what the dominant species in the different borehole samples are. Stiff diagrams can assist in the water chemistry comparison between different borehole samples. In this study, the concentrations of the following chemical species: Na K , Ca^2 , Mg^2 , HCO_3^-, SO_4^{2-} and Cl^- were used to construct the Stiff diagrams. *Rockworks15* was used to draw the Stiff diagrams. *Corel draw X3* was used to redraw the diagrams; this was done for quality purposes only.

Diagrams are shown in Appendix H.

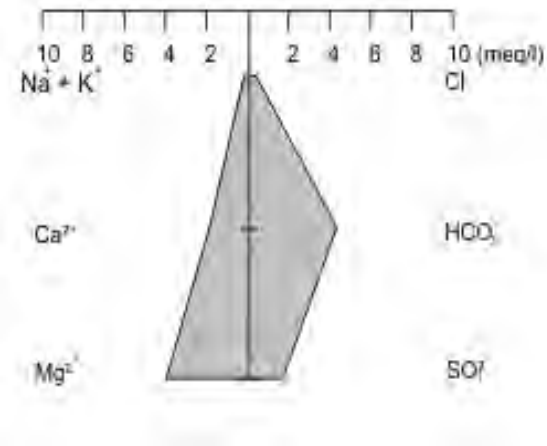

Figure 26: Illustration of a Stiff diagram, showing the concentrations of the representative cations and anions.

3.6.3 Water Sampling

Borehole sampling was conducted in April 2013 and January 2014. In January 2014, only six boreholes could be sampled. The two DWA boreholes and VAN 7 could not be sampled on the two occasions. The DWA monitoring boreholes had monitoring equipment which was not allowed to be removed. The VAN 7 borehole was completely dried up. In January 2014, VAN 6 had a water pump which could not be removed and was non-operational. In April 2013, VAN 6 was sampled. VAN 2 and 3 were not sampled in April 2013 due to the location not being known.

An upgraded electrical water sampler (as shown in Figure 27) from the NWU (Potchefstroom Campus) was used to sample the various boreholes in the study area.

The water sampler consists of a through-flow that can be closed at different depths and does not only take the water sample at the top of water level in the borehole. Three water samples were collected per locality for various analyses (and marked as A, B and C) as follows:

A: TAL determination (was done a.s.a.p. within the first 24 hours after sampling).

B: Major ions: Na^+, K^+, Ca^{2+}, Mg^{2+}, NH^{4+}, F^-, Cl^-, $(SO_4)^{2-}$ and $(NO_3)^-/(NO_2)^-$ [all in mg/ℓ].

C: Trace metal elements (samples were acidified with one drop of pure 95% HNO_3).

All the samples were filtered prior to storage within a 50 ml plastic bottle as shown in Figure 28; pH and EC were also measured beforehand, utilizing a Hannah multi-meter, which was calibrated prior to the measurements. All water samples were kept cool by making use of cold packs and a cooling container (e.g. cool box) which was kept clean and out of direct sunlight.

Figure 27: Photograph illustrating water being sampled with an electrical upgraded water sampler. Photograph taken by Daniell (2014).

Figure 28: Photograph of borehole water being filtered prior to storage. Photograph taken by Daniell (2014).

3.6.4 Water Analysis

The water samples were sent to Eco-Analytica laboratory (NWU, Potchefstroom) where the water samples were tested for TAL, major ions and trace metal elements.

3.6.4.1 Total Alkalinity (TAL) Analysis

Firstly, 25 ml of the water sample was placed in a beaker, where after pH and volume (d) was measured. The water was then titrated with 0.005 N HCl to a pH of 8.2, after which the volume was noted (a). If the original pH was lower than 8.2, then no CO_3^{2-} species were present.

The water was titrated again with 0.005 N HCl to a pH of 4.5; the volume (b) was noted. The water sample was titrated once again using 0.005 N HCl to a pH of 4.2, and volume (c) was noted. The following calculations were used to calculate the total alkalinity of the water:

Carbonate CO_3^{2-}: p-Alkalinity:

$$\frac{a \times N \times 50\,000}{d} \quad \text{mg } CaCO_3/l \qquad \text{Eq. 17}$$

Bicarbonate HCO_3^-: m-Alkalinity:

$$\left(\frac{c \times N \times 50\,000}{d}\right) 0.05 \times 50 \quad \text{mg } CaCO_3/l \qquad \text{Eq. 18}$$

Total alkalinity (TAL):

$$\frac{(2b\ c) \times N \times 50\,000}{d} \quad \text{mg } CaCO_3/l \qquad \text{Eq. 19}$$

where:

a = volume in ml of 0.005 N HCl to pH 8.2

b = volume in ml of 0.005 N HCl to pH 4.5

c = volume in ml of 0.005 N HCl to pH 4.2

d = volume in ml of the water sample

N = normality of the acid (0.005 N HCl)

3.6.4.2 Major Ion Analysis

The major ions that were analysed include: Na , K , Mg^2 , Ca^2 , Cl^-, SO_4^{2-}, F^-, NO_3^- and NH_4. The concentrations of Na , K , Mg^2 and Ca^2 within the water samples were analysed by making use of the SpectrAA 250 Plus instrument from VARIAN.

The concentrations of Cl^-, SO_4^{2-}, $F^-$and NO_3^- within the water samples were analysed by making use of the 761 Compact IC instrument from Metrohm, and the TTT85 Titrator instrument from Radiometer was used to analyse the NH_4 concentration of the water samples. The entire set of water sample was filtered prior to analysis. The water samples were prepared using a 1:2 extract.

3.6.4.3 Trace Element Analysis

First, 50 ml of Suprapur 65% nitric acid was mixed with 50 ml of deionised water. Three ml of this mixture was taken and mixed again with one litre of deionised water; nine ml of the second mixture was extracted and mixed with one ml of the water sample, thus diluting it ten times.

The sample was acidified before analysis with pure nitric acid to ensure stability and comparability with calibration standards according to the EPA 3050B (1996) method. The final mixed sample was analysed with the ICP-MS according to the EPA 3050B (1996) method for Na^+, K^+, Ca^{2+}, Mg^{2+}, Cl^-, $(SO_4)^{2-}$ and $(CO_3)^-$ and trace metal elements (V, Cr, Co, Ni, Cu, Zn, As, Se, Mo, Pd, Ag, Cd, Ba, Pt, Au, Hg, Tl, Pb and U), as explained in Chapter 3.3.7.

3.6.5 Down-hole Camera Survey

The down-hole camera survey was conducted in order to see if any joints, fractures and cavities, which may create pathways for the water to flow from TDF No. 5 to the study site were present in the dolomites. Existing boreholes in the study area were used to conduct the survey, as shown in Figure 29. A total of 10 boreholes were used in this survey as shown in Appendix J.

A down-hole camera was used from the NWU (Potchefstroom Campus), as shown in Figure 30. A tripod was placed directly over the boreholes to ensure that the camera was guided and supported correctly into the borehole, as shown in Figure 31. The image from the camera was displayed on a monitor, which was then recorded.

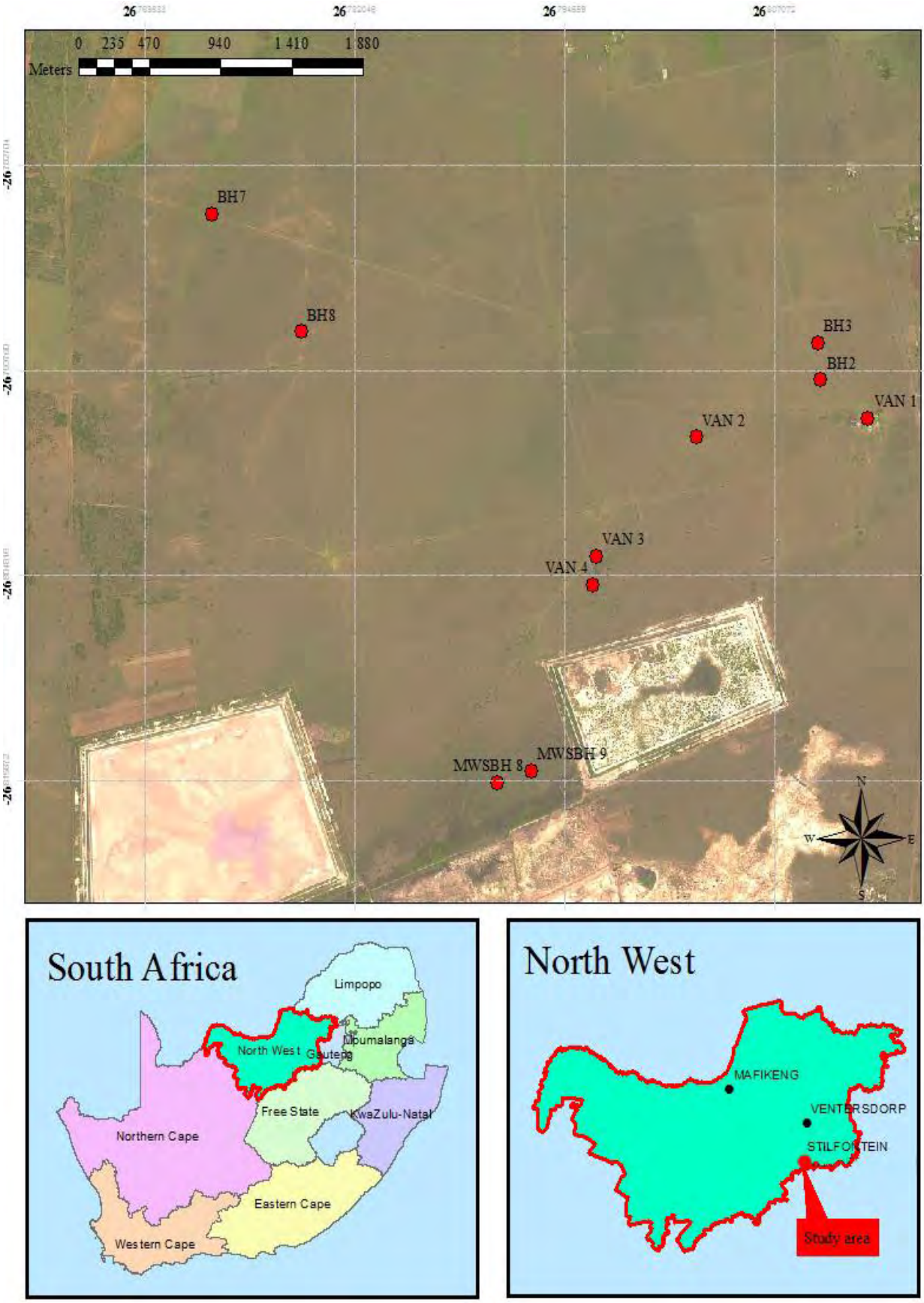

Figure 29: Map showing the locations of the boreholes that were used to conduct the down-hole camera survey (Google Earth, 2013).

Figure 30: Down hole camera from the NWU used to conduct the down-hole camera survey. Photograph taken by Daniell (2014).

Figure 31: Tripod placed directly over the boreholes for guidance and support of the camera. Photograph taken by Daniell (2014).

3.7 MAGNETIC SURVEY

There is a lot of speculation about the subsurface characteristics of the study area and therefore it was suggested that a magnetic survey should be conducted in order to confirm the location of the diabase dyke and to locate any other possible dykes in the area that may be associated with the pollution plume.

3.7.1 Geo-magnetic Survey

Geo-magnetic surveys are used to investigate subsurface geology based on anomalies in the earth's magnetic field, which are the result of the magnetic properties of the underlying rocks (Mariita, 2007). The magnetic content of the underlying geology is extremely variable depending on the rock type and the environment it is in (Mariita, 2007).

The G5 proton memory magnetometer from Geotron Potchefstroom was used to conduct this survey on the farm. Four survey lines, all with an eastern-western direction, were selected over the extent of the pollution plume, as shown in Figure 32. Another two lines were monitored in a northern-southern direction on the footprints (Figure 32); all the survey lines were monitored at 20 m intervals between readings. The SI unit for the magnetic field measurement is tesla (T), i.e. 10^9 nanotesla (nT). Three readings (nT) were taken at each point to ensure that the instrument was placed correctly and that no interference was recorded.

A base station with the following coordinates, S 26.79350, E 26.79573, was selected in approximately the centre of the farm, which was measured every two hours. Changes occur during the course of a day, which are normally referred to as diurnal drifts and which are a few tens of nT; however, changes of hundreds or thousands of nT can occur over a few hours (Mariita, 2007). Therefore, the base station was selected for the correction of diurnal drift (Mariita, 2007).

The G5 proton memory magnetometer specifications:

- 0.1 nT sensitivity and accuracy.
- The total field strength is displayed in nT.
- Light, compact, reliable and rugged design.
- Lower power consumption.
- Short time necessary to take a measurement.

Detailed specification can be obtained from Geotron's website at:
http://www.geoarmatech.com/home_htm_files/magnetometer.pdf

Data are shown in Appendix I.

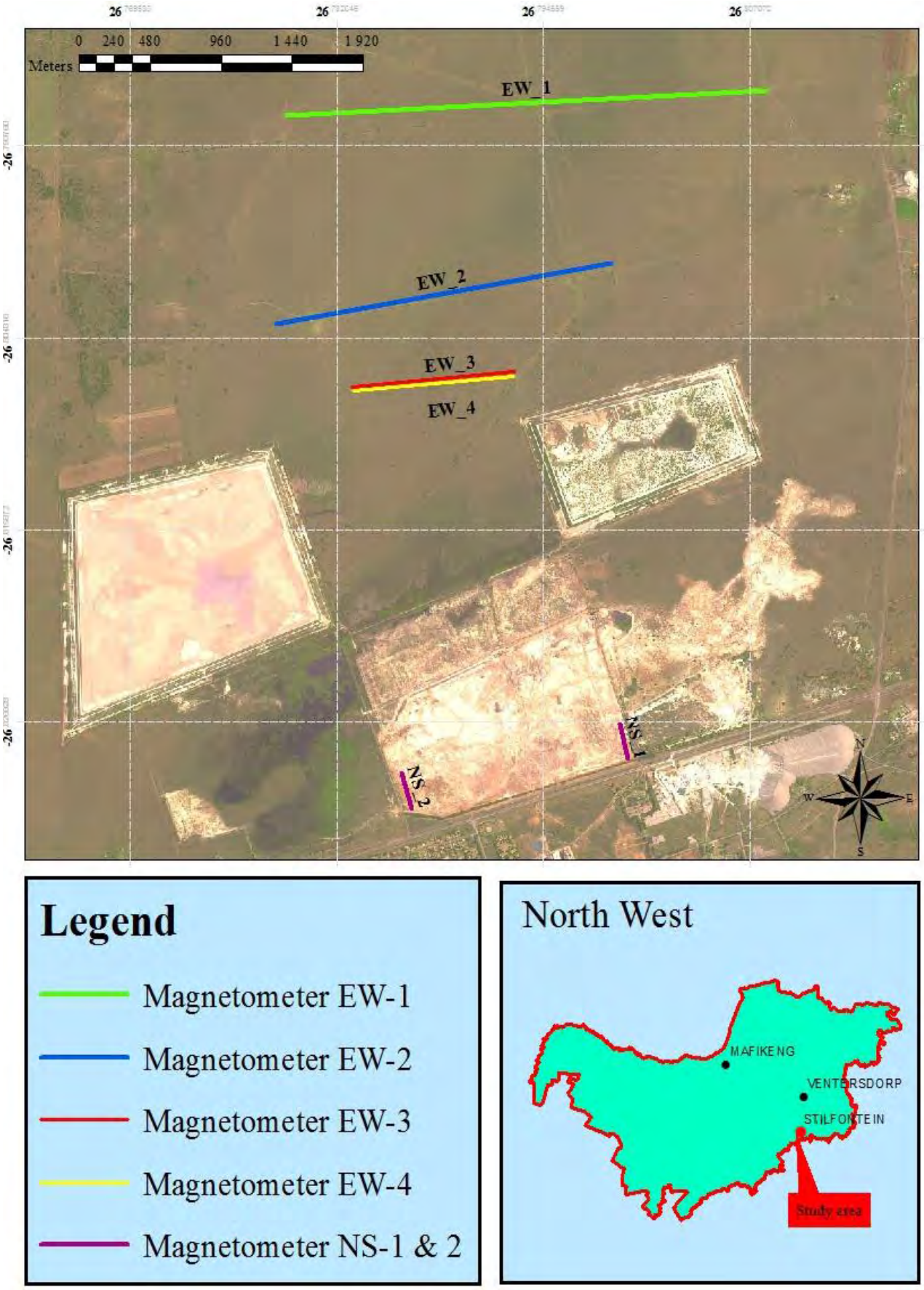

Figure 32: Map showing the locations of the magnetometer lines (Google Earth, 2013).

3.8 VEGETATION

3.8.1 Vegetation Sampling

The vegetation sampling was done from April 2012 up to May 2012 and again in April 2013 and March 2014. This timeframe represents the end of the growing season when most herbaceous plants would be in flower, in order to identify the specific grasses and annual plants in the study area (Haagner, 2008).

Three species namely: *Cynodon dactylon, Eragrostis chloromelas and Setaria sphacelata* var. *torta* were sampled, if present in a 20 m radius around the FP's. This was decided by Malo (2012) due to the fact that these species were the most prevalent grasses present in the study sites at the time. The sampling was done by making use of standard pruning scissors. The plants were cut 10 cm above surface and did not include any roots (whole plant, directly above ground).

3.8.2 Plant Tissue Preparation

The plant tissue samples that were collected were first washed thoroughly with distilled water before they were left to dry at the NWU soil laboratory, out of direct sunlight. After the samples were completely dried, they were milled with a plant mill into smaller fragments and fine powder at Eco-Analytica laboratory (NWU, Potchefstroom).

This was done due to the fact that larger particles are poorly extractable, whereas small particles have a higher surface area which makes extraction much more efficient.

3.8.3 Plant Tissue Analysis

Plant tissue analysis was done by Eco-Analytica laboratory (NWU, Potchefstroom) according to the EPA 3050B (1996) method for total acid digestion. The same procedure was used as described in Chapter 3.3.7 to analyse the vegetation samples for total metal elements (V, Cr, Co, Ni, Cu, Zn, As, Se, Mo, Pd, Ag, Cd, Ba, Pt, Au, Hg, Tl, Pb and U).

Data are shown in Appendix K.

3.8.4 Landscape Function Analysis (LFA)

- The fieldwork was done between the end of January 2012 and April 2012 by DS Malo. In February 2014, a separate LFA was conducted on the same sites and transects. This gives an indication of the recovery or degradation of the LFA over time, which then directly influences the ability of the landscape to regulate ecosystem properties and services. There are three principle steps to be executed during the implementation of an LFA (Tongway and Hindley, 2004):, namely
- Site Description: Description of the geographical setting of the study site.
- Landscape Organisation: Characterising the landscape organisation; the distribution of patches and inter-patches.
- Soil surface assessment (SSA): SSA of each of the patches and inter-patches in step 2.

3.8.4.1 Field Procedure

- **Site Description**

This procedure was done for all of the 12 FPs and control sites. The location, position (crest, upper slope, mid slope, lower slope, closed depression/lake, flat and open depression/stream channels), compass bearing of the different transects, slope, aspect, lithology, soils and the site‘s land uses were described in detail.

- **Landscape Organisation**

A measuring tape of 50 m was laid out as close as possible to the soil surface, marking the upslope and downslope boundaries of the transect line. The LFA conducted for this study included three transect lines of 20 m per site at the same nine FP and the three control sites.

The transect lines on the different sites were divided into a series of patches and inter-patches from the upslope boundary to the downslope boundary of the line, as shown in Figure 33.

The patches and inter-patches were named according to the nature of the soil surface and were measured in meters for length.

The width of each patch was measured in centimeters on the contour. This step was done in order to map the study area in relation to the spatial pattern of resource losses or accumulations (Tongway and Hindley, 2004).

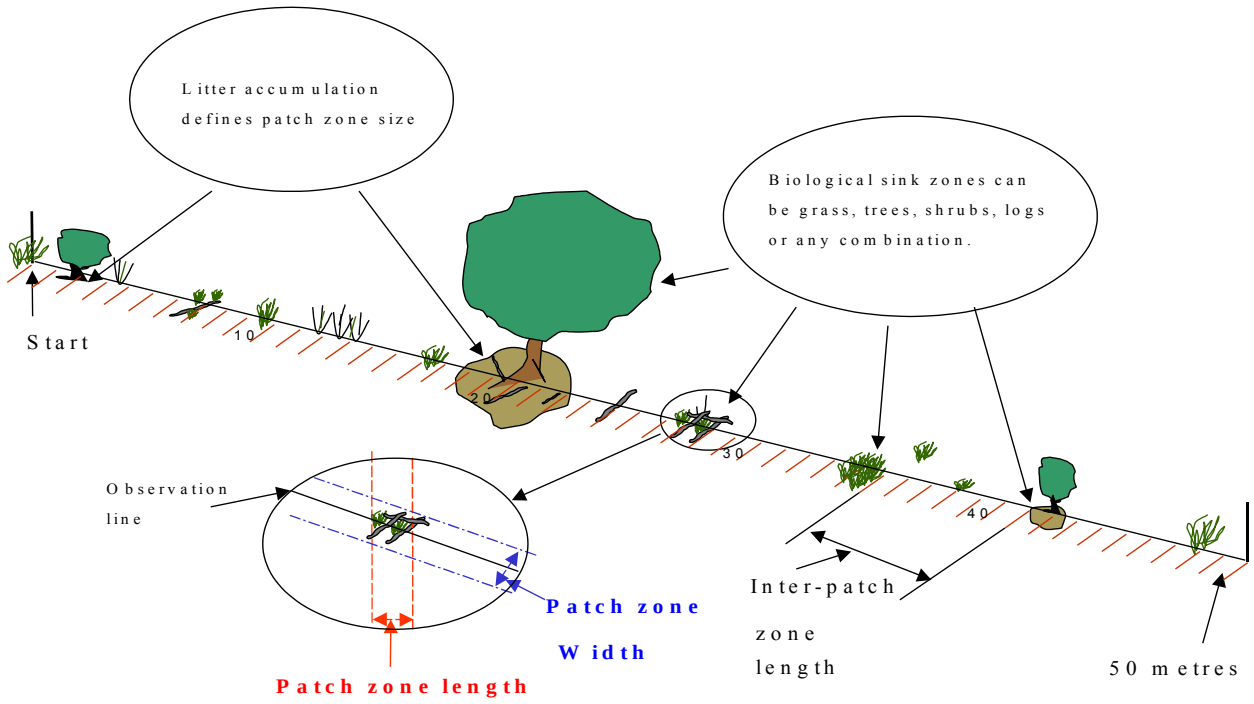

Figure 33: Landscape organisation schematic to illustrate, a transect layout, in the direction of resource flow and the various measurements necessary to conduct an LFA. (Tongway and Hindley, 2004; Tongway and Ludwig, 2011).

- **Landscape Function Analysis (LFA) Patch and Inter-patch Description**

The landscape organisation was described by making use of the required patches and inter-patches which represent the different sites. The different sites consist of a series of patches and inter-patches which will be described briefly.

The description used was the same description DS Malo used in 2012. This was done to ensure that the LFA was consistent, reliable and provided a consistency amongst multiple assessors.

Below is a short description of each of the patches and inter-patches used to define the landscape organisation.

➢ *Dense Grass Patch (DGP)*

Figure 34 indicates a simple dense grass patch (DGP) unit displayed by a single plant. The DGPs can overlap and form large distinct units; these units are primarily made up of living plants, perennial grasses and have strongly developed root tufts. DGPs may also be a grouping of plants growing closely together in a specific area.

Figure 34: Photograph displaying a dense grass patch, with measurements which indicate the extent of the patch. Photograph taken by Malo (2012), with permission.

- *Forb Patch (FbP)*

Forb patches (FbPs), as shown in Figure 35, are plant species that are not classified as grasses, such as *Sersia lancea.* The FbPs were not the most common patches found to be present on the fixed point sites. Throughout the LFA, the FbPs on the different sites varied in terms of species, size and length.

Figure 35: Photograph showing a single forb patch with measurements which indicate the extent of the patch. Photograph taken by Daniell (2014).

- *Grass Patch (GP)*

Figure 36 shows a single grass patch (GP) unit; it was one of the most frequent patches that occurred on the different sites. These patches also showed the most external variation. The GPs are often overlapped by plants or swards to form larger functional units and often comprise perennial grasses which have strong root tufts (Haagner, 2008). The GPs contribute significantly towards all LFA indices due to high functionality.

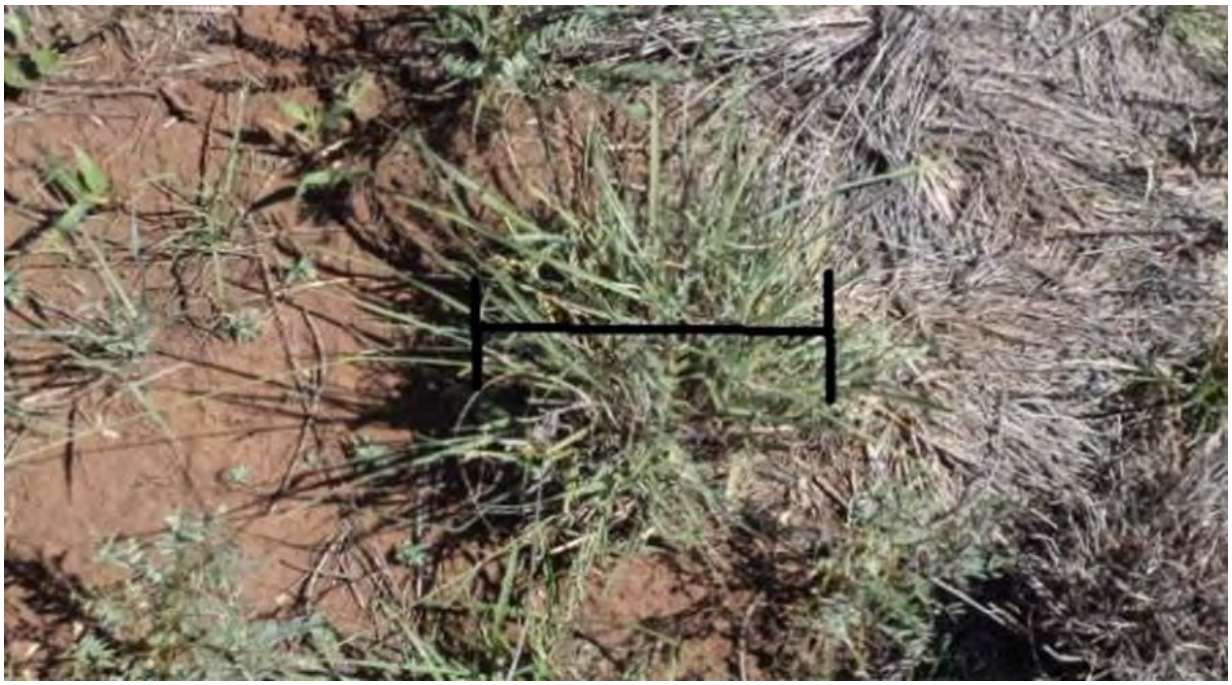

Figure 36: Photograph shows a single grass patch with measurements which indicate the extent of the patch. Photograph taken by Malo (2012), with permission.

- *Forb-Grass Patch (FGP)*

Forb-grass patches (FGPs) were identified by a mixture of forbs and grass species that grow in between one another. These patches generally consist of a great basal area, due to the large tufts of grasses covering a significant amount of area, which causes more resources to be trapped.

- *Litter Patch (LP)*

Litter patches (LPs), as shown in Figure 37, were found at all 12 fixed point sites. The LPs were identified by litter material without any living perennial plant material. The LPs contribute greatly to the infiltration and nutrient cycle abilities of the soil, but not the stability thereof, due to the fact that litter material is easily eroded, removed and burnt (Haagner, 2008).

Figure 37: Photograph displaying a litter patch with measurements which indicate the extent of the patch. Photograph taken by Malo (2012), with permission.

- *Grass-litter Patch (GLP)*

Grass-litter patches (GLPs), as displayed in Figure 38, consist of locally-produced litter within the perennial grass patches. It is essential to make sure that the litter comes in contact with the soil and plants, which is indicative that the litter forms part of the single plant unit to control the cycle and flow of mobile resources (Haagner, 2008).

The GLPs are considered highly functional due their ability to act as reservoirs for the accumulation of seeds, water and nutrients, and to reduce erosion by raindrops as well as create habitats for microorganisms and seed germination (Haagner, 2008). The GLPs also contribute towards the organic matter content of SOM-poor soils (Haagner, 2008).

- *Rock Patch (RP)*

Rock patches (RPs), as shown in Figure 39, consist of rock which is unbroken by soil and vegetation, and is bigger than two centimeters (Haagner, 2008).

Haagner (2008) stated that RPs may prevent the formation of physical crusting on the soil surfaces which would lower the infiltration and nutrient cycling abilities of the soil, as well as

contribute towards the stability of the landscape, but do not have an abundant effect on the infiltration and nutrient cycle of the soil.

The RPs provide shelter for macro invertebrates and microorganism which themselves play a highly functional role in the aeration of, and contribution to, the structure of the soil, and which might have an indirect effect on the nutrient cycle (Haagner, 2008).

Figure 38: Photograph showing a grass litter patch with measurements which indicate the extent of the patch. Photograph taken by Malo (2012), with permission.

- *Inter-patch (IP)*

Figure 40 shows an inter-patch (IP) which occurred at all the fixed point sites; it was the main IP which separated the patches from one another (Haagner, 2008). The IPs generally have high stability; however, most inter-patches have a low infiltration rate due to texture and surface crusting abilities. The IPs consist of bare soil patches with no covering whatsoever.

- *Dung Patch (DP)*

Dung patches (DPs), as displayed in Figure 41, were only found at the sites which were used for grazing. No DPs were found when DS Malo conducted the LFA in 2012 since the farm was sold to AngloGold Ashanti in 2012. The DPs contribute significantly towards the infiltration and

nutrient cycle abilities of the soil, but not the stability due to the fact that dung material is easily eroded, removed and burnt (Haagner, 2008).

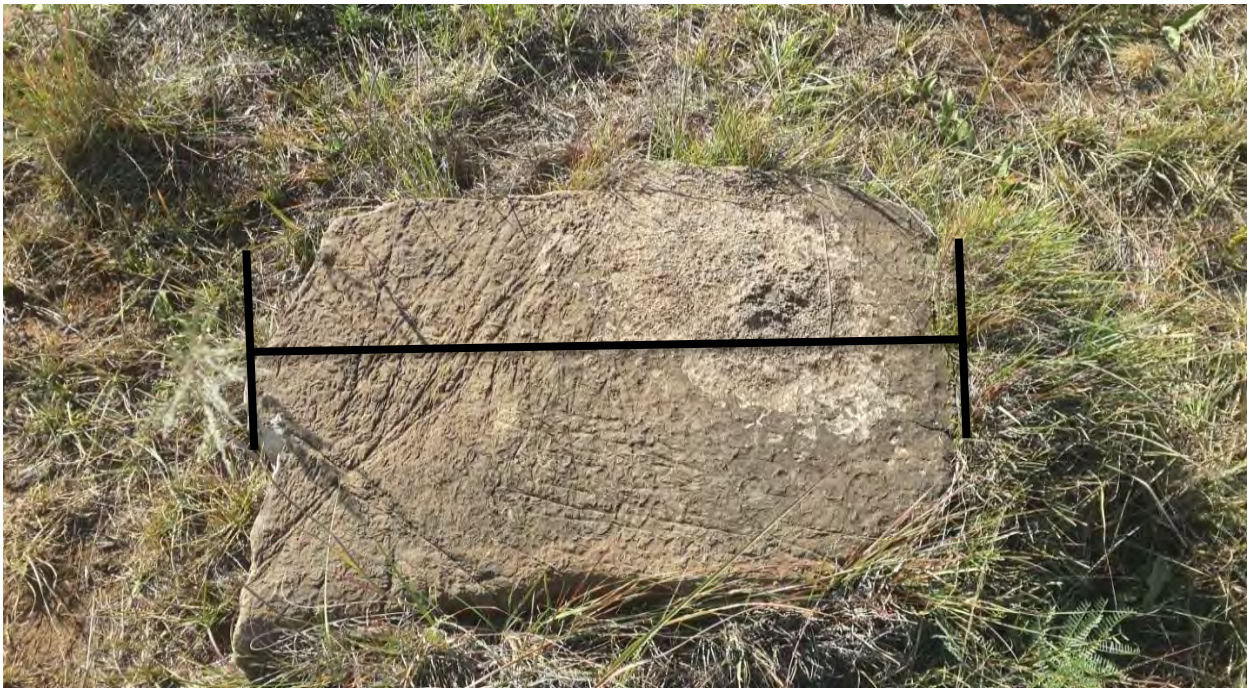

Figure 39: Photograph displaying a rock patch with measurements which indicate the extent of the patch. Photograph taken by Daniell (2014).

Figure 40: Photograph showing an inter-patch with measurements which indicate the extent of the patch. Photograph taken by Malo (2012), with permission.

Figure 41: Photograph showing a dung patch with measurements which indicate the extent of the patch. Photograph taken by Daniell (2014).

- *Seriphium plumosum Patch (SPP/SVP)*

Seriphium plumosum patches (SPPs), as shown in Figure 42, were found at five sites in this study. They consisted of individual/ clumps of *S. plumosum* (*Afr.* Bankrotbos). This is an indigenous grass to South Africa which is widley spread throughout the country. *S. plumosum* is an aggressive encroacher that mostly invades where overgrazing is prominent.

They contribute significantly to the LFA indices (Malo, 2012). The criterion according to which the SPPs were identified was that the plant must either come into contact or be very close to the soil surface in order to act as a resource catchment area for wind or water-borne resources (Malo, 2012).

- *Sparse Grass Patch (SGP)*

Sparse grass patches (SGPs), as displayed in Figure 43, constantly comprise annual grasses and semi-annual grasses (Haagner, 2008). The SGPs do not vary a great deal from the GPs but were identified mainly based on the botanical composition of the area (Haagner, 2008).

The SGP‘s litter cover mainly consisted of transported litter that accumulated at the base of the patch (Haagner, 2008). The SGPs were identified according to a high occurrence in low

efficiency areas, with low biomass, low resource retention capacity, and soils with amplified erosion and crusting abilities (Haagner, 2008).

Figure 42: Photograph showing a *Seriphium plumosum* patch with measurements which indicate the extent of the patch. Photograph taken by Daniell (2014).

Figure 43: Photograph showing sparse grass patches scattered over the area. Photograph taken by Daniell (2014).

- **Soil Surface Assessment**

The soil surface assessment (SSA) was conducted after the landscape organisation. During the SSA, five duplicates of each of the different patches recorded in the landscape organisation field data sheet were selected randomly, but preferably not too close to one another on the gradsect (a gradient-oriented transect). The SSA comprised 11 indicators as set out in Table 7 and was conducted at each of the selected patches. The SSA indicators were evaluated using the field procedure as set out in the LFA training manual v3.5. A class value is assigned to each indicator according to Tongway and Hindley (2004) and Tongway and Ludwig (2011). The datasets were inserted into a *Microsoft Excel* spreadsheet (LFA software Version 2.2), which was designed by Tongway and Hindley (2004) to automatically calculate the indices.

Table 7: SSA-11 indicators and the measurement of the objectives for the different SSA indicators (Tongway and Hindley, 2004; Haagner, 2008).

Indicator	Objective
1.Rainsplash Protection	Evaluate the degree to which the surface cover and projected plant cover ameliorate the effects of raindrops on the soil surface in terms of rainsplash, erosion and physical crust formation.
2. Perennial Vegetation Cover	Estimate the basal cover of perennial grasses and canopy cover of trees/shrubs to assess the contribution of the below-ground biomass.
3. Litter	Measure the amount, origin and degree of decomposing plant litter to evaluate the nutrient cycling of the soil.
4. Cryptogram Cover	Evaluate the cover of cryptograms visible on the soil surface, indicating soil stability and available nutrients.
5. Crust Brokenness	Evaluate the extent to which crust is broken, leaving loose, erodible soil material.
6. Erosion Type & Severity	Evaluate the type and severity of recent/current soil erosion.
7. Deposited Materials	Evaluate the nature and amount of alluvium transported and material deposited.
8. Soil Surface Roughness	Evaluate surface roughness for the ability to retain and capture mobile resources.
9. Surface Nature	Evaluate the ease with which the soil is mechanically disturbed to yield erodible material.
10. Slake Test	Evaluate the stability of natural soil fragments to rapid wetting.
11. Texture	Categorize the texture of surface soil, and compare this to permeability.

The following diagram (Figure 44) from Tongway and Hindley (2004) shows the 11 indicators which were measured during the SSA and how they contribute in different ways to the three LFA indices of stability, infiltration and nutrient cycling, which have significance for the landscape function.

Each patch and inter-patch functionality was calculated. The weighted mean for the transect line was also calculated in order for a comparison to be drawn with other transects. The patch and inter-patch values may be compared alongside a single transect line or with sawn-rowed patches and inter-patches on other transect lines (Malo, 2012).

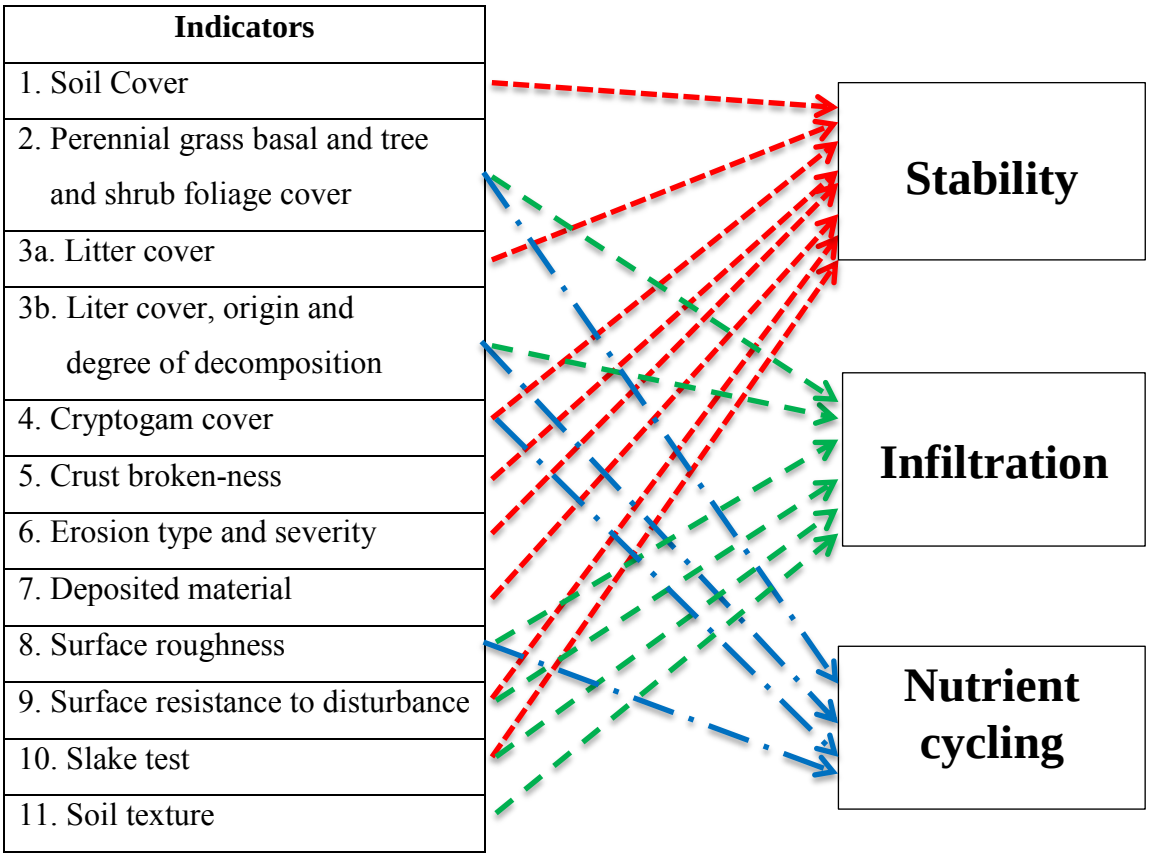

Figure 44: The 11 SSA indicators and the allocation of these indicators to the three LFA indices. (Tongway and Hindley, 2004).

The LFA software provided by Tongway and Hindley (2004) summarized the outputs as follows: (a) landscape organisation in three reflecting tables, (b) LFA soil surface assessment indices [stability, infiltration and nutrient cycle] (Figure 44) for each individual patch and inter-patch that was identified and measured in step 2-landscape organisation.

The functionality of the landscape as a biophysical division is best described by the various indicators that were measured during step 3-SSA (Table 7), which contributes to the three LFA indices in diverse ways (Figure 44).

The Landscape Organisation Index (LOI) is calculated from the landscape organisation in step 2. It is calculated by the division of the sum of the patch zone by the length of the transect line, in this case 20 m (Tongway and Ludwig, 2011). This was done in order to calculate the portion of the landscape that was covered with patches (Haagner, 2008).

- **Data Analyses**

According to Haagner (2008), the LFA software comprises the analytical calculation of the indices calculated at the patch and inter-patch scale with their standard error values. These values can be compared over time for different transects; however, these values do not provide a complete assessment of the functionality of the landscape (Haagner, 2008).

The three indices that were used and compared using *Microsoft Excel* 2010 and *CANOCO* 4.5 were stability, infiltration and nutrient cycling.

3.8.5 Descending Point Method

The Descending-Point Method was done by setting out transects with regular point intervals (one meter) at the 12 FPs in the same three directions used in the LFA in order to compare the data. This method involves the recording of the nearest basal cover in a 30 cm radius and a hit can be only noted when the point of the spike strokes the root area of the basal cover.

CHAPTER 4: SOIL ANALYSES RESULTS AND DISCUSSION

All soil analyses were completed as outlined in Chapter 3 of this report. The soil data were used to monitor the pollution in the study area in terms of quality and quantity. The soil evaluations for the 30-month monitoring period were compared at monthly intervals in order to determine whether the pollution process on the soil did indeed decline or cease.

4.1 BASELINE ASSESSMENT

The tables in Appendix A1 show the results of the baseline assessment of this study, which show that the composite samples were representative for the 11 samples taken around the FP and that the composite sample can be used to represent the whole FP in its entirety. Therefore, it was recommended that only one thoroughly mixed composite sample would suffice.

There are a few variations in the EC and pH values of the composite and the average of the 11 samples at the beginning and end of the sampling period. This is mainly due to the presence of shale lenses within the Oaktree Formation dolomites, as shown in Figure 45, which alter the EC and pH values slightly. These shale lenses do not outcrop frequently, although they have a significant effect on the soil analysis results such as an increase in sodium.

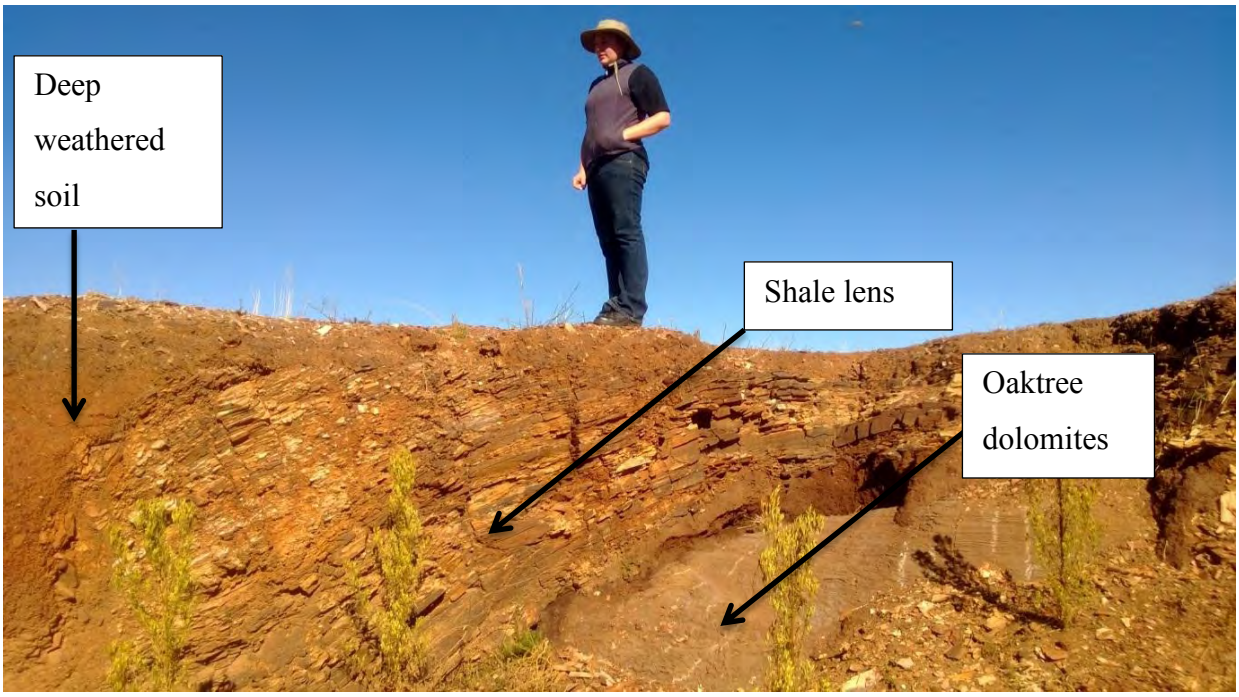

Figure 45: Photograph showing a shale lens within the Oaktree Formation dolomites in a borrow pit in the study area. Photograph taken by Boneschans (2013), with permition.

4.2 pH

The pH of the soil was slightly acidic to slightly alkaline, with neutral values being dominant; the pH values of the FP and transect lines ranged between 5 and 9 throughout the monitoring period. This is an indication that bicarbonate is the most significant carbonate species present in the soil moisture water (Sweeting, 1972). The dolomitic bedrock of the Oaktree Formation buffers the acidity generated from the MWS No.5 TDF and ensures the neutral to alkaline nature of the soil (Ratlhogo, 2011). This is an important ability due to the mobilization of pollutants such as trace metal elements in to the groundwater which, in this case, is not an issue as stated by Ritchie (2005):

"The presence of calcitic minerals and soils with high acid buffer capacity in and around the tailings facility is desirable to neutralise acidic seepage water and thereby precipitating heavy metals in solution".

4.3 ELECTRICAL CONDUCTIVITY (EC)

The complete monitoring of EC values of the soil samples are shown in Appendix B, from August 2011 to January 2014. The EC of FP-1 and -6 are shown in Figure 46 before the No. 5 TDF became dormant. The EC values of only August 2011, 2012 and 2013 are shown in Figure 47 to Figure 50 in order to display the overall trends in EC values over the years.

From Figure 46 and Figure 47, it is clear that FP-1 and -6 EC values decreased dramatically from August 2010 to August 2011 after the TDF became dormant (April 2011), decreasing from 11 683.2 mS/m (FP-1) and 3289.6 mS/m (FP-6) to 57.04 mS/m (FP-1) and 39.56 mS/m (FP-6), respectively. Figure 47 shows that the EC values for FP 1 and 6 are significantly higher than the EC values for the other FP and control sites, but never exceed the critical (high risk) EC value of 360 mS/m. There is a general decrease in EC values for all of the FPs from the beginning (August 2011) to the end (January 2014) of the monitoring period, as shown in Appendix B1 and B2. As shown in Appendix B1, a definite increase for the FP from September 2011 to December 2011 can be seen, which can be attributed to rainfall pattern throughout the year.

According to Hillel (1998), water infiltrates the soil and the infiltrated water dissolves additional solutes. As the water moves through the profile, it carries the solute loads to the groundwater and leaves some of the solutes behind in the soil, and in some cases precipitates where the solute

concentrations exceed their solubility. This concept explains why the EC values increase during the dry seasons and decrease during the wet periods.

The EC values for the control sites as shown in Appendix B2 do not show major increases during the monitoring period; this is due to the fact that these sites do not lie in the pollution plume zone and the EC values for the control sites do not exceed 35 mS/m throughout the monitoring period.

From Figure 48, it is clear that none of the sample sites exceeded the high risk EC value (360 mS/m); however, NS-08 and -09 values were dramatically higher than the other sample site values. The EC values for all the north-south transect line sample sites decreased from August 2011 to November 2013 (Appendix B3).

Transect line east-west 1 (Figure 49) shows elevated levels at site EW1-06 in August 2011, with a significant decrease in August 2013. The EC values for all the samples sites of the east-west 1 transect showed a significant decrease from August 2011 to November 2013 (Appendix B4). Figure 50 shows that none of the east-west transect 2 line sample sites exceeded the high risk EC value, with EC elevated levels for sample sites EW2-16, -17, -18, -19, -37 and -43; however, these values are acceptable. The general pattern for transect line EW2 shows an overall decrease in EC from August 2011 to November 2013, as shown in Appendix B5.

The overall trend of the EC values for all the FP and transect line samples shows a clear decrease in EC values from 2010 to January 2014.

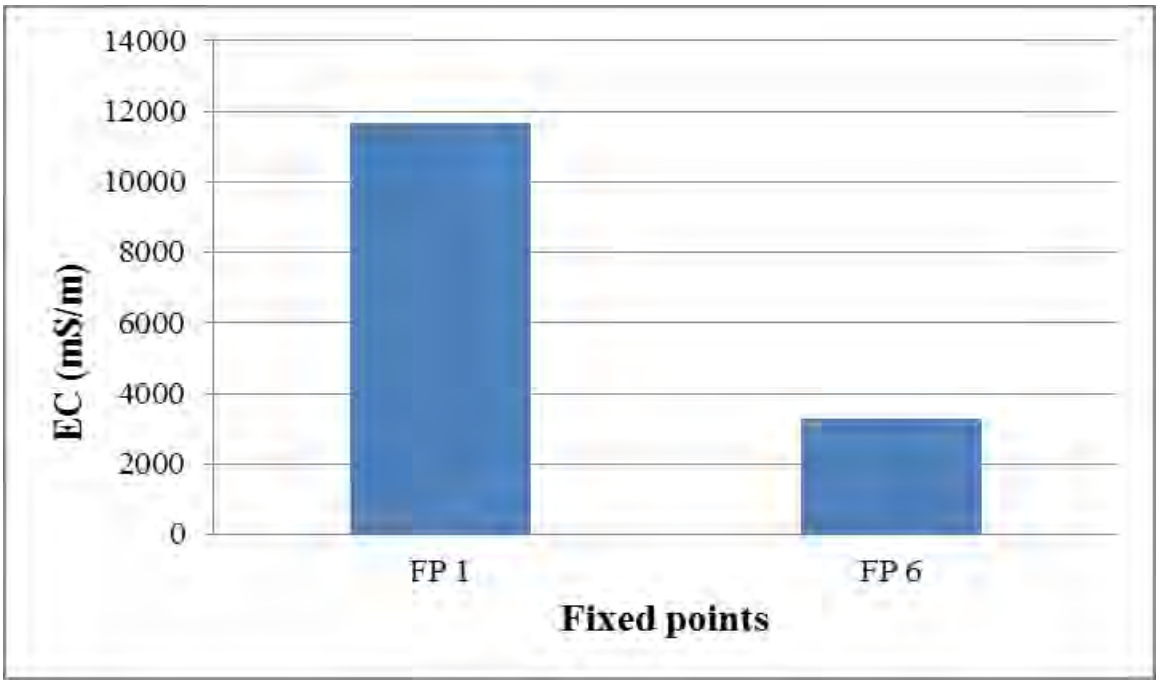

Figure 46: Electrical conductivity of FP–1 and -6 in August 2010 (Van Deventer, 2011b).

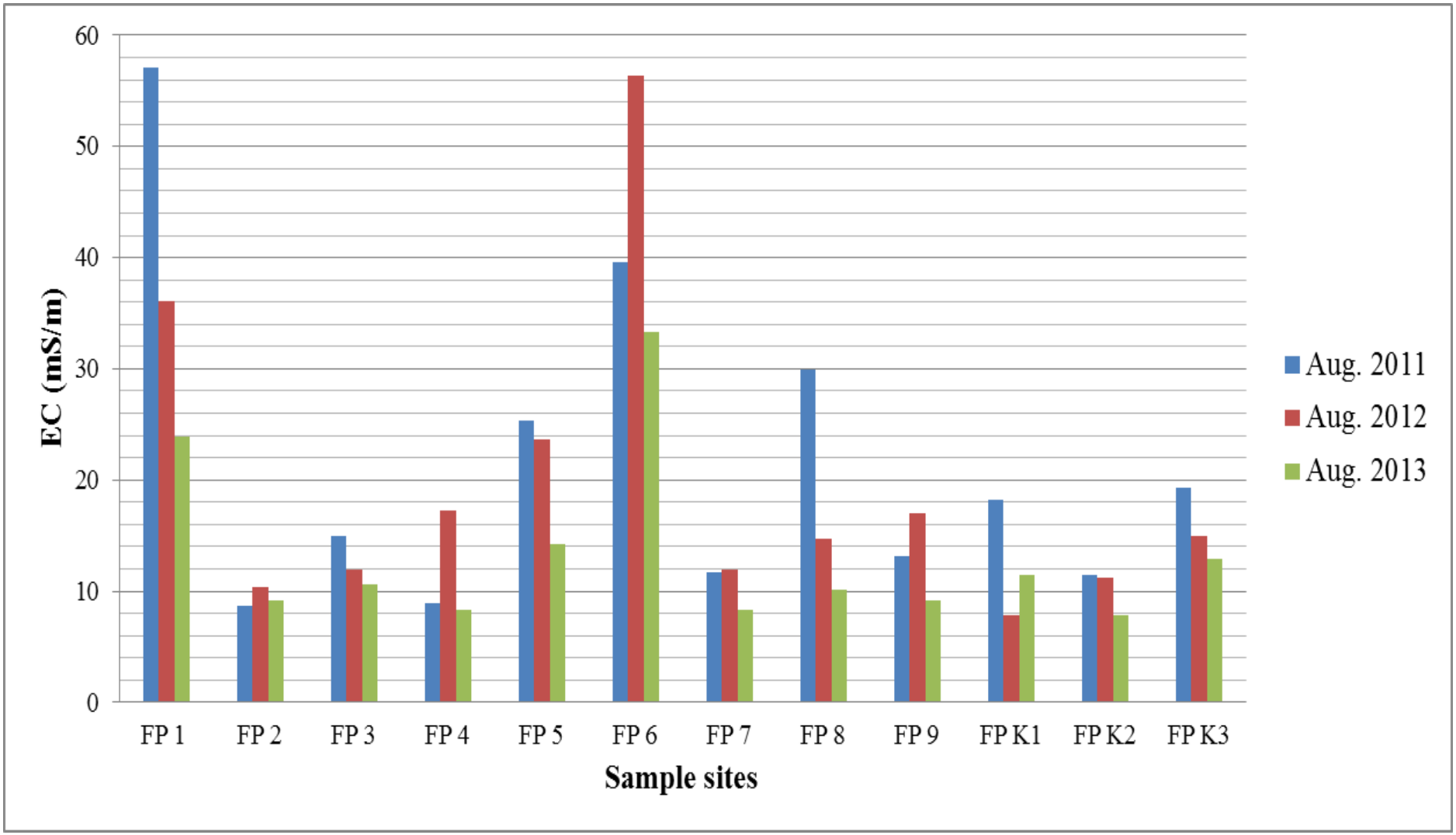

Figure 47: Electrical conductivity (EC) of the nine FPs and three control sites in August 2011, 2012 and 2013.

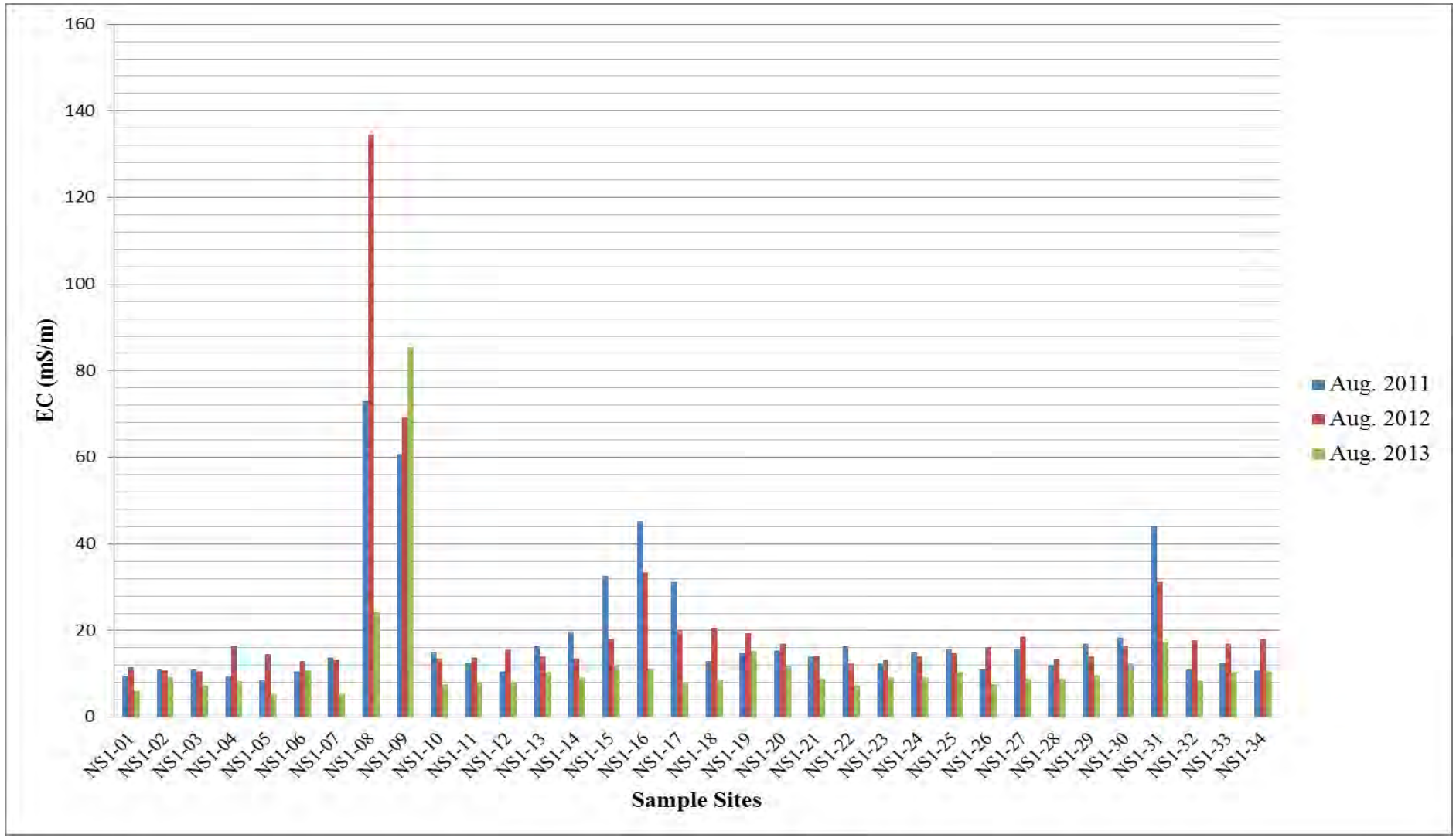

Figure 48: Electrical conductivity of the north-south transect line in August 2011, 2012 and 2013.

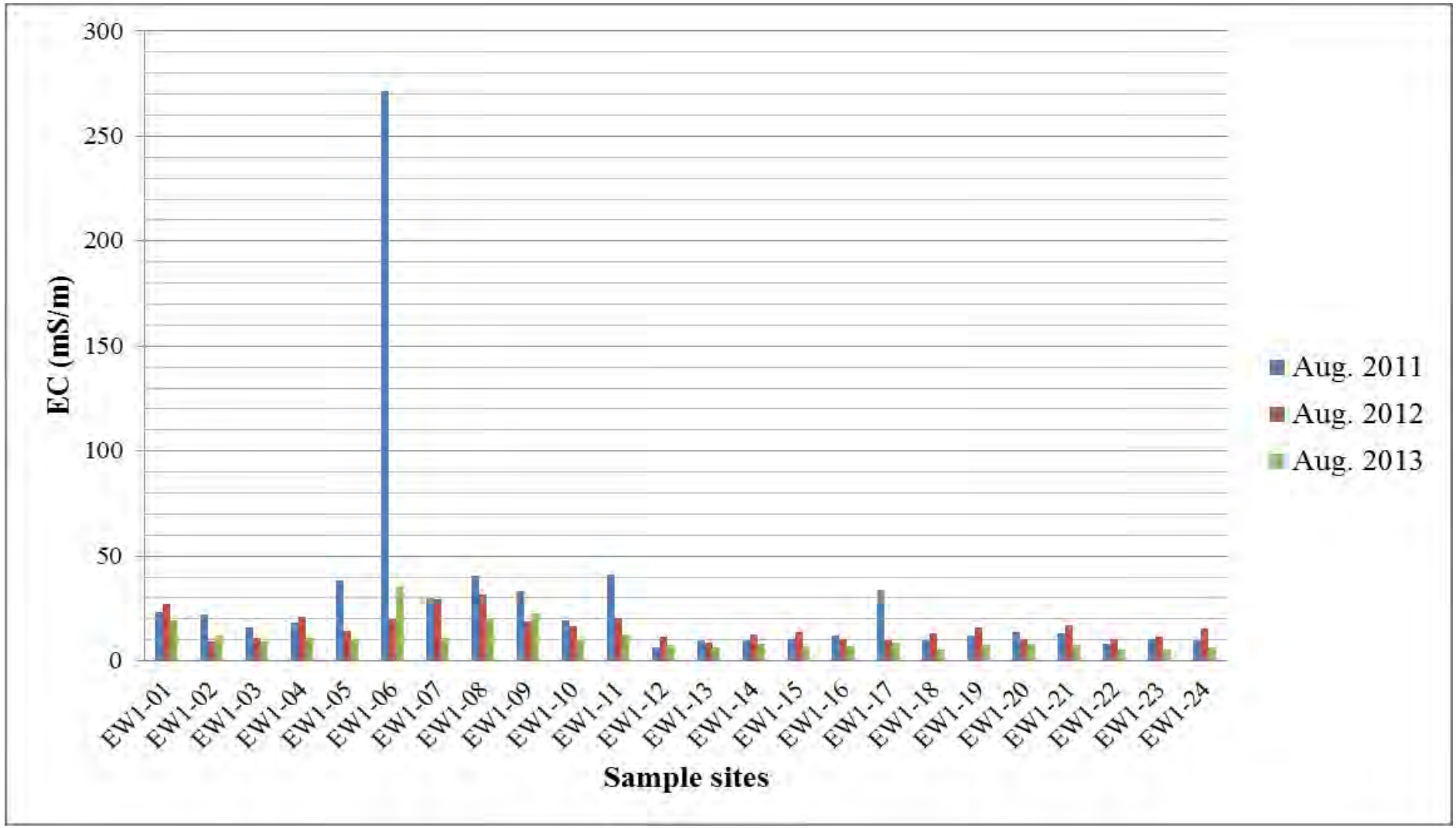

Figure 49: Electrical conductivity of east-west 1 transect line in August 2011, 2012 and 2013.

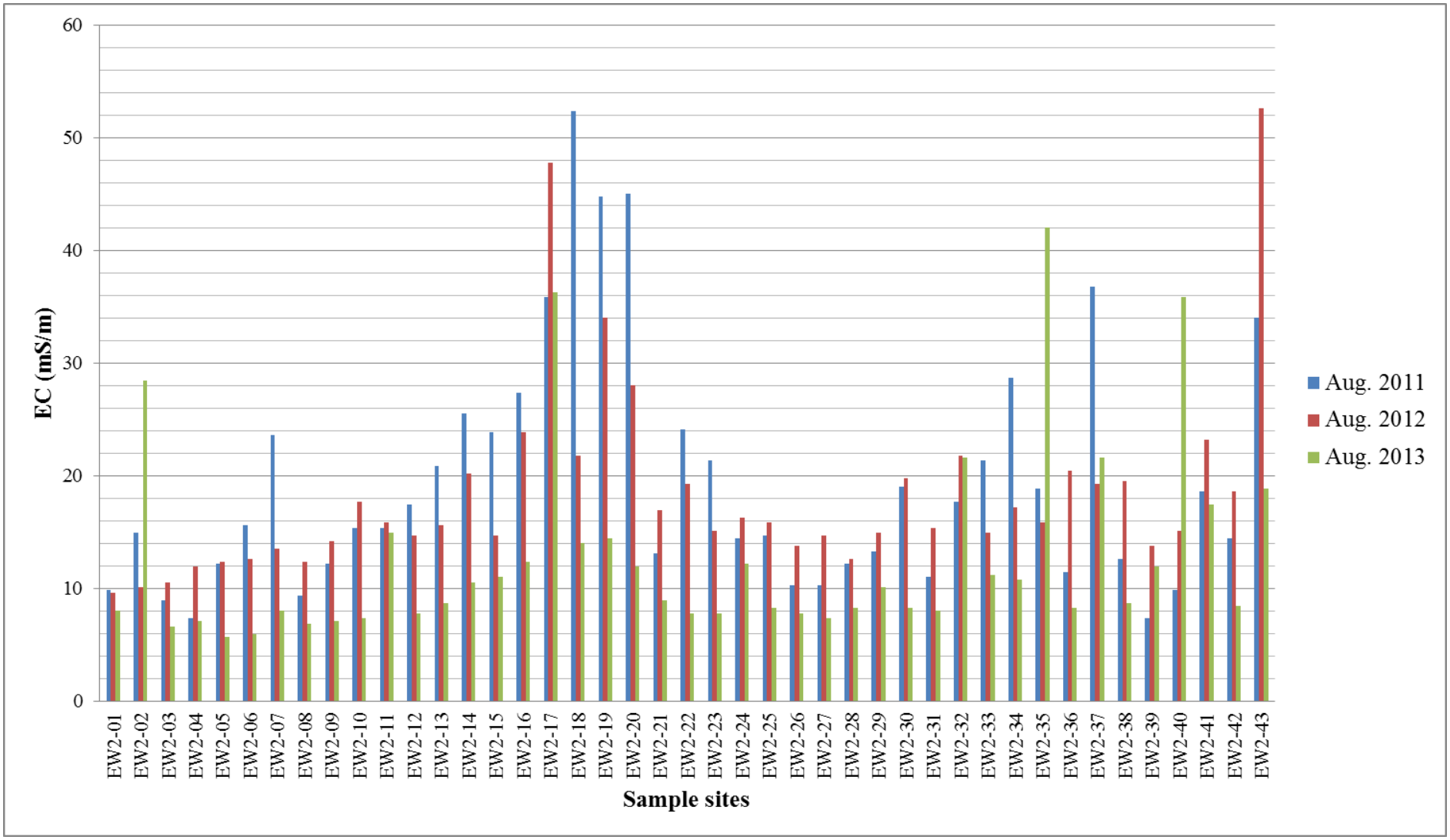

Figure 50: Electrical conductivity of the east-west 2 transect line in August 2011, 2012 and 2013.

4.4 EXCHANGEABLE CATION AND CATION EXCHANGE CAPACITY (CEC)

The exchangeable cations, CEC and calculations of the 12 FP samples in 2012 and 2013 are shown in Appendix C. Figure 51 and Figure 52 depicts the exchangeable cations and CEC values for all the FPs and control sites in 2012 and 2013, respectively. FP-6 shows the highest exchangeable cations and CEC values for 2012 and 2013 due to the higher amount of clays within the soil. According to Metson (1961, cited by Hazelton and Murphy, 2007), the CEC values for all the FPs and control sites for 2012 and 2013 can be grouped within the low to moderate CEC values, ranging from 6-25 cmol(+)/kg. This is mainly due to the low clay content of the FP and control site soils.

The Ca^{2+} (cmol(+)/kg) of all the sites, with the exception of FP-6 in 2012 (20.05 cmol(+)/kg), are classified according to Metson (1961, cited by Hazelton and Murphy, 2007) as low to moderate, ranging from 2-10 cmol(+)/kg.

The Mg^{2+} (cmol(+)/kg) for all the sites, with the exception of FP-6 (13.57 cmol(+)/kg in 2012 and 10.87 cmol(+)/kg in 2013, which is classified as very high), varied from low to high (0.3-8 cmol(+)/kg) from 2012 to 2013 (Metson, 1961, cited by Hazelton and Murphy, 2007).

The K^{+} (cmol(+)/kg) for all the sample sites are classified as very low to moderate, ranging from 0-0.7 cmol(+)/kg (Metson, 1961, cited by Hazelton and Murphy, 2007).

The Na^{+} (cmol(+)/kg) for all the sites, with the exception of FP-9 in 2013 (1.34 cmol(+)/kg), are classified as very low to low, ranging from 0-0.3 cmol(+)/kg (Metson, 1961, cited by Hazelton and Murphy, 200).

Table 8 and Table 9 display the proportion of cations as a percentage of effective CEC. Effective CEC values are the sum of all the exchangeable cations that were measured (Hazelton and Murphy, 2007).

According to Abbott (1989, cited by Hazelton and Murphy, 2007) and (FSSA, 2007), the Ca^{2+} as a percentage of effective CEC in 2012 for the 12 FPs is in close approximation to the optimal range of 60-80%, for some FPs being lower than the range percentage (Table 8); however, these percentages are still acceptable, and in 2013 the Ca^{2+} percentages increased significantly.

The 2012 and 2013 (as displayed in Table 8 and Table 9) Mg^{2+} percentages are significantly higher than the range percentage presented by Abbott (1989, cited by Hazelton and Murphy, 2007) of 10-15%; however, the South African standards for Mg^{2+} as a percentage of effective

CEC range between 20-25% (FSSA, 2007). Although the Mg^{2+} percentages exceed the FSSA (2007) range it is common for the percentages to exceed the standard in the presence of dolomitic bedrock, such as in this case.

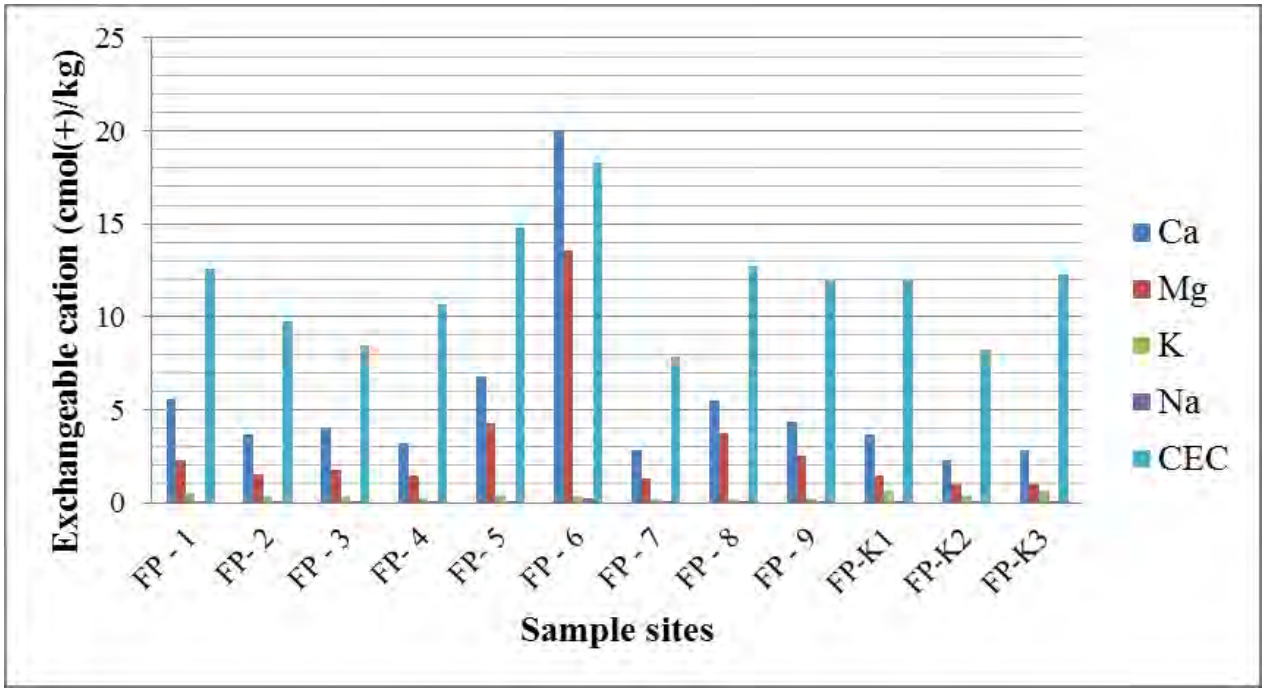

Figure 51: Exchangeable cations and cation exchange capacity (CEC) of the fixed points and control sites in 2012.

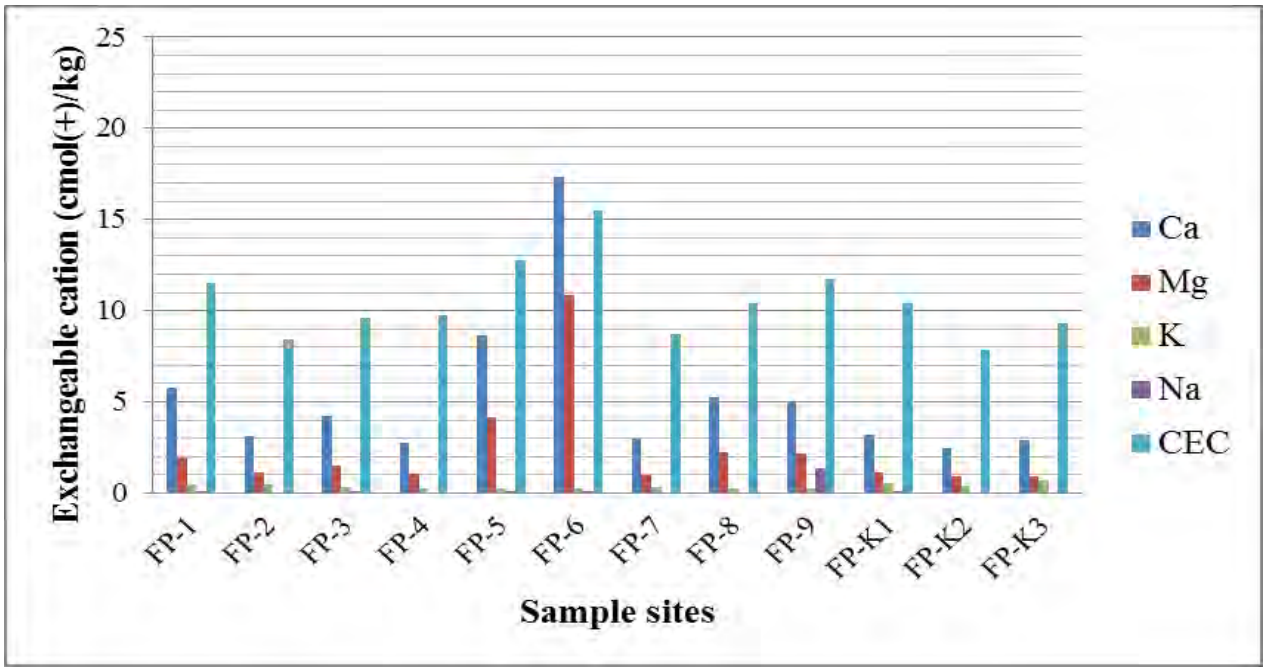

Figure 52: Exchangeable cations and cation exchange capacity (CEC) of the fixed points and control sites in 2013.

The K^+ percentages for all the FPs in 2012 and 2013 vary from 0.9-15.7%. Some of these percentages fall within the ranges of the percentage presented by Abbott (1989, cited by Hazelton and Murphy, 2007) of 1-5%, and the FSSA (2007) percentage of 6-10%; however, field experts commonly argue that the K^+ percentage relative to the CEC should normally be 12% for optimal plant transpiration to occur.

Therefore none of the percentages exceed or fall short of the percentages ranges given for K^+ as there is a lot of controversy in this regard. The Na^+ percentages for all the FPs in 2012 and 2013, except for FP-9 in 2013, do not exceed the ranges presented by Abbott (1989, cited by Hazelton and Murphy, 2007) of 0-1% and the FSSA (2007) of < 5%. This indicates that dispersion [> 15 exchangeable sodium percentage (ESP)] in these areas is not a concern and that sodicity is not relevant.

According to the FSSA (2007), the Ca:Mg ratio values that are commonly considered as normal/standard range between 1.5-4.5. All the FPs for 2012 and 2013 fall within the range, therefore this is not a concern in this case.

Table 8: Proportions of cations to the effective cation exchange capacity (CEC) and Ca:Mg ratio of the 12 fixed points in 2012.

	Ca/Effective CEC	**Mg/Effective CEC**	**K/Effective CEC**	**Na/Effective CEC**	**Ca:Mg ratio**
	(65-80%)	(10-15%)	(1-5%)	(0-1%)	
FP-1	65.71	27.13	6.25	0.83	2.42
FP-2	66.36	28.00	5.27	0.36	2.37
FP-3	65.90	28.52	5.25	0.33	2.31
FP-4	66.43	29.12	4.10	0.21	2.28
FP-5	59.38	37.22	3.33	0.09	1.60
FP-6	58.67	39.71	0.99	0.61	1.48
FP-7	65.23	30.44	3.89	0.23	2.14
FP-8	58.36	39.76	1.60	0.21	1.47
FP-9	60.95	35.42	3.49	0.14	1.72
FP-K1	64.00	24.94	10.99	0.17	2.57
FP-K2	62.99	26.52	10.22	0.28	2.38
FP-K3	63.07	22.73	14.04	0.22	2.77

Table 9: Proportions of cations to the effective cation exchange capacity (CEC) and Ca:Mg ratio of the 12 fixed points in 2013.

	Ca/Effective CEC	**Mg/Effective CEC**	**K/Effective CEC**	**Na/Effective CEC**	**Ca:Mg ratio**
	(65-80%)	(10-15%)	(1-5%)	(0-1%)	
FP-1	70.1	23.9	5.7	0.2	2.9
FP-2	66.3	24.3	9.5	0.0	2.7
FP-3	69.9	25.0	5.0	0.2	2.8
FP-4	67.4	26.3	5.9	0.0	2.6
FP-5	66.2	31.7	1.9	0.1	2.1
FP-6	60.7	38.2	0.9	0.2	1.6
FP-7	70.0	22.6	7.1	0.0	3.1
FP-8	67.9	28.9	3.0	0.0	2.3
FP-9	57.3	24.8	2.8	15.1	2.3
FP-K1	66.4	22.7	10.8	0.2	2.9
FP-K2	66.4	24.0	9.6	0.0	2.8
FP-K3	64.8	19.7	15.7	0.0	3.3

4.5 TOTAL MACRO ELEMENT CONCENTRATION

The total macro element concentrations were determined using the EPA 3050B (1996) method. Eco-Analytica conducted the analyses and measured the total macro element concentrations using an ICP-MS, the same as the method described in Chapter 3.3.7.

The total macro element concentrations of the 12 FPs are shown in Figure 53 to Figure 65. All the FP sites show high concentrations of macro elements in August 2011, January to May 2012 and again in January 2014. The overall lowest concentrations of macro elements, for all the FP sites, were found in November and December 2011.

Figure 53 shows an increase in macro element concentrations from January to April 2012, which might be due to the fluctuating water table in the area. The high Ca^{2+} of FP-1 can be explained by the dissolution of the dolomitic bedrock. The overall trend shows an increase in macro element concentration from the beginning to the end of the monitoring period however this increase is not statistically worthwhile. Figure 54 shows a raise in macro element concentrations

from January to April 2012. The high Ca^{2+} of FP-2 can also be explained by the dissolution of the Oaktree dolomitic bedrock of this area. Most of the macro element concentrations (Figure 54) show an increase from the beginning to the end of the monitoring period, with the exception of Ca^{2+} that decreased slightly.

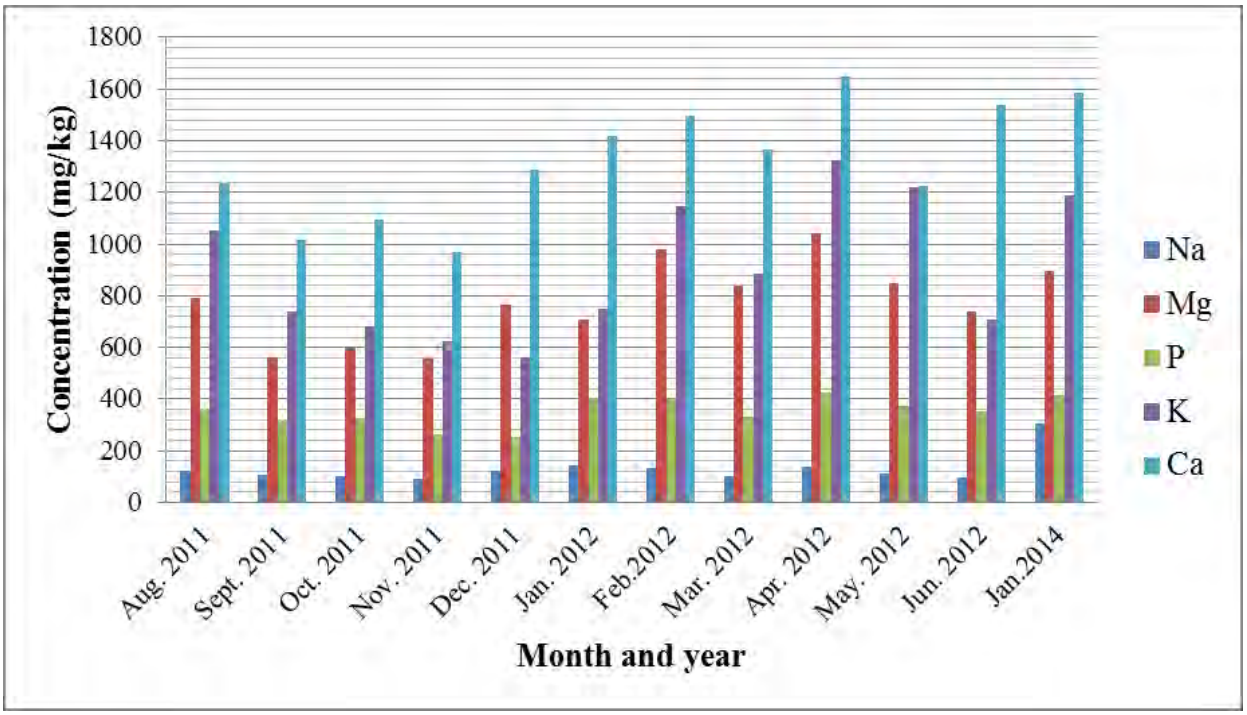

Figure 53: Total macro element concentration for FP-1 (EPA 3050B, 1996).

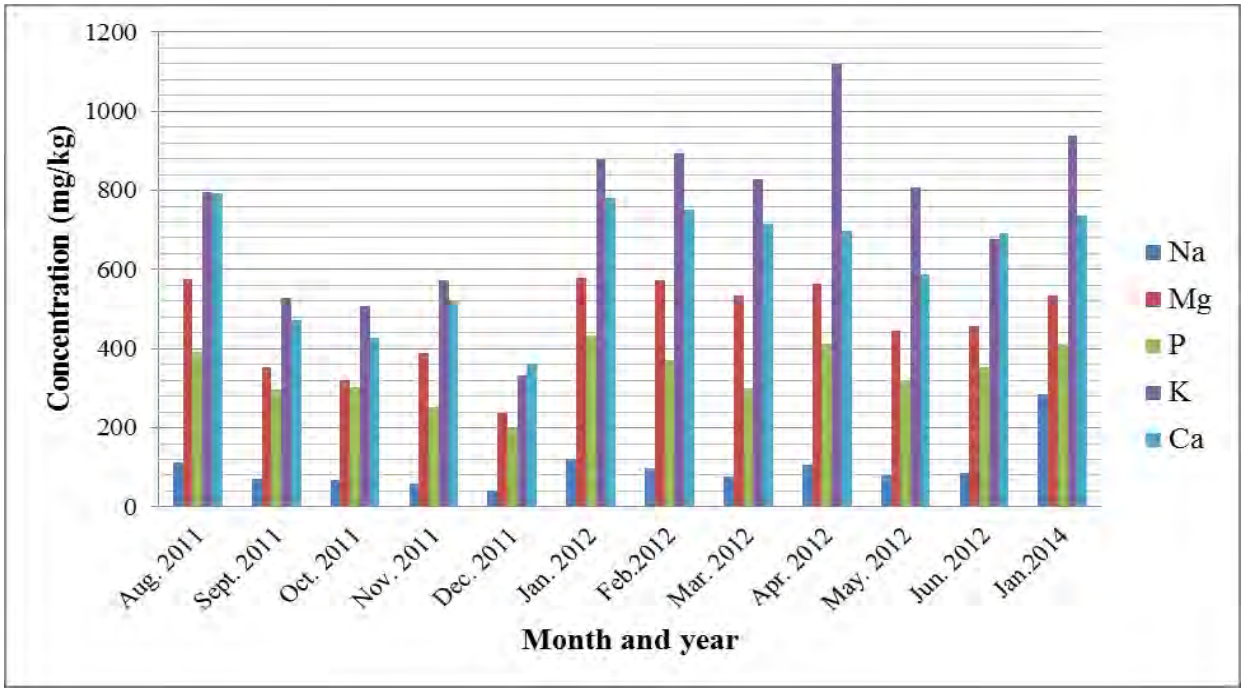

Figure 54: Total macro element concentration for FP-2 (EPA 3050B, 1996).

Figure 55 shows an increase in macro element concentration in January to April 2012 which, similar the other FPs, can be contributed to seasonal changes that occur. The macro element concentration also increased from the beginning to the end of the monitoring period (Figure 55).

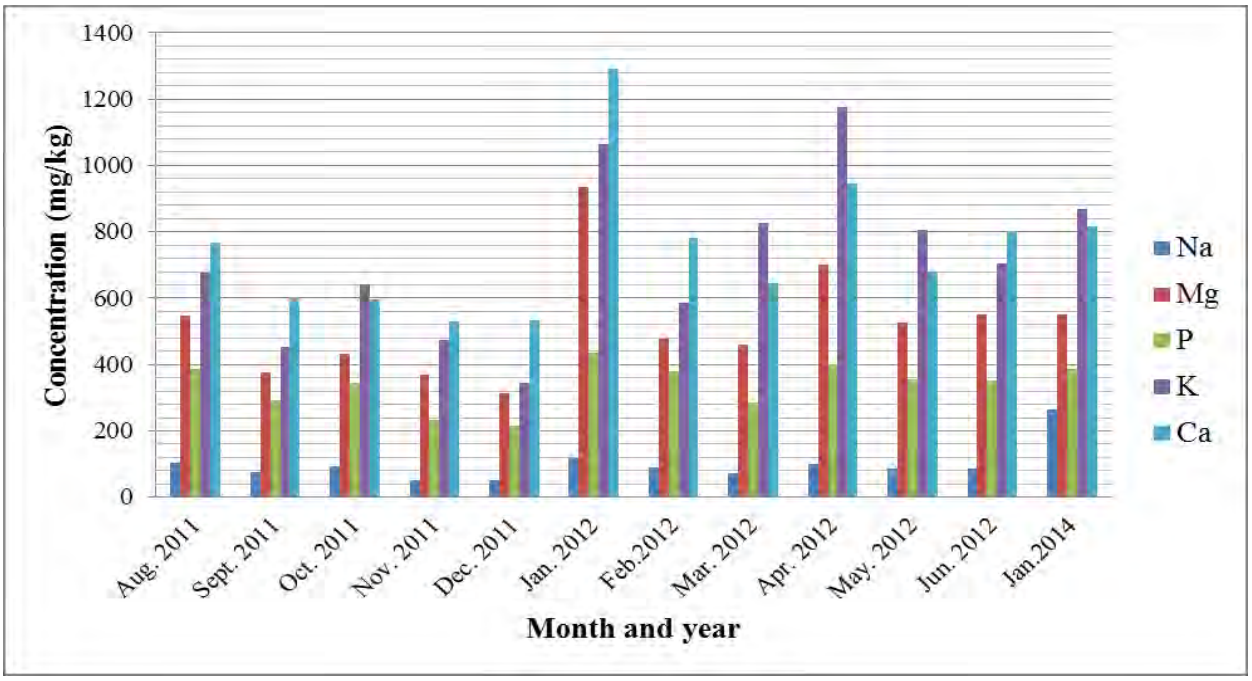

Figure 55: Total macro element concentration for FP-3 (EPA 3050B, 1996).

Figure 56 also shows an increase in macro element concentrations from January to April 2012. The Mg^{2+} and Ca^{2+} concentrations showed an increase in November 2011 (Figure 56).

The overall trend shows an increase in total macro element concentration from the beginning to the end of the monitoring period (Figure 56).

Figure 57 shows a steady decrease in macro element concentration from August to December 2011 and shows a significant increase again from January 2012, after which it remained constant.

The Ca^{2+} and Mg^{2+} concentrations of FP-5 are the second highest of all the FPs, while concentrations in FP-6 are the highest. However, these two FPs lie in close range to each other as indicated in Figure 16. The overall trend shows an increase in total macro element concentrations from the beginning to the end of the monitoring period.

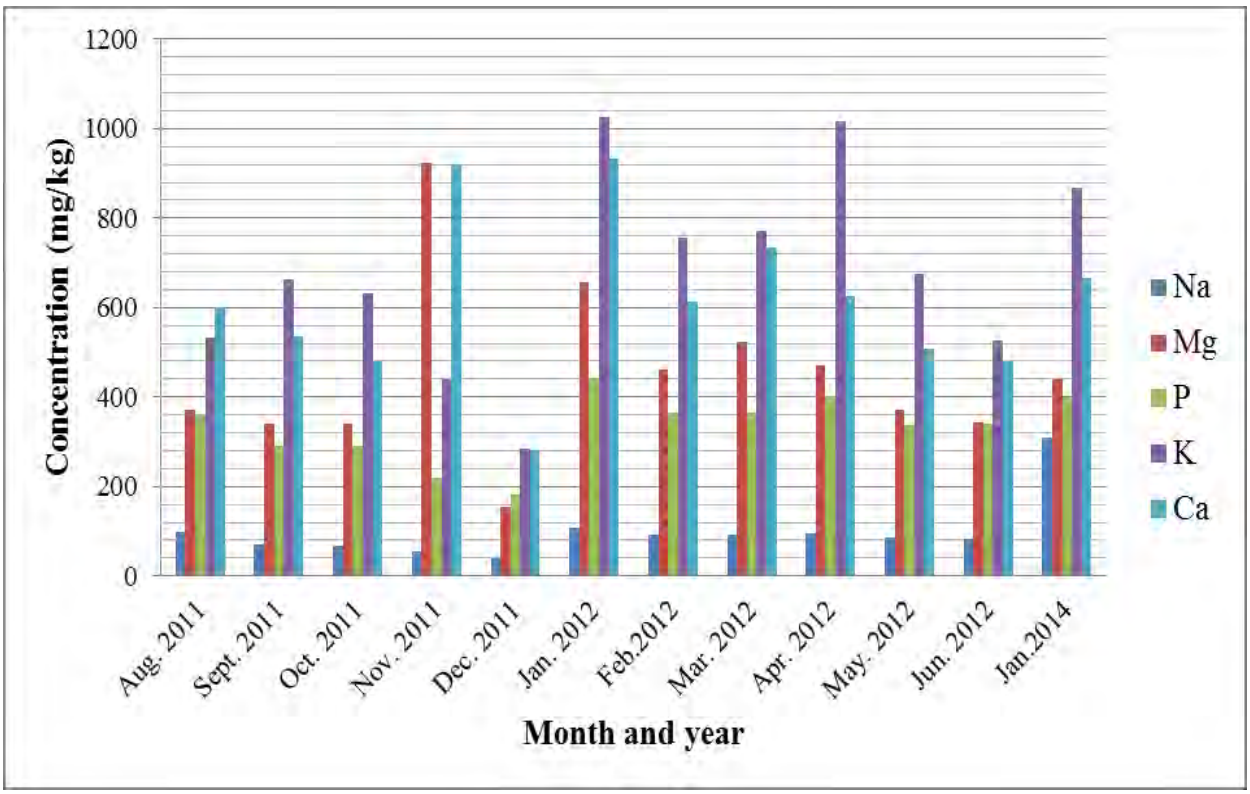

Figure 56: Total macro element concentration for FP-4 (EPA 3050B, 1996).

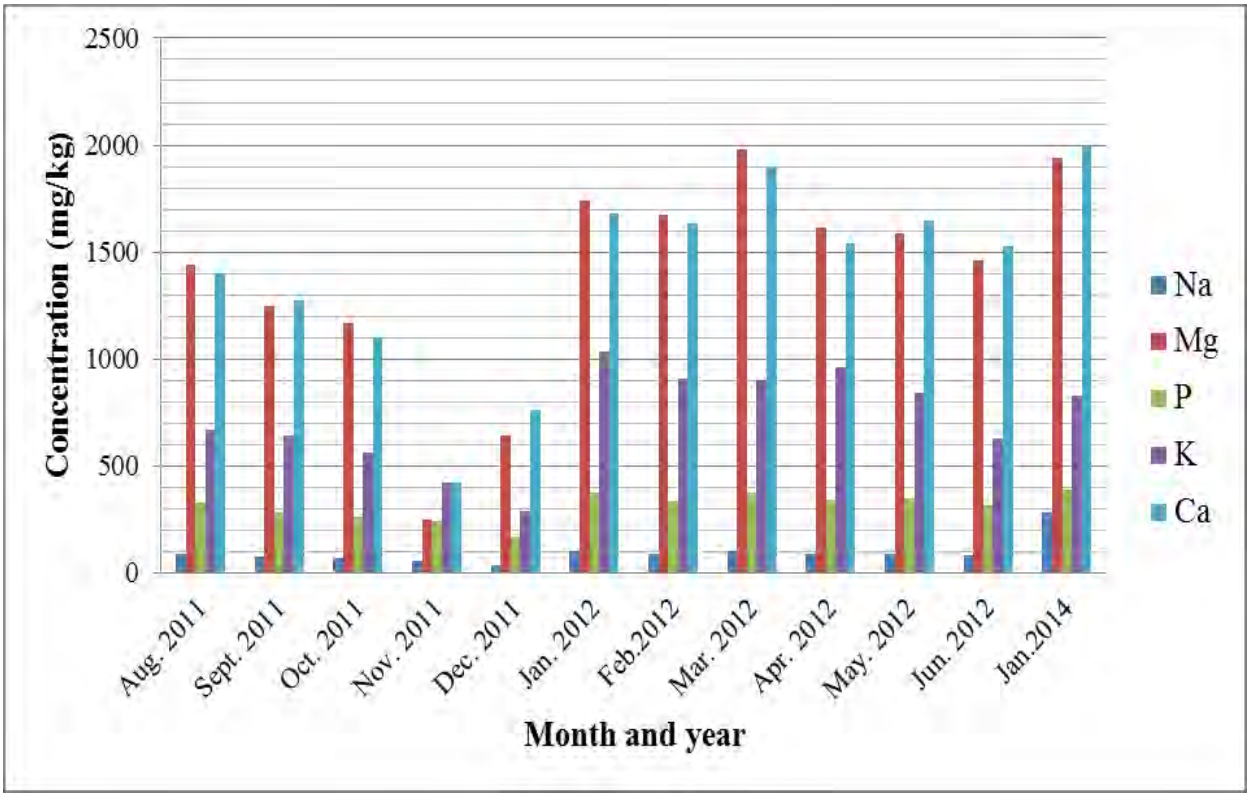

Figure 57: Total macro element concentration for FP-5 (EPA 3050B, 1996).

Figure 58 only shows the concentrations of Ca^{2+} and Mg^{2+} of FP-6 due to the extremely lower concentrations of the other macro elements which are displayed in Figure 59. These higher concentrations of Ca^{2+} and Mg^{2+} for both FP-5 and FP-6 (Figure 57 and Figure 58) may be due to the excess smectite, other 2:1 clays and manganese oxides present in these areas. Fixed point-5 and -6 lies in low lying areas therefore the soil is darker in colour, while the remaining FPs display a red brownish colour.

Figure 58 and Figure 59 show an increase in macro element concentrations from January to April 2012. Figure 58 and Figure 59 also reveal that the overall trend increased in total macro element concentration from the beginning to the end of the monitoring period.

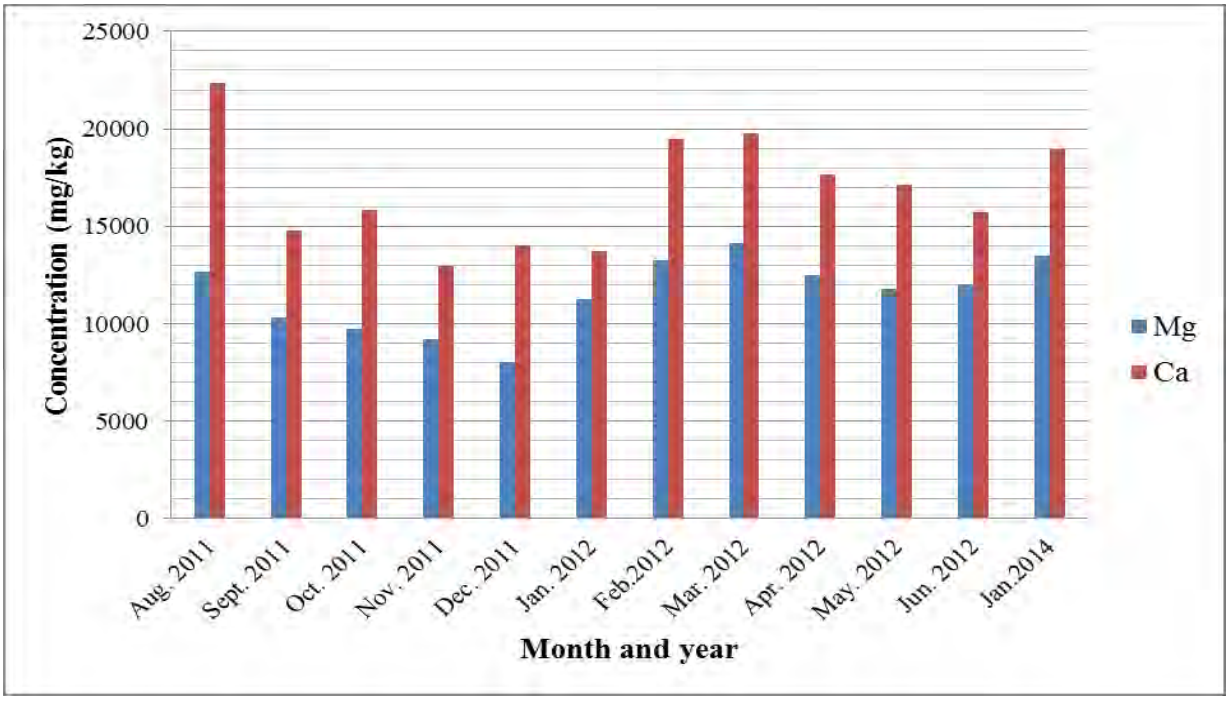

Figure 58: Total macro element (Mg^{2+} and Ca^{2+}) concentration for FP-6 (EPA 3050B, 1996).

Figure 60 shows the second lowest concentrations for macro elements of all the FPs, with FP-K2 showing the lowest values. Figure 60 shows the same trend as all the other FPs with increased concentrations from January to May 2012, and also shows an increase in concentrations from the beginning to the end of the monitoring period. Figure 61 and Figure 62 show a decrease in macro elements from August to December 2011, where after the concentrations increased again from January 2012 to June 2012. Both Figure 61 and Figure 62 show an increase in concentrations from the beginning to the end of the monitoring period. The increase and decrease are not statistically worthwhile.

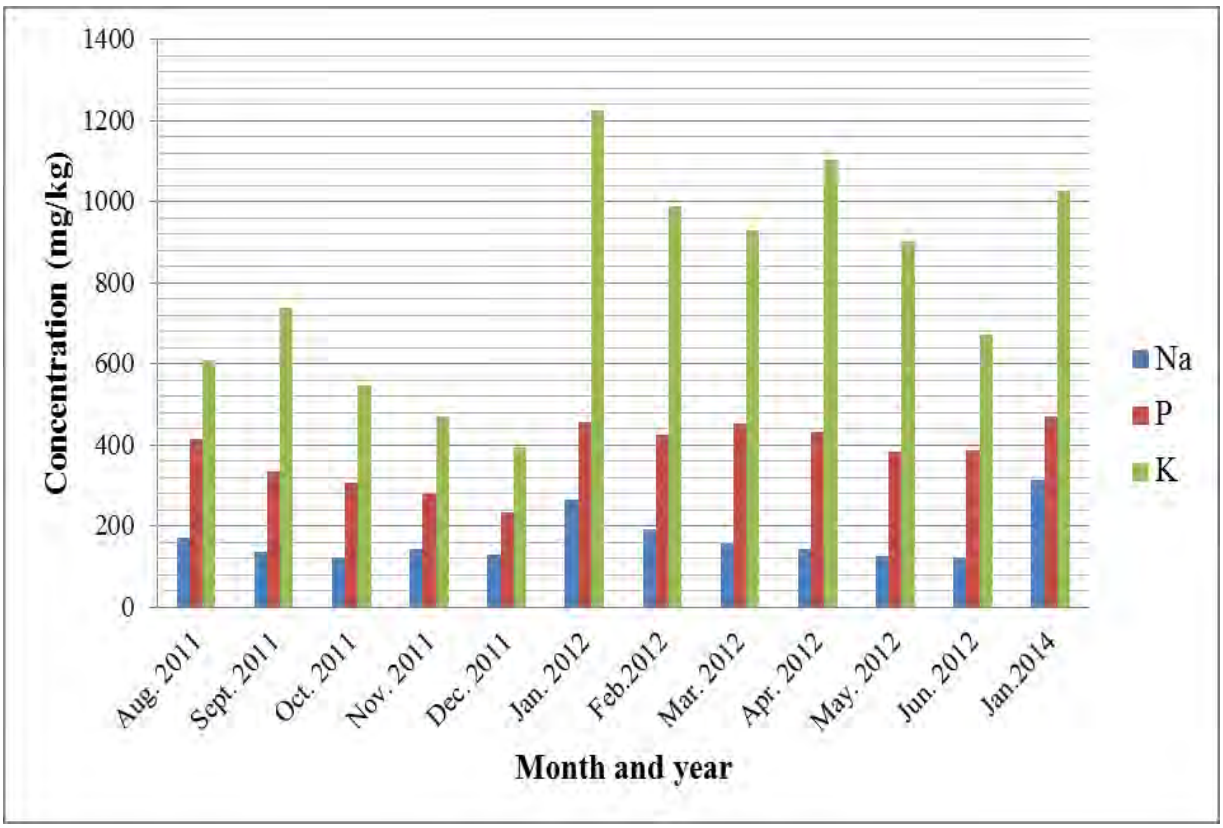

Figure 59: Total macro element (Na^+, P^{3-} and K^+) concentration for FP-6 (EPA 3050B, 1996).

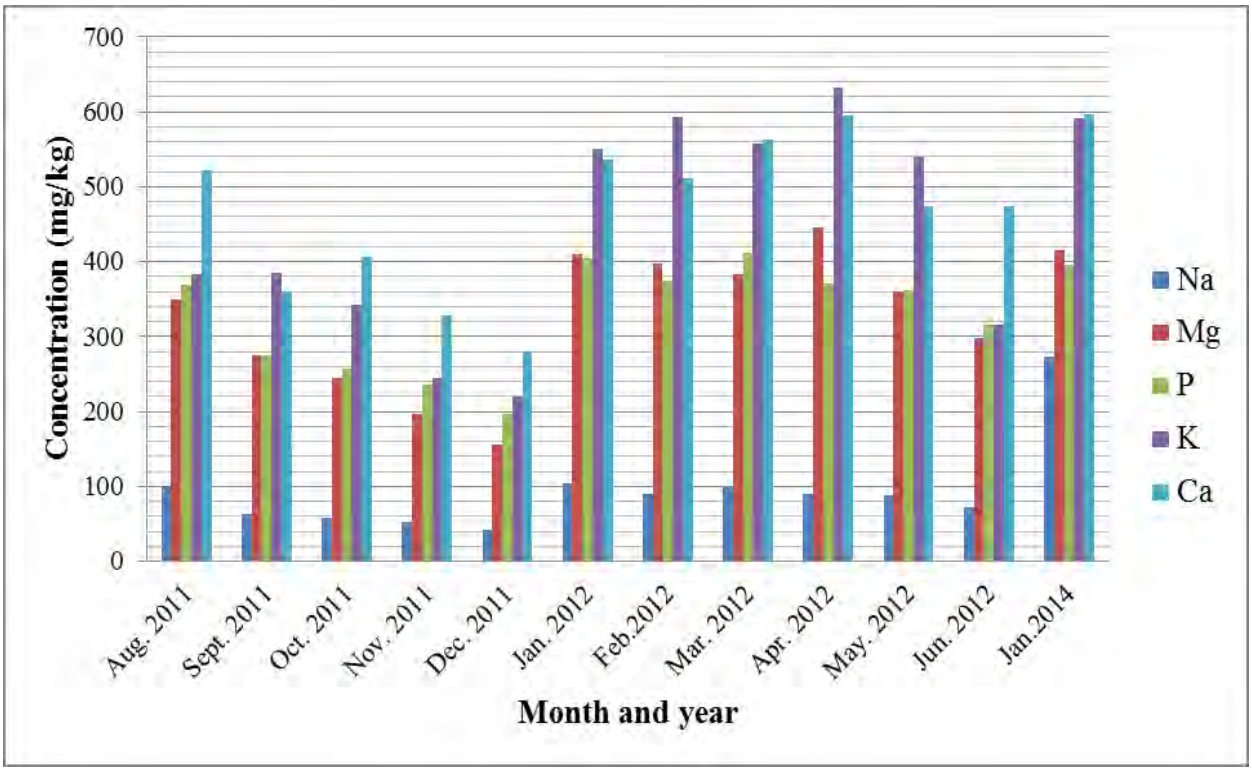

Figure 60: Total macro element concentration for FP-7 (EPA 3050B, 1996).

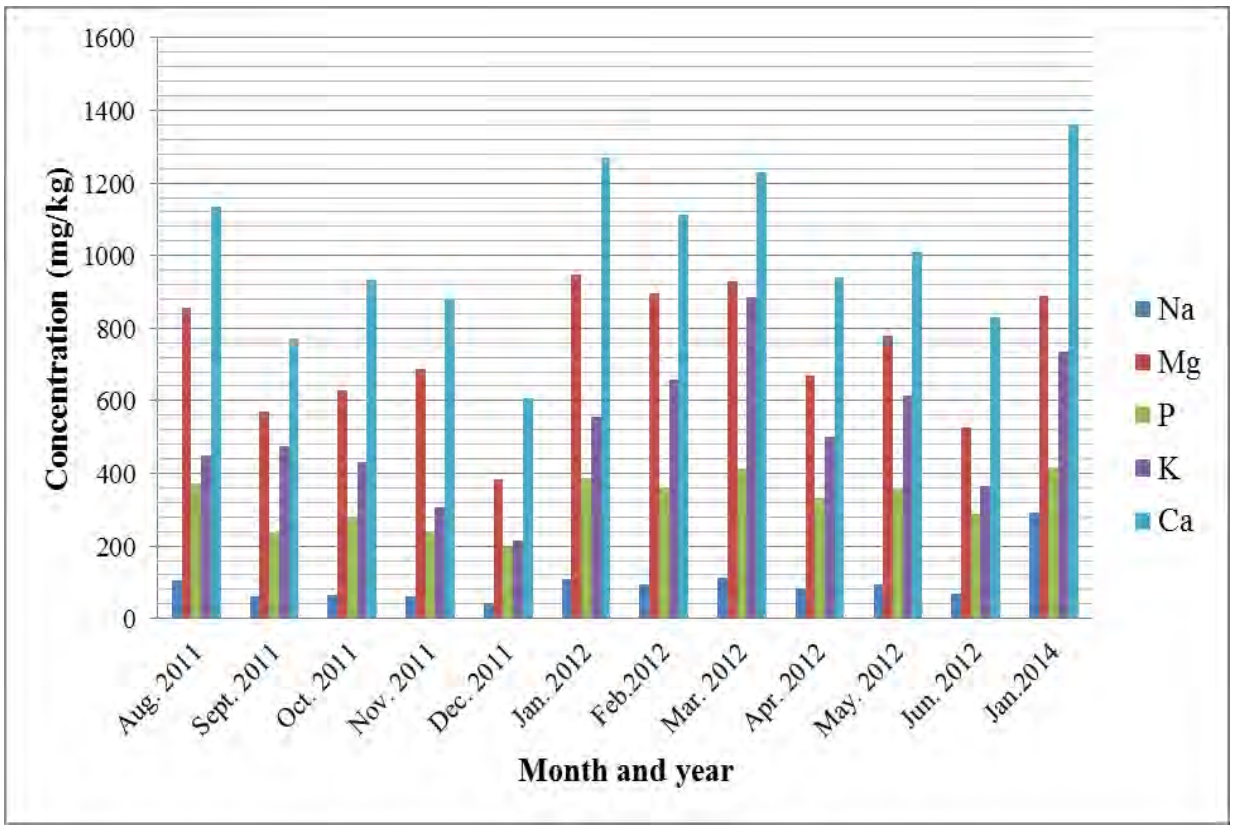

Figure 61: Total macro element concentration for FP-8 (EPA 3050B, 1996).

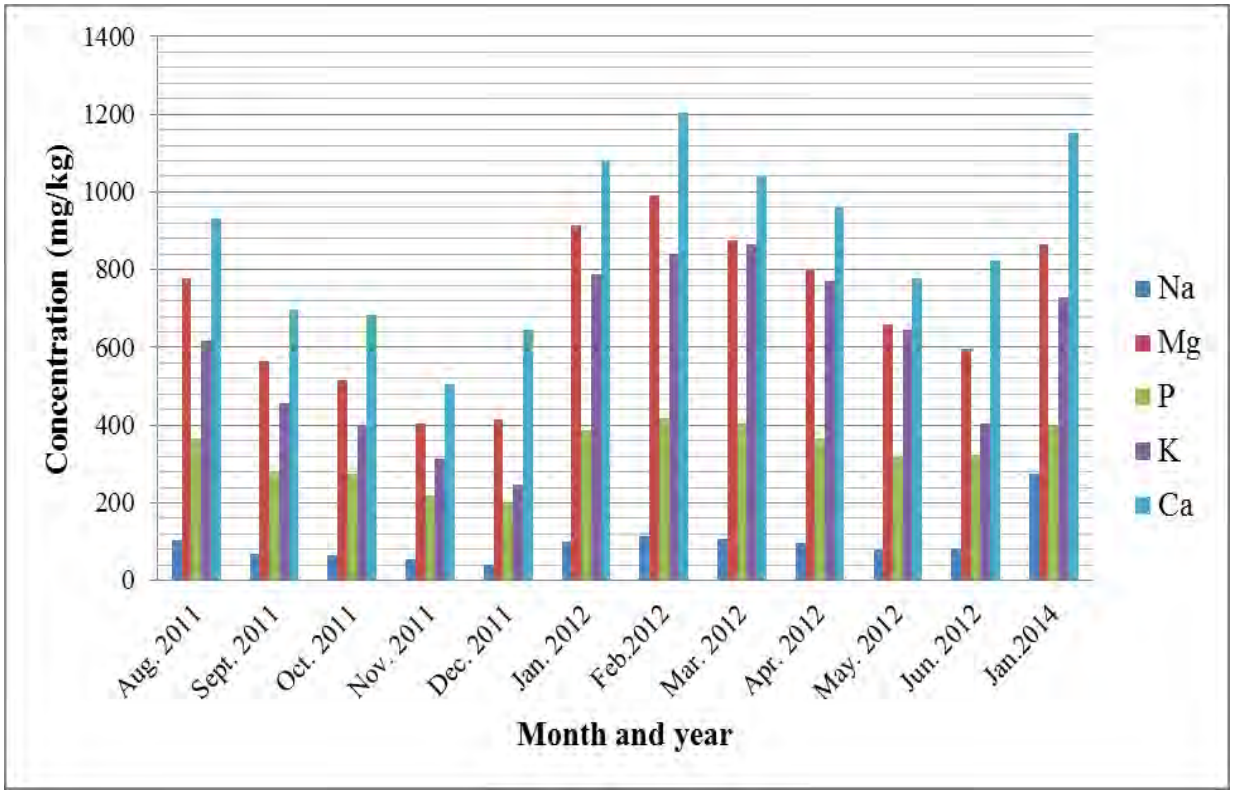

Figure 62: Total macro element concentration for FP-9 (EPA 3050B, 1996).

The macro element concentration for FP-K1, as illustrated in Figure 63, display a similar trend as the rest of the FPs and control sites, with the exception of February 2012 which shows a significantly lower concentration of macro elements that those for all the other FPs. The K^+ concentration of FP-K1 is the highest of all the FP sites. Figure 63 also shows an increase in concentrations from the beginning to the end of the monitoring period.

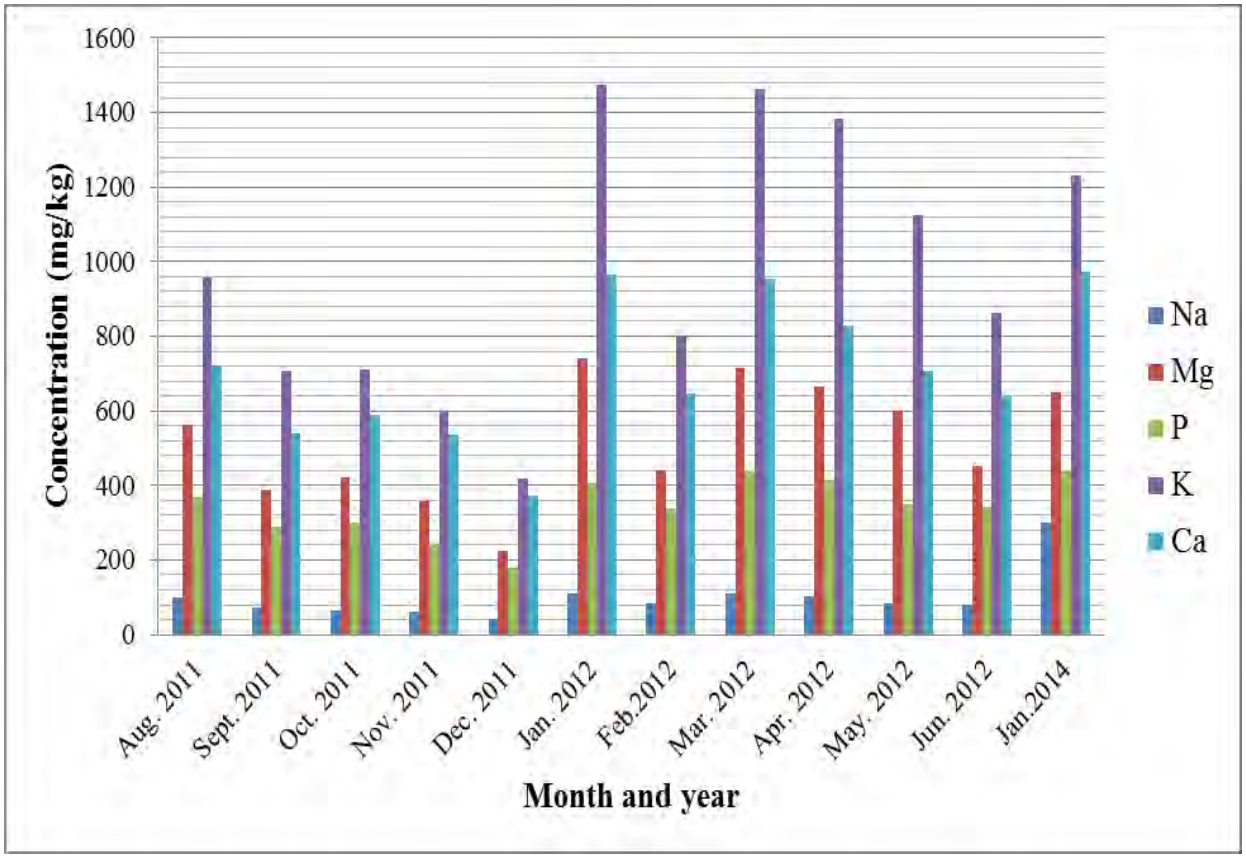

Figure 63: Total macro element concentration for FP-K1 (EPA 3050B, 1996).

FP-K2 shows the lowest concentrations of total macro elements of all the FP sites (Figure 64). The overall trend of the concentrations for FP-K2 is similar to the rest of the FP sites and control sites with a significant increase in concentrations from the beginning to the end of the monitoring period, as illustrated in Figure 64.

Figure 65 shows the macro element concentrations of FP-K3 which are similar to the rest of the FPs, with a decrease in macro element concentrations from August to December 2011, an increase in January 2012, and then again from March to April 2012. FP-K3 shows relatively high concentrations of K^+ relative to the other FP sites. The overall trend of FP-K3 increased in total macro element concentration from the beginning to the end of the monitoring period.

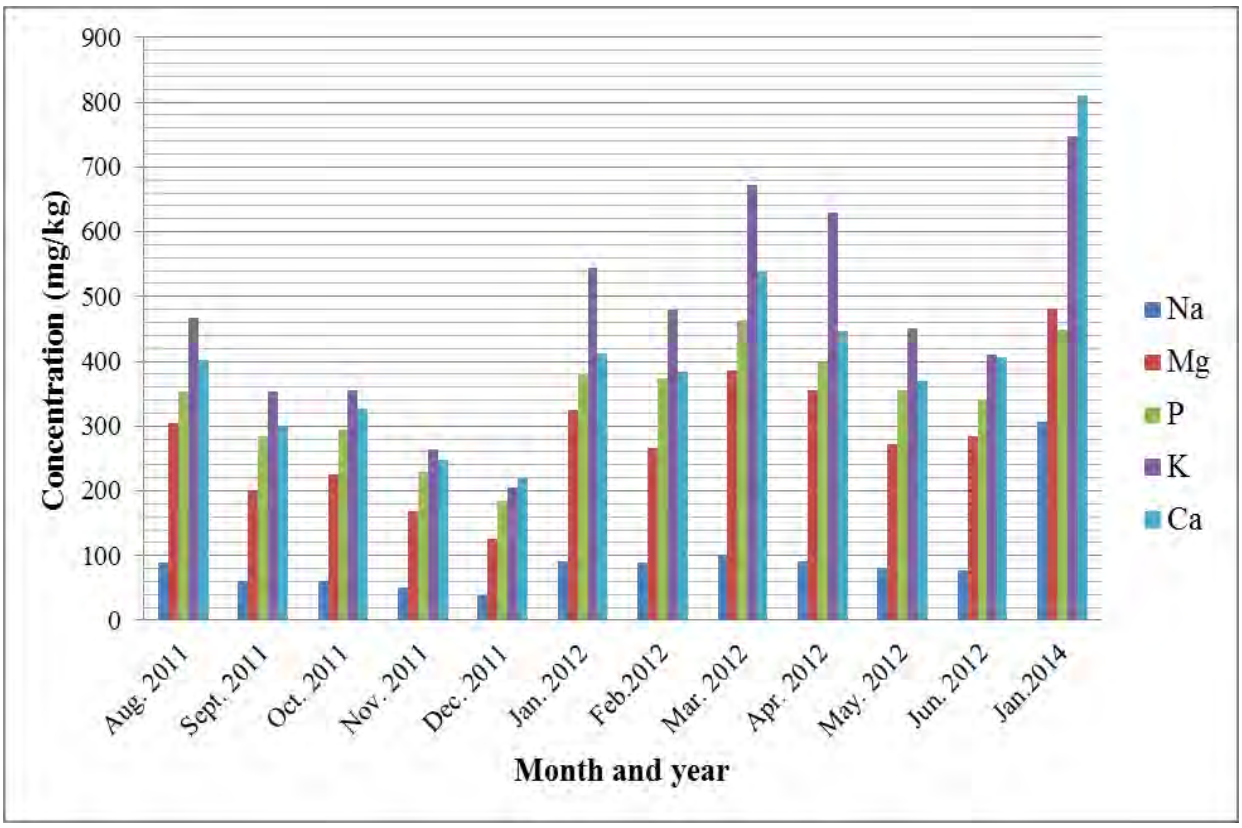

Figure 64: Total macro element concentration for FP-K2 (EPA 3050B, 1996).

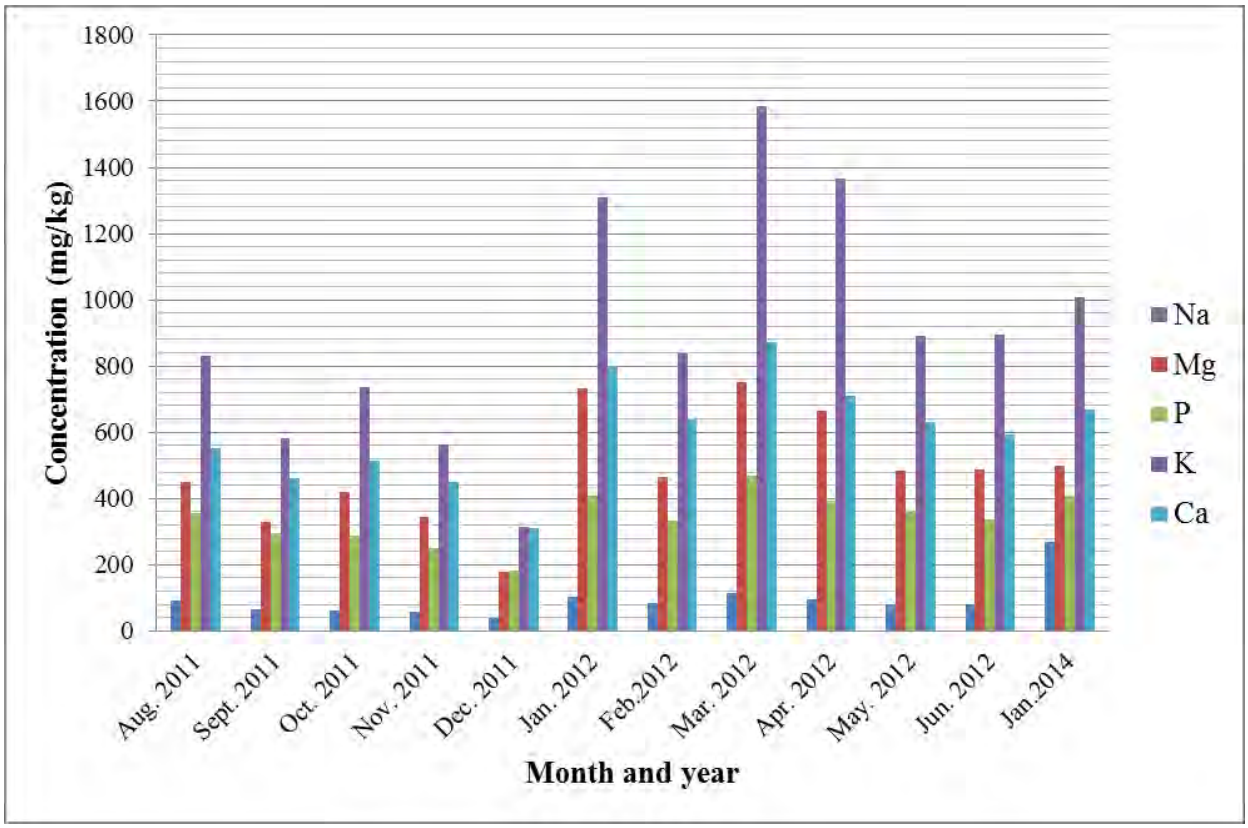

Figure 65: Total macro element concentration for FP-K3 (EPA 3050B, 1996).

4.6 TOTAL ANION CONCENTRATIONS

The total anion concentration data are shown in Appendix D, from August 2011 to June 2012 and again in August 2013. The data that were used include those for August 2011 and August 2013 in order to determine whether any changes may have occurred in the two-year timeframe. The overall monthly variations in the total anion concentrations can be explained in the same way as the variations in the EC values, as described by Hillel (1998) in Chapter 4.3; this explains why the anion concentrations increase in dry periods and decrease during wet periods. The anion concentrations (Cl^-, NO_3^- and SO_4^{2-}) for the 12 FPs in August 2011 and August 2013 are shown in Figure 66, Figure 67 and Figure 68.

The fluoride concentrations are very low throughout the monitoring period at all the FP and control sites. Therefore, the fluoride concentration will not be presented in the graphs; however, the data are presented in Appendix D.

From Figure 66, it is clear that the chloride concentrations in August 2011 are the highest for FP–1 and -6, which confirms the assumptions made in 2010 that these FP sites were the most polluted by AMD from the MWS No.5 TDF.

According to Ratlhogo (2011) the amounts of Cl^- and SO_4^{2-} are directly related to AMD. The chloride concentrations decreased from August 2011 to August 2013, except for FP-2, which showed a small increase in August 2013. However, this indicates that the seepage and leaching process from the MWS No. 5 TDF decreased from 2011 to 2013.

Bacteria that live in the soil perform nitrification, and warm, moist soils with abundant oxygen provide perfect conditions for the process to proceed (Mellin, 2005). Nitrification occurs in two stages – first, NH_4 is oxidised to NO_2^-, and then the NO_2^- is oxidized to NO_3^-.

In 2011, the NO_3^- concentration was extremely high for FP–1, K2 and K3 (Figure 67); this could be due to the explosive substances used during the mining phase which were distributed over this area, as well as the very high solubility of this anion. The NO_3^- concentration decreased in 2013. The NO_3^- concentrations in 2013 are normal which, according to Mellin (2005), should only reach trace amounts (10 mg/l) of normal standards. The sulphate (SO_4^{2-}) concentrations are also the highest in 2011 at FP-1 and -6, as shown in Figure 68; this confirms the assumptions made in 2010 that these FPs were the sites most polluted by AMD from the MWS No.5 TDF.

The main trend in SO_4^{2-} concentration shows an overall decrease from 2011 to 2013, with only minor increases in values. However, these increases are not significant enough to be considered as polluted.

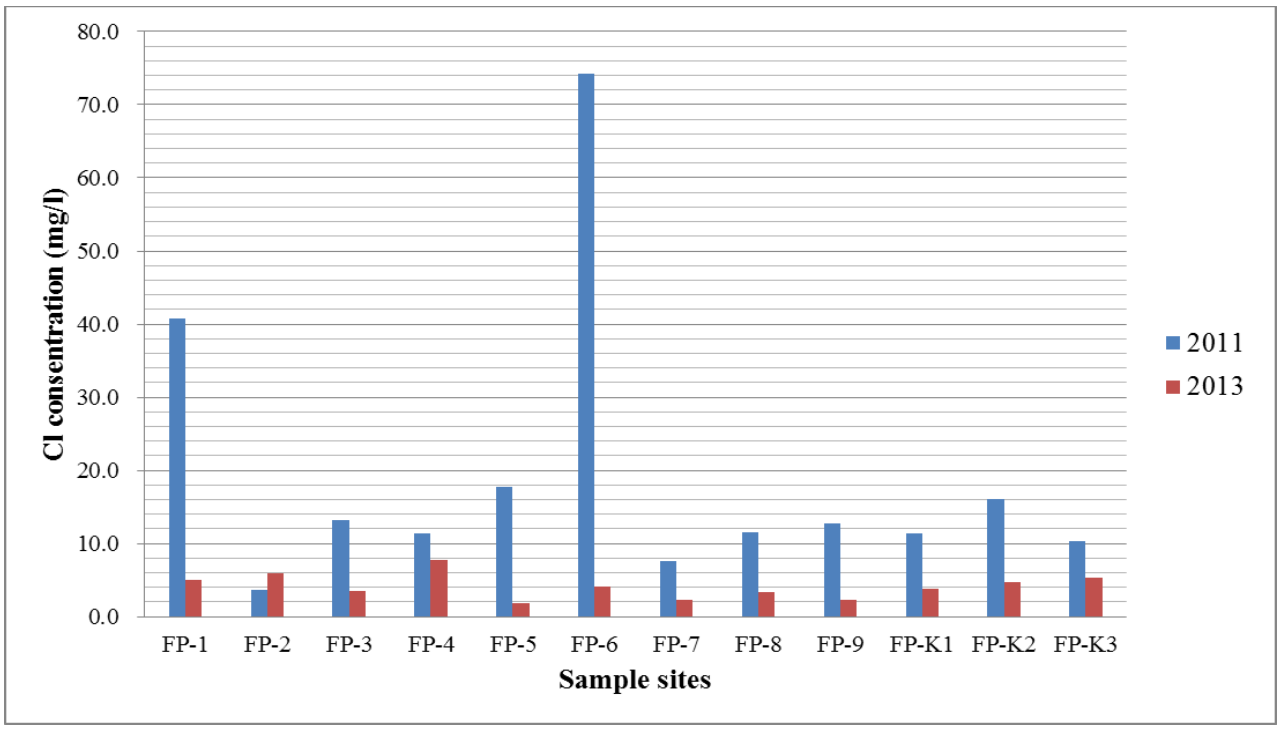

Figure 66: Chloride concentration of the 12 fixed points in August 2011 and 2013.

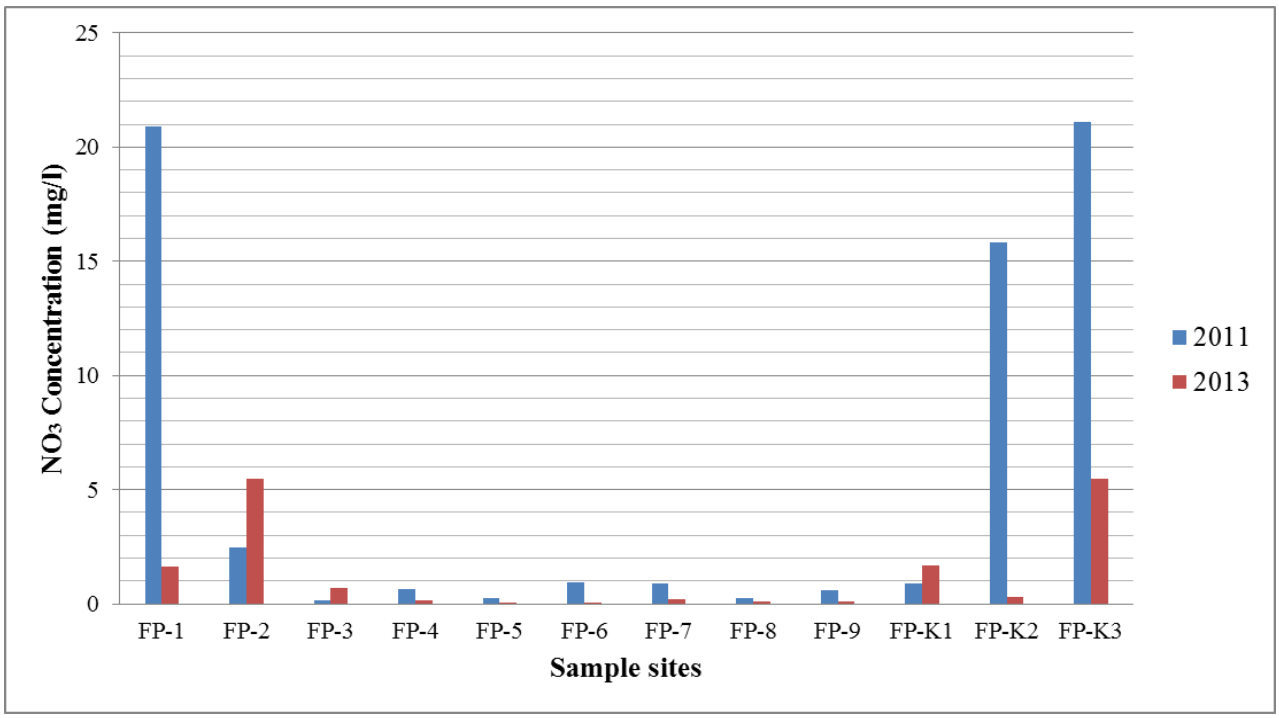

Figure 67: Nitrate concentration (mg/l) of the 12 fixed points in August 2011 and 2013.

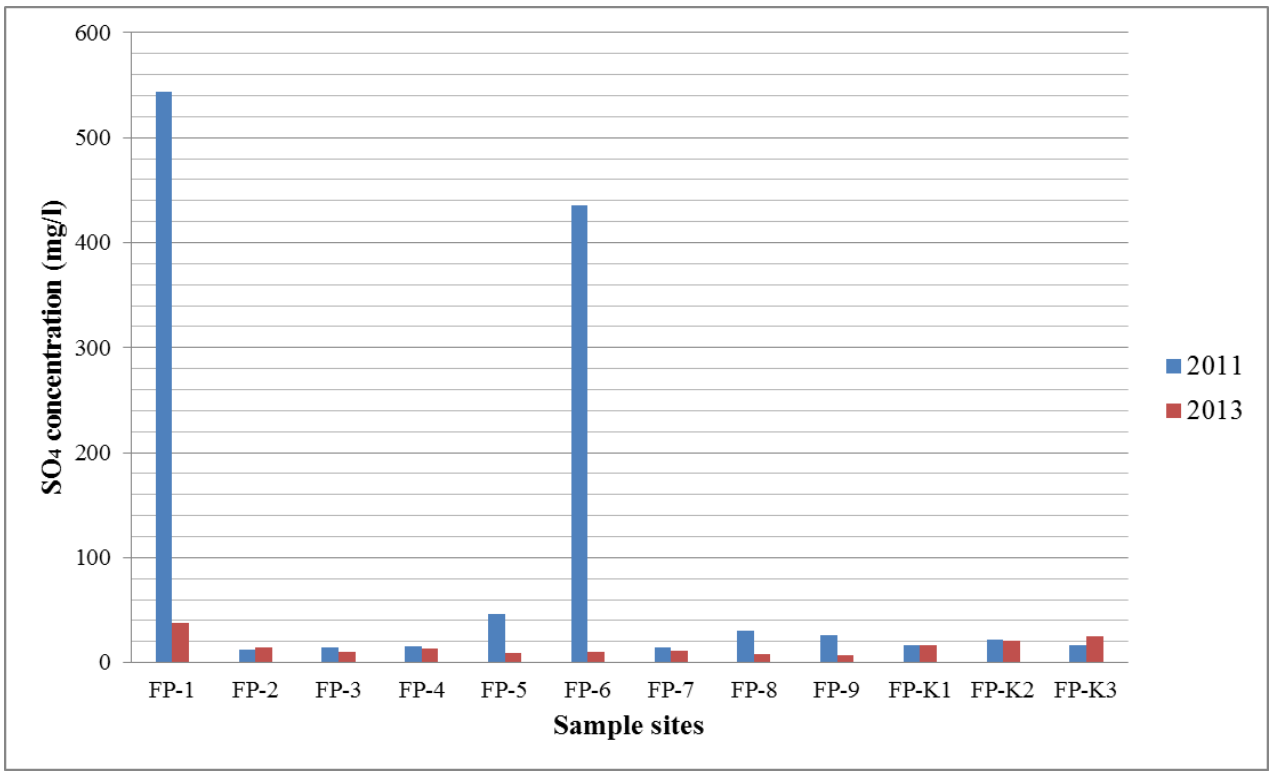

Figure 68: Sulphate concentration (mg/l) of the 12 fixed points in August 2011 and 2013.

4.7 TOTAL AND SOLUBLE/AVAILABLE TRACE METAL ELEMENTS IN THE SOIL

The total and soluble/available trace metal elements of the soil samples of the 12 FPs are shown in Appendix E. The nine trace metal elements considered for this study include Cr, Co, Ni, Cu, Zn, As, Cd, Pb and U.

Various values for the maximum permissible trace metal elements concentrations (mg/kg) for soils in South Africa were provided by the Department of National Health and Population Development (DNHPD) in 1991 and the Water Research Commission in 1997 however, Herselman (2007) stated that these value restrictions are too conservative for natural trace metal elements of South African soils and therefore proposed a new Total Maximum Threshold (TMT) and Maximum Available Threshold (MAT).

The maximum threshold levels of the metal used are presented in Table 10.

Table 10: Total and available (soluble) thresholds/guidelines for specific potentially toxic trace metal elements.

	Totals (Total maximum threshold [TMT])*	**References**	**Available (Maximum available threshold [MAT])#**	**Reference**
	mg/kg	mg/kg		
Cd	3	[1]	0.1	[1]
Cr	350	[1]	0.1	[1]
Co	20	[2]	0.5	[4]
Ni	150	[1]	1.2	[1]
Cu	120	[1]	1.2	[1]
Zn	200	[1]	5	[1]
Pb	100	[1]	3.5	[1]
As	2	[1]	0.014	[1]
U	16	[3]	0.04	[4]
	**Total acid digestion method (EPA 3050)*		*# NH_4NO_3 extraction method*	

[1]Snyman and Herselman, 2006; Prüeß, 1997 (cited by Herselman, 2007)
[2]DNHPD, 1991; WRC, 1997
[3]Coetzee *et al.,* 2006
[4]Prüeß *et al.,* 1991 (cited by Rösner *et al.,* 2001)

4.7.1 Total Trace Metal Elements in the Soil

The total trace metal element datasets that were analyzed are shown in Appendix E1. The total trace metal elements of the 12 FPs analysed at the beginning and end of the monitoring period are shown in Figure 69 to Figure 77.

None of the FPs in 2011 and 2014 exceeded the total maximum threshold that is presented in Table 10, with the exception of FP-K3 in 2014 that had an As concentration of 2.0715 mg/kg. All of the FPs are, to a great extent, lower than the total maximum threshold (TMT) for eight of the trace metal elements; however, the arsenic for all the FPs are truly closer to the TMT for arsenic of 2 mg/kg, which might cause problems in the future.

Fixed point-1, FP-K1 and FP-K3 show the highest overall trace metal element concentrations throughout this study. This can be explained by the geological setting of these FPs (Figure 3 and Figure 16) which is located near the contact between the Oaktree Formation dolomites and the

Black Reef Formation, which consists of feldspathic quartzites, shales and conglomerates [refer to Chapter 1.2.2] (Van Deventer, 2011b). Herselman (2007) stated that higher amounts of trace metal elements are found in shales due to the shale‘s capability to adsorb trace metal ions during sedimentation; during the weathering process, they are reintroduced into the soil profile. Thus, the high concentration of trace metal elements of FP-1,-K1 and –K3 are due to natural weathering processes.

The nine metal trace element concentrations across nearly all of the FPs show elevations in 2014, from 2011. This is due to the rise in maximum temperature and lower rainfall from 2011 to 2014, which lead to the precipitation of these trace metals in the soil.

According to Herselman (2007), Cd is largely adsorbed by clays and organic matter in the soil; between pH 6-7, the adsorption capacity of a soil is the highest. This explains the low Cd concentration of the FPs (Figure 69) which, for sedimentary rock, ranges between 0.3-11 mg/kg.

Chromium concentrations are generally determined by the parent rocks in certain areas; Cr concentrations (Figure 70) normal for sedimentary rocks range between an average of 60-120 mg/kg in soils (Herselman, 2007).

The Co concentration for dolomites is generally low, ranging between 0.1-10 mg/kg (Herselman, 2007). In Figure 71, it is clear that for FP-1; -K1 and –K3, the FPs closest to the Black Reef Formation have higher Co concentrations than the FPs on the Oaktree dolomites; however, Herselman (2007) stated that shales have higher Co concentrations ranging from 11-20 mg/kg.

The Zn concentration shows excessive elevations from 2011 to 2014 (Figure 74). The Zn concentrations are the highest at FP-1, -6, -K1 and K-3 which is mostly attributed to the shales of the Black Reef (FP-1, -K1 and –K3) and the clay content (FP-6). However, these Zn concentrations still fall within the ranges for dolomites of 10-30 mg/kg, as set out by Korte (1999, cited by Herselman, 2007).

The Pb concentration shows a dramatic increase for FP-K2 in 2014, as shown in Figure 75. The Pb concentration associated with dolomites ranges between 0.1-10 mg/kg and 10-40 mg/kg for shales (Herselman, 2007); therefore, these Pb concentration values presented in Figure 75 for all the FPs in 2011 and 2014 are considered as normal weathering Pb concentrations.

The As concentrations (as presented in Figure 76) show that only FP-K3 exceeds the TMT value of 2 mg/kg in 2014, however the other FPs do not show significantly lower concentrations than

FP-K3. Therefore, As in this study area needs to be monitored due to the effects it has on the growth potential of plants.

Arsenic and U are well-known pollutants associated with gold mine tailings disposal facilities (Winde, 2010; Rösner *et al,* 2001, cited by Seiderer, 2011).

The U concentration (Figure 77) for FP-1 shows elevations in 2014; however, none of the FPs exceed the TMT of 16 mg/kg.

These U concentrations may be from the parent rock and not necessarily from the TDF, however dolomites are normally low in U.

Although the total trace metal elements increased at most sites in 2014, it cannot be said that the quality of the soil is starting to degrade due to the fact that most of these trace metal elements are present within the parent (bedrock) material.

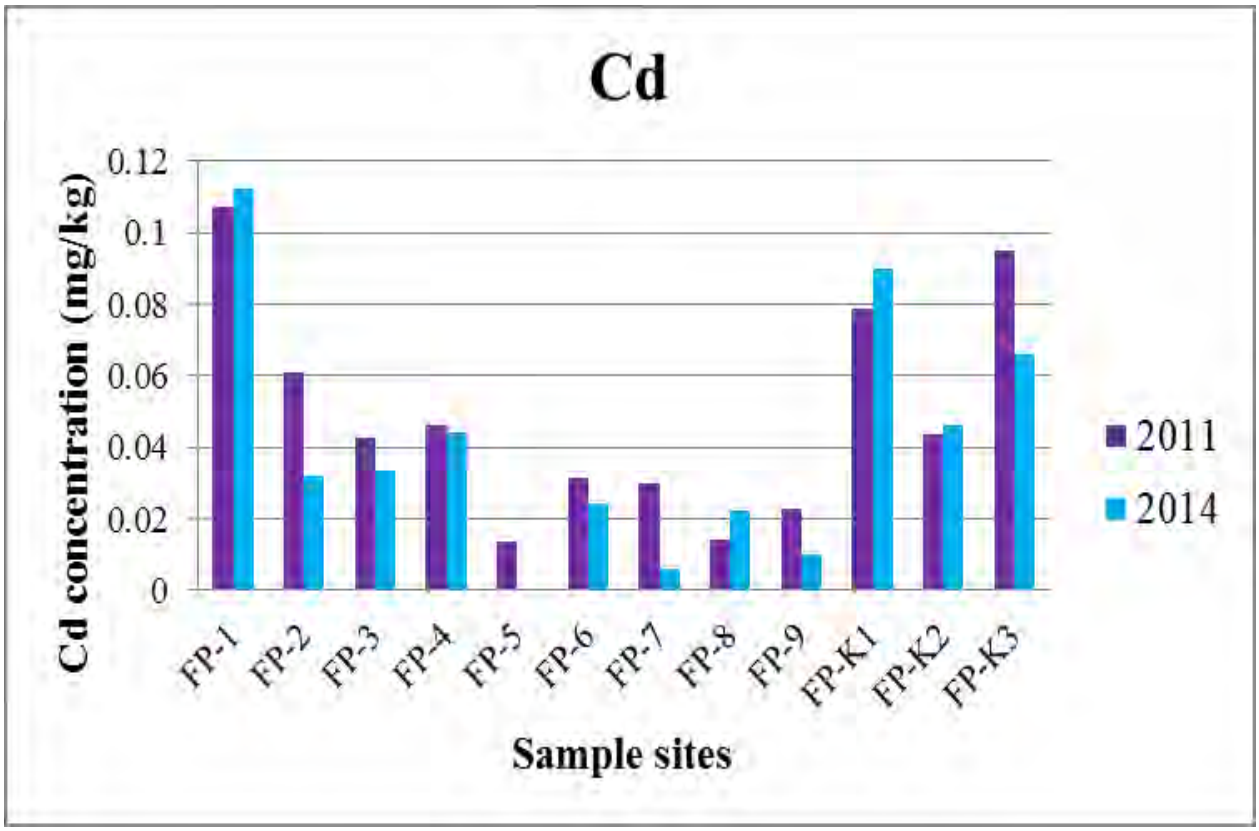

Figure 69: Cadmium concentration (mg/kg) of the 12 fixed points in 2011 and 2014. (EPA 3050B, 1996).

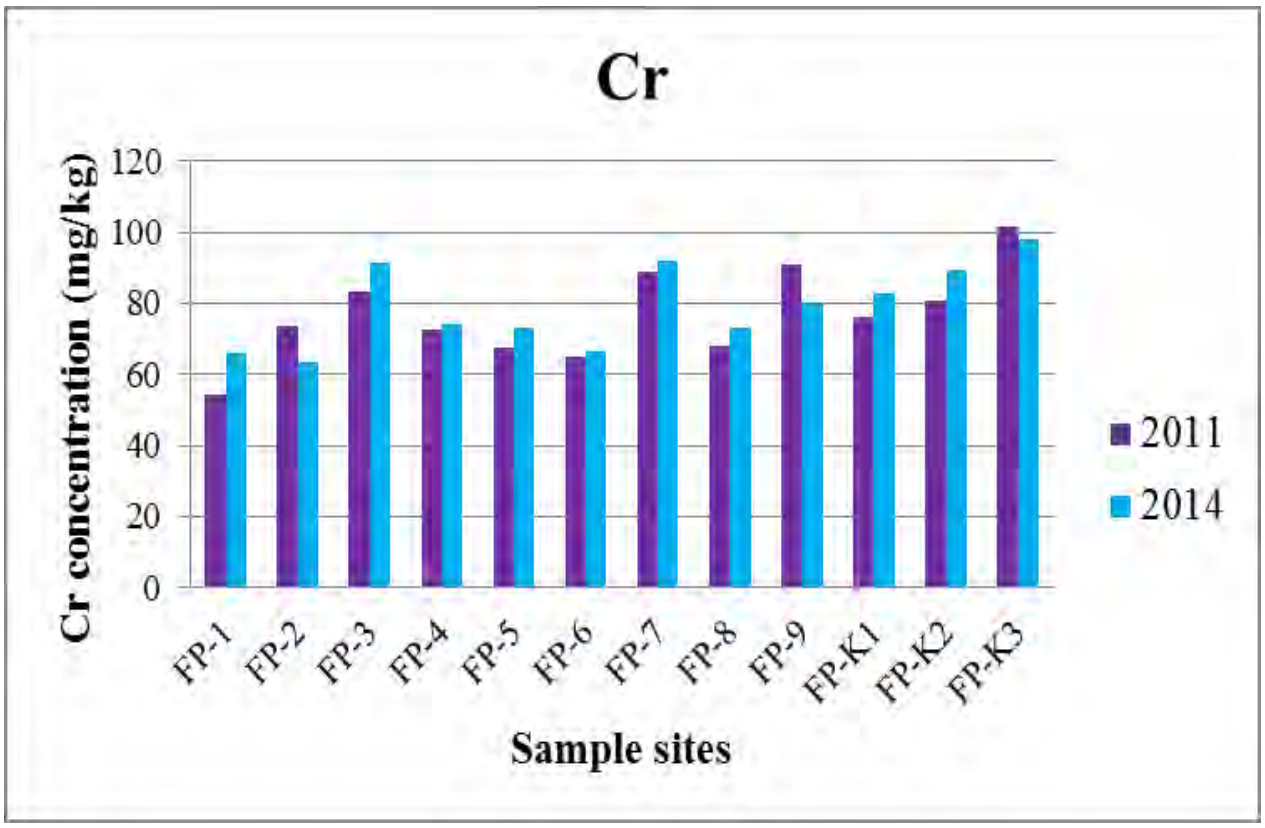

Figure 70: Chromium concentration (mg/kg) of the 12 fixed points in 2011 and 2014. (EPA 3050B, 1996).

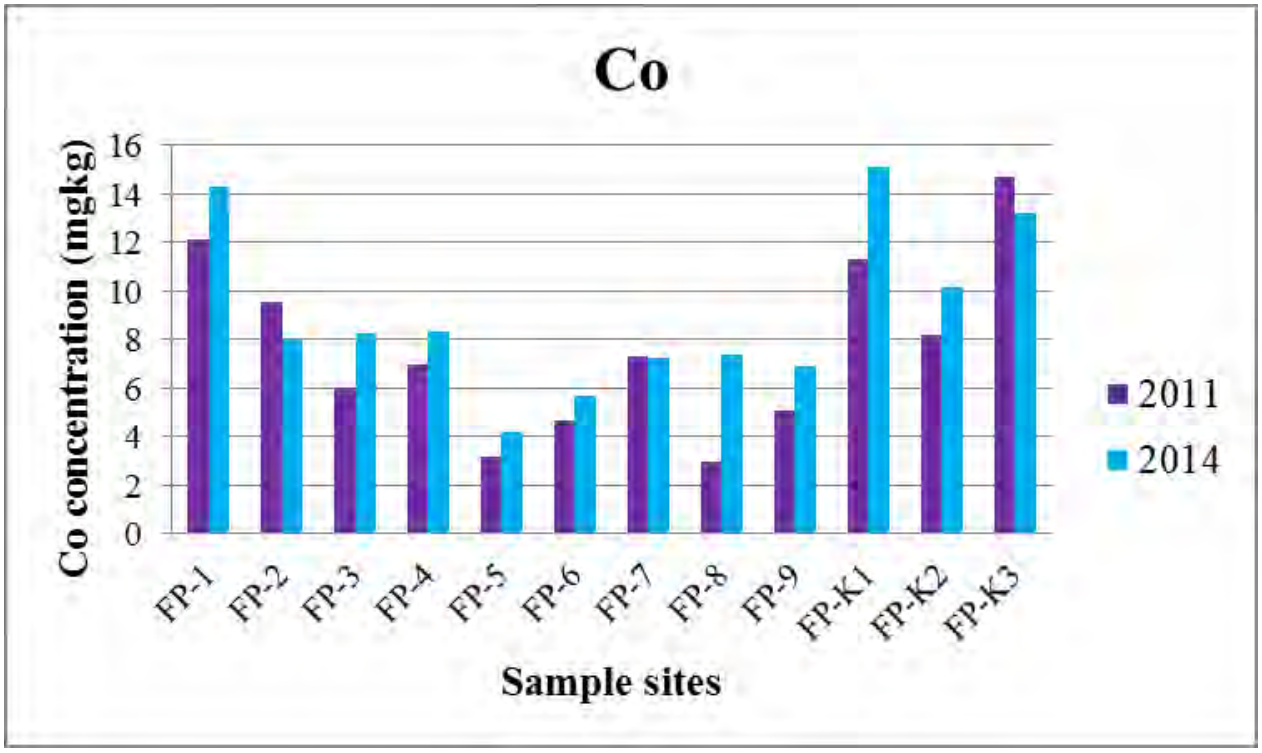

Figure 71: Cobalt concentration (mg/kg) of the 12 fixed points in 2011 and 2014. (EPA 3050B, 1996).

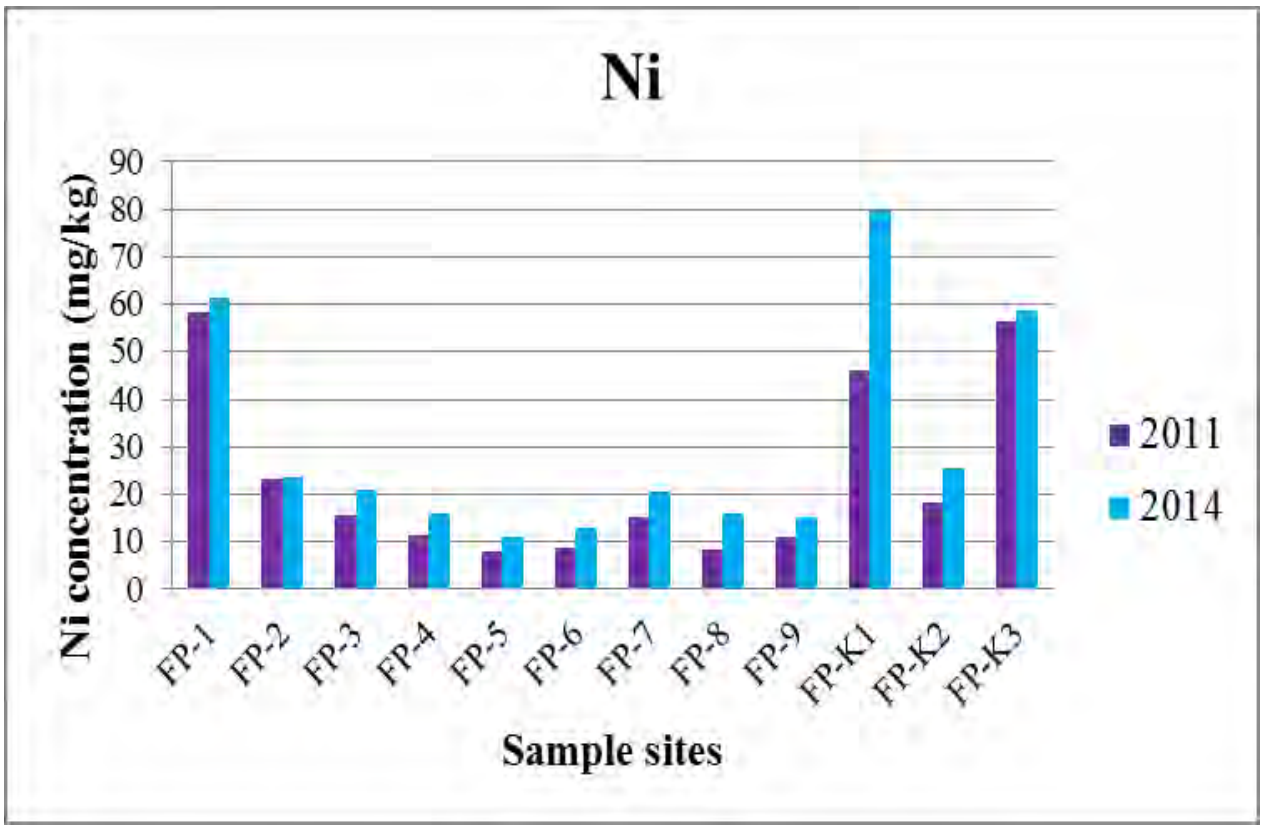

Figure 72: Nickel concentration (mg/kg) of the 12 fixed points in 2011 and 2014. (EPA 3050B, 1996).

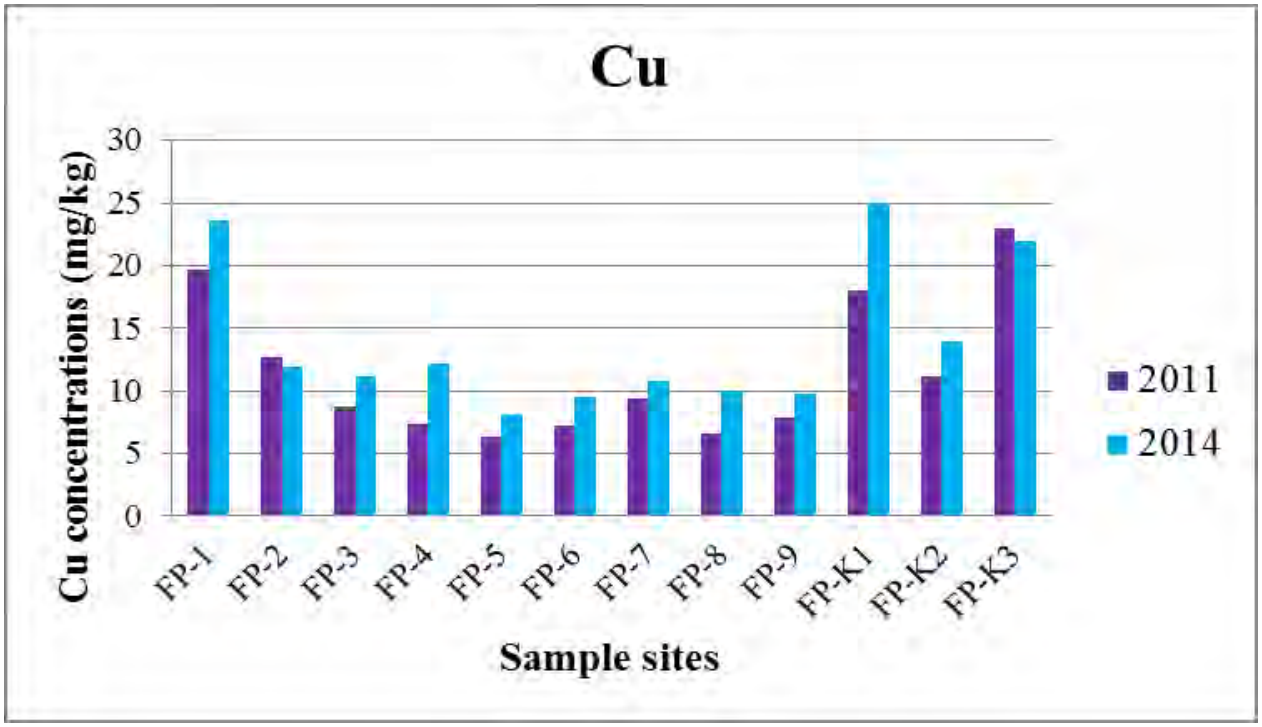

Figure 73: Copper concentration (mg/kg) of the 12 fixed points in 2011 and 2014. (EPA 3050B, 1996).

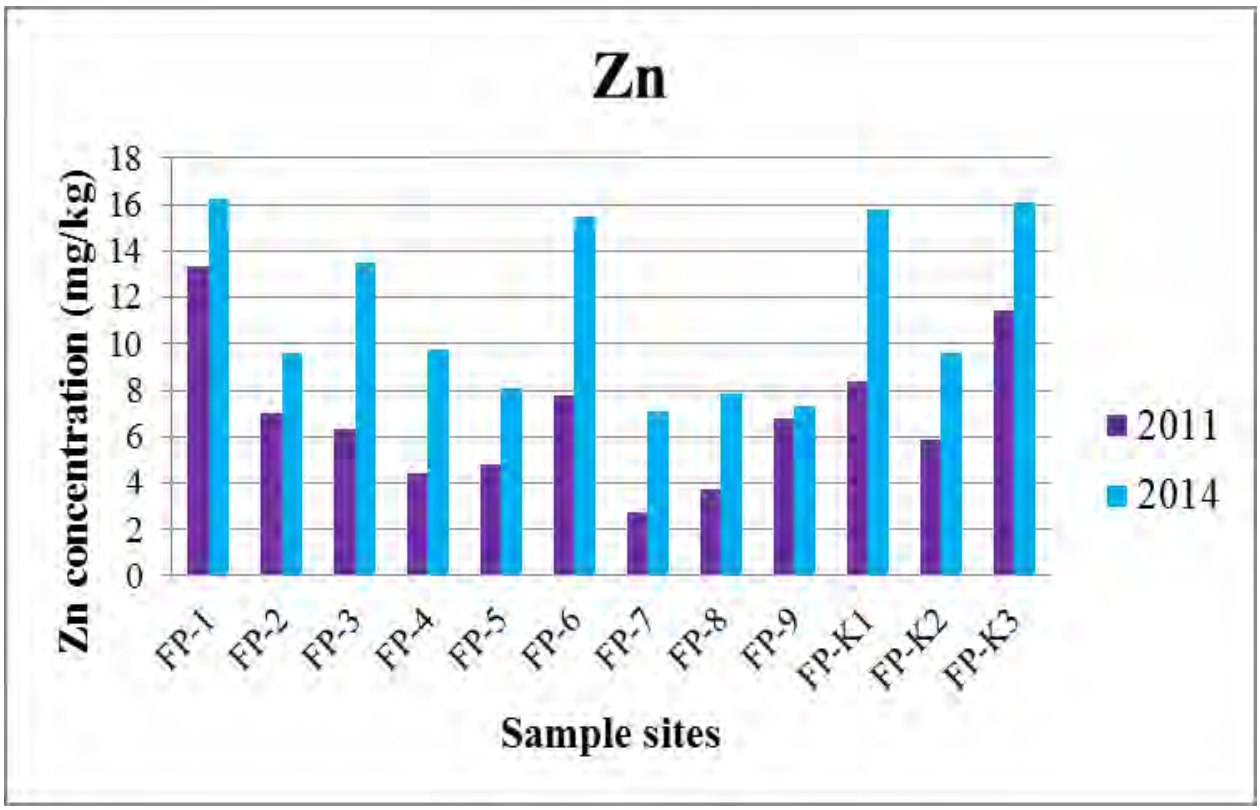

Figure 74: Zinc concentration (mg/kg) of the 12 fixed points in 2011 and 2014. (EPA 3050B, 1996).

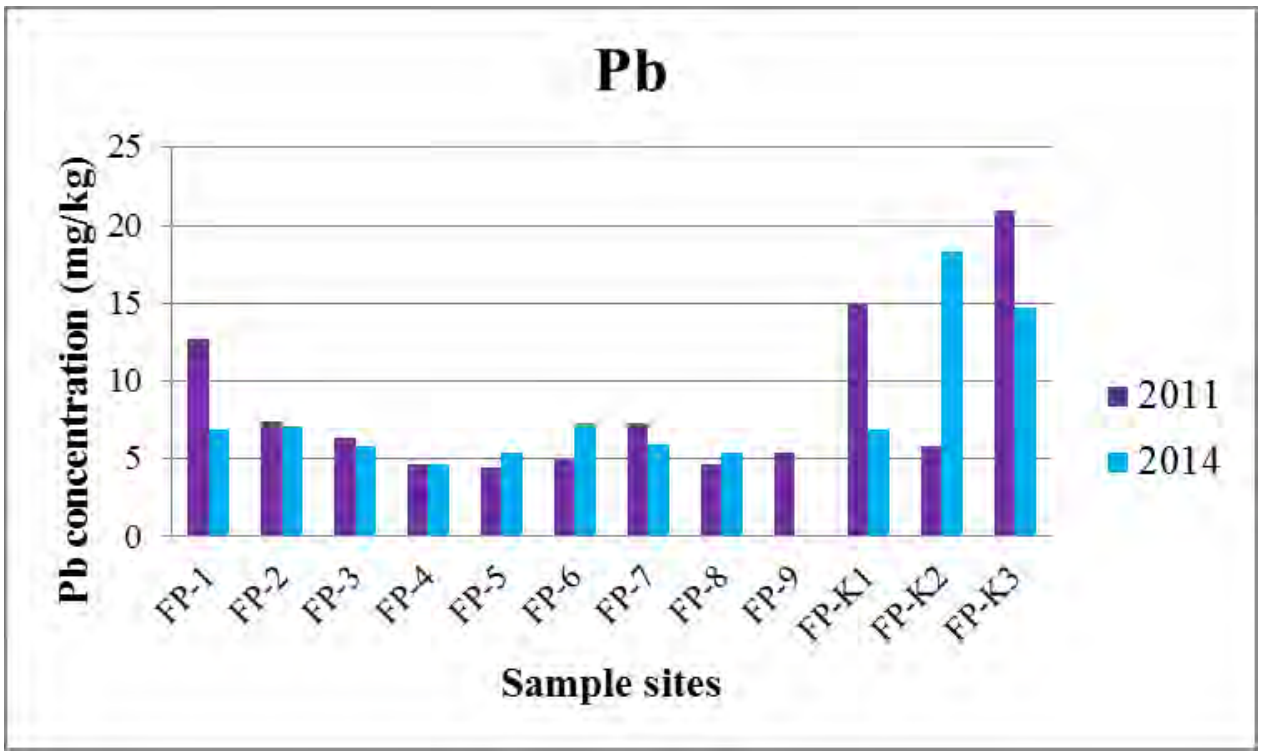

Figure 75: Lead concentration (mg/kg) of the 12 fixed points in 2011 and 2014. (EPA 3050B, 1996).

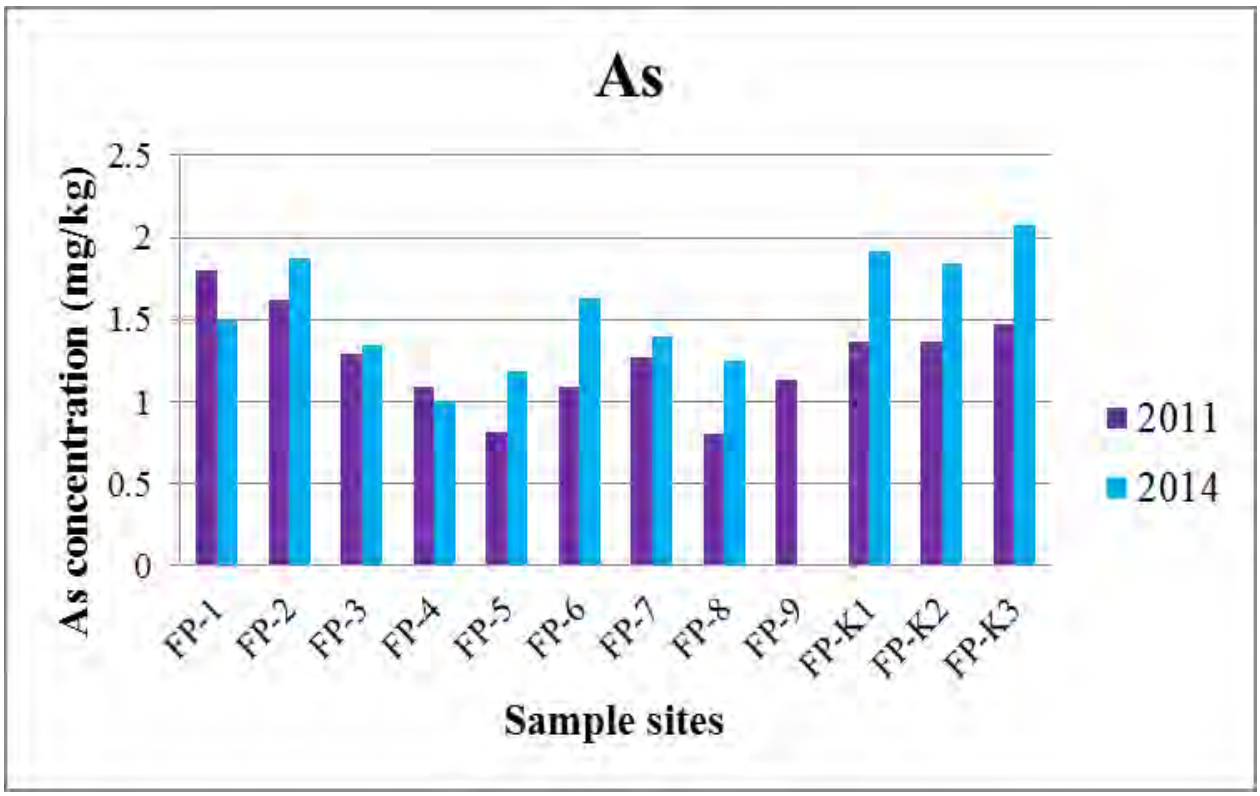

Figure 76: Arsenic concentration (mg/kg) of the 12 fixed points in 2011 and 2014. (EPA 3050B, 1996).

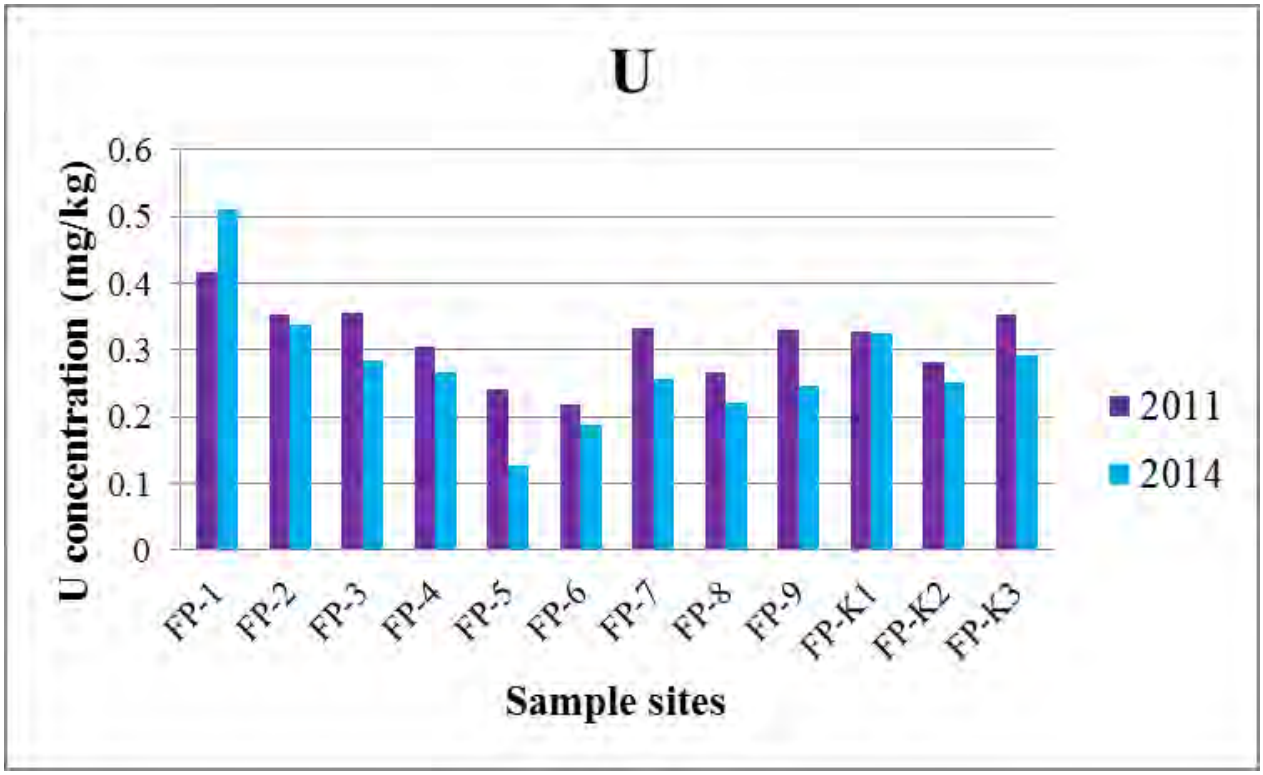

Figure 77: Uranium concentration (mg/kg) of the 12 fixed points in 2011 and 2014. (EPA 3050B, 1996).

4.7.2 Soluble/Available Trace Metal Elements in the Soil

The soil soluble/available trace metal elements were assessed in August 2011, April 2013 and January 2014 in order to correspond with the total trace metal elements assessed within the plant material, and is shown in Table 11.

The complete sets of data are shown in Appendix E. The FP sites that exceed the maximum available threshold (MAT) values in mg/kg (Table 10) are indicated in red in Table 11.

The trace metal elements that exceed the MAT are Cr and U in 2011. In 2011, Cr exceeded the MAT for FP-1, -3 and -8; U exceeded the MAT for all 12 FPs.

Although the Cr and U concentrations at some sites do exceed the MAT in 2011, these values are too minor to be considered as contaminated sites due to the fact that Cr only becomes phytotoxic between 1-5 mg/kg (Herselman, 2007).

All the trace metal elements decreased from 2011 to 2014 for all the FPs, with the concentrations almost being insignificant.

The soluble/available trace metals indicated the bio-availability of these trace metal elements for plant uptake; therefore, the trace metal concentrations of these soils display no sign of being potentially contaminated, and thus phytotoxicity is not of great concern.

Some of these trace metal elements are essential for plants, hence some of the concentrations (mg/kg) measured in 2014 may cause a deficiency in plants which can also affect the plant in a negative way.

Table 11: Soluble/available trace metal element concentrations (mg/kg) of the 12 fixed points in 2011, 2013 and 2014 (DIN 19730, 1997).

mg/kg	Year	FP-1	FP-2	FP-3	FP-4	FP-5	FP-6	FP-7	FP-8	FP-9	FP-K1	FP-K2	FP-K3
Cr	2011	0.11	0.05	0.17	0.03	0.074	0.01	0.02	0.11	0.01	1×10^{-4}	2×10^{-4}	3×10^{-4}
	2013	1×10^{-4}	1×10^{-4}	1×10^{-4}	1×10^{-4}	1×10^{-4}	1×10^{-4}	1×10^{-4}	1×10^{-4}	1×10^{-4}	1×10^{-4}	1×10^{-4}	1×10^{-4}
	2014	0.01	4×10^{-5}	5×10^{-5}	1×10^{-4}	1×10^{-4}	1×10^{-4}	5×10^{-5}	4×10^{-5}	4×10^{-5}	1×10^{-4}	1×10^{-4}	1×10^{-4}
Co	2011	0.13	0.1	0.071	0.056	0.08	0.08	0.06	0.08	0.08	0.06	0.07	0.07
	2013	0.001	1×10^{-5}	3×10^{-5}	3×10^{-5}	2×10^{-5}	2×10^{-5}	3×10^{-5}	3×10^{-5}	3×10^{-5}	3×10^{-5}	3×10^{-5}	3×10^{-5}
	2014	3×10^{-5}	4×10^{-5}	4×10^{-5}	1×10^{-5}	3×10^{-5}	4×10^{-5}	3×10^{-5}	1×10^{-5}	1×10^{-5}	0.00	3×10^{-5}	4×10^{-5}
Ni	2011	0.16	0.18	0.27	0.25	0.188	0.17	0.26	0.22	0.15	0.22	0.30	0.56
	2013	3×10^{-5}	0.014	0.01	0.025	3×10^{-5}	0.00	0.04	5×10^{-5}	4×10^{-5}	0.02	0.04	0.03
	2014	0.021	0.0014	0.035	3×10^{-5}	0.012	0.003	0.03	0.002	4×10^{-4}	0.03	3×10^{-4}	1×10^{-5}
Cu	2011	0.523	0.67	0.66	0.26	0.60	0.8	0.6	0.81	0.43	0.73	0.65	0.45
	2013	0.037	0.027	0.023	0.02	0.044	0.04	0.021	0.02	0.014	0.03	0.02	0.05
	2014	0.02	0.01	0.004	0.03	0.013	0.02	0.01	0.02	0.03	0.01	0.01	0.02
Zn	2011	0.014	0.012	0.8	0.62	0.014	0.003	0.012	0.4	0.13	0.6	0.62	1
	2013	0.001	4×10^{-4}	5×10^{-4}	3×10^{-4}	0.001	0.001	0.01	0.001	0.001	0.001	2×10^{-4}	3×10^{-4}
	2014	0.001	0.001	0.001	0.001	0.001	0.001	0.001	0.001	0.001	0.001	0.001	0.001
As	2011	4×10^{-4}	4×10^{-4}	4×10^{-4}	5×10^{-4}	4×10^{-4}	4×10^{-4}	4×10^{-4}	4×10^{-4}	5×10^{-4}	5×10^{-4}	6×10^{-4}	5×10^{-4}
	2013	1×10^{-4}	1×10^{-4}	1×10^{-4}	1×10^{-4}	1×10^{-4}	1×10^{-4}	1×10^{-4}	1×10^{-4}	1×10^{-4}	1×10^{-4}	1×10^{-4}	1×10^{-4}
	2014	2×10^{-4}	2×10^{-4}	2×10^{-4}	2×10^{-4}	2×10^{-4}	2×10^{-4}	2×10^{-4}	2×10^{-4}	2×10^{-4}	2×10^{-4}	2×10^{-4}	2×10^{-4}
Cd	2011	2×10^{-4}	2×10^{-4}	2×10^{-4}	2×10^{-4}	2×10^{-4}	2×10^{-4}	2×10^{-4}	2×10^{-4}	2×10^{-4}	2×10^{-4}	2×10^{-4}	2×10^{-4}
Cd	**2013**	5×10^{-5}	5×10^{-5}	5×10^{-5}	5×10^{-5}	5×10^{-5}	5×10^{-5}	5×10^{-5}	5×10^{-5}	5×10^{-5}	4×10^{-5}	5×10^{-5}	4×10^{-5}
	2014	6×10^{-5}	6×10^{-5}	6×10^{-5}	6×10^{-5}	5×10^{-5}	6×10^{-5}	6×10^{-5}	6×10^{-5}	6×10^{-5}	6×10^{-5}	7×10^{-5}	6×10^{-5}
Pb	**2011**	5×10^{-4}	2×10^{-4}	0.092	3×10^{-4}	0.06	6×10^{-4}	4×10^{-4}	0.009	4×10^{-4}	4×10^{-4}	2×10^{-4}	1×10^{-4}
	2013	3×10^{-4}	2×10^{-4}	2×10^{-4}	3×10^{-4}	3×10^{-4}	3×10^{-4}	2×10^{-4}	2×10^{-4}	0.0003	2×10^{-4}	0.0003	2×10^{-4}

Table 11: Soluble/available trace metal element concentrations (mg/kg) of the 12 fixed points in 2011, 2013 and 2014 (DIN 19730, 1997).

mg/kg	Year	FP-1	FP-2	FP-3	FP-4	FP-5	FP-6	FP-7	FP-8	FP-9	FP-K1	FP-K2	FP-K3
	2014	2×10^{-4}	2×10^{-4}	2×10^{-4}	3×10^{-4}	2×10^{-4}	2×10^{-4}	2×10^{-4}	2×10^{-4}	2×10^{-4}	2×10^{-4}	2×10^{-4}	2×10^{-4}
U	**2011**	0.068	0.067	0.071	0.067	0.067	0.089	0.067	0.068	0.067	0.066	0.066	0.066
	2013	0.0014	0.0021	0.0014	0.0013	0.003	0.003	0.001	0.001	0.001	0.001	0.001	0.001
	2014	2×10^{-5}	2×10^{-5}	2×10^{-5}	2×10^{-5}	2×10^{-5}	2×10^{-5}	2×10^{-5}	2×10^{-5}	2×10^{-5}	2×10^{-5}	2×10^{-5}	2×10^{-5}

4.8 PARTICLE SIZE DISTRIBUTION

Soil particles can be divided into different size ranges (Winegardner, 1995) and they define the relative amounts of sand, silt and clay present in a soil (Hazelton and Murphy, 2007). The particle size distribution is shown in Appendix F. The particle size distribution for the nine FPs and three control FPs are very similar, as illustrated in Figure 78.

From Figure 78 it is also clear that the soil is well graded but poorly sorted. This implies that the soil comprises particles with an extensive range of sizes.

The texture classes of the 12 FPs were assigned by making use of the USDA Soil Texture Calculator at the following website:
http://www.nrcs.usda.gov/wps/portal/nrcs/detail/soils/survey/?cid=nrcs142p2_054167

Figure 79 illustrates the texture classes in which the 12 FP soil samples fell; it is clear that all of the FPs fall in the loamy sand area, with the exception of FP 4 and FP-K2, which fell on the border of the loamy sand and the sand area. Table 12 summarizes the textural properties of the 12 FPs.

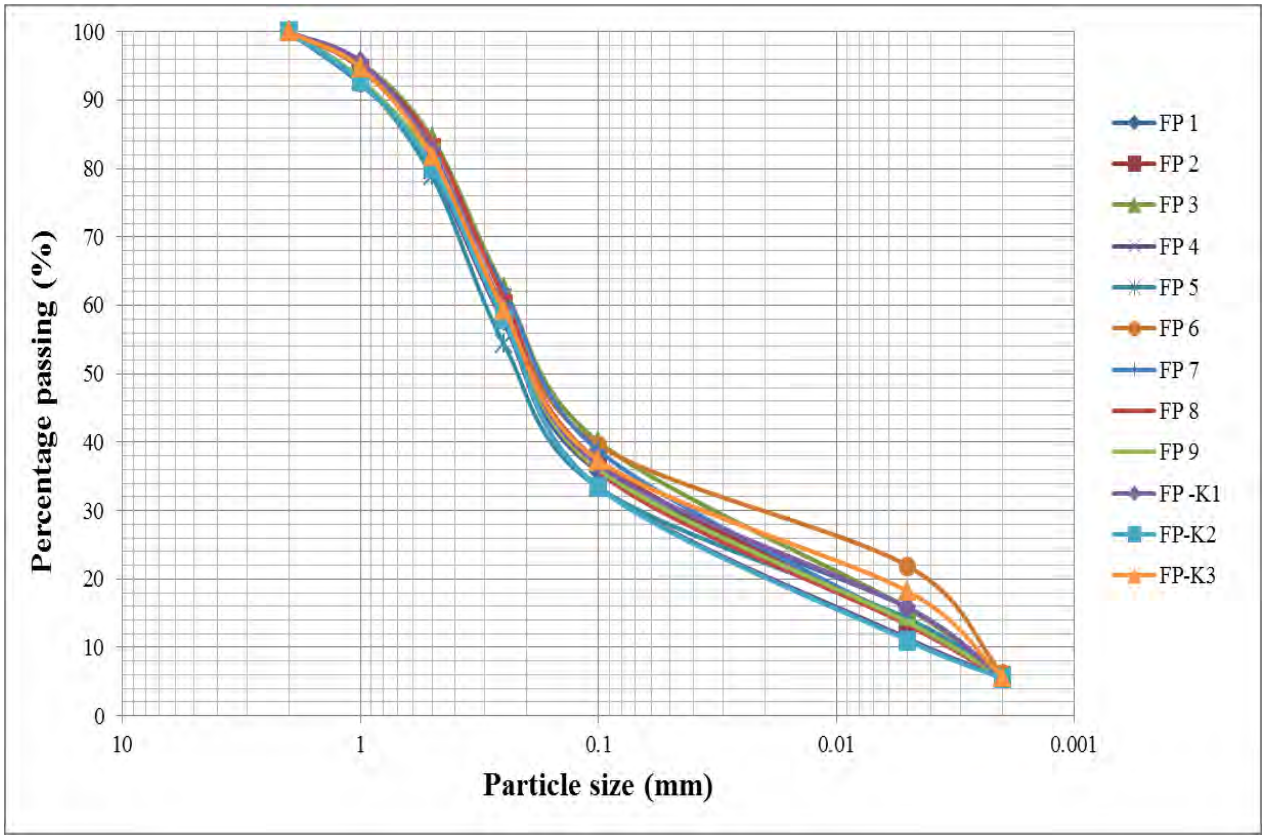

Figure 78: Particle size distribution curves of the 12 fixed point samples.

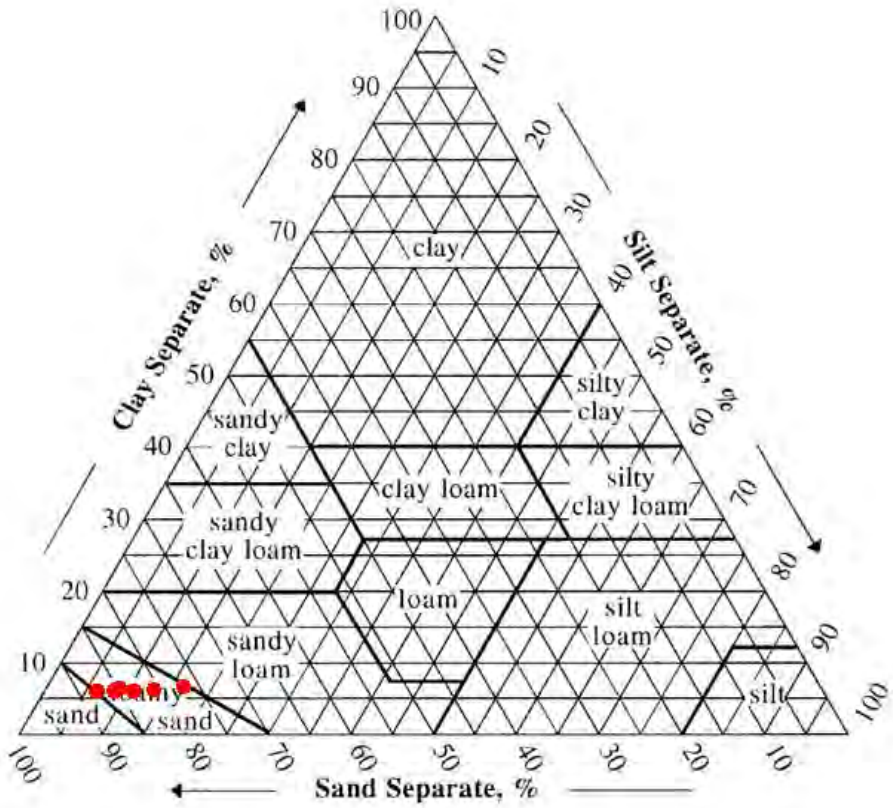

Figure 79: Soil textural triangle of the 12 fixed point soil samples (Calculated from USDA-NRCS, 2014).

Table 12: Summary of the textural properties of 12 fixed points.

Sample name	Texture	Sand %	Silt %	Clay %
FP-1	Loamy sand	84.2	10.2	5.6
FP-2	Loamy sand	86.3	8.0	5.7
FP-3	Loamy sand	84.3	10.1	5.6
FP-4	Sand	88.7	5.7	5.6
FP-5	Loamy sand	85.8	8.3	5.9
FP-6	Loamy sand	78.1	15.8	6.1
FP-7	Loamy sand	86.5	7.9	5.6
FP-8	Loamy sand	86.7	7.8	5.5
FP-9	Loamy sand	86.3	8.0	5.7
FP-K1	Loamy sand	84.2	10.2	5.6
FP-K2	Sand	89	5.5	5.5
FP-K3	Loamy sand	81.8	12.5	5.7

4.9 MINERAL PHASE IDENTIFICATION

The XRD data obtained from the 12 FPs shows a variation in salt accumulation along the pollution plume as well as in the mineralogy of the dolomitic soils in the area.

4.9.1 X-ray Diffraction

The X-ray diffractograms of the 12 FP samples are shown in Appendix G. The most common minerals expected to be in abundance in the soil in this area includes: Iron oxides (such as hematite) and in some cases manganese oxides is associated with iron oxides in plinthic soils (Fey, 2010), however it is mainly dependent of the parent material.

A list of minerals found in the 12 FP samples is set out in Table 13 to Table 17. The sulphate salts found at FP 1 (Table 13) and 6 (Table 14) are not very common minerals associated with dolomites, but are highly common in gold mining activities, and as such, these sulphate salts can be ascribed to the No. 5 TDF seepage. Although some of the sulphate salts were present again in 2013, their quantities decreased significantly, as shown in Table 15 and Table 16.

It should be noted that not one of these sulphate salts are toxic to humans or animals, but can cause irritation to the eyes and respiratory system if they fall into direct contact (Gibson, 1974 and Buck *et al.,* 2006, cited by Van Deventer, 2011b). There was a relative increase in quartz quantity, however not an absolute increase. This essentially means that as the other salts decrease the quartz % increases. The Na (Bldite) that was found could be from the shale lenses present in the dolomites. From Table 15 and Table 16 it is clear that the pollution is decreasing from 2010-2014.

The dolomites are dominated by manganese and iron as stated in Chapter 1.2.3, therefore presence the of Ca, Mg, Fe and Mn minerals, salts and oxides found in all the FP samples (Table 17) are the result of the weathering of the Oaktree Formation dolomites ($Ca,Mg(CO_3)_2$).

The presence of quartz in all the soil samples (Table 17) verify the loamy sand and sandy soils that were found with the particle size distribution analysis of the soils of the 12 FPs in Chapter 4.8.

Some of the minerals found in this area are not commonly associated with the dolomites in this area however they might be derived from the weathering of the diabase dyke and the

Ventersdorp Supergroup (such as forsterite, hedenbergite-ferrosilite, ilmenite, periclase and phlogopite).

Table 13: XRD analysis of FP-1 done in 2010.

Compound Name	Chemical Formula	SemiQuant (%)
Bldite	$Na_2Mg(SO_4)_2.4(H_2O)$	25
Gypsum	$Ca(SO_4)_2.2(H_2O)$	9
Hexahydrite	$MgSO_4.6(H_2O)$	66

Table 14: XRD analysis of FP-6 done in 2010.

Compound Name	Chemical Formula	SemiQuant (%)
Quartz	SiO_2	23
Bldite	$Na_2Mg(SO_4)_2.4(H_2O)$	12
Gypsum	$Ca(SO_4)_2.2(H_2O)$	13
Hexahydrite	$MgSO_4.6(H_2O)$	15
Epsomite	$MgSO_4.7(H_2O)$	5.4

Table 15: XRD analysis of FP-1 done in 2013.

Compound Name	Chemical Formula	SemiQuant (%)
Quartz	SiO_2	92.3
Bldite	$Na_2Mg(SO_4)_2.4(H_2O)$	3.1
Gypsum	$Ca(SO_4)_2.2(H_2O)$	0.2
Chloritoid	$(Fe,Mg,Mn)_2Al_4Si_2O_{10}(OH)_4$	3.0
Fluorophlogopite, ferroan	$KFe_2AlSi_2Al_2O_{10}(OH)_2$	1.5

Table 16: XRD analysis of FP-6 done in 2013.

Compound Name	Chemical Formula	SemiQuant (%)
Quartz	SiO_2	87.9
Bldite	$Na_2Mg(SO_4)_2.4(H_2O)$	4.5
Gypsum	$Ca(SO_4)_2.2(H_2O)$	1.3
Jacobsite	$MnFe_2O_4$	0.9
Calcite magnesian	$(Ca,Mg)CO_3$	5.4

Table 17: Results of the XRD analysis of the remaining 10 fixed points done in 2013.

Minerals	Chemical formula	FP-2	FP-3	FP-4	FP-5	FP-7	FP-8	FP-9	FP-K1	FP-K2	FP-K3
Quartz	SiO_2	X	X	X	X	X	X	X	X	X	X
Jacobsite	$MnFe_2O_4$	X	X	X	X		X	X	X	X	X
Chloritoid	$(Fe,Mg,Mn)_2Al_4Si_2O_{10}(OH)_4$	X	X	X	X	X	X	X	X	X	X
Periclase	MgO	X	X	X		X	X	X			X
Hematite	Fe_2O_3	X	X								
Manganite	$MnO(OH)$	X	X		X		X			X	
Calcite	$CaCO_3$	X					X	X		X	X
Forsterite	Mg_2SiO_4	X	X	X	X	X		X		X	X
Ilmenite	$FeTiO_3$	X	X				X	X			
Hedenbergite-Ferrosilite	$Fe_2Si_2O_6$	X	X	X				X			
Pyrochroite	$Mn(OH)_2$		X					X		X	X
Magnesioferrite	$MgFe_2O_4$		X		X	X	X	X		X	
Phlogopite	$KMg_3(AlSi_3O_{10})(F,OH)_2$								X	X	X

4.10 BASIC CONCLUSION

From the above data it is clear that the pollution plume did diminish in size, and the pollution process on the soil ceased. The soil did recover from the pollution due to the percolation and infiltration of rain water and the dolomitic bedrock of this area. The total trace metal elements did not exceed the TMT except for As (FP-K3) in 2014.

Most of the trace metal elements are present due to the natural weathering of the dolomites of the Oaktree Formation dolomites and the shales of the Black Reef Formation. The soluble/available trace metal elements decreased from 2011 to 2014 to potentially plant-deficient levels, even though Cr and U exceeded the MAT values in 2011.

CHAPTER 5: WATER ANALYSES RESULTS AND DISCUSSION

After the data evaluation, only 10 borehole sites remained with only 80 datasets, as shown in Table 6. The data used in this chapter were used to graph 24 diagrams (Ternary, Piper and Stiff), as shown in Appendix H.

The data that were employed contained ranges from 2010 to 2012, and in the case of VAN 6, 2002 up to 2004, and 2010 up to 2012. The samples taken in 2013 and 2014 filtered out with a ± 5% filter which could not be used as accurate data and were therefore discarded.

5.1 TERNARY DIAGRAMS

The ternary diagrams created for the three major anions (HCO_3^-, SO_4^{2-} and Cl^-) are shown in Appendix H1. The diagrams for the complete set of borehole sites and all the years show no evidence of sulphate or chlorine contamination. The diagrams show, according to Huizenga (2011), that chemical rock weathering is the main contributor to the inorganic chemistry of the groundwater.

All the sites plotted within the HCO_3 > 0.7 region, as shown in Table 18, with minor variations in the plots.

Table 18: Summative representation of the ternary diagrams for the borehole sites with plots greater than 0.7 HCO_3.

Borehole sites	**HCO_3 > 0.7 region (100%)**
VAN 1	2010-2012
VAN 2	2010-2012
VAN 3	2011-2012
VAN 4	2010-2012
VAN 6	2002-2004, 2010-2012
VAN 7	2010-2012
BH 3	2008
BH 8	2008
FS008	2003
FS009	2003

5.2 PIPER DIAGRAMS

The Piper diagrams created for the major cations and anions (Ca^{2} , Mg^{2} , Na , K , HCO_3^- Cl^- and SO_4^-) are shown in Appendix H2.

The diagrams for the complete set of borehole sites and all the years show that the stations have high Ca^{2} , Mg^{2} and HCO_3^- values, which are the result of the dolomitic ($CaMg(CO_3)_2$) bedrock. The diagrams also revealed that the water is low in Na , K , Cl^- and SO_4^- values. In 2012, VAN 2 showed an increased in Na and K ; however, the other sites remained almost the same with minor variations in plots. These diagrams indicate that sulfate or chlorine contamination is not present.

5.3 STIFF DIAGRAMS

The Stiff diagrams created for the major cations and anions (Ca^{2} , Mg^{2} , Na , K , HCO_3^- Cl^- and SO_4^-) are shown in Appendix H3. The Stiff diagrams have been created to represent the average concentrations in meq/ℓ for each station.

All the diagrams show the highest concentrations for HCO_3^- Mg^{2} Ca^{2} , with significantly low concentrations for Na K SO_4^- Cl^-. The general shape of the Stiff diagrams of stations VAN 1, 3, 4, 6 and 7, BH 3, 8 and FS009 are nearly identical with only minor variations in width.

VAN 2 Stiff diagrams show variation from 2010 to 2012, with a decrease in calcium in 2011 and 2012. In 2012, the sodium increased while the magnesium decreased.

FS008 depicts a low calcium concentration in relation to the other station; however, there is only one dataset for this station and thus it cannot be considered as a variation.

It should be noted that some of the boreholes (BH 3, BH 8, FS008 and FS009) only contained data from one year, and as such, comparisons cannot be drawn. However, it is regarded as evident that the water chemistry is controlled by chemical rock weathering and not pollution.

5.4 BASIC CONCLUSION

The groundwater results obtained during this study indicate that the groundwater quality of the area is not affected by the No. 5 TDF. The mechanism that controls the groundwater chemistry in this area was identified as chemical rock weathering of the dolomitic bedrock, which is indicated by the high concentrations of Ca^{2} , Mg^{2} and HCO_3^- in the groundwater; no chloride salinisation or sulphate contamination is present.

Therefore, it can be said that the groundwater is not polluted in this area.

CHAPTER 6: GEOPHYSICAL SURVEY, SURFACE OBSERVATIONS AND DOWN-HOLE CAMERA SURVEY RESULTS AND DISCUSSION

The geo-magnetic and down-hole camera survey were conducted to investigate the area for potential dyke systems which may divide the area into water compartments, faults, joints and cavities/sinkholes present in the dolomites; this may contribute towards the pollution plume that is visible in the study area.

6.1 MAGNETOMETER SURVEY

The geo-magnetic data are shown in Appendix I. The geo-magnetic survey revealed the presence of both minor and major anomalies. The minor anomalies are related to lithological changes such as the shale lenses, manganese and iron-rich dolomite variations and/or changes in topography, such as thin dolomite layers and underlying Black Reef and Ventersdorp lavas which, according to Van Deventer and Bloem (2007), have a higher magnetic susceptibility than the dolomites.

The six magnetometer transects (Figure 32) were conducted at 20 m intervals, three readings at each point were taken in order to obtain a high rate of accuracy. The EW-2 line, as indicated in Figure 32, displays no major anomalies, with only minor anomalies present along the line. This indicates that no geological structures occur on this transects. In the case of survey lines 1, 3 and 4 major anomalies was observe, these major anomalies are shown in Table 19 and Figure 80.

The diabase dyke that is shown on the 1:250 000, 2626 West Rand Geological Plan from the Council for Geoscience published in 1986 and was confirmed by Van Deventer and Bloem (2007), and is indicated in Figure 80 as the diabase dyke anomalies found in 2007.

An extension of the diabase dyke was found by Digby Wells & Associates and DWA (2008), and again in 2013, on the geo-magnetometer lines (EW-1, EW-3 and EW-4) as indicated in Figure 80, which confirms that the dyke extends over the area despite no field observations or outcrops. The other anomalies that were found, indicated as green dots in Figure 80, can be contributed to the bifurcation from the diabase dyke and/or underground water pipelines which are not visible on the surface. The NS magnetometer lines revealed the anomaly at 100–200 meters, which confirms the position of the dyke (as shown in Figure 80) that was observed underground (personal communication with P.W. Van Deventer, 2013) and found by GCS, Digby Wells & Associates and DWA (2008, cited by Labuschagne, 2008).

Table 19: Major magnetic anomalies found in the study area, during the magnetometer survey.

Line	Meter	Longitude	Latitude	nT
EW -1	1680	26.7912	-26.79212	27956.0
	1700	26.791	-26.79213	27969.3
	1720	26.7908	-26.79214	27973.7
	2000	26.78799	-26.79226	27957.5
	2020	26.78779	-26.79223	27971.3
	2240	26.7856	-26.79218	27955.7
	2260	26.7854	-26.79217	27965.4
	2800	26.78	-26.79213	27964.4
	2820	26.7798	-26.79214	27973.7
EW-3	340	26.7894	-26.80691	27956.74
	360	26.7892	-26.80691	27960.43
	380	26.789	-26.80693	27962.15
	460	26.7882	-26.80702	27959.81
	480	26.788	-26.80705	27964.86
	500	26.7878	-26.80708	27973.02
EW-4	80	26.792	-26.80717	27939.76
	100	26.7918	-26.80722	27950.54
	420	26.7884	-26.80786	27933.18
	440	26.7882	-26.80784	27970.38
	460	26.788	-26.80784	27937.13
	480	26.7878	-26.80784	27958.21
	780	26.7848	-26.80784	27910.09
	800	26.7846	-26.80784	27967.50
NS-1	100	26.79951	-26.82808	27940.48
	120	26.79944	-26.82782	27957.33
	140	26.79942	-26.82768	27962.85
	180	26.79920	-26.82752	27949.55
	200	26.79915	-26.82702	27957.80
NS-2	100	26.78633	-26.8309	27993.63
	120	26.78627	-26.83069	28030.33
	140	26.7862	-26.83048	27989.6
	160	26.78615	-26.83028	27995.2
	180	26.78604	-26.83009	27982.93

The dyke does not outcrop in this area and the distance below the surface is unknown. The dyke was classified as diabase from mineral composition and creates a compartment for water flow from the dolomites to underground mine workings; it is commonly known as the Scott Diabase dyke (Digby Wells & Associates and DWA, 2008).

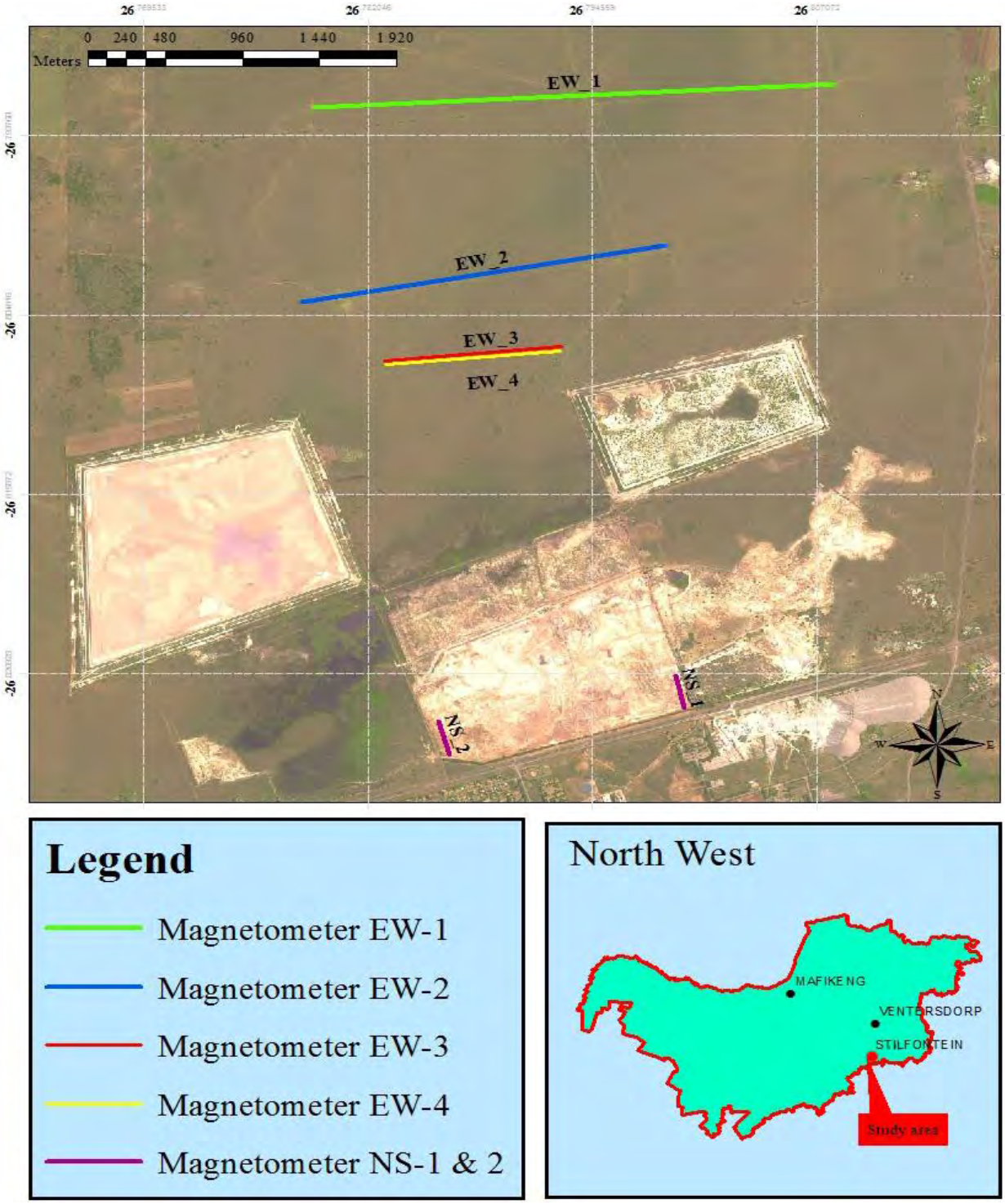

Figure 80: Potential dykes found and magnetometer anomalies found in the study area. (Google Earth, 2013).

6.2 SURFACE OBSERVATIONS AND DOWN-HOLE CAMERA SURVEY

6.2.1 Surface Observations

The surface dolomites of the Oaktree Formation show the presence of joints and fractures as illustrated in Figure 81. These joints and fractures are frequently found in the study area. There were no signs of any caves/sinkholes in this area, only that shallow holes are present which, as shown in Figure 82, form undulating structures in the Oaktree dolomites. These shallow hole structures tend to form in the absence of chert in the dolomites due to the fact that the chert creates a semi-impermeable layer over the dolomites; if the chert is not present, the dolomites have a tendency to weather in this way (Figure 82).

No visible geological structures such as faults were found in the Oaktree Formation in this area. Van Deventer and Bloem (2007) found some isolated vegetation anomalies in this area; however, no paleo sinkholes were found. Dolomite outcrops cover the whole area with no evidence of other dyke outcrops.

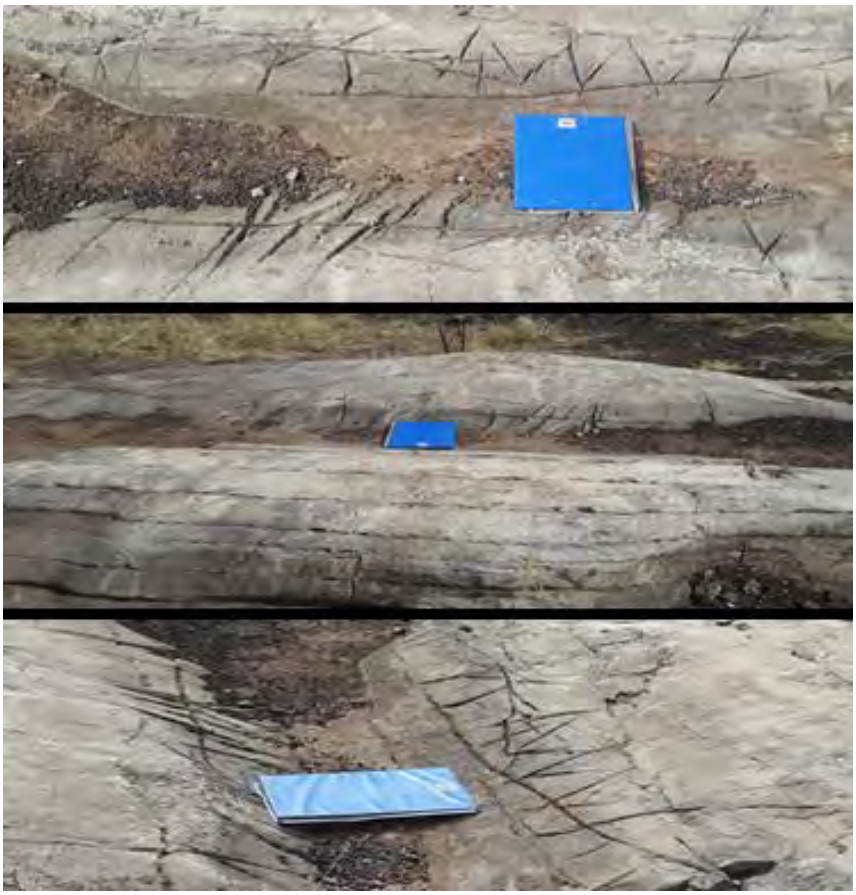

Figure 81: Photographs showing the fractures and joints present on the surface dolomites. Photographs taken by Daniell (2014).

Figure 82: Photograph showing a shallow hole present on the surface of the Oaktree Formation dolomites in the study area. Photograph taken by Daniell (2014).

6.2.2 Aerial Examination of the Plume

Aerial photographs were taken during this study to examine the plume; however, the photographs were not usable, due to the fact that the aeroplane could not fly at the necessary height in order for the target area to be correctly framed. The portions of the area that were photographed displayed no signs of the plume, nor in soil and/or vegetation anomalies.

6.2.3 Down-hole Camera Survey

The videos taken during the down-hole camera survey in selected boreholes are shown in Appendix J. A summary of the surveyed boreholes are shown in Appendix J1. The camera resolution was not sufficient enough to allow for differentiation between dolomites of the Oaktree Formation and/or the quartzite and shales of the Black Reef Formation.

The down-hole camera survey conducted in the 10 boreholes (Figure 29) revealed the presence of cavities, fractures and joints within the Oaktree dolomites, as shown in Figure 83.

No depressions such as dolines, sinkholes or large cavities (which are commonly associated with dolomites and gold mining activities) were found, although for approximately 56 years, the gold waste materials from the Stilfontein Gold Mine were deposited on this dolomitic formation.

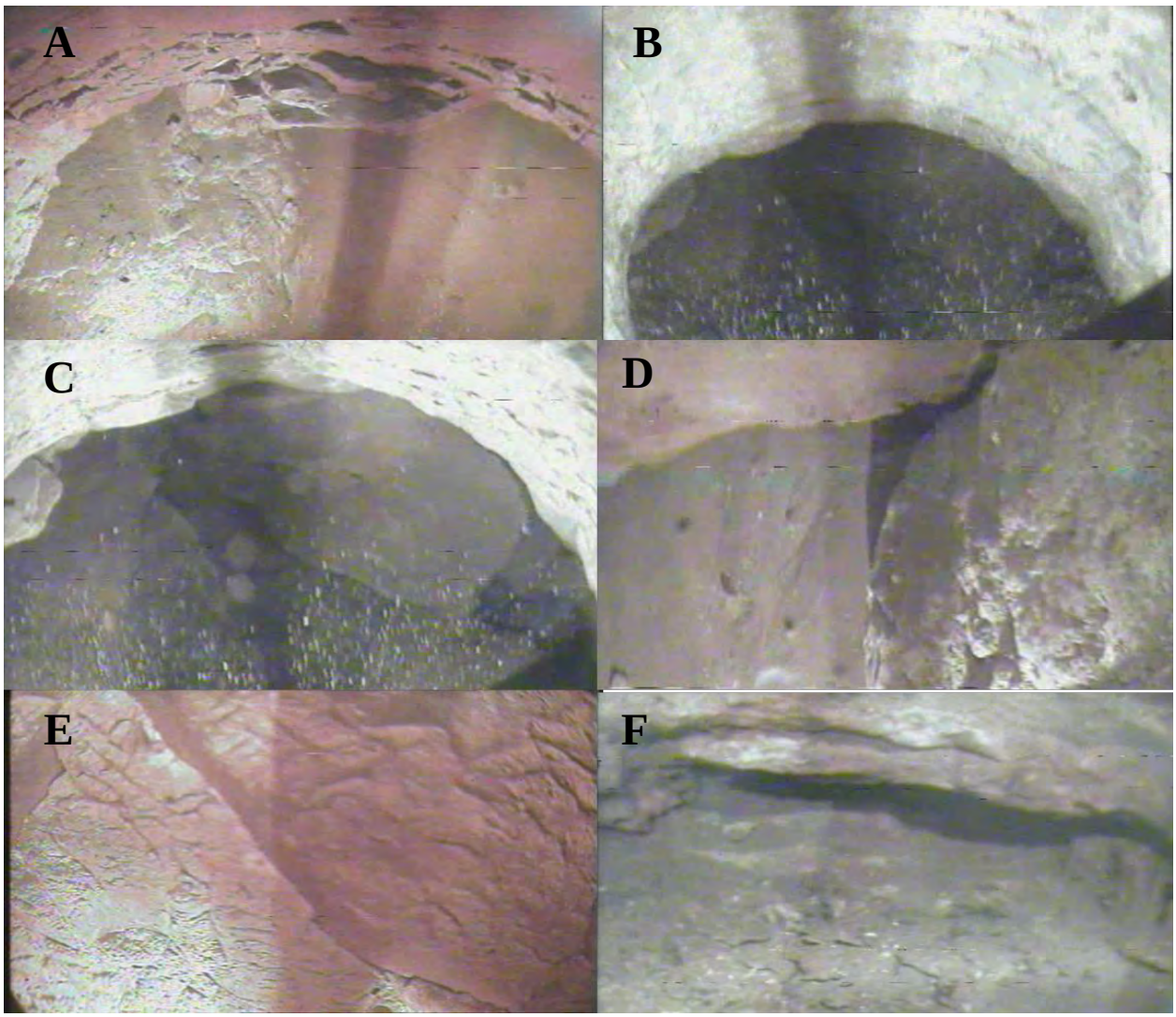

Figure 83: Down-hole camera photographs. A: Shows a cavity. B: Shows a cavity. C: Shows a cavity. D: Shows fractures. E: Shows joints. F: Shows fractures. All present within the Oaktree Formation dolomites.

6.3 BASIC CONCLUSION

From the data gathered during the geo-magnetic survey, the down-hole camera survey and the field observations, it is clear that there are dyke systems present which divide the area into compartments. Fractures, joints and cavities are also common features which serve as pathways for the groundwater to flow from the TDF to the study area. Evidence also suggests that the Oaktree dolomites do not form major depressions such as dolines, sinkholes or large cavities, although these are commonly associated with dolomites in South Africa. It should be noted that no differences in the groundwater chemistry at either sides of the dyke was found. The groundwater chemistry stayed the same throughout the study area.

CHAPTER 7: VEGETATION AND LANDSCAPE FUNCTION ANALYSIS (LFA) RESULTS AND DISCUSSION

This chapter contains the vegetation analysis result, LFA results and Descending Point Method analyses from 2012, which were conducted by DS Malo, as well as the results obtained in 2013 and 2014.

This was conducted in order for a comparison to be drawn against the findings from 2012 up to 2014, and to estimate if the vegetation quality on the farm decreased or increased in terms of density, functionality, chemistry and species variation relative to the time period.

7.1 VEGETATION CHEMICAL ANALYSES

In Table 20 to Table 22, the macro– and micronutrient uptake of the three different grass species (*Cynodon dactylon, Eragrostis chloromelas and Setaria sphacelata* var. *torta)* are shown in mg/kg for 2012, 2013 and 2014, respectively. The nutrients include: Na, K, Ca, Mg, Mn and Fe. The complete data sets are shown in Appendix K1.

In 2012 and 2013, sampling was conducted in April and May, and as a result, some species were already dormant (note: empty table rows) and therefore samples could not be taken. In 2014, sampling was conducted in March, resulting in 2014 being the year accompanied by the most abundant grass species out of the three years.

In 2012, 2013 and 2014, the Ca, Mg and K concentrations were the highest for some of the grass species, which is likely due to the dolomitic bedrock of the Oaktree Formation. The results from this analysis reveal that the three grass species accumulate high concentrations of Ca, Mg, K and phosphorus [P].

C. dactylon and *S. sphacelata* var. *torta* display a higher accumulation of K and P for the three years, as well as for Mn and Fe.

From Table 20, Table 21 and Table 22, it is clear that *C. dactylon* is the best suited amongst the three grass species to absorb chemical elements on most of the sites, although it occurred at a lower frequency than the other species in 2012.

Setaria sphacelata var. *torta* was ranked second in terms of nutrient accumulation and it was the most absent species in 2012, 2013 and 2014. The *E. chloromelas* species accumulated the least macro- and micronutrients throughout this study.

The high Mn and Fe concentrations in the grass species are most likely due to dolomites, which are typically Mn and Fe-rich, which results in soils being dominated by Mn and Fe oxides (oxisoils), as mentioned in Chapter 1.2.3.

The toxic level for Mn is considered to be 1000 mg/kg (Seiderer, 2011) and none of the sites exceeded this toxic level.

Römheld and Marscher (1991, cited by Madejon *et al.,* 2002) stated that the exact definition of the critical toxicity concentration for Fe is hard, since the quantity of Fe (III), which precipitates, especially in the apoplast, vs. the highly toxic Fe^{2+}, which easily circulates in the cytoplasm and cell organelles, is not known.

No toxicity or deficiencies of elements was found in any of the selected species.

The high concentrations of macro- and micronutrients in the vegetation samples correspond with the high concentrations in the soil. However, the concentrations in the grasses are higher than in the substrate, which indicates that the grasses do accumulate chemical elements in this area.

It is difficult to compare the years with each other due to the lack of certain species from 2012 to 2014; however, the overall macro and micronutrients concentration appears to be relatively the same for the different grass species in 2012, 2013 and 2014 (Table 20, Table 21 and Table 22) with minor variations.

Table 20: Vegetation chemical analyses of species for micro- and macro-nutrient concentration (mg/kg) in 2012.

Sites	Species	Ca	Mg	Na	K	P	Mn	Fe
FP 1	*Cynodon dactylon*	4655	1302.5	181.5	7267.5	1043.8	235	164.7
FP 1	*Eragrostis chloromelas*	2962.5	1103	152.4	7055	1007.5	51.7	86.4
FP 1	*S. sphacelata var. torta*	2299.8	1329.8	171.6	14952.5	939.5	50.6	81.2
FP 2	*Cynodon dactylon*	-	-	-	-	-	-	-
FP 2	*Eragrostis chloromelas*	2655	785	146.2	7545	1010.3	56.4	89.5
FP 2	*S. sphacelata var. torta*	2535	1347	148	15585	1078.5	58.9	70.8
FP 3	*Cynodon dactylon*	2660	1411.3	166.5	8342.5	1328.8	96.1	144.1
FP 3	*Eragrostis chloromelas*	1716	481.8	152.8	3665	622.8	27.1	75.6
FP 3	*S. sphacelata var. torta*	3235	1351.5	169.8	17002.5	1060.3	48.2	79.2
FP 4	*Cynodon dactylon*	3710	1991.3	159.8	8970	1299.8	100.5	174.7
FP 4	*Eragrostis chloromelas*	2022.3	662.3	150.2	4225	693	35.3	77.6
FP 4	*S. sphacelata var. torta*	-	-	-	-	-	-	-
FP 5	*Cynodon dactylon*	3157.5	1769	135.1	9862.5	1234.5	38.9	99.7
FP 5	*Eragrostis chloromelas*	1889.5	503.8	165	4877.5	787.3	46.6	68.5
FP 5	*S. sphacelata var. torta*	2950	2142.3	162.2	32325	1168.8	20.6	60.6
FP 6	*Cynodon dactylon*	3742.5	2260.8	168.6	32325	1401	32.9	106.3
FP 6	*Eragrostis chloromelas*	2570	2522.5	162.4	12847.5	1198.5	25	65.8
FP 6	*S. sphacelata var. torta*	-	-	-	-	-	-	-
FP 7	*Cynodon dactylon*	1886.5	817.5	137.1	22170	650	15.8	73.2
FP 7	*Eragrostis chloromelas*	-	-	-	-	-	-	-
FP 7	*S. sphacelata var. torta*	-	-	-	-	-	-	-
FP 8	*Cynodon dactylon*	-	-	-	-	-	-	-
FP 8	*Eragrostis chloromelas*	2682.5	1387.3	144.3	3397.5	680.8	27.7	103.8

Table 20: Vegetation chemical analyses of species for micro- and macro-nutrient concentration (mg/kg) in 2012.

Sites	Species	Ca	Mg	Na	K	P	Mn	Fe
FP 8	*S. sphacelata var. torta*	-	-	-	-	-	-	-
FP 9	*Cynodon dactylon*	-	-	-	-	-	-	-
FP 9	*Eragrostis chloromelas*	-	-	-	-	-	-	-
FP 9	*S. sphacelata var. torta*	3767.5	1638.3	140	7090	1059.8	94.1	134.9
FP K1	*Cynodon dactylon*	-	-	-	-	-	-	-
FP K1	*Eragrostis chloromelas*	-	-	-	-	-	-	-
FP K1	*S. sphacelata var. torta*	2642.5	1157.5	109.8	7852.5	1078.8	174.3	148.9
FP K2	*Cynodon dactylon*	2447	687	150.8	8042.5	909	43.3	77.5
FP K2	*Eragrostis chloromelas*	-	-	-	-	-	-	-
FP K2	*S. sphacelata var. torta*	3532.5	1421	144.8	4132.5	955.3	194	207.7
FP K3	*Cynodon dactylon*	3532.5	1421	144.8	8232.5	955.3	194	207.7
FP K3	*Eragrostis chloromelas*	-	-	-	-	-	-	-
FP K3	*S. sphacelata var. torta*	1569.8	845.3	165.5	13577.5	588.8	60.1	70

Table 21: Vegetation chemical analyses of species for micro- and macro-nutrient concentration (mg/kg) in 2013.

Sites	Species	Ca	Mg	Na	K	P	Mn	Fe
FP 1	*Cynodon dactylon*	4542.5	946.25	316.75	3907.5	705	165.95	216.6
FP 1	*Eragrostis chloromelas*	2149.25	442.25	348.25	3322.5	690.75	53	167.275
FP 1	*S. sphacelata var. torta*	-	-	-	-	-	-	-
FP 2	*Cynodon dactylon*	-	-	-	-	-	-	-
FP 2	*Eragrostis chloromelas*	1574.5	314	349	1948	593	62.3	354.5
FP 2	*S. sphacelata var. torta*	3370	1124.25	320.25	6092.5	686.25	141.025	347.25

Table 21: Vegetation chemical analyses of species for micro- and macro-nutrient concentration (mg/kg) in 2013.

Sites	Species	Ca	Mg	Na	K	P	Mn	Fe
FP 3	*Cynodon dactylon*	-	-	-	-	-	-	-
FP 3	*Eragrostis chloromelas*	1937.5	477	442	1920.75	508.5	30.9	174.35
FP 3	*S. sphacelata var. torta*	-	-	-	-	-	-	-
FP 4	*Cynodon dactylon*	3150	1682.25	358.5	5327.5	796.75	233.8	656.75
FP 4	*Eragrostis chloromelas*	2620	562.5	345	3580	838.5	61.5	220.925
FP 4	*S. sphacelata var. torta*	-	-	-	-	-	-	-
FP 5	*Cynodon dactylon*	2720	1597.75	351	6677.5	1009	84.65	241.375
FP 5	*Eragrostis chloromelas*	2892.5	1051.25	359	4672.5	820.25	35.1	227.875
FP 5	*S. sphacelata var. torta*	-	-	-	-	-	-	-
FP 6	*Cynodon dactylon*	3835	2116	356.25	4017.5	883	54.25	169.5
FP 6	*Eragrostis chloromelas*	2730	1343	367	3417.5	772	24	164.925
FP 6	*S. sphacelata var. torta*	-	-	-	-	-	-	-
FP 7	*Cynodon dactylon*	-	-	-	-	-	-	-
FP 7	*Eragrostis chloromelas*	-	-	-	-	-	-	-
FP 7	*S. sphacelata var. torta*	-	-	-	-	-	-	-
FP 8	*Cynodon dactylon*	-	-	-	-	-	-	-
FP 8	*Eragrostis chloromelas*	2497.75	690	369.75	2283.25	549.5	21.47	188.1
FP 8	*S. sphacelata var. torta*	5075	1785	398.25	4120	667.25	30.725	283.75
FP 9	*Cynodon dactylon*	-	-	-	-	-	-	-
FP 9	*Eragrostis chloromelas*	-	-	-	-	-	-	-
FP 9	*S. sphacelata var. torta*	-	-	-	-	-	-	-
FP K1	*Cynodon dactylon*	-	-	-	-	-	-	-
FP K1	*Eragrostis chloromelas*	1807.5	425.75	346.75	3402.5	694.25	116.325	358.75

Table 21: Vegetation chemical analyses of species for micro- and macro-nutrient concentration (mg/kg) in 2013.

Sites	Species	Ca	Mg	Na	K	P	Mn	Fe
FP K1	*S. sphacelata var. torta*	3495	1184.75	359	7010	656.75	199.375	228.1
FP K2	*Cynodon dactylon*	-	-	-	-	-	-	-
FP K2	*S. sphacelata var. torta*	-	-	-	-	-	-	-
FP K3	*Cynodon dactylon*	-	-	-	-	-	-	-
FP K3	*Eragrostis chloromelas*	2011	449	350.5	4235	656.5	112.4	218.275
FP K3	*S. sphacelata var. torta*	3702.5	1172.75	386.25	7680	647	133	184.65

Table 22: Vegetation chemical analyses of species for micro- and macro-nutrient concentration (mg/kg) in 2014.

Sites	Species	Ca	Mg	Na	K	P	Mn	Fe
FP 1	*Cynodon dactylon*	3730	1273.5	352.25	8910	858.5	93.575	107.95
FP 1	*Eragrostis chloromelas*	2592.5	566.25	355	4592.5	680.75	43.05	142.25
FP 1	*S. sphacelata var. torta*	-	-	-	-	-	-	-
FP 2	*Cynodon dactylon*	5375	1852.25	334	12955	1219.5	88.825	174.85
FP 2	*Eragrostis chloromelas*	-	-	-	-	-	-	-
FP 2	*S. sphacelata var. torta*	2512.5	1998.75	356.25	16617.5	947	118.675	93.175
FP 3	*Cynodon dactylon*	3462.5	1897.75	385.75	6567.5	1221	414.25	634.75
FP 3	*Eragrostis chloromelas*	1972.5	691.5	364.5	4462.5	692.25	43.375	171
FP 3	*S. sphacelata var. torta*	1915	1875	292	8670	698	96.525	240.475
FP 4	*Cynodon dactylon*	3932.5	2507.5	430.75	10262.5	1388.75	431.75	900.5
FP 4	*Eragrostis chloromelas*	1584.25	595.5	351.25	4670	868	148.4	415.25
FP 4	*S. sphacelata var. torta*	-	-	-	-	-	-	-
FP 5	*Cynodon dactylon*	2677.5	1548.75	367.5	8077.5	881.75	45.675	191.8

Table 22: Vegetation chemical analyses of species for micro- and macro-nutrient concentration (mg/kg) in 2014.

Sites	Species	Ca	Mg	Na	K	P	Mn	Fe
FP 5	*Eragrostis chloromelas*	2399.25	1259.25	361.75	4705	707	26.925	158.375
FP 5	*S. sphacelata var. torta*	-	-	-	-	-	-	-
FP 6	*Cynodon dactylon*	3277.5	2484.5	396.75	8412.5	1138.25	62.15	295
FP 6	*Eragrostis chloromelas*	2715	2072.25	378	4560	849.75	27.075	178.225
FP 6	*S. sphacelata var. torta*	-	-	-	-	-	-	-
FP 7	*Cynodon dactylon*	3302.5	1743	412	10450	1266	82.125	110.95
FP 7	*Eragrostis chloromelas*	2790	805.25	353.25	4365	924.5	37.825	99.125
FP 7	*S. sphacelata var. torta*	2322.25	2927.5	368.75	10185	925.5	70.575	73.4
FP 8	*Cynodon dactylon*	3922.5	2925	440.25	7317.5	845.25	60.15	224.8
FP 8	*Eragrostis chloromelas*	2243.75	1025	316	3442.5	628	29	127.05
FP 8	*S. sphacelata var. torta*	-	-	-	-	-	-	-
FP 9	*Cynodon dactylon*	3637.5	1760.25	407.5	6647.5	1057.25	61.95	188.825
FP 9	*Eragrostis chloromelas*	2186.25	938.25	350.5	4855	649.5	31.275	119.25
FP 9	*S. sphacelata var. torta*	-	-	-	-	-	-	-
FP K1	*Cynodon dactylon*	3260	1258.75	350.5	8210	1150.25	196.15	302.75
FP K1	*Eragrostis chloromelas*	1859.5	498.75	339	4317.5	660	86.775	181.3
FP K1	*S. sphacelata var. torta*	1434.75	1202.75	307.75	10652.5	636.25	190.675	101.075
FP K2	*Cynodon dactylon*	2652.5	1373	539.25	9475	1136	175.6	214.8
FP K2	*Eragrostis chloromelas*	1686	819.25	348.25	7622.5	1013.75	77.55	103.675
FP K2	*S. sphacelata var. torta*	1117.25	1113	311.25	11852.5	946	120.775	120.95
FP K3	*Cynodon dactylon*	2820	1495.75	374.25	10547.5	1033.25	241.575	387
FP K3	*Eragrostis chloromelas*	2005.25	757.5	298.5	4367.5	720.25	119.3	262.5
FP K3	*S. sphacelata var. torta*	-	-	-	-	-	-	-

7.2 TRACE METAL ELEMENTS CONCENTRATIONS IN THE VEGETATION

The high concentration of toxic trace metal elements in soils is reflected by higher concentrations of metal elements in plants, and consequently in animal and human bodies (Buszewski *et al.,* 2000). Heavy metal uptake is important for plants, but at a certain level the accumulation of heavy metals can become toxic to plants, and subsequently also animals and humans (Madejon *et al.,* 2002, cited by Malo, 2012). The nine trace metal elements are shown in Table 23 to Table 25. None of the species exceeded the TMTs for soluble/available trace metal elements as set out in Table 10.

Zinc showed the highest concentrations and greatest variations in the three grass species at all of the FP sites (Table 23, Table 24 and Table 25), with the highest values measured for *C. dactylon* at FP-1 - 49.3 mg/kg [2012] and 36.6 mg/kg [2013], and at FP-K1 - 82.5 mg/kg [2014]. This may also be from the dolomitic bedrock that contains natural Zn and Ni as indicated in Chapter 1.2.3 of this study.

All the species proved to be well adapted for the accumulation of Zn cations, although the concentrations in the plants are relatively low in relation to their toxic levels. Minor differences were observed for the other trace metal elements in the different species in 2012–2014. The grass species accumulated more Zn than there were observed in the soil samples (Table 11).

The other trace metal elements never exceeded 10 mg/kg throughout this investigation. The Cd concentration increased slightly from 2012 to 2014; however, this increase is not of concern due to the fact these values are substantially lower than the TMT values for Cd of 3 mg/kg.

Chromium concentrations increased at several sites (Table 25) in 2014, but remained nearly the same at the majority of the sites. Cobalt stayed the same over the three years. The Ni concentration decreased in 2013 (Table 24); however, it increased again in 2014 to nearly the same values as in 2012 (Table 23).

The Cu concentration remained close to the values which occurred in 2012, with the highest Cu concentrations in *E. chloromelas* at FP-5 in 2012 (9.7 mg/kg), and in *C. dactylon* at FP-4 in 2013 and 2014 (4.2 mg/kg and 8.5 mg/kg, respectively). Lead, As and U concentrations decreased from 2012 to 2014.

The highest As values were observed in *C. dactylon* (0.4 mg/kg) in 2012. Plants readily take up arsenite and arsenate, the major forms of As, which is greatly influenced by soil texture and competing phosphates (Malo, 2012). *Cynodon dactylon* was found to have the highest absorption of these heavy metals, followed by *S. sphacelata* var. *torta* and *E. chloromelas.*

Table 23: Total trace metal element concentration (mg/kg) of the different grass species samples on each site in 2012 (EPA 3050B, 1996).

Sites	Species	Cd	Cr	Co	Ni	Cu	Zn	Pb	As	U
FP 1	*Cynodon dactylon*	0.03	4.6	0.3	2.0	6.2	49.3	0.6	0.4	0.2
FP 1	*Eragrostis chloromelas*	0.01	4.5	0.2	1.2	6.5	11.2	0.5	0.2	0.1
FP 1	*S. sphacelata var. torta*	0.02	4.5	0.2	1.3	4.5	19.9	0.5	0.2	0.2
FP 2	*Cynodon dactylon*	-	-	-	-	-	-	-	-	-
FP 2	*Eragrostis chloromelas*	0.01	4.6	0.1	1.2	5.6	12.9	0.5	0.3	0.1
FP 2	*S. sphacelata var. torta*	0.01	4.5	0.2	1.0	4.2	16.7	0.5	0.2	0.1
FP 3	*Cynodon dactylon*	0.01	4.7	0.2	1.6	4.4	23.5	0.5	0.2	0.1
FP 3	*Eragrostis chloromelas*	0.005	4.3	0.1	1.0	4.8	9.9	0.5	0.2	0.1
FP 3	*S. sphacelata var. torta*	0.01	4.4	0.1	1.1	5.6	13.2	0.5	0.2	0.1
FP 4	*Cynodon dactylon*	0.01	4.7	0.2	1.2	5.1	21.7	0.5	0.2	0.1
FP 4	*Eragrostis chloromelas*	0.005	4.1	0.1	1.0	5.1	16.8	0.5	0.2	0.1
FP 4	*S. sphacelata var. torta*	-	-	-	-	-	-	-	-	-
FP 5	*Cynodon dactylon*	0.01	4.3	0.1	1.0	4.0	23.2	0.5	0.2	0.1
FP 5	*Eragrostis chloromelas*	0.01	4.4	0.1	0.9	9.7	21.8	0.5	0.2	0.1
FP 5	*S. sphacelata var. torta*	0.02	4.5	0.1	0.8	4.7	22.6	0.5	0.2	0.1
FP 6	*Cynodon dactylon*	0.01	4.5	0.1	0.9	5.7	20.9	0.4	0.2	0.1
FP 6	*Eragrostis chloromelas*	0.01	4.3	0.1	0.8	4.5	13.7	0.4	0.2	0.1
FP 6	*S. sphacelata var. torta*	-	-	-	-	-	-	-	-	-
FP 7	*Cynodon dactylon*	-	-	-	-	-	-	-	-	-
FP 7	*Eragrostis chloromelas*	0.01	4.1	0.1	0.9	3.7	9.0	0.8	0.2	0.1
FP 7	*S. sphacelata var. torta*	-	-	-	-	-	-	-	-	-
FP 8	*Cynodon dactylon*	-	-	-	-	-	-	-	-	-
FP 8	*Eragrostis chloromelas*	-	-	-	-	-	-	-	-	-

Table 23: Total trace metal element concentration (mg/kg) of the different grass species samples on each site in 2012 (EPA 3050B, 1996).

Sites	Species	Cd	Cr	Co	Ni	Cu	Zn	Pb	As	U
FP 8	*S. sphacelata var. torta*	0.01	4.1	0.2	0.8	4.8	20.3	0.7	0.2	0.1
FP 9	*Cynodon dactylon*	-	-	-	-	-	-	-	-	-
FP 9	*Eragrostis chloromelas*	-	-	-	-	-	-	-	-	-
FP 9	*S. sphacelata var. torta*	-	-	-	-	-	-	-	-	-
FP K1	*Cynodon dactylon*	0.01	4.1	0.1	0.8	4.1	23.1	0.5	0.2	0.1
FP K1	*Eragrostis chloromelas*	-	-	-	-	-	-	-	-	-
FP K1	*S. sphacelata var. torta*	-	-	-	-	-	-	-	-	-
FP K2	*Cynodon dactylon*	0.01	4.0	0.2	1.1	3.6	32.2	0.5	0.2	0.1
FP K2	*Eragrostis chloromelas*	0.01	3.9	0.1	0.9	3.9	39.1	0.5	0.2	0.1
FP K2	*S. sphacelata var. torta*	-	-	-	-	-	-	-		-
FP K3	*Cynodon dactylon*	0.01	4.1	0.2	1.1	3.8	29.0	0.6	0.2	0.1
FP K3	*Eragrostis chloromelas*	-	-	-	-	-	-	-	-	-
FP K3	*S. sphacelata var. torta*	0.01	4.1	0.1	0.9	3.3	17.0	0.6	0.2	0.1

Table 24: Total trace metal element concentration (mg/kg) of the different grass species samples on each site in 2013 (EPA 3050B, 1996).

Sites	Species	Cd	Cr	Co	Ni	Cu	Zn	Pb	As	U
FP 1	*Cynodon dactylon*	0.01	1.9	0.1	0.5	3.1	36.6	0.2	0.13	0.13
FP 1	*Eragrostis chloromelas*	0.01	2.4	0.1	0.6	3.7	13.6	0.2	0.13	0.2
FP 1	*S. sphacelata var. torta*	-	-	-	-	-	-	-	-	-
FP 2	*Cynodon dactylon*	-	-	-	-	-	-	-	-	-
FP 2	*Eragrostis chloromelas*	0.0	3.3	0.2	0.8	3.3	12.5	0.5	0.2	0.2
FP 2	*S. sphacelata var. torta*	0.0	3.0	0.2	0.6	2.7	14.9	0.2	0.12	0.1

Table 24: Total trace metal element concentration (mg/kg) of the different grass species samples on each site in 2013 (EPA 3050B, 1996).

Sites	Species	Cd	Cr	Co	Ni	Cu	Zn	Pb	As	U
FP 3	*Cynodon dactylon*	-	-	-	-	-	-	-	-	-
FP 3	*Eragrostis chloromelas*	0.0	2.1	0.04	0.3	2.6	11.6	0.3	0.06	0.06
FP 3	*S. sphacelata var. torta*	-	-	-	-	-	-	-	-	-
FP 4	*Cynodon dactylon*	0.0	4.1	0.2	0.8	4.2	22.8	0.2	0.12	0.03
FP 4	*Eragrostis chloromelas*	0.0	2.6	0.1	0.3	2.8	11.5	0.2	0.07	0.04
FP 4	*S. sphacelata var. torta*	-	-	-	-	-	-	-	-	-
FP 5	*Cynodon dactylon*	0.0	3.0	0.1	0.7	4.1	10.9	0.01	0.05	0.02
FP 5	*Eragrostis chloromelas*	0.01	3.2	0.04	0.3	3.6	9.6	0.05	0.05	0.02
FP 5	*S. sphacelata var. torta*	-	-	-	-	-	-	-	-	-
FP 6	*Cynodon dactylon*	0.0	2.0	0.02	0.3	3.1	21.9	0.0	0.0	0.01
FP 6	*Eragrostis chloromelas*	0.0	2.3	0.03	0.3	2.8	10.7	0.1	0.03	0.02
FP 6	*S. sphacelata var. torta*	-	-	-	-	-	-	-	-	-
FP 7	*Cynodon dactylon*	-	-	-	-	-	-	-	-	-
FP 7	*Eragrostis chloromelas*	-	-	-	-	-	-	-	-	-
FP 7	*S. sphacelata var. torta*	-	-	-	-	-	-	-	-	-
FP 8	*Cynodon dactylon*	-	-	-	-	-	-	-	-	-
FP 8	*Eragrostis chloromelas*	0.0	2.8	0.07	0.4	2.7	11.1	0.4	0.06	0.05
FP 8	*S. sphacelata var. torta*	0.01	2.7	0.15	0.6	3.4	12.8	0.4	0.08	0.04
FP 9	*Cynodon dactylon*	-	-	-	-	-	-	-	-	-
FP 9	*Eragrostis chloromelas*	-	-	-	-	-	-	-	-	-
FP 9	*S. sphacelata var. torta*	-	-	-	-	-	-	-	-	-
FP K1	*Cynodon dactylon*	-	-	-	-	-	-	-	-	-
FP K1	*Eragrostis chloromelas*	0.0	2.5	0.1	0.9	3.5	17.4	0.3	0.06	0.1

Table 24: Total trace metal element concentration (mg/kg) of the different grass species samples on each site in 2013 (EPA 3050B, 1996).

Sites	Species	Cd	Cr	Co	Ni	Cu	Zn	Pb	As	U
FP K1	*S. sphacelata var. torta*	0.01	2.3	0.15	0.5	3.2	23.1	0.2	0.04	0.05
FP K2	*Cynodon dactylon*	-	-	-	-	-	-	-	-	-
FP K2	*Eragrostis chloromelas*	-	-	-	-	-	-	-		
FP K2	*S. sphacelata var. torta*	-	-	-	-	-	-	-	-	-
FP K3	*Cynodon dactylon*	-	-	-	-	-	-	-	-	-
FP K3	*Eragrostis chloromelas*	0.0	2.8	0.1	0.6	3.7	19.6	0.2	0.03	0.02
FP K3	*S. sphacelata var. torta*	0.0	2.9	0.1	0.3	3.2	17.8	0.1	0.04	0.02

Table 25: Total trace metal element concentration (mg/kg) of the different grass species samples on each site in 2014 (EPA 3050B, 1996).

Sites	Species	Cd	Cr	Co	Ni	Cu	Zn	Pb	As	U
FP 1	*Cynodon dactylon*	0.02	7.6	0.05	0.9	3.6	28.7	0.2	0.0	0.04
FP 1	*Eragrostis chloromelas*	0.1	2.0	0.1	0.9	3.1	15.0	0.3	0.0	0.1
FP 1	*S. sphacelata var. torta*	-	-	-	-	-	-	-	-	-
FP 2	*Cynodon dactylon*	0.01	5.9	0.1	0.7	6.2	62.4	0.2	0.0	0.03
FP 2	*Eragrostis chloromelas*	-	-	-	-	-	-	-	-	-
FP 2	*S. sphacelata var. torta*	0.01	1.4	0.02	0.5	5.1	17.4	0.1	0.0	0.2
FP 3	*Cynodon dactylon*	0.1	5.1	0.3	1.4	4.8	16.5	0.4	0.0	0.04
FP 3	*Eragrostis chloromelas*	0.01	1.6	0.1	0.6	3.5	20.4	0.4	0.0	0.04
FP 3	*S. sphacelata var. torta*	0.04	8.78	0.1	0.5	4.4	17.5	0.3	0.0	0.04
FP 4	*Cynodon dactylon*	0.04	4.4	0.4	1.8	8.5	40.6	0.5	0.0	0.05
FP 4	*Eragrostis chloromelas*	0.1	4.0	0.2	1.0	5.5	19.1	0.7	0.0	0.1
FP 4	*S. sphacelata var. torta*	-	-	-	-	-	-	-	-	-

Table 25: Total trace metal element concentration (mg/kg) of the different grass species samples on each site in 2014 (EPA 3050B, 1996).

Sites	Species	Cd	Cr	Co	Ni	Cu	Zn	Pb	As	U
FP 5	*Cynodon dactylon*	0.04	3.8	0.1	0.7	4.9	23.3	0.3	0.0	0.03
FP 5	*Eragrostis chloromelas*	0.05	7.0	0.05	1.3	3.3	14.17	0.3	0.0	0.02
FP 5	*S. sphacelata var. torta*	-	-	-	-	-	-	-	-	-
FP 6	*Cynodon dactylon*	0.05	8.3	0.1	0.6	5.9	23.6	0.3	0.0	0.03
FP 6	*Eragrostis chloromelas*	0.1	2.2	0.1	0.8	3.6	12.3	0.3	0.0	0.02
FP 6	*S. sphacelata var. torta*	-	-	-	-	-	-	-	-	-
FP 7	*Cynodon dactylon*	0.04	4.1	0.03	0.7	4.5	32.1	0.2	0.0	0.02
FP 9	*Cynodon dactylon*	0.01	2.1	0.06	0.5	3.7	11.5	0.2	0.0	0.02
FP 9	*Eragrostis chloromelas*	0.05	5.12	0.03	0.3	3.0	11.9	0.2	0.0	0.03
FP 9	*S. sphacelata var. torta*	-	-	-	-	-	-	-	-	-
FP K1	*Cynodon dactylon*	0.01	1.7	0.1	1.1	7.0	58.9	0.2	0.0	0.03
FP K1	*Eragrostis chloromelas*	0.1	6.1	0.1	0.5	3.4	20.8	0.3	0.0	0.1
FP K1	*S. sphacelata var. torta*	0.0	2.9	0.03	0.5	3.5	19.7	0.2	0.0	0.03
FP K2	*Cynodon dactylon*	0.02	3.5	0.2	1.4	5.7	82.5	0.4	0.0	0.02
FP K2	*Eragrostis chloromelas*	0.03	1.5	0.1	0.4	3.3	25.4	0.4	0.0	0.02
FP K2	*S. sphacelata var. torta*	0.01	0.9	0.04	0.7	3.7	16.6	0.3	0.0	0.02
FP K3	*Cynodon dactylon*	0.1	1.4	0.2	0.8	4.9	53.8	0.3	0.0	0.02
FP K3	*Eragrostis chloromelas*	0.03	5.3	0.1	0.5	3.5	20.2	0.3	0.0	0.03
FP K3	*S. sphacelata var. torta*	-	-	-	-	-	-	-	-	-

7.3 DESCENDING POINT METHOD ANALYSES

The groupings of grasses based on their reactions to different grazing levels are commonly referred to as their ecological status since grasses usually react to grazing in two ways: they can either increase or decrease in number (Van Oudtshoorn, 2012).

All grasses are categorized into the following groups (Van Oudtshoorn, 2012):

Decreasers (D): This grouping includes grasses that are plentiful in good veld but decreases in total when overgrazing or under-grazing occurs. These grasses are mainly preferred by grass eaters. E.g. *Digitaria eriantha* (common finger grass) and *Themeda triandra* (red grass).

Increaser 1 (I1): This grouping includes grasses that are plentiful in underused veld. They are typically unpalatable species that can grow without any defoliation. E.g. *Hyperthelia dissoluta* and *Trachypogon spicatus*.

Increaser 2 (I2): This grouping includes grasses that are plentiful in overgrazed veld. These grasses commonly increase due to the disrupting effects of overgrazing and include pioneer and subclimax species, which are more commonly found in low rainfall areas. E.g. *Aristida congesta* subsp. *congesta* (tassel three-awn) and *E. chloromelas* (narrow curly leaf). These species establish quickly on newly exposed ground by means of producing many viable seeds.

Increaser 3 (I3): This grouping includes grasses that are found in overgrazed veld and are typically unpalatable, dense, climax grasses. For example *Cymbopogon pospischilii* (narrow leaf turpentine grass).

Invaders/Exotic (E): This grouping includes grasses that are not native to an area such as *Pennisetum clandestinum* (kikuyu grass).

This classification is commonly used as a future indicator regarding what will likely occur in the veld over time, as well as the current condition of the veld (Van Oudtshoorn, 2012). The species composition at the 12 FPs in 2012 and 2014 are shown in Table 26 and Table 27. In 2012, no I1 species were found; however, in 2014, three I1 species were found to be present, namely *Hyparrhenia hirta; Schizachyrium sanguineum* and *Triraphis andropogonoides*. The I2 species were the most dominant at all the sites in 2012 and 2014. This is an indication that the veld was exposed to overgrazing, causing palatable grasses to decrease. In 2012, only one I3 grass species

was found, namely *C. pospischilii*. In 2014, two increaser 3 grass species were found, *C. pospischilii* and *Aristida diffusa*.

As mentioned in Chapter 1.2.5, the natural grass species composition should consist of *T. triandra*, but it is frequently unstable due to unpredictable rainfall, which has led to variations in the structure of these grasslands (Haagner, 2008; Mucina & Rutherford, 2006). In 2012, *T. triandra* was only found to be present at one FP (FP-K1) and in 2014, *T. triandra* was found to be present at eight of the FPs (Table 27); this indicates that the natural grass species composition of this site is being restored.

The species diversity in this area changed from *C. dactylon*, *E. chloromelas* and *S. sphacelata* var. *torta* being the dominant grasses in 2012 to *Aristida scabrivalvis*, *Eragrostis gummiflua* and *Eragrostis plana* being the dominant grass species in 2014; all of which are I2 grass species, thus indicating that the land is mainly overgrazed despite the restoration of grasses.

In 2012, the vegetation composition of FP-K2 and FP-K3 (control sites) was lower than at some of the other polluted FPs. In 2014, only control site FP-K2 was lower than some of the other polluted sites; however, this is not statistically significant.

In 2012, FP-K1 was the greatest in species abundance compared to the other sites, comprising 55% of all the grass species that were recorded during the study. In 2014, FP-2 was the greatest in species abundance compared to the other sites, comprising 53% of all the grass species recorded during this study. In 2012, FP-6 and in 2014 FP-1 had the lowest species diversity of all the others due to the enrichment of the *Scirpus ficinioides* (bulrush) and *S. plumosum* (*Afr.* Bankrotbos), respectively.

In 2012, a total of 24 different grass species were found, whereas in 2014, a total of 36 different grass species were found. The overall vegetation quantity and species composition of all the FPs increased from 2012 to 2014, with no site species composition lower than 10 different grass species per site, although overgrazing is still taking place. The natural vegetation is also beginning to restore.

Table 26: Average relative frequency of species on the three transects per site in 2012. The table also illustrates the species composition and ecological status (Malo, 2012).

Species names and ecological status (D, I1, I2, I3, E)	FP 1	FP 2	FP 3	FP 4	FP 5	FP 6	FP 7	FP 8	FP 9	FP K1	FP K2	FP K3
Anthephora pubescens (D)	-	8.3	1.8	5.0	-	-	-	-	-	5.0	-	-
Aristida congesta subsp. *congesta* (I2)	-	26.7	21.8	38.3	-	-	-	-	-	40.0	3.3	-
Aristida congesta subsp. *barbicollis* (I2)	-	-	-	-	-	-	-	-	-	-	-	5.0
Aristida stipitata (I2)	-	-	-	-	-	-	5.0	-	-	-	11.7	-
Chloris gayana (D)	-	-	-	-	-	-	-	-	-	1.7	-	-
Chloris virgata (I2)	6.7	-	-	-	-	-	-	-	5.0	-	-	-
Cymbopogon pospischilii (I3)	-	-	5.0	1.7	13.3	-	-	-	-	5.0	-	-
Cynodon dactylon (I2)	-	-	-	-	-	5.0	1.7	-	-	1.7	3.3	-
Digitaria eriantha (D)	-	-	1.7	-	-	-	31.7	-	-	1.7	23.3	-
Eragrostis chloromelas (I2)	8.3	16.7	17.4	33.3	27.4	-	23.3	1.7	-	-	-	-
Eragrostis curvula (I2)	-	-	1.7	1.7	27.0	26.7	6.7	33.3	20.0	6.7	-	6.7
Eragrostis gummiflua (I2)	68.3	8.3	3.4	-	-	-	-	-	1.7	8.3	-	1.7
Eragrostis lehmanniana (I2)	-	-	-	-	-	-	-	-	-	-	13.3	-
Eragrostis obtusa (I2)	-	-	-	-	-	-	-	-	8.3	-	-	-
Eragrostis plana (I2)	5.0	13.3	13.5	6.7	5.2	-	-	1.7	41.7	15.0	18.3	46.7
Eragrostis superba (I2)	-	-	10.5	-	1.8	-	28.3	-	23.3	-	-	-
Eustachys paspaloides (D)	-	-	-	-	1.8	-	-	-	-	-	-	-
Heteropogon contortus (I2)	-	-	-	-	-	-	-	-	-	1.7	-	-
Melinis repens (I2)	-	1.7	-	-	-	-	-	-	-	-	-	-
Pennisetum clandestinum (E)	-	-	-	-	-	-	-	-	-	-	-	3.3
Setaria sphacelata var. *torta* (D)	11.7	20.0	11.9	-	18.3	68.3	-	63.3	-	5.0	-	33.3
Themeda triandra (D)	-	-	-	-	-	-	-	-	-	1.7	-	-
Trichoneura grandiglumis (I2)	-	-	-	-	-	-	3.3	-	-	1.7	8.3	-
Urochloa mosambicensis (I2)	-	-	-	5.0	5.3	-	-	-	-	-	-	-

Table 27: Average relative frequency of species on the three transects per site in 2014. The table also illustrates the species composition and ecological status.

Species names and ecological status (D, I1, I2, I3, E)	FP 1	FP 2	FP 3	FP 4	FP 5	FP 6	FP 7	FP 8	FP 9	FP K1	FP K2	FP K3
Anthephora pubescens (D)		5	1.7	3.3			5					
Aristida congesta subsp. *congesta* (I2)		1.7	1.7	10			16.7	3.3		5	10	1.7
Aristida congesta subsp. *Barbicollis* (I2)		6.7				3.3	5		1.7			
Aristida diffusa (I3)							3.3					
Aristida scabrivalvis (I2)		10	33.3	25	5	6.7	10	18	17	22		5
Aristida sciurus		11.7		1.7					3.3			5
Brachiaria advena						1.7						
Brachiaria serrata (D)		3.3	1.7		1.7			3.3		1.7		
Chloris pycnothrix (I2 and E)											1.7	
Cymbopogon pospischilii (I1 and I3)				1.67		3.3		5	1.7	5		1.7
Cynodon dactylon (I2)	11.7	3.3		1.7	1.7	23.3		3.3			6.7	1.7
Cynodon hirsutus (I2)							1.7					
Digitaria eriantha (D)							10		3.3		5	
Eragrostis chloromelas (I2)			8.3	8.3	6.7	3.3	1.7	1.7				1.7
Eragrostis curvula (I2)	6.7	3.3	8.3	3.3	26.7	6.7	5	18	8	13		1.7
Eragrostis gummiflua (I2)	45	5	1.7	8.3	3.3	11.7		3.3	26.7	3.3		1.7
Eragrostis inamoena (I2)												1.7
Eragrostis lehmanniana (I2)	3.3	10	3.3			8.3	1.7			1.7	13.3	
Eragrostis patentipilosa (I2)											3.3	
Eragrostis plana (I2)	18.3	6.7	21.7	16.7	13.3			18.3	25	10		33.3
Eragrostis superba (I2)		10	11.7		3.3	3.3	5	6.7	6.7	8.3	5	
Eragrostis tef (E)						3.3	1.7				3.3	
Eragrostis trichophora (I2)				10			8.3				31.7	1.7
Eustachys paspaloides (D)		1.7	3.3		6.7					10		18.3
Heteropogon contortus (I2)			1.7				6.7					

Table 27: Average relative frequency of species on the three transects per site in 2014. The table also illustrates the species composition and ecological status.

Species names and ecological status (D, I1, I2, I3, E)	FP 1	FP 2	FP 3	FP 4	FP 5	FP 6	FP 7	FP 8	FP 9	FP K1	FP K2	FP K3
Hypathenia hirta (I1 and E)	1.7				8.3	1.7				6.7		8.3
Melinis repens (I2)							6.7			1.7		
Panicum maximum (D and E)					8.3	18.3			3.3			
Pogonarthria squarrosa (I2)		1.7										
Schizachyrium Sanguineum (I1)	3.3											
Setaria Sphacelata var *torta* (D)	1.7	1.7						8.3		1.7		1.7
Stipagrostis hirtigluma (I2)		1.7					1.7					
Themeda triandra (D)		1.7		3.3	13.3	5			1.7	1.7	8.3	1.7
Trichoneura grandiglumis (I2)							6.7					
Triraphis andropogonoides (I1)	5	10	1.7					8.3		8.3		10
Urochloa trichopus	3.3	5		6.7	1.7		3.3	1.7	1.7		11.7	3.3

7.4 LANDSCAPE FUNCTION ANALYSIS (LFA)

7.4.1 Patch/Inter-patch Description

The different patches and inter-patch zone documentation and descriptions form part of the organisation step of LFA. These patches and inter-patches have diverse functions in the landscape; therefore, their contribution to one function can be greater than others (Malo, 2012). Zone description was intended to establish whether indicator values of specific types varied significantly across the 12 FP sites, and it should be noted that this would not affect the overall function of the sites (Malo, 2012).

Table 28 and Table 29 assist in the summary of the mean contribution of each patch and inter-patch to the LFA index (stability, infiltration and nutrient cycling) across the 12 FP sites in 2012 and 2014. These values are influenced by the frequency of these zone types on the three selected transects, and finally their overall frequency at all sites (Malo, 2012). The data were obtained from the summary page (SSA of the individual zones) of the LFA software.

In 2012, the GLP was the most functional patch type, followed by GPs, LPs and SGPs, respectively. Malo (2012) stated that the low nutrient cycling is due to the size of the grass patches, and the little or no litter present (that are able to increase nutrient cycling). Tree patches were one of the least functional zone types for all LFA indices and were not found again in 2014. In 2014, DPs were found to be present, which is due to the fact that the farm is once again being used for grazing purposes (which was not the case in 2012).

In 2014, DPs were the most functional patch types with stability, infiltration and nutrient cycles being the highest, followed by the *S. plumosum* patch. Although the *S. plumosum* patch contributes greatly to the LFA index, the presence of these aggressive encroacher species decreases the grazing capacity of the area. They are found to be present due to their unpalatability and smell, which results in cattle not grazing in these areas (Malo, 2012); nevertheless, they generated a micro-climate environment.

The frequency of the SPPs at the different sites decreased from eight sites in 2012 to only being present at five sites in 2014. From Table 29 it is clear that all the patches contribute the most to the stability of the soil. The stability created by the LP can be of concern due to the ease with which the material is removed. The overall LFA indices for the different patches and inter-patches increased from 2012 up to 2014.

Table 28: The mean patch and inter-patch contribution to the landscape function analysis (LFA) index function for the 12 fixed points in 2012 (Malo, 2012).

Zone types	Mean Stability	Mean Infiltration	Mean Nutrient cycling	Site frequency
Dense grass patch	29.1	23.1	17.0	10
Forb patch	27.0	19.3	12.8	6
Forb grass patch	40.1	30.6	22.6	10
Grass patch	55.7	41.9	27.8	12
Inter-patch	46.7	25.7	10.2	12
Litter patch	50.8	37.6	24.1	12
Grass litter patch	59.5	46.2	35.4	8
Rock patch	38.1	10.0	11.1	6
***Seriphium plumosum* patch**	47.6	38.6	28.4	8
Sparse grass patch	50.6	32.6	19.6	12
Tree patch	28.9	24.3	17.2	2

Table 29: The mean patch and inter-patch contribution to the landscape function analysis (LFA) index function for the 12 fixed points in 2014.

Zone types	Mean Stability	Mean Infiltration	Mean Nutrient cycling	Site frequency
Dense grass patch	64.1	35.9	28.1	11
Forb patch	60.2	29.2	20.5	5
Forb grass patch	61.7	33.6	26.3	8
Grass patch	61.5	32.3	23.8	12
Inter-patch	50.1	24.8	13.4	12
Litter patch	61.5	42.3	37.9	12
Grass litter patch	63.2	39.0	34.1	12
Rock patch	66.8	23.9	12.6	5
***Seriphium plumosum* patch**	69.5	46.3	41.5	5
Sparse grass patch	57.5	30.3	22.2	8
Dung patch	75.4	50.7	50.3	3

7.4.2 LFA Values

The LFA variables used by Malo (2012) were a combination of structural and functional parameters across the 12 FPs, which were included as described by Haagner (2008):

- Stability: the index of exposure to erosion.
- Infiltration: the index of the ratio of runoff:runon.
- Nutrient Cycling: the index of litter breakdown, mineralisation and microbial activity.
- LOI: the ratio of patches:inter-patches, to indicate significance of LFA indices. The nearer the value is to one, the larger quantity of landscape is covered in patches. A landscape with an LOI value of one comprised one large patch, whereas an LOI of zero indicated no patches present in the landscape.
- Inter-patch length: average distance between patches, to itemize bare soil/tailings.
- Patch area: average patch size (m^2), to elucidate width and efficiency of patches.
- Number of patches: physical number of patches on a gradsect, to elucidate patchiness.
- Density of patches: expressed as number of patches per 10 m of gradsect.

Table 30 and Table 31 show the complete set of LFA index variables in conjunction with the LFA software in 2012 and 2014. The stability values for both survey years were the highest for all the sites, which contributed more to the functionality of the landscape than the contribution of the infiltration and nutrient cycling. Nutrient cycling for both survey years were the lowest, marking it as the smallest contributor to functionality.

According to Haagner (2008), a high Stability index value is a good indication of organic matter being incorporated which increases the soil structure.

In order to give a status to the values presented in Table 30 and Table 31, and to finally classify the site as functional or dysfunctional, a threshold value is essential. The threshold of potential concern should be calculated to state whether the site is functional (above this value) or dysfunctional (below this value). The threshold values were calculated in the same way as by Malo (2012), for comparative purposes. According to Haagner (2008), these values represent the minimum boundary at which an ecosystem recovery is adequate to handle stress and disturbances, thus avoiding the loss of landscape functionality.

The ―threshold of potential concern" (TPC) values for Stability, Infiltration and Nutrient cycling indices were calculated using the following equation: (Tongway and Hindley, 2000, cited by Haagner, 2008):

$$\text{TPC} \quad \frac{\text{Max value Min value}}{2} \quad \text{Min value} \qquad \text{Eq. 20}$$

Tongway and Hindley (2004, cited by Haagner, 2008) stated that the TPC values are an indication of the point where the indicators make up the index values for landscape self-sustainability to initiate.

Malo (2012) stated that the data shows only small variations throughout the sites, thus making this threshold value method ineffective, due to the fact that the TPC assessment can only be properly applied when the most disturbed and least disturbed examples of the landscape are included in the analysis.

All of the LFA sites do not have adverse pollution effects on the soil properties; therefore, the TPC is an overestimation resulting in most of the sites falling below the TPC values in 2012 and 2014. Data can be seen in Appendix K3.

Table 30: Summary of the Landscape Function Analysis (LFA) variables for the 2012 survey.

Site	Nr of patches/ 10 m	Total Patch Area (m^2)	LOI*	Average inter-patch length (m)	Stability	Infiltration	Nutrient cycling
FP 1	18.0	6.2	0.9	0.5	55.8	36.7	25.7
FP 2	15.1	5.4	0.8	0.6	54.4	35.9	23.6
FP 3	15.0	5.4	0.7	0.5	60.7	43.6	26.7
FP 4	19.2	3.0	0.7	0.4	53.6	36.1	21.2
FP 5	17.2	4.4	0.7	0.6	53.1	36.4	20.9
FP 6	14.9	4.9	0.8	0.7	54.1	38.2	23.1
FP 7	14.2	4.2	0.6	0.6	52.6	35.3	20.8
FP 8	17.1	6.5	0.8	0.5	55.0	39.9	26.7
FP 9	21.2	3.4	0.7	0.4	52.0	37.1	22.5
FP K1	13.1	4.5	0.7	0.7	60.3	41.0	25.5
FP K2	19.9	1.4	0.5	0.4	50.3	30.1	16.1
FP K3	20.5	4.0	0.8	0.3	54.1	35.9	22.7

*The sum of all the individual patch lengths measured along the gradsect divided by the total length of the gradsect (Tongway and Ludwig, 2011).

Table 31: Summary of the Landscape Function Analysis (LFA) variables for the 2014 survey.

Site	Nr of patches/ 10 m	Total Patch Area (m^2)	LOI*	Average inter-patch length (m)	Stability	Infiltration	Nutrient cycling
FP 1	17.4	7.91	0.8	0.4	64.9	38.0	32.0
FP 2	22.3	3.4	0.5	0.3	58.8	30.1	23.0
FP 3	22.2	4.8	0.6	0.3	59.1	31.2	24.2
FP 4	22.7	3.4	0.6	0.2	57.4	31.0	20.7
FP 5	18.5	3.2	0.6	0.3	54.0	29.2	20.5
FP 6	21.1	5.1	0.6	0.3	56.0	29.5	19.3
FP 7	25.2	5.1	0.7	0.3	58.4	32.4	22.4
FP 8	21.5	4.6	0.6	0.3	55.1	35.7	27.9
FP 9	18.7	3.1	0.7	0.2	59.1	33.8	24.3
FP K1	22.1	3.7	0.6	0.3	59.0	31.9	22.1
FP K2	21.1	6.0	0.8	0.3	57.4	33.6	22.7
FP K3	25.2	3.9	0.5	0.3	54.1	30.0	21.7

*The sum of all the individual patch lengths measured along the gradsect divided by the total length of the gradsect (Tongway and Ludwig, 2011).

The Landscape Organization Index (LOI) is seen as the total functionality of the landscape, and is thus considered an accurate indication of the landscape health or functionality (Seiderer, 2011).

Figure 84 shows the LOI of all the LFA sites in 2012 and 2014. The LOI for 2014 decreased across all the LFA survey sites with FP-9 being the same in 2012 and 2014. This indicates that the area of patch cover decreased from 2012 to 2014.

However, from Table 30 and Table 31 it is clear that the density of the patches increased from 2012 to 2014, as well as the patch areas for certain sites.

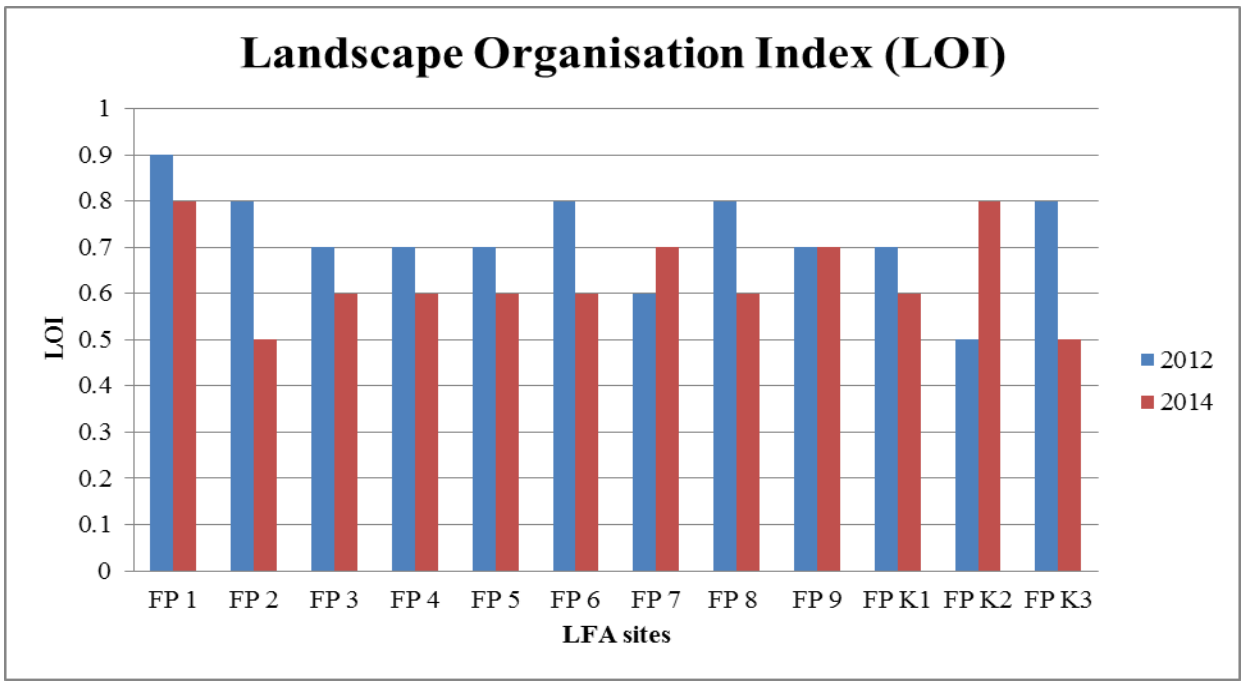

Figure 84: Landscape Organisation Index for the 12 fixed points of the 2012 and 2014 surveys.

7.4.3 Landscape Function Analysis (LFA) Data Comparison

Figure 85 and Figure 86 show that the index indicators contributed to the total SSA functionality of the sites in 2012 and 2014. The Stability index scored the highest values at all the LFA sites for both years, followed by Infiltration, and with lowest values being of the Nutrient cycle index (as stated previously, it is an indication that the Stability index contributes the most to the landscape functionality) for all of the LFA sites.

FP-3 was the most functional site in 2012 with the highest combined mean LFA index values, followed by FP-K1. Both of these sites are situated within 2 km of the MWS No. 5 TDF. In 2012, FP-K2 had the lowest overall functionality.

According to Malo (2012), the carbon monoxide released by passing vehicles on the Buffeldoorn road adjacent to FP-K2 may contribute to the vegetation in this area not thriving to its full potential, and as a result negatively affecting the LFA indices. The control sites in both 2012 and 2014 did not vary much from the other FPs (polluted areas) in landscape functionality.

In 2014, FP-1 was the most functional site; this is the result of the overgrowth of *S. plumosum* in this area. FP-5 was the least functional site in 2014; this can be due to the unexplained deaths of the *S. plumosum* patches in this area.

From Figure 85 and Figure 86 it is clear that the LFA index values decreased from 2012 to 2014. This can be attributed to the presence of cattle on the farm in 2014 and the heavy drought that occurred from the end of 2012 to the beginning of 2013. In 2012, the LFA indices varied greatly from site to site, and in 2014, the variation between sites was not that prominent, with the exception of FP-1.

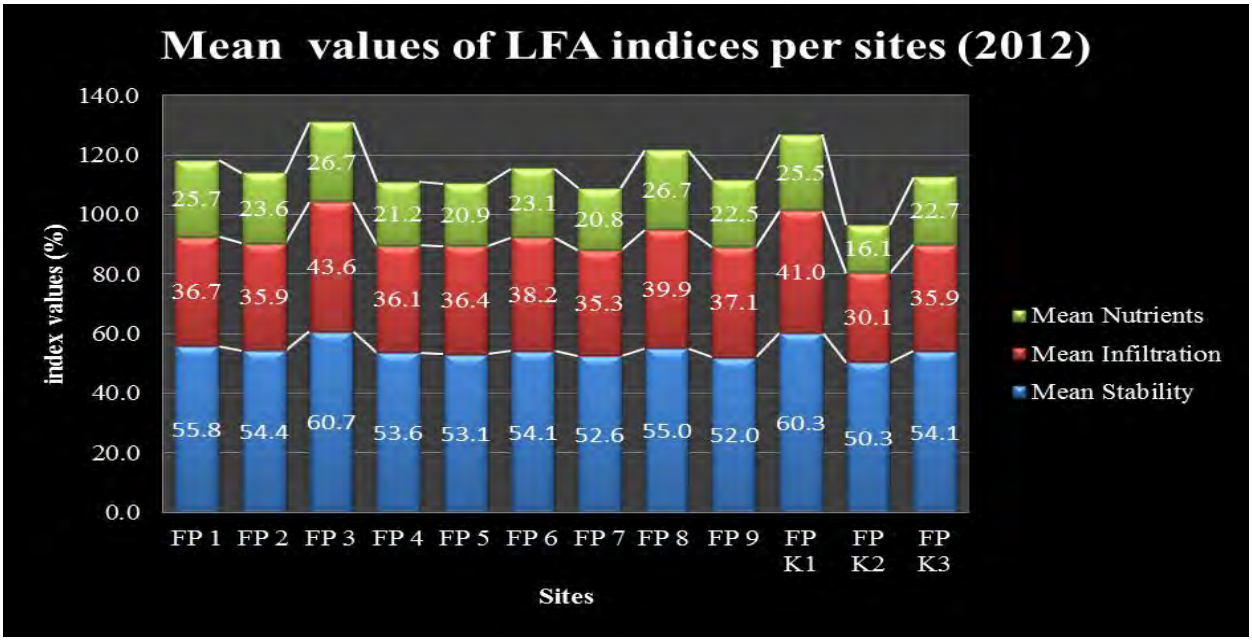

Figure 85: Mean values of the LFA indices with trend lines indicating a decrease or increase in LFA index values of the 2012 survey.

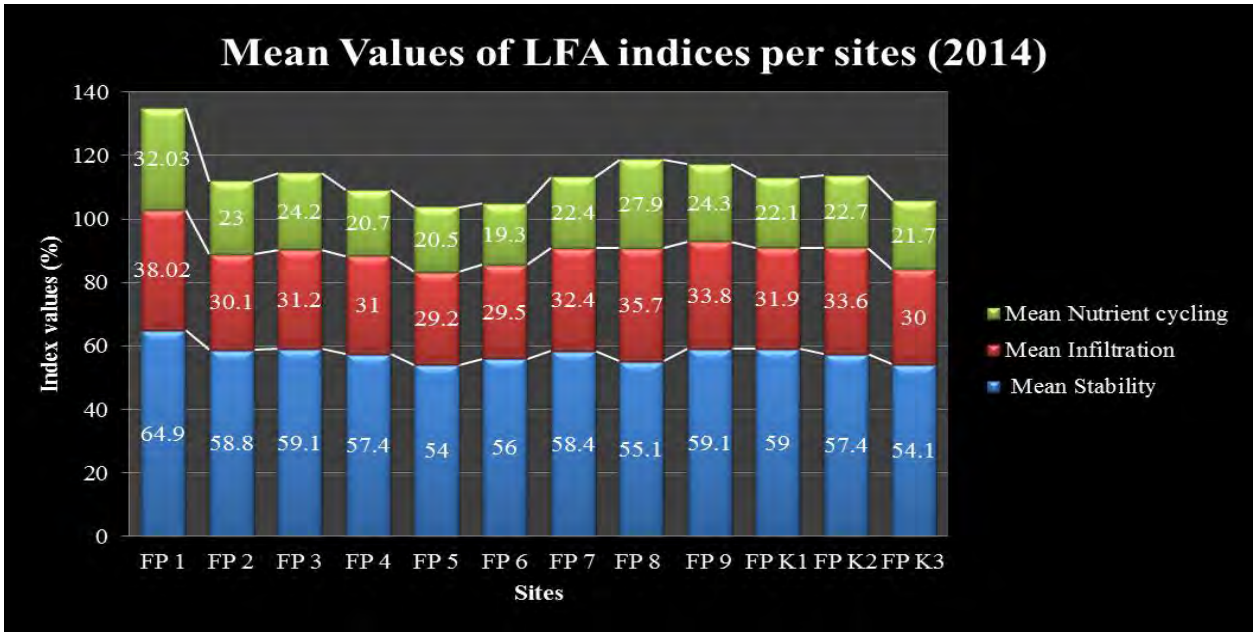

Figure 86: Mean values of the LFA indices with trend lines indicating a decrease or increase in LFA index values of the 2014 survey.

7.5 SITE COMPARISON

In order to find a relationship between the site‘s species composition, soil chemistry (EC [mS/m], pH) and LFA, canonical correspondence analysis (CCA) were used. Figure 87 and Figure 88 are tri-plots showing the abovementioned relationships.

The triangles represent individual grass species, circles represent the FP sites, while the arrows represent the environmental variable pointing in the direction of maximum change. Environmental variables with longer arrows are more closely related than those with short arrows (Kent and Coker, 1992, cited by Malo, 2012).

In Figure 87, it is clear that the LOI and pH are the two environmental factors that are more closely related than the other factors. The position of the species to environmental factors is relatively weakly related across most of the sites. A good correlation can be seen between FP-1 and the LOI, Nutrient cycling, Infiltration and EC.

The position of FP-6 and FP-8 show strong relationships with pH and EC. Figure 87 shows that *C. dactylon, E. chloromelas,* and *E. plana* are closely related to FP, -3, -4, -9 and -K1, whereas FP-6 and -8 are more closely related to *S. sphacelata* var. *torta* and *E. curvula.*

In Figure 88, it is clear that Stability, LOI, pH and EC are the environmental factors that are more closely related than the other factors. The position of the species to environmental factors is relatively weakly related across most of the sites.

A good correlation can be seen with FP-1 and LOI, Infiltration, Stability, Nutrient cycling, pH and EC, although the area is encroached by *S. plumosum.*

Fixed points-6, -7 and -K2 show good correlations with pH and EC. Figure 88 shows that most of the species are closely related with most of the sites. *Cynodon dactylon* shows good correlations with FP-6, -7 and -K1.

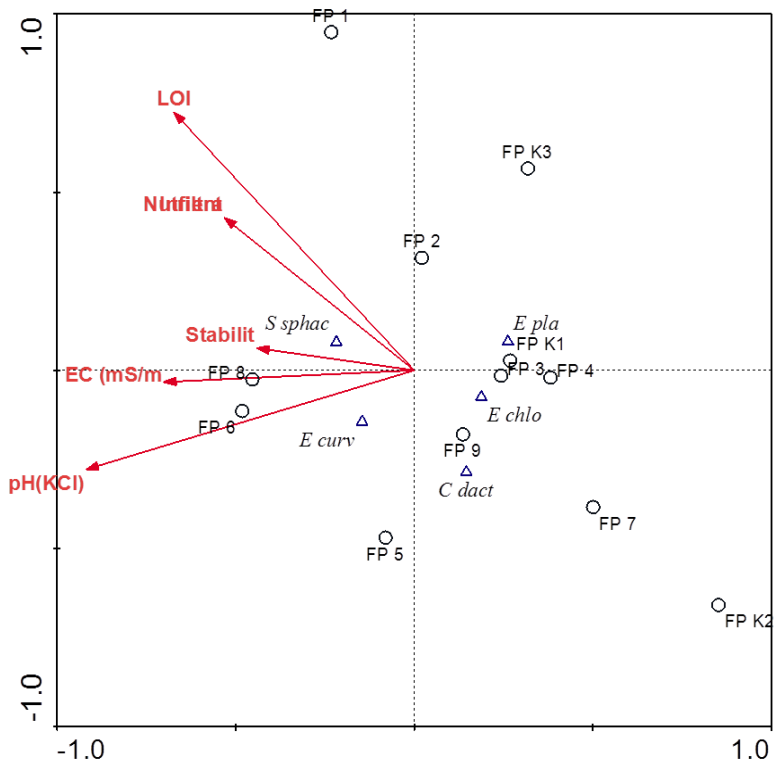

Figure 87: Species, environmental data and LFA data tri-plot from canonical correspondence analysis (CANOCO) in 2012 (Malo, 2012).

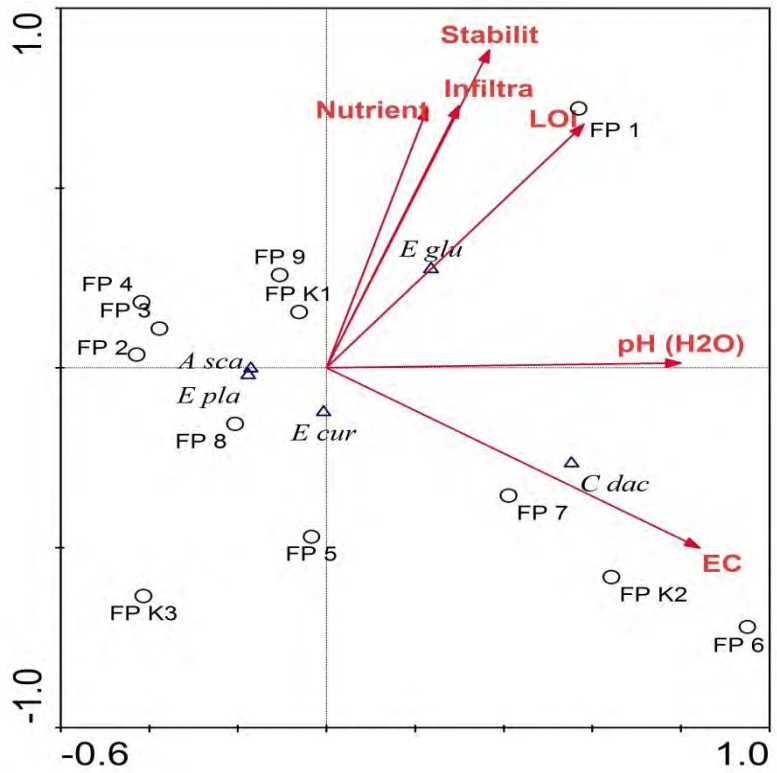

Figure 88: Species, environmental data and LFA data tri-plot from canonical correspondence analysis (CANOCO) in 2014.

7.6 BASIC CONCLUSION

The grass species in this area display a high accumulation of macro- and micronutrients in 2012 to 2014; this is due to the dolomitic bedrock and the accumulation capabilities of the grass species. There were no adverse effects of the pollution which formed the plume, on the grass quality of the area due to the low trace metal elements in the selected grass species.

The quantity of grass species increased from 24 in 2012 to 36 in 2014. The natural vegetation, as discussed in Chapter 1.2.5, should be *T. triandra,* which was found at only one site in 2012 and eight sites in 2014; this indicates that restoration of natural vegetation is underway. The LFA indices and LOI decreased due to overgrazing and the drought which took place end of 2011 and beginning of 2012.

CHAPTER 8: FINAL CONCLUSION AND RECOMMENDATIONS

8.1 CONCLUSIONS

8.1.1 MONITORING THE QUANTITATIVE, QUALITATIVE AND AERIAL EXTENT OF THE POLLUTION PLUME

The study investigated whether/stated that the MWS No. 5 TDF caused soil pollution which formed a pollution plume in this area. In order to monitor the extent of the pollution plume, 12 fixed monitoring sites were identified to be sampled monthly.

The 12 monitoring sites included nine FPs that had visible signs of pollution and three control sites that had no visible signs of pollution. Furthermore, three transect lines were identified to be sampled at 100 m intervals every third month, including two lines with east-west orientations and one with a north-south orientation.

Geochemical soil analyses were conducted on the twelve fixed points which included: pH, EC, CEC, exchangeable cations and anions, particle size distribution and mineral phase identification. Only pH and EC analyses were conducted on the three transect lines. The trace metal elements of the soil were analysed at the beginning (2011) and end of the monitoring period (2014).

Trace metal elements were also measured for the vegetation samples for comparison with the soil trace metal quantities.

Landscape Function Analysis and Descending Point Method were conducted in 2012 and 2014 at the same 12 sample sites. A groundwater samples was taken for analysis, however the data was filtered out by means of ± 5% of the useful dataset and could not be use.

A down-hole camera survey and geo-magnetic survey were conducted to find any potential linear structural anomalies as well as any weathered zones within the Oaktree dolomites. Aerial photograph was unsuccessful. Geographical Information Systems were used to construct maps to visually present the area of influence.

8.1.2 CONCLUSIONS OF THE MONITORING OF THE QUANTITATIVE, QUALITATIVE AND AERIAL EXTENT OF THE POLLUTION PLUME

8.1.2.1 Soil Monitoring

The MWS No. 5 tailings disposal facility (TDF) has been inactive from April 2011, and as the TDF material dried out, the phreatic water level inside the TDF lowered, which caused the pressure exerted by hydraulic head of the TDF to lower over the subsequent three and a half years, and this ended the pollution process on the soil. This is confirmed by the fact that the overall EC (mS/m) values of the soil samples decreased over time, and further substantiated by means of XRD and field observations that sulphate salts no longer precipitate on the soil surface at the nine fixed point sites (which displayed a substantial amount of sulphate precipitation in 2010).

The soil also recovered from the sulfate, nitrate and chloride pollution (pollution plume diminished in size) due to the percolation and infiltration of rain water and the dolomitic bedrock of this area as shown by the decrease in sulphate, nitrate and chlorite concentrations in the soil.

None of the total trace metal elements for the fixed points in 2011, 2012 and 2014 exceed the TMT except for As (FP-K3) in 2014. Most of the trace metal elements found during this investigation are present due to the natural weathering of the dolomites of the Oaktree Formation and the shales from the Black Reef Formation.

The soluble/available trace metal elements decreased from 2011 to 2014, with levels that may potentially result in plant deficiency, even though Cr and U exceeded the MAT values in 2011.

The dolomitic bedrock and soils in this area also made it possible for the extent of the plume to diminish greatly without any rehabilitation performed on this area.

8.1.2.2 Water Monitoring

The pollution derived from the No. 5 TDF (sulphate and chloride pollution) did not affect the groundwater in this area. The groundwater chemistry in this area is controlled by the natural rock weathering from the dolomites present.

8.1.2.3 Surveys Conducted in the Area

The dykes in the area (which were found during the geo-magnetic survey) are responsible for the creation of water compartments, and the fractures, joints and cavities (which are classified as weathered zones) create pathways for the seepage water of the TDF to flow in a slightly upslope direction (north-east) as indicated by the pollution plume that formed in 2011. The slope of the area is 5-8º in a south-eastern direction, and this is possible due to the 40 m pressure head of the No. 5 TDF at that time.

Evidence also suggests that the Oaktree dolomites do not form major depressions such as dolines, sinkholes or large cavities although they are commonly associated with dolomites in South Africa.

8.1.2.4 Vegetation Monitoring

The vegetation in this area is recovering to its natural state; it was also observed that the species compositions in 2012 and 2014 did not differ between the polluted sites and the control sites. Species compositions at some of the polluted sites were better than at some of the control sites. The species composition increased from 24 different species in 2012 to 36 in 2014. This indicates that the pollution did not have any adverse pollution effects on the vegetation dynamics. In 2012 and 2014, the grass species composition is predominantly Increaser 2 species, which is a result of poor management practices since these grasses commonly increase due to the disruptive effects of overgrazing.

The negative grazing qualities that were observed in 2010 can be due to the presence *S. plumosum* in some areas and other unpalatable grasses that were present at the time. Although *S. plumosum* is associated with the negative grazing qualities at the sites, it contributed greatly to LFA indices and created microhabitats for other species to colonize. It was observed that the plants do not show any signs of phytotoxicity from the trace metal elements in this area.

Minor variations occur between the most functional and least functional sites, thus reducing the effectiveness of the LFA data. These variations resulted in the TPC being rendered an ineffective test. It should be noted that the LFA data is not due to adverse effects caused by pollution from the No. 5 TDF, but rather due to other sources with minor effects, such as overgrazing and/or the drought experienced during the study period. The study area is ecologically functional, with minor signs of dysfunctionality at certain sites.

8.1.2.5 Final Conclusion

From all the above data interpretations and conclusions it can finally be concluded that as predicted in the hypothesis, the pollution plume did indeed diminish and the pollution process on the soil has receded. In summary:

- Referred to Chapter 4.10 and 8.1.2.1: Soil monitoring revealed that the pollution plume did reduced in size, EC values decreased from 2010 to 2014, sulphate, chloride and nitrate concentrations decreased and no trace metal pollution was found.
- Referred to Chapter 5.4 and 8.1.2.2: The ground water in this area is not polluted by sulphates and/or chlorides, the data only showed that natural rock weathering is the dominant factor controlling the groundwater chemistry in this area.
- Referred to Chapter 6.3 and 8.1.2.3: The dykes in the area are responsible for the creation of water compartments, and the fractures, joints and cavities in the dolomite create pathways for the seepage water from the TDF to flow in a slightly upslope direction (north-east) as indicated by the pollution plume that formed in 2011.
- Referred to Chapter 7.6 and 8.1.2.4: The natural vegetation is recuperating, however it is going to take some time for the species to recover. The specie quantity also improved from 2012 to 2014 however monitoring is a necessity.

8.2 RECOMMENDATIONS

- The arsenic concentration of FP-K3 needs to be monitored on a yearly basis to observe whether any increases/changes in arsenic concentration takes place.
- The capability of manganese oxide to adsorb pollutants needs to be examined.
- Trace metal element concentration of the groundwater needs to be evaluated to confirm the dolomite rehabilitation capabilities.
- Monitoring of grazing in this area due to the sensitivity of the natural grasses resulted in the classification of decreaser species, which suggests that they are plentiful in good veld but decrease in total when overgrazing or under-grazing occurs, together with the ascendancy of Increaser 2 species in this area. Therefore, grazing camp rotation is recommended.
- Monitoring and maintenance of *S. plumosum* is recommended in this area.

It can be further be said that it is more viable to construct new gold TDFs on the Oaktree Formation dolomites due to the natural rehabilitation capabilities, as well as the fact that no

dolines, sinkholes or large cavities were found during the 56 years that the Stilfontein Gold Mine deposited waste material on these dolomites.

CHAPTER 9: REFERENCES

Abbott, T. S. (Ed). 1989. BCRI Soil Testing: Methods and Interpretation. Biological and Chemical Research Institute: NSW Agriculture & Fisheries.

Anderson, D.W. and Gregorich, E.G. 1984. Effects of soil erosion on soil quality and productivity. (*In* Soil erosion and degradation. Proceedings of 2nd Annual Western Provincial Conference on rationalization of water and soil research and management. Saskatoon, Sask., Canada. p. 105-113).

Appelo, C.A.J. and Postma, D. 1994. Geochemistry, groundwater and pollution. Rotterdam: AA Balkema Publishers.

Appelo, C.A.J. and Postma, D. 2005. Geochemistry, Groundwater and Pollution. 2nd ed. Rotterdam: AA Balkema Publishers.

Aronson, J., Milton, S.J. and Blignaut, J.N. 2007. Restoring natural capital: definitions and rationale. (*In* Aronson, J., Milton, S.J. and Blignaut, J.N., *ed*. Restoring Natural Capital. SER International. p. 3-8).

Aucamp, P. 2003. Trace-element pollution of soils by abandoned gold-mine tailings near Potchefstroom, South Africa. Pretoria: Council for Geoscience.

Bell, F.G. 1999. Geological Hazards: Their Assessment, Avoidance and Mitigation. London: E & FN Spon.

Bell, F.G. and Donnelly, L.J. 2006. Mining and its Impact on the Environment. Oxon: Taylor & Francis.

Bengtsson, J. 1998. Which species? What kind of diversity? Which ecosystem function? Some problems in studies of relations between biodiversity and ecosystem function. *Applied Soil Ecology,* 10(3):191–199.

Blom, J.J. 2011. Identification and characterization of hardsetting and other layers in gold tailings disposal facilities. Potchefstroom: NWU (Mini-dissertation – B.Sc. Hons.).

Boneschans, R.B. 2013. Field Photographs with permission. Potchefstroom: NWU.

Bucas, K. 2006. Natural and anthropogenic influences on the water quality of the Orange River, South Africa. Johannesburg: UJ. (Dissertation – M.Sc).

Buck, B.J., Wolff, K., Merkler, D.J. and McMillan, N.J. 2006. Salt Mineralogy of Las Vegas Wash, Nevada: Morphology and Subsurface Evaporation. *Soil Science Society of America Journal,* 70(5):1639-1651.

Buszewski, B., Jastrzębska, A., Kowalkowski, T. and Górna-Binkul, A. 2000. Monitoring of selected heavy metals uptake by plants and soils in the area of Toruń, Poland. *Polish Journal of Environmental Studies,* 9(6):511-515.

Cadisch, G. and Giller, K.E. 1997. Driven by Nature, Plant Litter Quality and Decomposition. Wallingford: CAB International.

Cairns, J. 1995. Rehabilitating Damaged Ecosystems. London: Lewis publishers.

Carter, M.R. 2002. Soil quality for sustainable land management: Organic matter and aggregation interactions that maintain soil functions. *Agronomy Journal,* 94:38-47.

Central Materials Laboratory. 2000. Laboratory Testing Manual 2000. Tanzania: The United Republic of Tanzania Ministry of Works.

Coetzee, H. Winde, F. and Wade, P.W. 2006. An assessment of sources, pathways, and mechanisms and risks of current and potential future contamination of water and sediments in gold-mining areas of the Wonderfonteinspruit catchment. WRC Report No. 1214/1/06, Pretoria.

Council for Geoscience. 1986. 1:250 000, 2626 West Rand Geological Plan [Geographical map]. Pretoria: Council for Geoscience.

Crain, E.R. 2001. Crain's Petrophysical Handbook. http://www.spec2000.net/09-xrd.htm Date of access: 23 July 2012.

Cramer, V.A. and Hobbs, R.J. 2007. Why old fields? Socioeconomic and Ecological Causes and Consequences of Land Abandonment. (*In* Cramer, V.A. and Hobbs, RJ., *ed.* Old fields, dynamics and restoration of abandoned farmland. SER International/Island Press. p. 1-14).

Crater, M.R., Gregorich, E.G., Anderson, D.W., Doran, J.W., Janzen, H.H. and Pierce F.J. 1997. Concept of soil quality and their significance. (*In* Gregorich, E.G. and Carter, M.R., *ed.* Soil quality for crop production and ecosystem health. Netherlands: Elsevier. p. 1-20).

Daniell, A. 2014. Field Photographs. Potchefstroom: NWU.

Dennis, I., Pretorius, J. and Van Deventer, P.W. 2008. Impact of tailings dams on the groundwater system in South Africa. (*In* Robinson, B., *ed*. Proceedings of the 4th International Mining and Waste Management Conference on the tailings life cycle- managing waste for life. 11-12 March 2008. South Africa: NAUE; Frazer Alexander and ECMP. Session 2. p. 1-9).

Department of Environmental Affairs and Tourim (DEAT) South Africa. 2006. South Africa Environmental Outlook. A report on the state of the environment. Pretoria: Department of Environmental Affairs and Tourism.

Department of National Health and Population Development (DNHPD) South Africa. 1991. Guide: Permissible utilization and disposal of sewage sludge. Ref: A11/2/5/4. Pretoria.

Department of Water Affairs and Forestry (DWAF). 2007. Best Practice Guideline Series H2: Pollution Prevention and Minimisation of Impacts. Pretoria.

Department of Water Affairs and Forestry (DWAF). 2008a. Best Practice Guideline Series H1: Integrated Mine Water Management. Pretoria.

Department of Water Affairs and Forestry (DWAF). 2008b. Best Practice Guideline Series G5: Water Management Aspects for Mine Closure. Pretoria.

Deutsches Institut für Normung (DIN) 19730. 1997. Extraction of trace elements in soils using ammonium nitrate solutions. Berlin: Beuth Verslag.

Digby Wells and Associates and Department of Water Affairs (DWA). 2008. Impact assessment report for Margaret Shaft pumping arrangement on the water resources & associated ecology. Randburg SA: Environmental Solutions Providers. (Unpublished).

Doran, J.W. and Jones, A.J. 1996. Methods for Assessing Soil Quality. Soil Science Society of America Special Publication, vol. 49. Wisconsin: Soil Science Society of America.

Doran, J.W., Sarrantonio, M. and Lieberg, M.A. 1996. Soil health and sustainability. *Advances in Agronomy,* 56:1-54.

Drinkwater, L.E., Cambardella, C.A., Reeder, J.D. and Rice, C.W. 1996. Potentially mineralizable nitrogen as an indicator of biologically active soil nitrogen. (*In* Doran, J.W. and Jones, A.J., *ed.* Methods for Assessing Soil Quality. Wisconsin: Soil Science Society of America. p. 217–229).

Dutrow, B.L. and Clark, C.M. 2012. Geochemical Instrumentation and Analysis: X-ray Powder Diffraction (XRD). http://serc.carleton.edu/research_education/geochemsheets/techniques/XRD.html Date of access: 21 July 2012.

Eriksson, P.G., Altermann, W. and Hartzer, F.J. 2006. The Transvaal Supergroup and its precursors. (*In* Johnson, M.R., Anhaeusser, C.R. and Thomas, R.J., *ed*. The Geology of South Africa. Geological Society of South Africa, Johannesburg: Council for Geoscience, Pretoria. p. 237-260).

Fairbanks, D.H.K., Thompson, M.W., Vink, D.E., Newby, T.S., Van den Berg, H.M. and Everard, D.A. 2000. South African land-cover characteristics database: a synopsis of the landscape. *South African Journal of Science,* 96(2):69-82.

Fertilizer Society of South Africa (FSSA). 2007. Fertilizer Handbook. 6th ed. Lynwood Ridge: Fertilizer Society of South Africa.

Fey, M. 2010. Soils of South Africa: Their distribution, properties, classification, genesis, use and environmental significance. South Africa: Cambridge University Press.

Gagliano, W.B. and Brigham, J.M. 2006. Acid Mine Drainage. (*In* Lal, R., *ed.* Encyclopaedia of Soil Science. 2nd ed. Florida: CRC Press. p. 1-4).

Gibson, R.J. 1974. Descriptive human pathological mineralogy. *The American Mineralogist,* 59:1177-1182.

Goldich, S.S. 1938. A study in rock-weathering. *Journal of Geology*, 46(1):17-58.

Google Earth. 2013. Mine Waste Solutions Tailings Complex 26º48'24.05"S, 26º47'14.45"E, elevation 1351 m and Imagery Date 10/10/2013. Available through: http://www.google.com/earth/index.html. [Accessed 5 May 2013].

Gotkowitz, M. 2010. Groundwater recharge. http://wisconsingeologicalsurvey.org/pdfs/espdf/es50_2_recharge.pdf Date of access: 3 Mar 2014

Graham, D.J. and Midgley, N.G. 2000. Graphical representation of particle shape using triangular diagrams: an Excel spread sheet method. *Earth Surface Processes and Landforms*, 25(13):1473-1477.

Gray, N.F. 1997. Environmental impact and remediation of acid mine drainage: a management problem. *Environmental Geology,* 30(1/2):62-71.

Gregorich, E.G. and Acton, D.F. 1995. Understanding soil health. (*In* Acton, D.F. and Gregorich, E.G., *ed*. The health of our soils-towards sustainable agriculture in Canada. Ottowa: Centre for Land and Biological Resource Research, Research Branch, Agriculture and Agri-food Canada. p. 5-10).

Haagner, A.S.H. 2008. The role of vegetation in characterising landscape function on rehabilitating gold tailings. Potchefstroom: NWU. (Dissertation – M.Sc).

Hazelton, P. and Murphy, B. 2007. Interpreting soil test results: What do all the numbers mean? Australia: CSIRO Publishing.

Herselman, J.E. 2007. The concentration of selected trace metals in South African soils. Stellenbosch: University of Stellenbosch. (Thesis – Ph.D).

Hesse, P.R. 1971. A textbook of soil chemical analysis. New York: Chemical Publishing Co.

Hillel, D. 1998. Environmental soil physics. London: Academic Press.

Huizenga, J.M. 2012. Environmental Geochemistry. Potchefstroom: NWU, Potchefstroom Campus. (Study guide OMSG 611).

Huizenga, JM. 2011. Characterisation of the inorganic chemistry of surface waters in South Africa. *Water SA,* 37(3):401-410.

International Business Publications (IBP), USA Staff. 2013. South Africa mining industry business opportunities handbook. Volume 1: Strategic information and regulations. Washington: International business Publications.

Kent, M. and Coker, P. 1992. Vegetation Description and Analysis: A Practical Approach. New York: John Wiley and Sons.

King, H.L., Pringle, I.C., Oosterhuis, W.R. and Ehlers, D.L. 2007. The metallogeny of the West Rand. Pretoria: Council for Geoscience South Africa.

Kinyangi, J. 2007. Soil health and soil quality: A review.
http://www.worldaginfo.org/files/Soil%20Health%20Review.pdf Date of access: 10 Feb 2014.

Klein, C. and Dutrow, B. 2008. Mineral Science. 23rd ed. New Jersey: John Wiley and Sons.

Knödel, K., Lange, G. and Voigt, H.J. 2007. Environmental Geology: Handbook of field methods and case studies. Berlin: Springer.

Koch, J. 2013. Migration and gamma ray assessment of uranium in a gold tailings disposal facility. Potchefstroom: NWU. (Dissertation – M.Sc).

Korte, N. 1999. A guide for the technical evaluation of environmental data. Lancaster, USA: Technomic Publishing Co.

Labuschagne, P.E. 2008. Mine Waste Solutions: Reworking of Tailings Dams Project: Hydrogeological Assessment – 1st Draft for Review. Johannesburg: GCS. (Unpublished).

Larson, W.E. and Pierce, F.J. 1991. Conservation and enhancement of soil quality. (*In* Dumanski, J., Pushparajah, E., Latham, M. and Myers, R., *eds*. Evaluation for Sustainable Land Management in the Developing World. Technical Papers. Proc. Int. Workshop., Chiang Rai, Thailand, 15-21 September 1991: Int. Board for Soil Res. and Management, Bangkok. 2(12). p.175-203).

Lloyd, J.W. 1986. A Review of aridity and groundwater. *Hydrological Processes,* 1(1): 63-78.

Lottermoser, B.G. 2010. Mine Wastes: Characterization, Treatment and Environmental Impacts. 3rd ed. Berlin: Springer.

Mabuza, M. 2006. The role of mining in South Africa beyond 2010. http://www.docstoc.com/docs/5382083/THE-ROLE-OF-MINING-IN-SOUTH-AFRICA-BEYOND-MOSA Date of access: 27 Feb 2014.

Madejon, P. Maranon, T. Murillo, J. 2002. Bioaccumulation of As, Cd, Cu, Fe and Pb in wild grasses affected by the Aznalco´llar mine spill. Spain. *The Science of the Total Environment*, 290:105–120.

Malo, D.S. 2012. The effect of seepage pollution from gold mine tailings on vegetation change. Potchefstroom: NWU. (Mini-dissertation – B.Sc. Hons).

Marais, M., Van Deventer, P.W. and Van Wyk, SJ. 2006. Closure of the Stilfontein Gold Mine. (*In* Fourie, A. and Tibbett, M., *eds*. Mine Closure: Proceedings of the 1st International Seminar on Mine Closure. Perth: Australian Centre for Geomechanics. p. 261-268).

Mariita, N.O. 2007. The magnetic method. http://www.os.is/gogn/unu-gtp-sc/UNU-GTP-SC-05-18b.pdf Date of access: 12 Feb. 2014.

McCarthy, T. and Rubidge, B. 2005. The story of Earth and Life – A South African perspective on a 4.6 billion year old journey. Cape Town: Struik.

McCarthy, T.S. 2006. The Witwatersrand Supergroup. (*In* Johnson, M.R., Anhaeusser, C.R. and Thomas, R.J., *eds*. The Geology of South Africa. Geological Society of South Africa, Johannesburg: Council for Geoscience, Pretoria. p. 155-186).

McCarthy, T.S. 2011. The impact of acid mine drainage in South Africa. *South African Journal of Science*, 107(5/6):1-7.

Mellin, A. 2005. Nitrogen mineralization in a sludge-amended sandy clay loam in South Africa. Switzerland: Swedish University of Agricultural Science. (Dissertation – M.Sc).

Metson, A. J. 1961. Methods of chemical analysis for soil survey samples. Soil Bureau Bulletin No. 12. Wellington, New Zealand: Dept. of Scientific and Industrial Research. p. 168-175.

Milton, S.J. 2001. Re-thinking ecological rehabilitation in arid and winter rainfall regions of Southern Africa. *South African Journal of Science,* 97:47-48.

Möhr-Swart, M., Coetzee, F. and Blignaut, J. 2008. Sustainable Development in the South African Mining Industry: The Role of Cleaner Production and EMA. (*In* Schaltegger, S., Bennett, M., Burritt, R.L. and Jasch, C., *eds*. Environmental accounting for Cleaner Production. Netherlands: Springer. p.165-191).

Mucina, L. and Rutherford, M.C., *eds*. 2006. The vegetation of South Africa, Lesotho and Swaziland. Strelitzia 19. Pretoria: South African National Biodiversity Institute.

Naicker, K., Cukrowska, E. and McCarthy, T.S. 2003. Acid mine drainage arising from gold mining activity in Johannesburg, South Africa and environs. *Environmental Pollution,* 122:29-40.

Nel, L., Truter, M.A. and Willemse, J. 1939. The Geology of the country around Potchefstroom and Klerksdorp: An explanation of sheet no.61 (Potchefstroom). Pretoria: Government Printer.

North-West Department of Agriculture, Conservation and the Environment (NWDACE). 2002. The State of the Environment Report, North-West Province, South Africa. Mafikeng: NWDACE.

Odendaal, J., Van Heerden, D., Muller, C. and Sternberg, H. 2008. Technical report on the Mine Waste Solutions ("MWS") Tailings recovery Project located near Stilfontein, North West Province, South Africa. Stilfontein: First Uranium Corporation.

Pinkney, E.T. 1956. The chemistry of the uranium leaching process in South Africa. *The South African Industrial Chemist*, 10(11):264-272.

Prüeß, A., Turian, G. and Schweikele, V. 1991. Ableitung kritischer Gehalte an NH4NO3-extrahierbaren ökotoxikologisch relevanten Spurenelementen in Böden SW-Deutschlands. Mittlg. *Dtsch. Bodenk. Ges.,* 66:385-388.

Prüeβ, A. 1997. Action values for mobile (NH4NO3-extractable) trace elements in soils based on the German national standard DIN 19730. (*In*: Prost, R., *ed*. Contaminated soils. 3rd International conference on the biogeochemistry of trace elements. Paris: Institut National de la Recherche Agronomique. pp. 415-423).

Rashed, M.N. 2010. Monitoring of contaminated toxic and heavy metals, from mine tailings through age accumulation, in soil and some wild plants at Southeast Egypt. *Journal of Hazardous Material,* 178:739-746.

Ratlhogo, B.T. 2011. Acid mine drainage potential of a tailings disposal facility, Stilfontein, South Africa. Potchefstroom: NWU. (Mini-dissertation – B.Sc. Hons).

Ritchie, M. 2005. Tailings management in gold plants. *Hydrometallurgy*, 78:3-20.

Römheld, V. and Marschner, H. 1991. Function of micronutrients in plants. (*In*: Mortvedt, J.J., Cox, F.R., Shuman, L.M., Welch, R.M., *eds*. Micronutrients in agriculture. SSSA book series no.4. Madison, WI, USA: Soil Science Society of America. p.297 –328)

Rösner, T., Boer, R., Reyneke, R., Aucamp, P. and Vermaak, J. 2001. A preliminary assessment of pollution contained in the unsaturated and saturated zone beneath reclaimed gold mine residue deposits. WRC Report No. 797/1/01, Pretoria.

Sabah, A.A. and Fouzul, A.M. 2012. The environmental impact of gold mines: pollution by heavy metals. *Central European Journal of Engineering,* 2(2):304-313.

Seiderer, M. 2011. Evaluation of rehabilitation attempts at Harties No. 7 TDF 11 years on: The effect of slope flattening and topsoil additions. Potchefstroom: NWU. (Mini-dissertation – B.Sc. Hons).

Simmers, I. 1997. Recharge of Phreatic Aquifers in (semi-) arid Areas. Balkema: Rotterdam.

Simmers, I. 1998. Groundwater recharge: an overview of estimation _problems' and recent developments. (*In*: Robins, N.S., *ed*. Groundwater Pollution, Aquifer Recharge and Vulnerability. London: The Geological Society. p. 107-116.)

Slabbert, A. J. 2014. Surface impacts of gold mining activities on the Kromdraai/Koekemoerspruit: a situation analysis. Potchefstroom: NWU. (Dissertation – M.Sc).

Smyth, A.J. and Dumansky, J. 1993. FESLM: An international framework for evaluation of sustainable land management. World Soil Resources Report 73. Rome: FAO.

Snyman, H.G. and Herselman, J.E. 2006. Volume 2: Requirements for the agricultural use of wastewater sludge. Guidelines for the utilisation and disposal of wastewater sludge. WRC Report No. TT 262/06, Pretoria.

Spangenberg, A. 2000. The management of recharge and quality of the underground water in the Klerksdorp area with specific reference to post closure at the Stilfontein Gold Mine (1952-2000). Johannesburg: UJ. (Dissertation – M.Sc).

Steenekamp, S.J. and Haagner, A. 2010. Impacts of pollution plume emanating from Chemwes TD5 on vegetation and grazing capacity on the farm Stilfontein. Stilfontein: Agreenco environmental projects. (Unpublished).

Stenberg, B. 2010. Monitoring Soil Quality of Arable Land: Microbiological Indicators. *Acta Agriculturae Scandinavica, Section B - Soil & Plant Science,* 49(1):1-24.

Stephens, D.B. 1996. Vadose Zone Hydrology. Florida: Lewis.

Stilwell, L.C., Minnitt, R.C.A., Monson, T.D. and Kuhn, G. 2000. An input-output analysis of the impact of mining on the South African economy. *Resources Policy*, 26(1):17-30.

Sweeting, M.M. 1972. Karst Landforms. London: The Macmillan Press.

Swift, M.J., Izac, A. and Van Noordwijk, M. 2004. Biodiversity and ecosystem services in agricultural landscapes—are we asking the right questions? *Agriculture, Ecosystems and Environment,* 104(1):113-134.

Tainton, N.M. 1999. The ecology of the main grazing lands of South Africa: the Savanna Biome. (*In* Tainton, N.M., *ed.* Veld Management in South Africa, Pietermaritzburg: University of Natal Press. Chapter 2).

The International Network for Acid Prevention (INAP). 2009. Global Acid Rock Drainage Guide (GARD Guide). http://www.gardguide.com/index.php/Chapter_2 Date of access: 21 Mar 2014.

The Non-Affiliated Soil Analysis Work Committee. 1990. Handbook of standard soil testing methods for advisory purposes. Soil Sci. Soc. South Africa: Pretoria.

Tongway, D.J. and Hindley, N.L. 2004. Landscape Function Analysis: Procedures for Monitoring and Assessing Landscape with Special Reference to Mine sites and Rangelands. Australia: CSIRO.

Tongway, D.J. and Ludwig, J.A. 2011. Restoring Disturbed Landscapes: Putting Principles into Practice. London: Island press.

U.S. EPA (Environmental Protection Agency). 1996. Acid Digestion of Sediments, Sludges, and Soils. EPA Method 3050B.

United States Department of Agriculture (USDA), Natural Resources Conservation Service (NRCS). 2014. Soil Texture Calculator. http://www.nrcs.usda.gov/wps/portal/nrcs/detail/soils/survey/?cid=nrcs142p2_054167 Date of access: 19 Mei 2014.

Van der Merwe, M. 2012. The geochemical monitoring of potential soil pollution from a gold tailings dam facility. Potchefstroom: NWU. (Mini-dissertation – B.Sc. Hons).

Van Deventer, P.W. 2011a. Environmental Geology of Stilfontein Gold Mine. *Forum Geoökol*, 22(3):22-27.

Van Deventer, P.W. 2011b. Investigation into potential soil pollution from the Chemwes No. 5 TDF on the Farm Stilfontein. Potchefstroom: NWU. (Unpublished).

Van Deventer, P.W. 2011c. Criteria for topsoil stripping for topsoil covers. Potchefstroom: North West University. (Unpublished).

Van Deventer, P.W. 2012. Project insight [Personal communication in the field]. 19 November 2012, South Africa.

Van Deventer, P.W. 2013. Geomagnetic observation of diabase dyke [Personal communication in the field]. 15 August 2013, South Africa.

Van Deventer, P.W. and Bloem, A.A. 2007. Reconnaissance geological investigation on the Farm Stilfontein. Potchefstroom: NWU. (Unpublished).

Van Deventer, P.W. and Hattingh, J.M. 2009. Concepts of rehabilitation and mine closure of mine TDFs. Fraser Alexander Tailings Disposal Course. 14 - 18 November 2011 Witfield: Fraser Alexander. Part 3: Chapter 2.

Van Deventer, P.W. and Marais, M. 2003. The Historical overview of the operations of the Stilfontein Gold Mining Company Limited. (Unpublished).

Van Deventer, P.W., Hattingh, A.M., Botha, F. and du Plessis, F. 2009. Conceptual study on reclamation of mine residue areas for development purposes. Gauteng: Department of Agriculture and Rural Development (GDARD).

Van Deventer, P.W., Hattingh, J. and Bloem, D. 2008. Some rehabilitation issues on Witwatersrand gold tailings dams. *Civil Engineering,* 25-29.

Van Oudtshoorn, F. 2012. Gids tot Grasse van Suider-Afrika. Queenswood: Briza Publikasies.

Van Zyl, D. 2008. The mine life cycle system and mine waste management. (*In* Robinson, B., *ed*. Proceedings of the 4th International Mining and Waste Management Conference on the tailings life cycle- managing waste for life. 11-12 March 2008. South Africa: NAUE; Fraser Alexander and ECMP. p. 1-13).

Van Zyl, F. 2014. Rainfall data of the Stilfontein area from 2011 – 2014 [E-mail]. 4 Feb 2014, South Africa.

Water Research Commission (WRC). 1997. Permissible Utilisation and Disposal of Sewage Sludge. 1st Edition. TT85-97. Pretoria: Water Research Commission.

Weaver, A. and Caldwell, P. 1999. Environmental Impact Assessment for mining projects. (*In* Petts, J., *ed*. Handbook of Environmental Impact Assessment. London: Blackwell Science, Inc. p. 377-403).

Wendel, G. 1998. Radioactivity in mines and mine water – sources and mechanisms. *Journal of the South African Institute of Mining and Metallurgy,* 98(2):87-92.

Winde, F. 2010. Uranium pollution of the Wonderfonteinspruit, 1997-2008 Part1: Uranium toxicity, regional background and mining related sources of uranium pollution. *Water SA*, 36(3).

Winegardner, D.L. 1995. An introduction to soils for environmental professionals. Boca Raton: Lewis Publishers.

Wolf, R.E. 2005. What is ICP-MS?... and more importantly, what can it do? http://minerals.cr.usgs.gov/icpms/intro.html Date of access: 2 August 2012.

Zhu, C. and Andersen, G. 2002. Environmental Applications of Geochemical Modelling. New York: Cambridge University Press.

Zhu, J. 2001. Plant salt tolerances. *Trends in Plant Science,* 6(2):66-71.

CHAPTER 10: APPENDICES DESCRIPTION

LIST OF APPENDICES

APPENDIX A: BASELINE ASSESSMENT SOIL (pH AND EC) DATA AND SAMPLE COORDINATES OF THE SOIL SAMPLES ON THE STUDY AREA. 182

APPENDIX B: THE EC OF THE SOIL SAMPLES OF THE FIXED POINTS AND TRANSECT LINES ON THE STUDY AREA ACCUMULATED OVER A 30-MONTH PERIOD. 188

APPENDIX C: EXCHANGEABLE CATIONS AND CATION EXCHANGE CAPACITY (CEC) OF THE SOIL SAMPLES COLLECTED AT FIXED POINT ON THE STUDY AREA (ANALYST: TERINA VERMEULEN, ECO-ANALYTICA LABORATORY, NWU). 193

APPENDIX D: ANION CONCENTRATION OF THE SOIL SAMPLES COLLECTED AT FIXED POINT ON THE STUDY AREA (ANALYST: TERINA VERMEULEN, ECO-ANALYTICA LABORATORY, NWU). 195

APPENDIX E: ICP-MS ANALYSIS OF THE SOIL SAMPLES FOR TOTAL AND SOLUBLE/AVAILABLE TRACE METAL ELEMENTS OF THE 12 FIXED POINTS (ANALYST: YVONNE VISAGIE, ECO-ANALYTICA, NWU). 199

APPENDIX F: PARTICLE SIZE DISTRIBUTION OF THE SOIL SAMPLES COLLECTED AT THE 12 FIXED POINTS ON THE STUDY AREA (ANALYST: TERINA VERMEULEN, ECO-ANALYTICA LABORATORY, NWU). 210

APPENDIX G: X-RAY DIFFRACTION DATA OF THE MINERAL PHASES PRESENT IN THE SOIL SAMPLES COLLECTED AT THE 12 FIXED POINTS. 211

APPENDIX H: REPRESENTATION OF THE WATER CHEMISTRY DATA OF THE SAMPLED BOREHOLES IN THE STUDY AREA. 223

APPENDIX I: GEO-MAGNETIC SURVEY CONDUCTED IN THE STUDY AREA. 237

APPENDIX J: DOWN-HOLE CAMERA SURVEY VIDEOS. 243

APPENDIX K: VEGETATION AND LANDSCAPE FUNCTION ANALYSIS. 244

Appendix A: Baseline assessment soil (pH and EC) data and sample coordinates of the soil samples on the study area.

A1: Baseline assessment.

A1-1: Baseline assessment at the beginning of the sampling period in August 2011.

		FP-1	**FP-2**	**FP-3**	**FP-4**	**FP-5**	**FP-6**	**FP-7**	**FP-8**	**FP-9**	**FP-K1**	**FP-K2**	**FP-K3**
Average	pH	6.8	7.1	7.6	7.6	7.4	7.8	7.1	7.2	7.1	6.8	6.9	6.7
	EC*	58.4	15.1	11.9	9.4	25.4	60.8	12.6	23.3	19.8	16.5	12.5	14.0
Composite	pH	6.6	7.2	7.2	7.4	7	7.7	7.4	7.6	6.7	6.8	6.6	6.7
	EC*	57.0	8.7	15	9	25.3	39.6	11.7	29.9	13.11	18.2	11.5	19.3

*: mS/m

A1-2: Baseline assessment at the end of the sampling period in January 2014.

		FP-1	**FP-2**	**FP-3**	**FP-4**	**FP-5**	**FP-6**	**FP-7**	**FP-8**	**FP-9**	**FP-K1**	**FP-K2**	**FP-K3**
Average	pH	7.9	7.1	7.1	6.9	8.0	8.6	7.1	7.4	7.4	7.4	7.4	7.4
	EC*	18.5	11.0	10.6	8.5	17.5	32.0	17.8	13.7	10.5	13.3	32.5	13.2
Composite	pH	8.1	6.5	6.5	7	7.9	8.7	6.7	7.7	7.1	7.2	6.6	6.2
	EC*	17.3	10.8	10	8.7	20.5	34.5	19.6	13.3	10.6	13.34	21.6	13.3

*: mS/m

A2: Fixed point (FP) sample coordinates (see Figure 16).

	S°	E°
SAMPLE		
FP-1	26.81022	26.77835
FP-2	26.80896	26.78189
FP-3	26.80278	26.78536
FP-4	26.80024	26.79661
FP-5	26.79350	26.79573
FP-6	26.79170	26.79798
FP-7	26.79087	26.80804
FP-8	26.78171	26.79672
FP-9	26.79676	26.79507
FP-K1	26.80311	26.77797
FP-K2	26.79006	26.81339

A3: Transect line North-South 1 coordinates (see Figure 16).

	S°	E°
SAMPLE		
NS1-01	26.80661	26.79340
NS1-02	26.80603	26.79398
NS1-03	26.80521	26.79477
NS1-04	26.80442	26.79556
NS1-05	26.80382	26.79614
NS1-06	26.80311	26.79681
NS1-07	26.80244	26.79687
NS1-08	26.80138	26.79662
NS1-09	26.80106	26.79661
NS1-10	26.80025	26.79643
NS1-11	26.79913	26.79621
NS1-12	26.79818	26.79602
NS1-13	26.79730	26.79584
NS1-14	26.79656	26.79569
NS1-15	26.79560	26.79549
NS1-16	26.79460	26.79530
NS1-17	26.79386	26.79515
NS1-18	26.79299	26.79497
NS1-19	26.79202	26.79477
NS1-20	26.79134	26.79446
NS1-21	26.79018	26.79443
NS1-22	26.78936	26.79506
NS1-23	26.78859	26.79569
NS1-24	26.78784	26.79628
NS1-25	26.78723	26.79676
NS1-26	26.78639	26.79741
NS1-27	26.78538	26.79751
NS1-28	26.78462	26.79743
NS1-29	26.78344	26.79726
NS1-30	26.78260	26.79715
NS1-31	26.78169	26.79703
NS1-32	26.78083	26.79690
NS1-33	26.78003	26.79680
NS1-34	26.77931	26.79670

A4: Transect line East-West 2 coordinates (see Figure 16).

	S°	E°
SAMPLE		
EW2-01	26.78986	26.81357
EW2-02	26.78997	26.81290
EW2-03	26.79006	26.81194
EW2-04	26.79016	26.81101
EW2-05	26.79027	26.80985
EW2-06	26.79036	26.80888
EW2-07	26.79046	26.80804
EW2-08	26.79057	26.80701
EW2-09	26.79059	26.80564
EW2-10	26.79066	26.80482
EW2-11	26.79072	26.80374
EW2-12	26.79088	26.80286
EW2-13	26.79098	26.80187
EW2-14	26.79110	26.80080
EW2-15	26.79121	26.79977
EW2-16	26.79131	26.79878
EW2-17	26.79138	26.79801
EW2-18	26.79151	26.79699
EW2-19	26.79164	26.79588
EW2-20	26.79173	26.79486
EW2-21	26.79166	26.79422
EW2-22	26.79096	26.7934
EW2-23	26.79062	26.79212
EW2-24	26.79036	26.79118
EW2-25	26.79012	26.79035
EW2-26	26.78990	26.78957
EW2-27	26.78961	26.78863
EW2-28	26.78931	26.78757
EW2-29	26.78907	26.78670
EW2-30	26.78878	26.78568
EW2-31	26.78853	26.78480
EW2-32	26.78822	26.78370
EW2-33	26.78797	26.78282
EW2-34	26.78764	26.78169
EW2-35	26.78733	26.78057
EW2-36	26.78710	26.77974
EW2-37	26.78688	26.77900

A4: Transect line East-West 2 coordinates (see Figure 16).

Sample	Sº	Eº
EW2-38	26.78660	26.77796
EW2-39	26.78634	26.77705
EW2-40	26.78601	26.77586
EW2-41	26.78578	26.77502
EW2-42	26.78555	26.77422
EW2-43	26.78522	26.77293

A5: Transect line East-West 1 coordinates (see Figure 16).

	S°	E°
SAMPLE		
EW1-01	26.81178	26.77292
EW1-02	26.81156	26.77378
EW1-03	26.81128	26.77488
EW1-04	26.81107	26.77577
EW1-05	26.81090	26.77654
EW1-06	26.81064	26.77753
EW1-07	26.81044	26.77846
EW1-08	26.81023	26.77939
EW1-09	26.81002	26.78038
EW1-10	26.80980	26.78126
EW1-11	26.80959	26.78218
EW1-12	26.80924	26.78303
EW1-13	26.80898	26.78405
EW1-14	26.80879	26.78482
EW1-15	26.80855	26.78586
EW1-16	26.80838	26.78664
EW1-17	26.80815	26.78757
EW1-18	26.80794	26.78847
EW1-19	26.80791	26.78910
EW1-20	26.80793	26.78927
EW1-21	26.80770	26.79019
EW1-22	26.80746	26.79121
EW1-23	26.80726	26.79214
EW1-24	26.80711	26.79274

Appendix B: The EC of the soil samples of the fixed points and transect lines on the study area accumulated over a 30-month period.

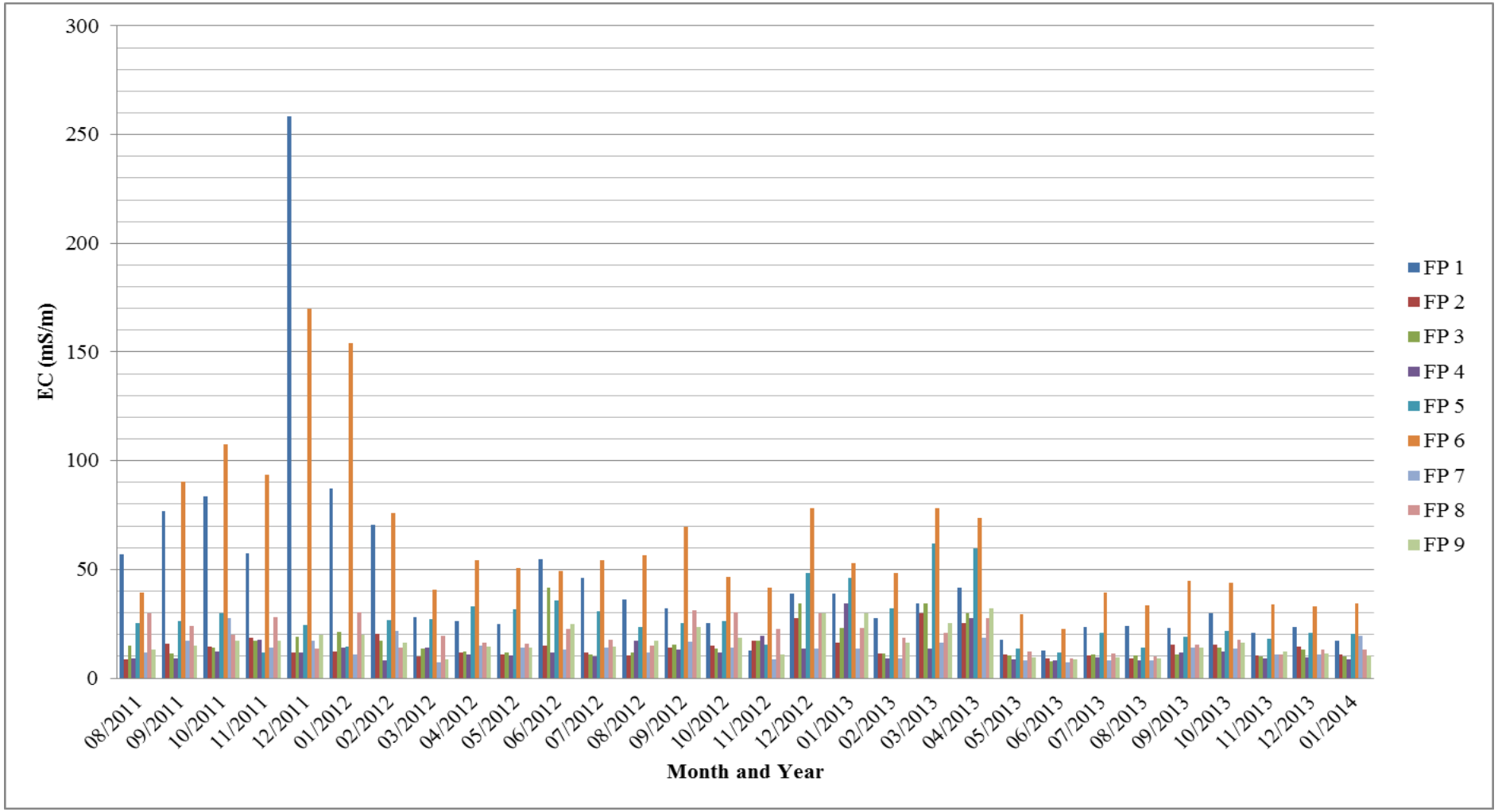

B1: The EC (mS/m) of the soil for nine fixed points over a 30 month period.

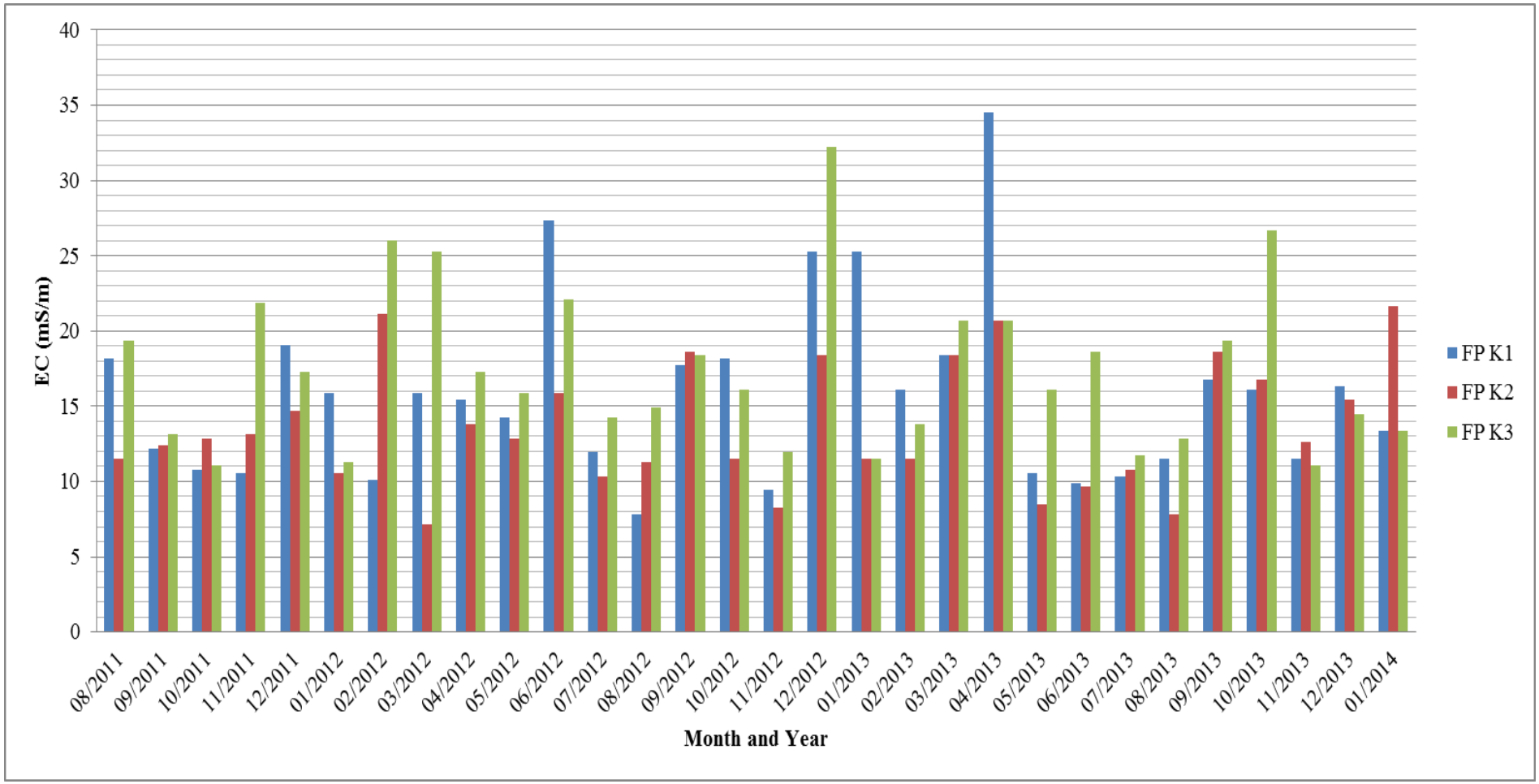

B2: The EC (mS/m) of the soil for the three control fixed points over a 30 month period.

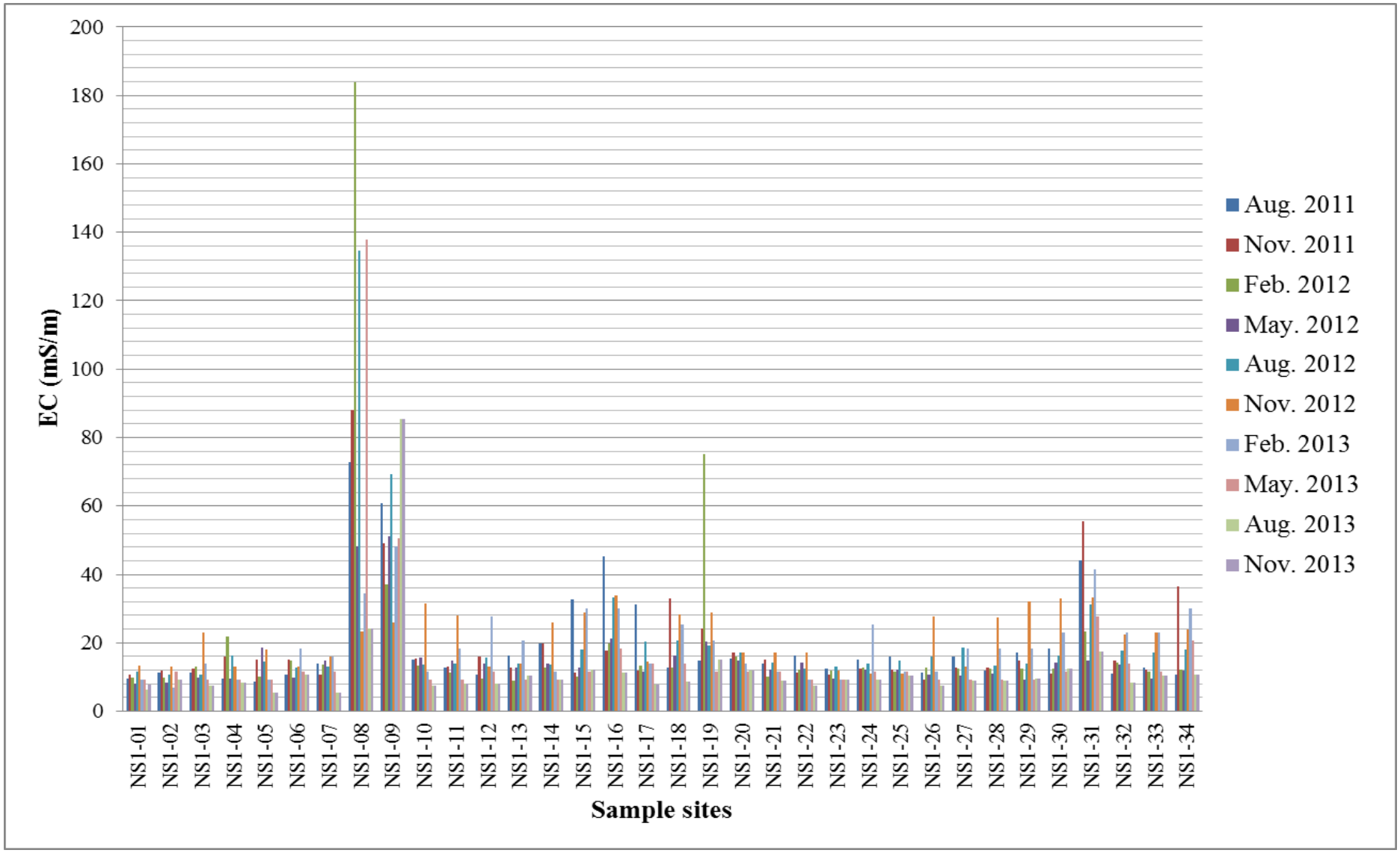

B3: The EC (mS/m) of the soil for the north-south transect line over a 30 month period.

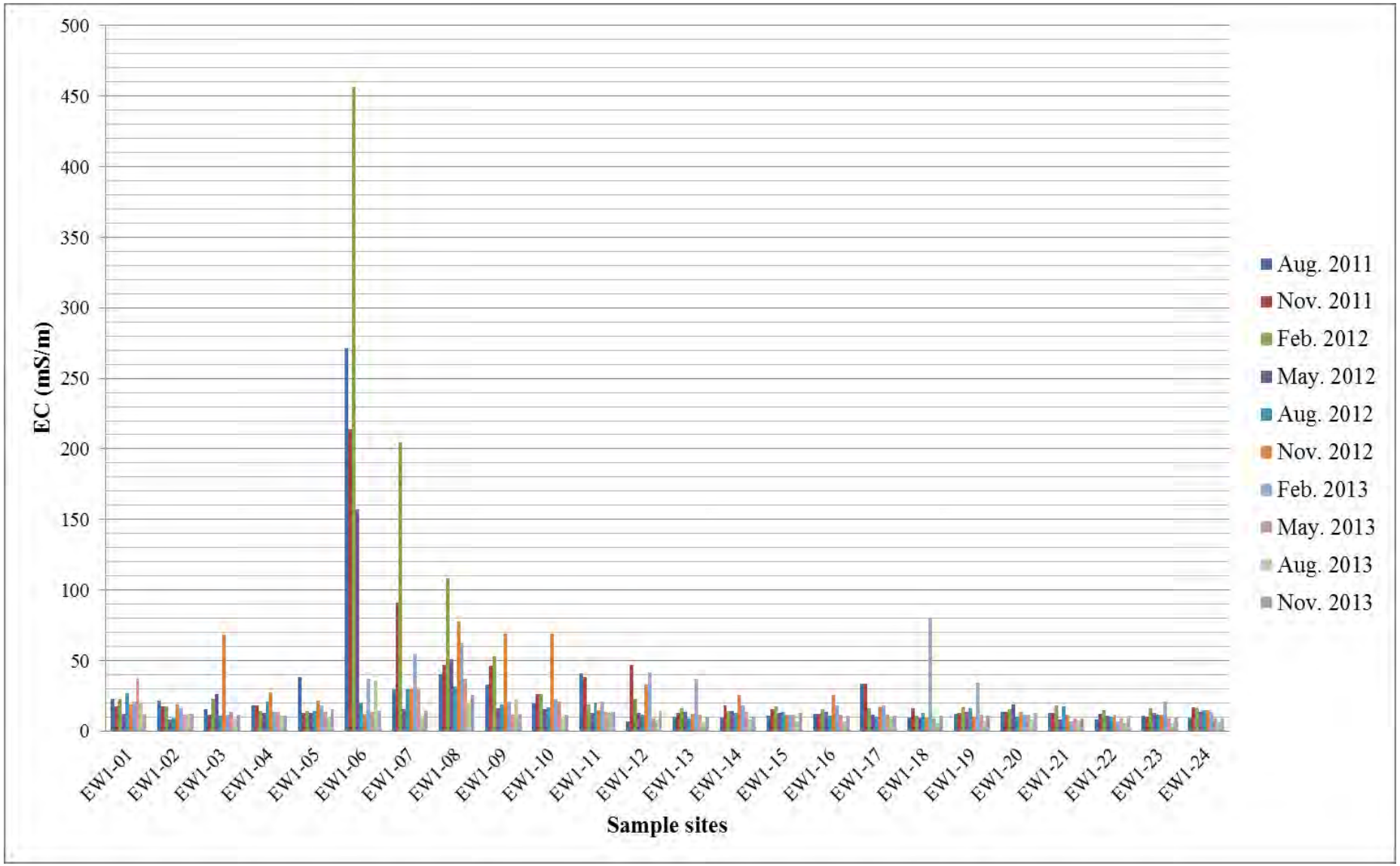

B4: The EC (mS/m) of the soil for the east-west 1 transect line over a 30 month period.

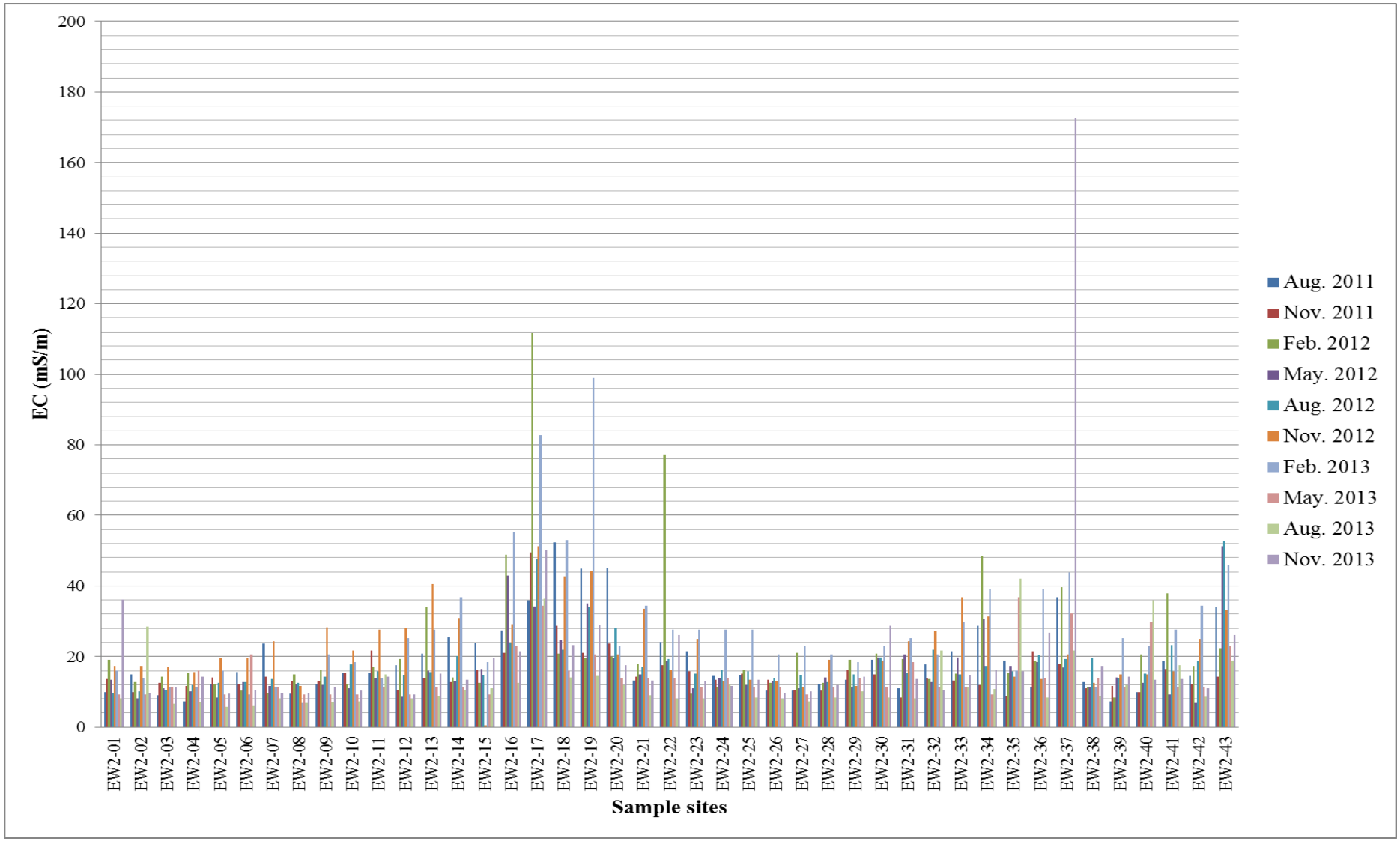

B5: The EC (mS/m) of the soil for the east-west 2 transect line over a 30 month period.

Appendix C: Exchangeable cations and cation exchange capacity (CEC) of the soil samples collected at fixed point on the study area (Analyst: Terina Vermeulen, Eco-Analytica Laboratory, NWU).

C1: Exchangeable cations and cation exchange capacity (CEC) of the composite soil samples of the 12 fixed point in March 2012.

Sample no.	Ca	Mg	K	Na	CEC	Effective CEC	Base Saturation	Ca:Mg ratio
	(cmol(+)/kg)						%	
FP - 1	5.57	2.30	0.53	0.07	12.57	8.48	67.42	2.42
FP- 2	3.65	1.54	0.29	0.02	9.78	5.50	56.22	2.37
FP - 3	4.02	1.74	0.32	0.02	8.45	6.10	72.17	2.31
FP- 4	3.24	1.42	0.20	0.01	10.70	4.88	45.60	2.28
FP- 5	6.78	4.25	0.38	0.01	14.75	11.42	77.42	1.60
FP - 6	20.05	13.57	0.34	0.21	18.29	34.17	186.86	1.48
FP - 7	2.85	1.33	0.17	0.01	7.82	4.37	55.89	2.14
FP - 8	5.46	3.72	0.15	0.02	12.76	9.36	73.34	1.47
FP - 9	4.37	2.54	0.25	0.01	12.00	7.17	59.75	1.72
FP-K1	3.67	1.43	0.63	0.01	11.96	5.73	47.96	2.57
FP-K2	2.28	0.96	0.37	0.01	8.21	3.62	44.10	2.38
FP-K3	2.83	1.02	0.63	0.01	12.29	4.49	36.52	2.77

C2: Exchangeable cations and cation exchange capacity (CEC) of the composite soil samples of the 12 fixed point in April 2013.

Sample no.	Ca	Mg	K	Na	CEC	Effective CEC	Base Saturation	Ca:Mg ratio
	(cmol($^+$)/kg)						%	
FP-1	5.75	1.96	0.47	0.02	11.49	8.20	71.38	2.9
FP-2	3.14	1.15	0.45	0.00	8.43	4.74	56.17	2.7
FP-3	4.20	1.50	0.30	0.01	9.63	6.01	62.39	2.8
FP-4	2.74	1.07	0.24	0.00	9.78	4.06	41.55	2.6
FP-5	8.68	4.16	0.25	0.01	12.77	13.11	102.68	2.1
FP-6	17.30	10.87	0.25	0.07	15.47	28.49	184.18	1.6
FP-7	2.97	0.96	0.30	0.00	8.70	4.25	48.77	3.1
FP-8	5.24	2.23	0.23	0.00	10.40	7.71	74.16	2.3
FP-9	5.07	2.19	0.25	1.34	11.74	8.85	75.36	2.3
FP-K1	3.21	1.10	0.52	0.01	10.42	4.84	46.43	2.9
FP-K2	2.49	0.90	0.36	0.00	7.84	3.75	47.79	2.8
FP-K3	2.93	0.89	0.71	0.00	9.28	4.52	48.76	3.3

C3: Calculations.

- Calculation was done as discribed by Hazelton and Murphy (2007).

C3.1: Proportions of the exchangeable cations of the cation exchange capacity (CEC) expressed as a precentage.

$$\frac{Ca^2}{\text{Effective CEC}} \times 100 \quad \text{Proportion of CEC} \qquad \frac{Mg^2}{\text{Effective CEC}} \times 100 \quad \text{Proportion of CEC}$$

$$\frac{K}{\text{Effective CEC}} \times 100 \quad \text{Proportion of CEC} \qquad \frac{Na}{\text{Effective CEC}} \times 100 \quad \text{Proportion of CEC}$$

C3.2: Ca:Mg Ratio.

$$\frac{Ca^2 \quad (\text{cmol}(\ )/\text{kg})}{Mg^2 \quad (\text{cmol}(\ )/\text{kg})}$$

Appendix D: Anion concentration of the soil samples collected at fixed point on the study area (Analyst: Terina Vermeulen, Eco-Analytica Laboratory, NWU).

D1: Anion concentration (mg/l) of the fixed point soil samples over a 30 month period.

Date	Sample no.	NO_2 (mg/l)	NO_3 (mg/l)	PO_4 (mg/l)	SO_4 (mg/l)	Cl (mg/l)	F (mg/l)
Aug. 2011	**FP-1**	25.48	20.90	0.09	543.87	40.76	0.86
	FP-2	5.97	2.47	<0.01	12.90	3.65	0.02
	FP-3	1.95	0.16	<0.01	14.85	13.27	0.06
	FP-4	2.31	0.66	<0.01	15.20	11.32	0.07
	FP-5	0.10	0.26	0.03	46.12	17.77	0.10
	FP-6	0.45	0.92	0.15	435.45	74.18	0.08
	FP-7	5.40	0.88	0.09	14.42	7.60	0.19
	FP-8	0.04	0.26	<0.01	30.50	11.52	0.19
	FP-9	0.45	0.58	<0.01	26.38	12.81	0.04
	FP-K1	3.32	0.90	0.01	16.68	11.35	0.08
	FP-K2	29.98	15.82	<0.01	22.07	16.01	0.14
	FP-K3	7.21	21.11	0.02	16.44	10.30	0.31
Sep. 2011	**FP-1**	22.58	7.16	<0.01	561.72	64.96	0.21
	FP-2	0.11	0.27	0.32	46.48	12.50	17.35
	FP-3	0.57	1.14	0.12	35.81	13.39	0.37
	FP-4	0.14	0.38	0.01	22.28	9.14	0.07
	FP-5	0.15	0.43	<0.01	121.59	26.98	0.03
	FP-6	1.15	7.70	1.11	877.85	203.43	0.13
	FP-7	7.99	15.17	0.07	49.33	11.39	1.02
	FP-8	0.35	0.42	<0.01	69.94	15.88	0.09
	FP-9	0.55	1.41	0.01	34.36	15.06	13.99
	FP-K1	2.58	0.66	0.1	31.14	15.03	0.03
	FP-K2	4.89	2.11	<0.01	29.42	8.78	0.02
	FP-K3	0.20	0.64	0.01	27.62	12.46	0.07
Oct. 2011	**FP-1**	47.15	6.62	<0.01	865.87	76.38	1.11
	FP-2	0.18	1.06	0.02	39.41	20.14	0.05
	FP-3	0.32	0.68	0.02	26.78	13.86	0.05
	FP-4	0.19	0.66	<0.01	24.54	15.16	0.04
	FP-5	4.92	66.34	<0.01	77.78	26.54	0.02
	FP-6	1.86	4.64	<0.01	630.87	116.73	0.12
	FP-7	65.97	141.15	<0.01	43.90	16.83	0.01
	FP-8	0.40	0.88	0.06	76.81	14.68	0.29
	FP-9	0.24	2.65	0.08	46.42	21.84	0.08

D1: Anion concentration (mg/l) of the fixed point soil samples over a 30 month period.

Date	Sample no.	NO_2 (mg/l)	NO_3 (mg/l)	PO_4 (mg/l)	SO_4 (mg/l)	Cl (mg/l)	F (mg/l)
Oct. 2011	**FP-K1**	0.36	1.70	0.05	35.03	18.05	0.05
	FP-K2	2.07	0.88	0.01	28.85	10.55	0.02
	FP-K3	1.39	1.11	<0.01	27.82	16.04	0.07
Nov. 2011	**FP-1**	1.49	7.83	<0.01	766.10	58.65	1.10
	FP-2	32.09	2.66	<0.01	39.34	10.31	0.05
	FP-3	1.58	1.81	<0.01	24.89	13.11	0.06
	FP-4	0.17	0.20	0.04	55.95	17.29	0.03
	FP-5	4.25	2.17	<0.01	24.88	7.84	0.04
	FP-6	1.52	6.86	<0.01	1286.22	110.30	0.02
	FP-7	32.13	0.10	<0.01	24.38	6.47	0.02
	FP-8	0.39	0.79	0.01	110.76	12.47	0.11
	FP-9	0.26	3.42	0.01	72.80	17.00	0.05
	FP-K1	5.68	1.25	<0.01	18.51	4.84	0.08
	FP-K2	30.94	3.40	<0.01	22.39	5.34	0.05
	FP-K3	34.54	2.76	<0.01	22.84	17.54	0.07
Dec. 2011	**FP-1**	2.64	37.55	<0.01	2935.16	235.88	0.16
	FP-2	16.49	1.16	0.02	43.51	7.80	0.04
	FP-3	0.41	0.60	<0.01	46.55	13.81	0.05
	FP-4	0.24	0.61	<0.01	20.40	6.96	0.03
	FP-5	0.12	0.31	<0.01	37.66	10.60	0.03
	FP-6	164.95	8.19	<0.01	1232.52	23.77	3.98
	FP-7	25.76	1.50	<0.01	25.93	4.25	0.02
	FP-8	0.19	0.30	<0.01	25.23	5.64	0.08
	FP-9	0.21	0.72	0.01	25.58	8.49	0.10
	FP-K1	0.41	0.51	<0.01	22.72	4.53	0.14
	FP-K2	4.79	5.25	<0.01	20.41	4.29	0.08
	FP-K3	0.33	0.73	0.02	34.57	7.92	0.15
Jan. 2012	**FP-1**	4.37	16.82	<0.01	688.51	63.67	0.10
	FP-2	0.15	1.39	0.04	31.69	4.90	0.06
	FP-3	3.53	1.26	0.02	61.32	15.44	0.25
	FP-4	3.84	2.23	0.04	23.55	3.14	0.10
	FP-5	0.04	0.11	<0.01	25.16	7.19	0.12
	FP-6	0.15	1.89	0.42	840.49	117.74	0.04
	FP-7	3.06	0.55	<0.01	17.40	5.07	0.12
	FP-8	0.15	0.67	<0.01	172.50	6.30	0.75
	FP-9	0.25	0.91	<0.01	42.86	6.45	0.07
	FP-K1	2.25	2.40	0.04	15.67	3.92	0.11
	FP-K2	1.45	5.99	<0.01	26.43	2.94	2.77

D1: Anion concentration (mg/l) of the fixed point soil samples over a 30 month period.

Date	Sample no.	NO_2 (mg/l)	NO_3 (mg/l)	PO_4 (mg/l)	SO_4 (mg/l)	Cl (mg/l)	F (mg/l)
Jan. 2012	**FP-K3**	12.31	31.96	0.01	53.48	6.57	0.11
Feb. 2012	**FP-1**	1.00	2.50	0.31	618.05	25.72	3.42
	FP-2	1.17	165.99	<0.01	36.60	6.91	1.95
	FP-3	1.54	83.69	0.01	26.55	6.70	0.01
	FP-4	19.07	8.05	<0.01	21.22	5.89	0.17
	FP-5	0.25	0.26	0.04	23.48	7.54	0.09
	FP-6	0.97	3.68	<0.01	277.19	35.74	0.01
	FP-7	37.50	12.21	<0.01	18.59	12.07	0.03
	FP-8	0.80	0.79	<0.01	18.39	7.11	0.04
	FP-9	0.69	0.88	0.10	20.42	7.14	1.33
	FP-K1	5.10	48.91	<0.01	24.49	5.12	0.07
	FP-K2	15.31	81.18	<0.01	41.11	6.35	0.09
	FP-K3	52.02	94.81	0.02	32.00	12.12	0.34
Mar. 2012	**FP-1**	0.27	0.13	<0.01	369.73	12.52	0.12
	FP-2	1.00	1.11	0.01	21.49	2.26	0.06
	FP-3	0.45	0.54	<0.01	17.82	4.20	0.04
Mar. 2012	**FP-4**	0.86	0.76	0.12	22.53	4.07	0.03
	FP-5	0.02	0.15	<0.01	15.63	4.48	2.07
	FP-6	0.06	0.48	0.03	77.70	9.77	0.01
	FP-7	0.24	0.54	0.02	19.27	5.81	0.02
	FP-8	0.27	0.32	0.02	16.46	4.65	0.01
	FP-9	0.14	0.26	<0.01	13.93	6.18	0.04
	FP-K1	0.25	0.30	<0.01	24.57	5.23	0.03
	FP-K2	1.02	1.00	0.03	18.20	5.05	0.06
	FP-K3	38.01	4.53	0.03	17.20	8.11	7.65
Apr. 2012	**FP-1**	0.21	0.67	0.10	298.12	13.32	0.20
	FP-2	2.14	2.08	0.04	13.87	5.04	4.72
	FP-3	0.21	2.33	0.02	13.19	4.18	0.27
	FP-4	0.42	1.34	<0.01	18.61	13.56	0.04
	FP-5	0.10	0.45	<0.01	14.88	5.92	0.05
	FP-6	0.25	0.39	<0.01	75.18	17.51	0.02
	FP-7	1.34	8.83	<0.01	15.28	6.36	0.03
	FP-8	0.25	1.63	<0.01	12.07	7.94	0.05
	FP-9	0.38	0.72	<0.01	11.86	7.46	0.05
	FP-K1	6.46	2.49	0.07	20.45	11.65	0.06
	FP-K2	3.94	47.17	<0.01	16.21	6.81	0.09
	FP-K3	11.55	7.74	0.01	22.78	7.59	0.04

D1: Anion concentration (mg/l) of the fixed point soil samples over a 30 month period.

Date	Sample no.	NO_2 (mg/l)	NO_3 (mg/l)	PO_4 (mg/l)	SO_4 (mg/l)	Cl (mg/l)	F (mg/l)
May 2012	**FP-1**	0.26	0.76	0.01	196.38	21.09	0.08
	FP-2	0.24	0.56	0.07	15.15	7.05	0.03
	FP-3	0.11	0.73	0.03	14.07	5.89	0.06
	FP-4	0.23	1.13	0.01	19.37	6.53	0.07
	FP-5	0.10	0.20	0.02	22.18	7.91	0.10
	FP-6	0.21	0.30	<0.01	31.38	13.21	0.10
	FP-7	0.36	0.99	<0.01	13.97	6.35	0.02
	FP-8	0.17	1.28	0.06	20.06	7.47	0.09
	FP-9	0.11	0.56	0.05	10.90	6.66	0.05
May 2012	**FP-K1**	0.63	0.68	0.01	19.59	10.68	0.04
	FP-K2	0.42	2.23	<0.01	18.00	8.00	1.32
	FP-K3	5.69	2.01	0.08	23.08	10.58	0.03
Jun. 2012	**FP-1**	0.23	2.42	0.34	205.18	15.63	0.21
	FP-2	2.00	1.16	0.01	22.96	9.02	0.11
	FP-3	125.27	9.72	0.23	35.73	148.41	0.12
	FP-4	0.44	0.45	0.08	24.55	13.76	0.02
	FP-5	0.53	3.87	<0.01	27.06	6.60	0.04
	FP-6	0.76	3.14	<0.01	50.30	18.82	0.03
	FP-7	3.27	0.99	<0.01	19.90	6.06	0.07
	FP-8	0.14	2.99	<0.01	22.23	6.82	0.33
	FP-9	0.43	2.07	<0.01	27.85	6.86	0.66
	FP-K1	14.88	1.95	0.55	59.40	15.20	1.09
	FP-K2	6.52	3.89	0.62	30.04	5.64	1.12
	FP-K3	0.10	0.39	0.98	31.00	10.45	0.09
Aug.2013	**FP-1**	1.35	1.64	<0.01	38.11	5.02	-
	FP-2	2.61	5.48	<0.01	14.55	5.88	
	FP-3	0.71	0.69	<0.01	10.12	3.54	-
	FP-4	0.10	0.14	<0.01	13.79	7.76	-
	FP-5	0.02	0.03	<0.01	9.28	1.82	-
	FP-6	0.04	0.07	<0.01	10.08	4.12	-
	FP-7	0.11	0.21	<0.01	11.19	2.29	-
	FP-8	<0.01	0.11	<0.01	7.68	3.35	-
	FP-9	<0.01	0.10	<0.01	6.75	2.36	-
	FP-K1	3.04	1.69	<0.01	16.85	3.77	-
	FP-K2	2.51	0.29	<0.01	20.96	4.79	-
	FP-K3	0.74	5.47	<0.01	24.61	5.40	-

Appendix E: ICP-MS analysis of the soil samples for total and soluble/available trace metal elements of the 12 fixed points (Analyst: Yvonne Visagie, Eco-Analytica, NWU).

E1 ICP-MS analysis of the soil samples for total trace metal elements of the 12 fixed points.

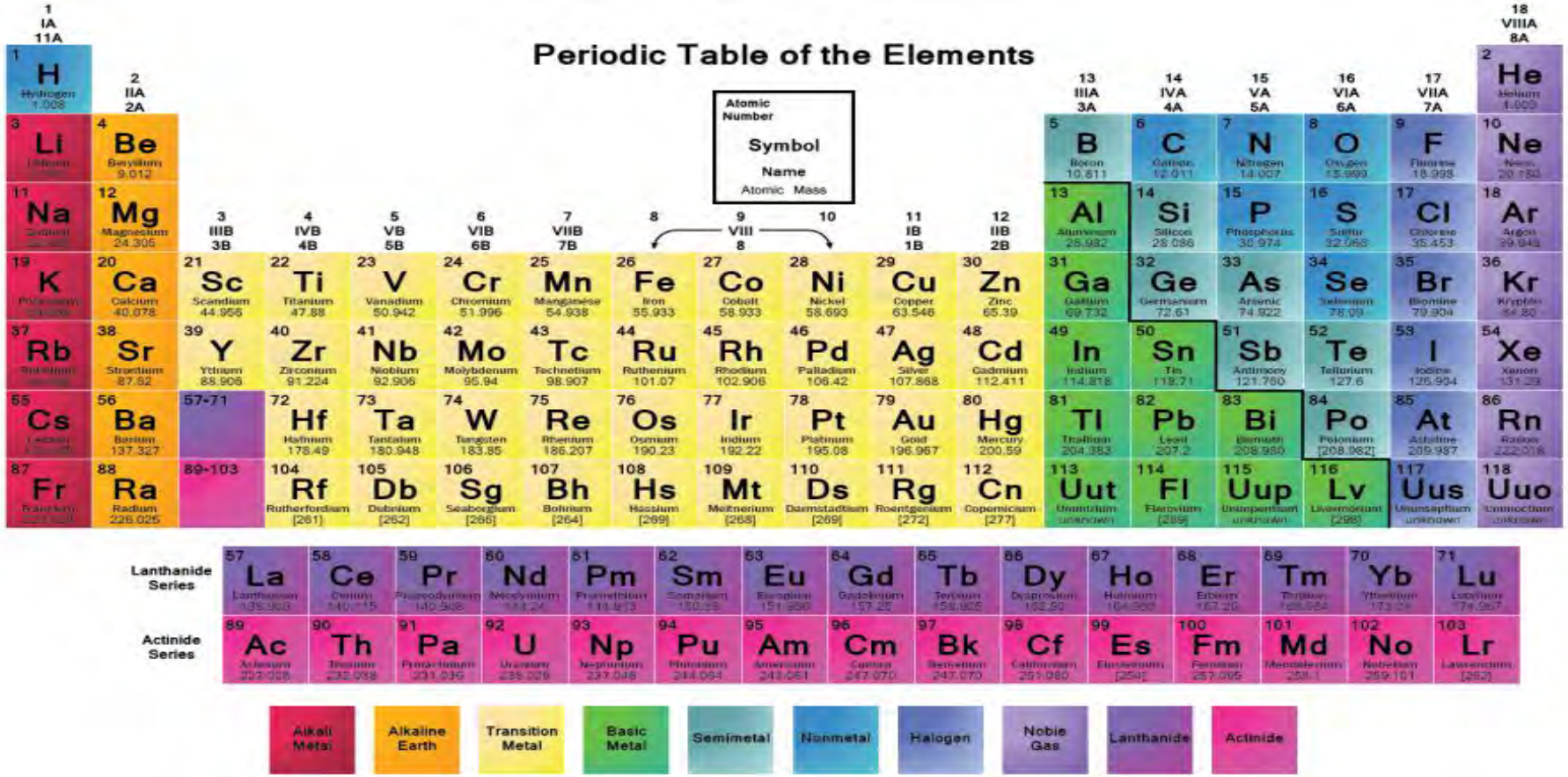

E1: Periodic Table of the elements. Retrieved from http://sciencenotes.org/color-printable-periodic-table/ Date of access: 20 Nov 2014.

E1.1: ICP-MS analysis of the soil samples for total trace metal elements of the 12 fixed points sampled in August 2011 complete dataset.

Sample no	**FP-1**	**FP-2**	**FP-3**	**FP-4**	**FP-5**	**FP-6**	**FP-7**	**FP-8**	**FP-9**	**FP-K1**	**FP-K2**	**FP-K3**
Major elements *mg/kg*												
Ti	170.1	149.2	131.1	123.3	81.5	86	104.9	102.6	162.1	154.9	122.2	167.4
Al	11275	9090	7912.5	5432.5	5037.5	5640	4995	6152.5	7567.5	9002.5	6082.5	8067.5
Fe	17550	16067.5	12912.5	11195	8525	10445	11180	8585	12317.5	13912.5	11097.5	18177.5
Mn	15265	9512.5	5305	7355	2830	3662.5	5237.5	2727.5	3812.5	9027.5	5985	10685
Mg	791.5	576	546.3	371.8	1441.5	12667.5	350	854.5	776.5	560.8	304	449.3
Ca	1234.3	793.8	768.8	602.5	1404	22325	522.8	1133.8	930.5	720.5	401.8	550
Na	125.3	113.65	105.5	99	90.9	171.3	101.3	105.4	103	97.4	89.6	93.5
K	1051.8	794.5	676.5	533.5	673.5	609.5	382.8	448.3	617.3	958	466.8	831.75
P	359.3	391	386.5	359	330	413.8	369.8	371.5	367	367.5	354.25	356.25
B	0.9	0.001	0.002	0.006	0.002	1.6	0.011	0.004	0.003	0.02	0.008	0.008
Trace elements *mg/kg*												
Ba	986.8	736.8	423	656.8	365.5	365.3	999.5	292	447	800	773.8	805
Be	0.7	0.6	0.5	0.4	0.4	0.4	0.5	0.5	0.4	0.6	0.4	0.6
Co	12.1	9.6	6.0	6.9	3.2	4.7	7.3	3	5.1	11.3	8.2	14.7
Cr	54.4	73.7	83.5	72.9	67.6	65.1	88.9	68.3	91.1	76.3	80.9	101.6
Cu	19.7	12.7	8.8	7.3	6.4	7.3	9.4	6.7	7.9	18.1	11.1	23
Ni	58.5	23.3	15.5	11.3	7.9	8.7	15.4	8.3	11.1	46.1	18.4	56.4
Sr	22.1	19	11.2	23.7	9.4	21.7	7.3	11.2	11.3	15.5	9.2	22.8

E1.1: ICP-MS analysis of the soil samples for total trace metal elements of the 12 fixed points sampled in August 2011 complete dataset.

Sample no	**FP-1**	**FP-2**	**FP-3**	**FP-4**	**FP-5**	**FP-6**	**FP-7**	**FP-8**	**FP-9**	**FP-K1**	**FP-K2**	**FP-K3**
Trace elements *mg/kg*												
V	36.6	31.9	24.8	23.9	14.7	16.9	25.9	14.8	25.4	28	24.2	35.4
Zn	13.3	7	6.4	4.4	4.8	7.8	2.7	3.7	6.8	8.4	5.9	11.5
U	0.4	0.4	0.4	0.3	0.2	0.2	0.3	0.3	0.3	0.3	0.3	0.4
As	1.8	1.6	1.3	1.1	0.8	1.1	1.3	0.8	1.1	1.4	1.4	1.5
Se	0.3	0.3	0.2	0.2	0.1	0.3	0.2	0.1	0.2	0.2	0.1	0.3
Mo	1.4	1	0.7	0.8	0.4	0.4	0.8	0.4	0.5	1.3	0.8	1.5
Pd	0.2	0.2	0.2	0.2	0.2	0.2	0.2	0.2	0.2	0.2	0.2	0.2
Ag	0.3	0.2	0.1	0.3	0.1	0.1	0.2	0.1	0.1	0.1	0.1	0.1
Cd	0.1	0.1	0.04	0.05	0.01	0.03	0.03	0.01	0.02	0.1	0.04	0.1
Sb	0.3	0.3	0.3	0.3	0.3	0.3	0.3	0.3	0.3	0.3	0.3	0.3
Pt	0.1	0.1	0.1	0.2	0.1	0.1	0.1	0.1	0.1	0.1	0.1	0.1
Au	02	0.1	0.1	0.1	0.1	0.1	0.1	0.2	0.1	0.1	0.1	0.2
Hg	0.0	0.003	0.0	0.001	0.0002	0.0003	0.02	0.05	0.0	0.0	0.0	0.00
Tl	0.5	0.4	0.3	0.5	0.3	0.3	0.5	0.3	0.3	0.4	0.5	0.5
Pb	12.7	7.4	6.3	4.6	4.4	5	7.3	4.6	5.4	14.9	5.8	20.9

E1.2: ICP-MS analysis of the soil samples for total trace metal elements of the 12 fixed points sampled in January 2014 complete dataset.

Sample no	**FP-1**	**FP-2**	**FP-3**	**FP-4**	**FP-5**	**FP-6**	**FP-7**	**FP-8**	**FP-9**	**FP-K1**	**FP-K2**	**FP-K3**
Major elements *mg/kg*												
Ti	145.1	120.7	101.8	124.6	89	105.5	97.9	103.8	129.0	124.5	113.6	135.0
Al	10057.5	9255	8465	7442.5	7282.5	9062.5	7345	7315	7612.5	10092.5	6980	9160
Fe	17012.5	12897.5	15100	12627.5	10312.5	12142.5	12395	12150	12685	16667.5	13340	19150
Mn	18077.5	8442.5	8622.5	10365	3540	4557.5	5112.5	8782.5	5585	13735	8630	11220
Mg	895	534	552.3	440	1943	13505	414.8	890.5	865.5	649.3	481.3	498
Ca	1585	736.5	815	665.3	1997.3	18977.5	597.5	1360.3	1152.3	973.8	810.8	667.5
Na	305.5	285.75	265.75	309.5	285.25	314.5	272.75	293.25	276.25	300.25	305.75	268.5
K	1190.3	937.3	870.5	867.3	832	1025.8	591	733.5	728	1232.8	747	1007.3
P	417.3	412	387	400.3	394.3	470.8	396.3	418.3	396.5	436.8	449.5	407.5
B	0.01	0.004	0.015	0.01	0.001	2.6	0.01	0.008	0.01	1.9	0.01	0.01
Trace elements *mg/kg*												
Ba	1124	599.8	588.8	722	362.8	370.8	706	743	455.3	880.5	787.5	585.5
Be	0.7	0.5	0.5	0.4	0.3	0.4	0.4	0.4	0.4	0.7	0.4	0.6
Co	14.3	8	8.3	8.3	4.2	5.7	7.3	7.4	6.9	15.1	10.1	13.2
Cr	66	63.5	91.5	74.2	73.2	66.5	92.2	73.3	80.5	82.7	89.5	98
Cu	23.6	11.9	11.2	12.2	8.1	9.5	10.8	10.1	9.8	24.9	14	22
Ni	61.4	23.6	21.1	16.1	11.2	12.9	20.4	15.9	15.1	79.6	25.7	58.7
Sr	26.3	16.9	16.9	29.1	10.4	20.2	7	26.7	14.4	19.8	12.4	16.5
V	42.6	30.1	35.7	32.4	24.7	24.4	30.9	30.7	31.1	37.8	34.575	39.9

E1.2: ICP-MS analysis of the soil samples for total trace metal elements of the 12 fixed points sampled in January 2014 complete dataset.

Sample no	**FP-1**	**FP-2**	**FP-3**	**FP-4**	**FP-5**	**FP-6**	**FP-7**	**FP-8**	**FP-9**	**FP-K1**	**FP-K2**	**FP-K3**
Zn	16.3	9.6	13.5	9.8	8.1	15.5	7.1	7.9	7.3	15.7	9.6	16.1
U	0.5	0.3	0.3	0.3	0.1	0.2	0.3	0.2	0.3	0.3	0.3	0.3
As	2.1	1.5	1.9	1.3	1.0	1.2	1.6	1.4	1.3	1.8	1.9	1.8
Se	0.003	0.004	0.003	0.004	0.005	0.003	0.004	0.004	0.004	0.003	0.003	0.003
Mo	1.6	0.8	0.8	0.8	0.4	0.4	0.7	0.7	0.5	1.8	1	1.3
Pd	0.2	0.1	0.1	0.2	0.1	0.2	0.1	0.2	0.1	0.2	0.1	0.2
Ag	0.06	0.00	0.00	0.00	0.00	0.00	0.00	0.00	0.00	0.04	0.00	0.01
Cd	0.11	0.03	0.03	0.04	0.00	0.02	0.01	0.02	0.01	0.09	0.05	0.07
Sb	0.24	0.16	0.18	0.21	0.18	0.18	0.25	0.23	0.20	0.31	0.28	0.25
Pt	0.0004	0.0004	0.0004	0.0004	0.0004	0.0188	0.0004	0.0003	0.0003	0.0003	0.0004	0.0004
Au	0.12	0.11	0.11	0.11	0.11	0.30	0.11	0.12	0.10	0.12	0.11	0.18
Hg	0.0002	0.0002	0.0002	0.0002	0.0002	0.0002	0.0002	0.0002	0.0002	0.0001	0.0002	0.0002
Tl	0.57	0.30	0.37	0.50	0.20	0.19	0.29	0.47	0.24	0.43	0.40	0.28
Pb	14.7	6.9	7.1	5.8	4.7	5.4	7.3	5.9	5.4	15.6	6.9	18.3

E2: ICP-MS analysis of the soil samples for soluble/available trace metal elements of the 12 fixed points.

E2.1: ICP-MS analysis of the soil samples for soluble/available trace metal elements of the 12 fixed points sampled in August 2011 complete dataset.

Sample no	**FP-1**	**FP-2**	**FP-3**	**FP-4**	**FP-5**	**FP-6**	**FP-7**	**FP-8**	**FP-9**	**FP-K1**	**FP-K2**	**FP-K3**
Major elements *mg/kg*												
Ti	1.0	2.4	4.3	2.2	2.0	1.2	2.8	4.1	2.1	0.8	1.7	1.0
Al	19.1	31.7	72.1	30.0	32.2	19.0	42.9	76.2	20.6	18.2	26.2	20.8
Fe	53.4	46.1	69.5	34.6	55.4	53.2	34.6	59.2	34.1	28.0	31.9	32.5
Mn	18.7	20.5	50.7	41.4	24.5	8.4	46.5	68.7	73.0	26.3	46.5	120.4
Mg	2436.5	1745.3	1924.8	1516.0	5345.0	13882.5	1326.8	3745.0	2810.0	1524.3	947.5	1026.0
Ca	10067.5	6395.0	7075.0	5800.0	12867.5	14105.0	4730.0	8672.5	7747.5	6060.0	3657.5	5072.5
Na	247.2	56.6	41.3	41.3	43.4	661.5	25.7	60.4	29.2	29.5	17.3	27.1
K	2221.5	1253.25	1310.5	853.5	1704.5	1344.25	716.75	622.75	1054.25	2363.25	1317	2550
P	4.9	5.4	6.5	5.4	5.7	8.5	5.0	6.0	4.5	5.7	4.5	5.1
B	0.408	0.099	0.412	0.000	0.002	0.002	0.003	0.006	0.003	0.005	0.005	0.005
Trace elements *mg/kg*												
Ba	27.3	5.5	12.8	19.3	14.7	6.3	18.3	16.6	6.7	16.7	18.1	35.1
Be	0.05	0.05	0.05	0.05	0.05	0.05	0.05	0.05	0.05	0.05	0.05	0.05
Co	0.13	0.07	0.07	0.06	0.08	0.08	0.06	0.08	0.08	0.06	0.07	0.07
Cr	0.1	0.05	0.2	0.03	0.07	0.007	0.02	0.1	0.009	0.0002	0.0002	0.0003
Cu	0.5	0.7	0.7	0.3	0.6	0.8	0.6	0.8	0.4	0.7	0.6	0.5

E2.1: ICP-MS analysis of the soil samples for soluble/available trace metal elements of the 12 fixed points sampled in August 2011 complete dataset.

Sample no	**FP-1**	**FP-2**	**FP-3**	**FP-4**	**FP-5**	**FP-6**	**FP-7**	**FP-8**	**FP-9**	**FP-K1**	**FP-K2**	**FP-K3**
Trace elements *mg/kg*												
Ni	0.2	0.2	0.3	0.3	0.2	0.2	0.3	0.2	0.1	0.2	0.3	0.6
Sr	11.7	10.3	13.3	14.9	16.5	12.9	8.8	6.7	12.9	12.4	11.2	16.4
V	0.2	0.3	0.3	0.2	0.2	0.2	0.2	0.3	0.2	0.2	0.2	0.2
Zn	0.01	0.01	0.8	0.6	0.01	0.003	0.01	0.4	0.1	0.6	0.6	1.0
U	0.1	0.1	0.1	0.1	0.1	0.1	0.1	0.1	0.1	0.1	0.1	0.1
As	0.0004	0.0004	0.0004	0.0005	0.0004	0.0004	0.0005	0.0004	0.0005	0.0005	0.0006	0.0005
Se	0.001	0.001	0.001	0.001	0.001	0.001	0.001	0.001	0.001	0.001	0.001	0.001
Mo	0.05	0.04	0.05	0.04	0.04	0.05	0.04	0.04	0.04	0.03	0.04	0.04
Pd	0.1	0.1	0.1	0.1	0.1	0.1	0.1	0.1	0.1	0.1	0.1	0.1
Ag	0.0001	0.003	0.0001	0.0002	0.0002	0.05	0.0001	0.0001	0.0001	0.00005	0.01	0.0001
Cd	0.0002	0.0002	0.0002	0.0002	0.0002	0.0002	0.0002	0.0002	0.0002	0.0002	0.0002	0.0001
Sb	0.2	0.2	0.2	0.2	0.2	0.2	0.2	0.2	0.2	0.2	0.2	0.2
Pt	0.1	0.1	0.1	0.1	0.1	0.1	0.1	0.1	0.1	0.1	0.1	0.1
Au	0.1	0.1	0.1	0.1	0.1	0.1	0.1	0.1	0.1	0.1	0.1	0.1
Hg	0.00003	0.00002	0.00003	0.00003	0.00003	0.00002	0.00004	0.00003	0.00003	0.00004	0.00004	0.00004
Tl	0.09	0.05	0.06	0.06	0.07	0.06	0.07	0.08	0.06	0.06	0.07	0.08
Pb	0.0005	0.0002	0.0915	0.0003	0.0632	0.0006	0.0004	0.0092	0.0003	0.0004	0.0001	0.0001

E2.2: ICP-MS analysis of the soil samples for soluble/available trace metal elements of the 12 fixed points sampled in April 2011 complete dataset.

Sample no	**FP-1**	**FP-2**	**FP-3**	**FP-4**	**FP-5**	**FP-6**	**FP-7**	**FP-8**	**FP-9**	**FP-K1**	**FP-K2**	**FP-K3**
Major elements *mg/kg*												
Ti	0.0	0.01	0.01	0.006	0.002	0.007	0.008	0.005	0.004	0.003	0.006	0.009
Al	0.01	0.2	0.5	0.1	0.0001	0.05	0.1	0.0001	0.00001	0.04	0.1	0.2
Fe	3.6	2.2	2.5	2.1	5.2	5.6	1.8	3.0	3.0	2.6	1.7	2.4
Mn	0.9	2.9	2.5	4.1	0.1	0.2	4.3	0.4	1.0	0.9	4.0	4.3
Mg	214.4	139.0	162.9	133.2	491.8	1386.8	130.6	298.0	296.8	162.9	114.9	123.6
Ca	911.3	575.5	610.3	551.3	1346.0	1409.8	478.8	768.3	786.3	679.0	429.0	620.0
Na	8.4	3.9	3.3	2.8	4.1	25.2	3.2	4.2	3.9	4.1	3.0	3.2
K	206.7	197.5	120.6	126.2	105.3	156.5	122.9	75.3	100.8	266.8	135.5	295.3
P	0.1	0.7	0.2	0.1	0.2	0.2	0.2	0.2	0.2	0.3	0.2	0.3
B	0.1	0.1	0.1	0.1	0.1	0.1	0.2	0.2	0.2	0.2	0.2	0.2
Trace elements *mg/kg*												
Ba	3.9	1.3	1.5	3.2	2.2	1.2	2.7	2.6	0.9	3.1	3.2	4.8
Be	0.00003	0.00003	0.00003	0.00003	0.00003	0.00003	0.00003	0.00003	0.00003	0.00003	0.00003	0.00003
Co	0.001	0.00001	0.00003	0.00003	0.00002	0.00002	0.00003	0.00003	0.00003	0.00003	0.00003	0.00003
Cr	0.0001	0.0001	0.0001	0.0001	0.0001	0.0001	0.0001	0.0001	0.0001	0.0001	0.0001	0.0001
Cu	0.04	0.03	0.02	0.02	0.04	0.04	0.02	0.02	0.01	0.03	0.02	0.05
Ni	0.00003	0.01	0.01	0.03	0.00003	0.00	0.04	0.0001	0.00004	0.01	0.04	0.03
Sr	1.2	1.4	1.4	2.0	1.4	1.3	1.1	0.8	1.2	1.5	1.1	2.0

E2.2: ICP-MS analysis of the soil samples for soluble/available trace metal elements of the 12 fixed points sampled in April 2011 complete dataset.

Sample no	**FP-1**	**FP-2**	**FP-3**	**FP-4**	**FP-5**	**FP-6**	**FP-7**	**FP-8**	**FP-9**	**FP-K1**	**FP-K2**	**FP-K3**
Trace elements *mg/kg*												
V	0.0001	0.0001	0.0001	0.0001	0.0001	0.0001	0.0001	0.0001	0.0001	0.0001	0.0001	0.0001
Zn	0.0007	0.0005	0.0005	0.0003	0.0009	0.0009	0.007	0.0006	0.0009	0.0007	0.0002	0.0003
U	0.001	0.002	0.001	0.001	0.003	0.003	0.001	0.001	0.001	0.001	0.001	0.001
As	0.0001	0.0001	0.0001	0.0001	0.0001	0.0001	0.0001	0.0001	0.0001	0.0001	0.0001	0.0001
Se	0.001	0.001	0.001	0.001	0.001	0.001	0.001	0.001	0.001	0.001	0.001	0.001
Mo	0.003	0.002	0.002	0.002	0.002	0.01	0.008	0.01	0.004	0.002	0.002	0.01
Pd	0.0006	0.001	0.0007	0.001	0.0007	0.0007	0.0004	0.0001	0.0006	0.0008	0.0006	0.002
Ag	0.0001	0.0001	0.0001	0.0001	0.0001	0.0001	0.0001	0.0001	0.0001	0.0001	0.0001	0.0001
Cd	0.00005	0.00005	0.00004	0.00005	0.00005	0.00005	0.00005	0.00005	0.00005	0.00004	0.00004	0.00004
Sb	0.01	0.01	0.01	0.01	0.01	0.01	0.01	0.01	0.01	0.01	0.01	0.02
Pt	0.00003	0.00003	0.00003	0.00003	0.00003	0.00003	0.00003	0.00003	0.00003	0.00003	0.00003	0.00003
Au	0.008	0.008	0.008	0.008	0.008	0.008	0.008	0.007	0.008	0.007	0.007	0.007
Hg	0.00001	0.00001	0.00001	0.00001	0.00001	0.00001	0.00001	0.00001	0.00001	0.00001	0.00001	0.00001
Tl	0.00005	0.00005	0.00005	0.00004	0.00005	0.00004	0.00003	0.00004	0.00005	0.00005	0.00003	0.00003
Pb	0.0003	0.0002	0.0002	0.0003	0.0003	0.0003	0.0002	0.0003	0.0002	0.0002	0.0003	0.0002

E2.3: ICP-MS analysis of the soil samples for soluble/available trace metal elements of the 12 fixed points sampled in January 2014 complete dataset.

Sample no	**FP-1**	**FP-2**	**FP-3**	**FP-4**	**FP-5**	**FP-6**	**FP-7**	**FP-8**	**FP-9**	**FP-K1**	**FP-K2**	**FP-K3**
Major elements *mg/kg*												
Ti	0.006	0.02	0.007	0.07	0.07	0.07	0.07	0.04	0.03	0.01	0.003	
Al	0.4	0.4	0.3	1.3	2	1.5	1.3	1	0.5	0.6	0.4	
Fe	3.8	2.4	2.7	2.6	6.1	5.4	2.6	3.9	3.3	2.5	2.5	
Mn	0.4	1.4	1	2.3	0.3	0.3	6.3	0.7	0.4	1.1	2.9	
Mg	193.2	118.3	142.7	103.9	441.8	959.3	116	302.8	251.5	102.8	102.6	
Ca	780.3	473	577	392	1154.5	1092.8	452.8	770.3	705.3	412.8	483.5	
Na	5.6	3	2.9	2.5	3.3	9.8	2.9	4.4	2.9	5.3	2.7	
K	177.4	134.6	76.5	67.7	94.5	111	78.1	72.2	88.8	186.4	236.4	
P	0.3	0.2	0.3	0.3	0.3	0.4	0.4	0.5	0.4	0.3	0.3	
B	0.002	0.002	0.002	0.002	0.002	0.002	0.002	0.002	0.002	0.002	0.002	
Trace elements *mg/kg*												
Ba	2.4	1.0	1.5	2.2	1.8	0.6	2.5	1.6	0.8	2.9	2.0	4.4
Be	0.00004	0.00004	0.00004	0.00004	0.00004	0.00004	0.00004	0.00004	0.00004	0.00004	0.00004	0.00004
Co	0.00001	0.00003	0.00004	0.00003	0.00001	0.00001	0.00000	0.00003	0.00003	0.00003	0.00004	0.00004
Cr	0.00005	0.0001	0.0001	0.00005	0.00004	0.00005	0.0001	0.0001	0.0001	0.01	0.00004	0.00005
Cu	0.03	0.01	0.02	0.01	0.02	0.03	0.01	0.01	0.02	0.02	0.01	0.004
Ni	0.00003	0.01	0.003	0.03	0.002	0.0004	0.03	0.0003	0.00001	0.02	0.001	0.04

E2.3: ICP-MS analysis of the soil samples for soluble/available trace metal elements of the 12 fixed points sampled in January 2014 complete dataset.

Sample no	**FP-1**	**FP-2**	**FP-3**	**FP-4**	**FP-5**	**FP-6**	**FP-7**	**FP-8**	**FP-9**	**FP-K1**	**FP-K2**	**FP-K3**
Trace elements *mg/kg*												
Sr	1.1	1.2	1.2	1.5	1.4	1.1	1.0	0.8	1.1	1.4	1.0	1.7
V	0.0002	0.0002	0.0002	0.0002	0.0002	0.0002	0.0002	0.0002	0.0002	0.0002	0.0002	0.0002
Zn	0.001	0.001	0.001	0.001	0.001	0.001	0.001	0.001	0.001	0.001	0.001	0.001
U	0.00002	0.00002	0.00002	0.00002	0.00002	0.00002	0.00002	0.00002	0.00002	0.00002	0.00002	0.00002
As	0.0002	0.0002	0.0002	0.0002	0.0002	0.0002	0.0002	0.0002	0.0002	0.0002	0.0002	0.0002
Se	0.001	0.001	0.001	0.001	0.001	0.001	0.001	0.001	0.001	0.001	0.001	0.001
Mo	0.002	0.002	0.002	0.002	0.002	0.002	0.002	0.003	0.001	0.005	0.004	0.002
Pd	0.001	0.001	0.001	0.002	0.001	0.002	0.001	0.001	0.001	0.002	0.001	0.002
Ag	0.0001	0.0001	0.0001	0.0001	0.0001	0.0001	0.0001	0.0001	0.0001	0.0001	0.0001	0.0001
Cd	0.00006	0.00005	0.00006	0.00006	0.00006	0.00006	0.00006	0.00006	0.00006	0.00006	0.00006	0.00006
Sb	0.008	0.008	0.008	0.008	0.008	0.009	0.011	0.008	0.008	0.008	0.008	0.008
Pt	0.00004	0.00004	0.00004	0.00004	0.00004	0.00004	0.00003	0.00004	0.00004	0.00004	0.00003	0.00004
Au	0.01	0.01	0.01	0.01	0.01	0.01	0.01	0.01	0.01	0.01	0.01	0.01
Hg	0.00002	0.00002	0.00002	0.00002	0.00002	0.00002	0.00002	0.00002	0.00002	0.00002	0.00002	0.00002
Tl	0.00005	0.00005	0.00005	0.00004	0.00004	0.00004	0.00002	0.00004	0.00005	0.00004	0.00004	0.00004
Pb	0.0002	0.0002	0.0002	0.0002	0.0002	0.0002	0.0002	0.0002	0.0002	0.0002	0.0002	0.0002

Appendix F: Particle size distribution of the soil samples collected at the 12 fixed points on the study area (Analyst: Terina Vermeulen, Eco-Analytica Laboratory, NWU).

F1: Particle size distribution of the soil samples collected at the 12 Fixed Points.

%	Very coarse sand	Coarse sand	Medium sand	Fine sand	Very fine sand	Slit	Clay
FP-1	5.0	13.2	24.0	22.1	19.9	10.2	5.6
FP-2	5.3	12.5	22.7	22.2	23.6	8.0	5.7
FP-3	4.4	11.1	21.9	22.5	24.4	10.1	5.6
FP-4	7.0	13.2	22.3	24.0	22.2	5.7	5.6
FP-5	7.1	14.0	24.5	21.0	19.2	8.3	5.9
FP-6	7.4	12.1	20.5	20.4	17.7	15.8	6.1
FP-7	7.6	10.8	19.3	23.5	25.3	7.9	5.6
FP-8	5.0	11.0	22.8	25.5	22.4	7.8	5.5
FP-9	6.9	12.1	22.4	22.5	22.4	8.0	5.7
FP-K-1	4.4	12.9	23.2	22.8	20.9	10.2	5.6
FP-K-2	7.2	12.6	22.3	24.5	22.4	5.5	5.5
FP-K-3	5.2	12.9	22.5	22.0	19.2	12.5	5.7

Appendix G: X-ray Diffraction data of the mineral phases present in the soil samples collected at the 12 fixed points.

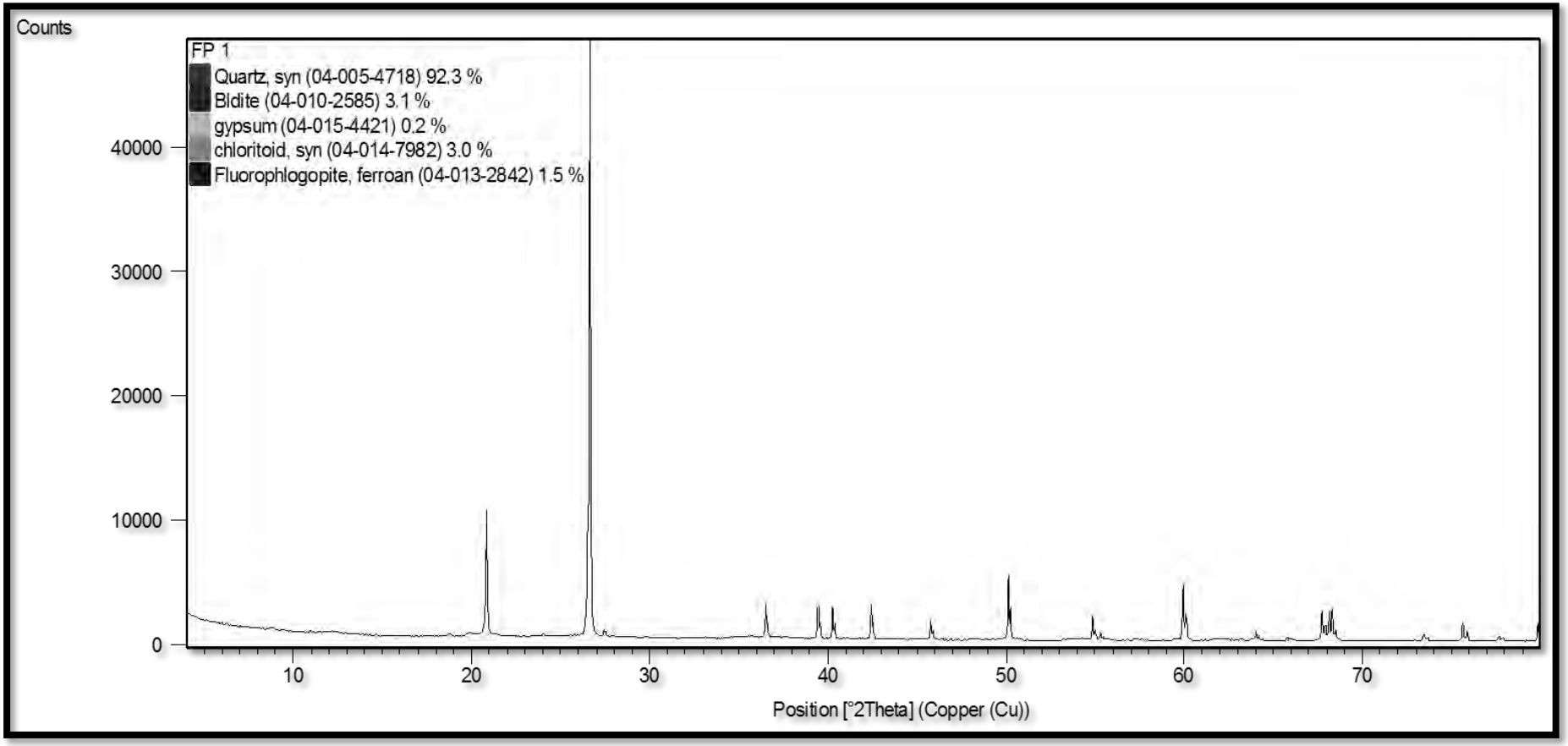

G1: XRD Analysis Diffractogram of FP-1. (Analyst: Belinda Venter, Geo XRD & XRF Laboratory, NWU).

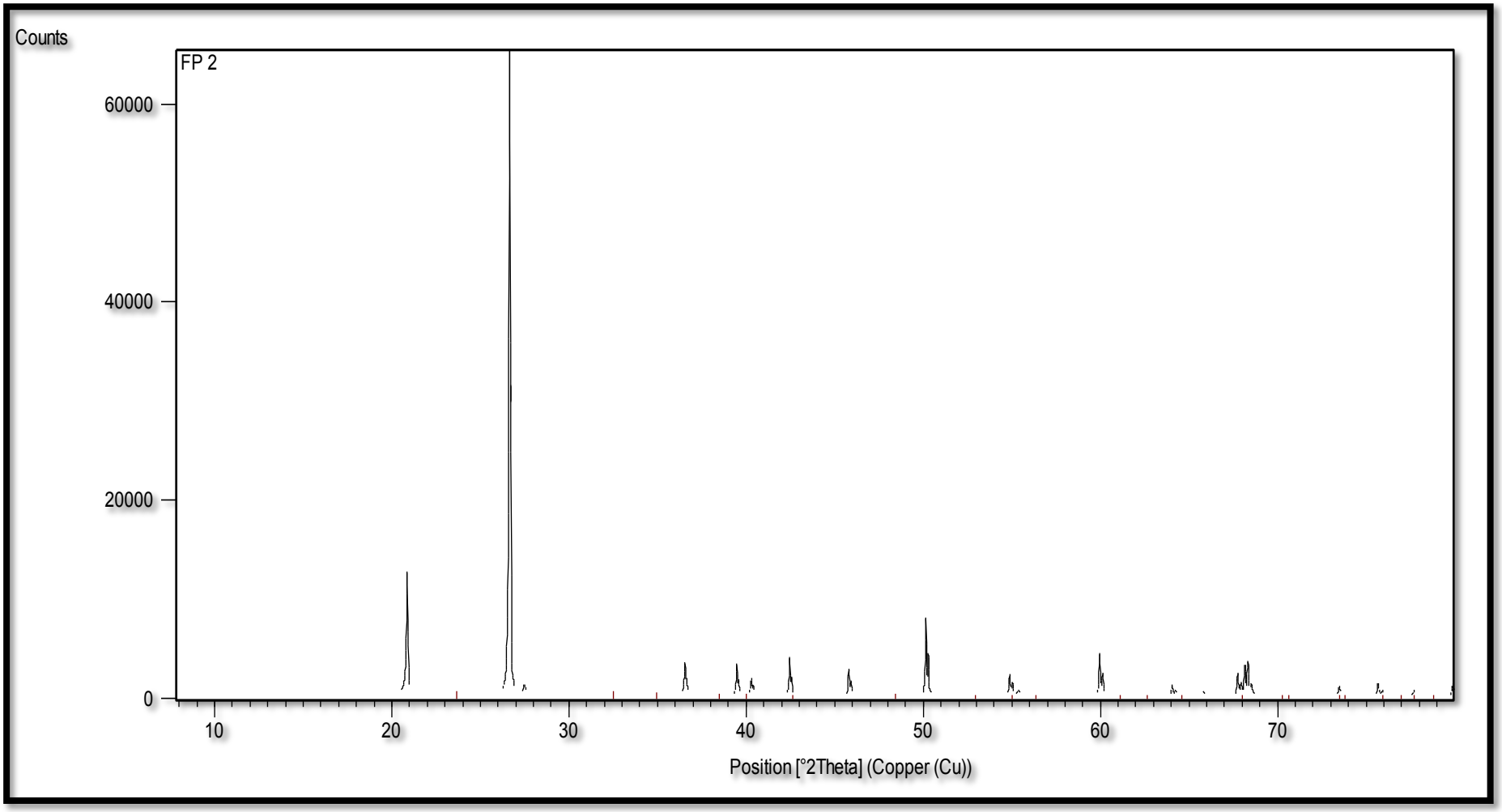

G2: XRD Analysis Diffractogram of FP-2. (Analyst: Belinda Venter, Geo XRD & XRF Laboratory, NWU).

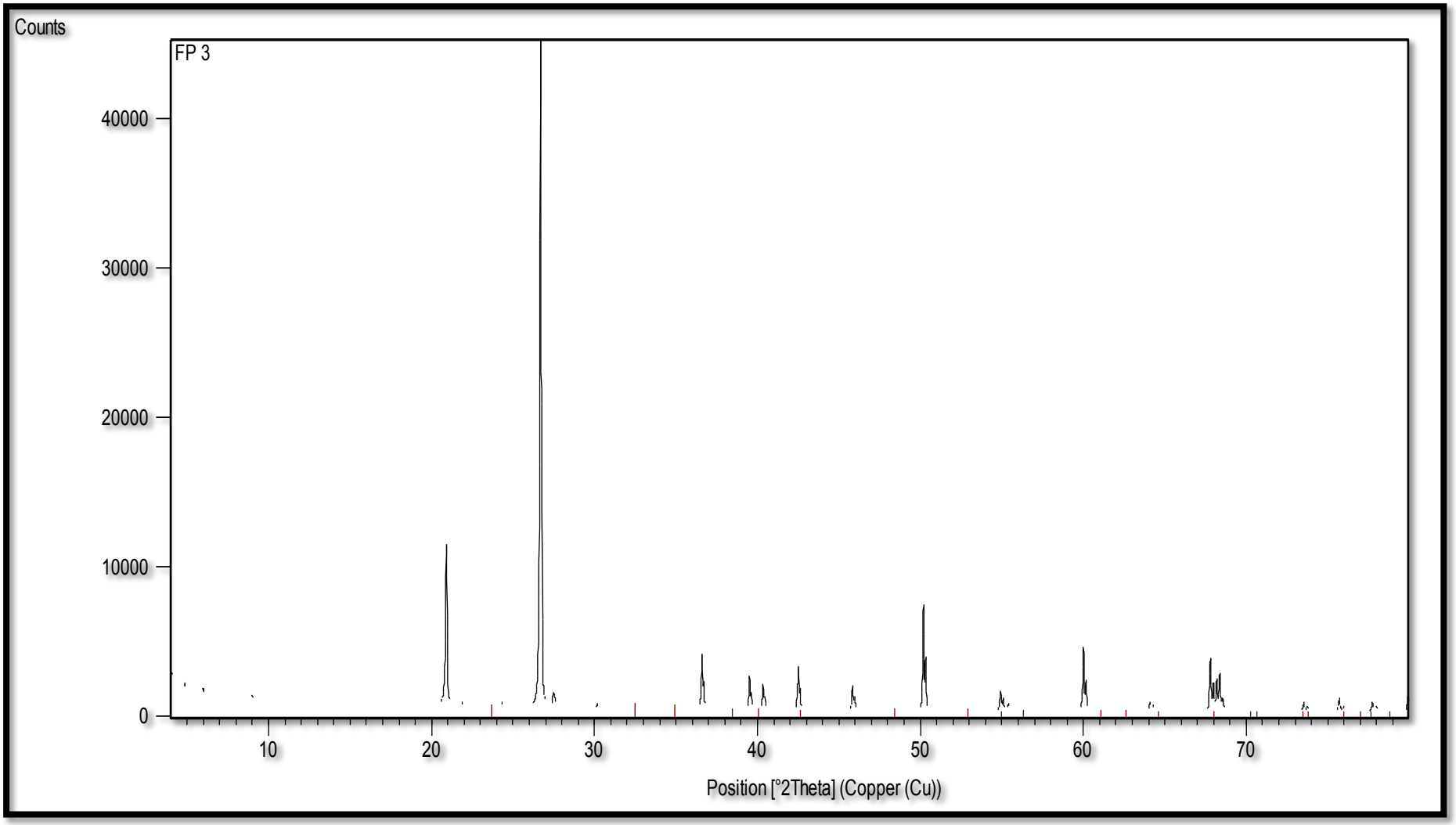

G3: XRD Analysis Diffractogram of FP-3. (Analyst: Belinda Venter, Geo XRD & XRF Laboratory, NWU).

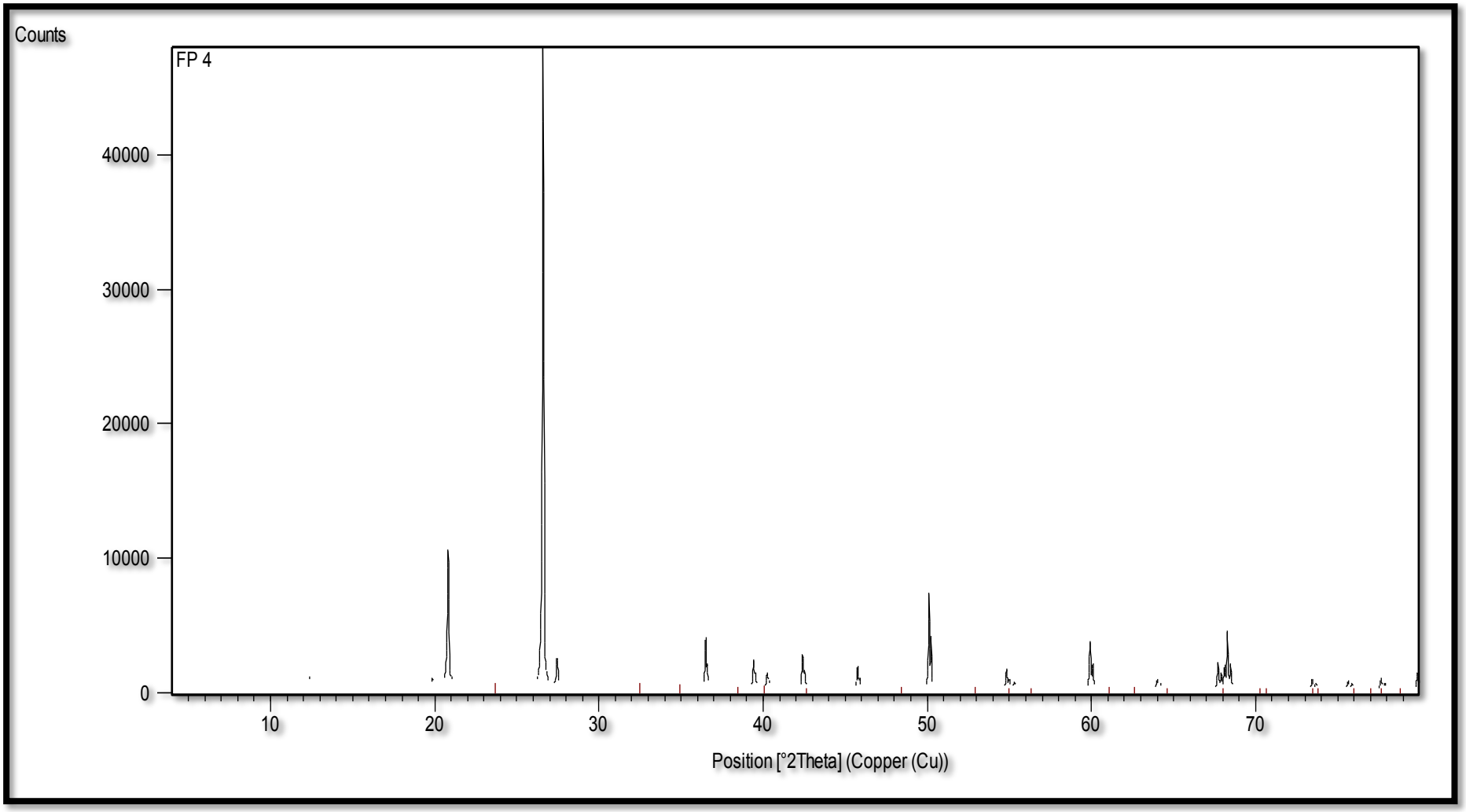

G4: XRD Analysis Diffractogram of FP-4. (Analyst: Belinda Venter, Geo XRD & XRF Laboratory, NWU).

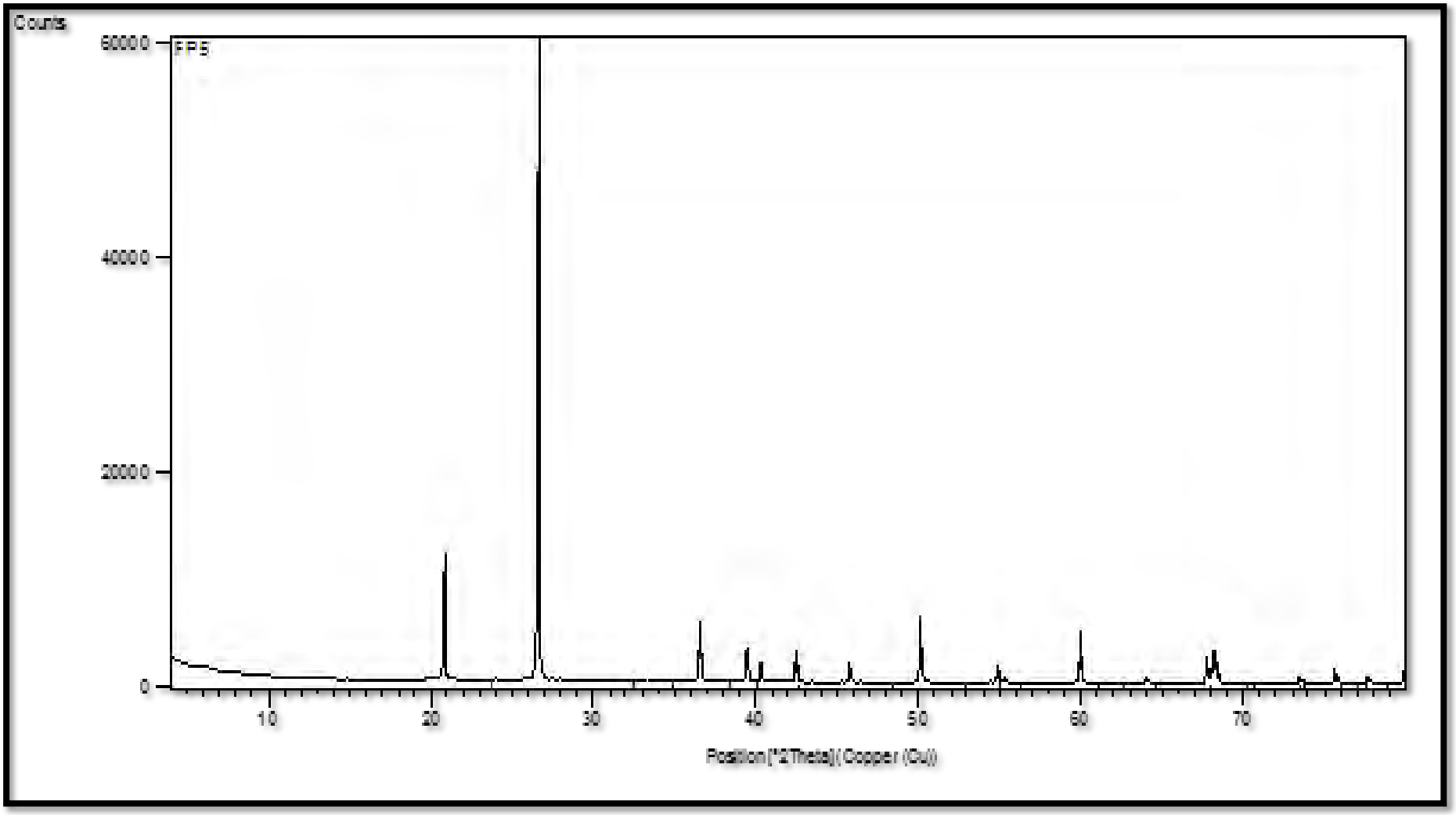

G5: XRD Analysis Diffractogram of FP-5. (Analyst: Belinda Venter, Geo XRD & XRF Laboratory, NWU).

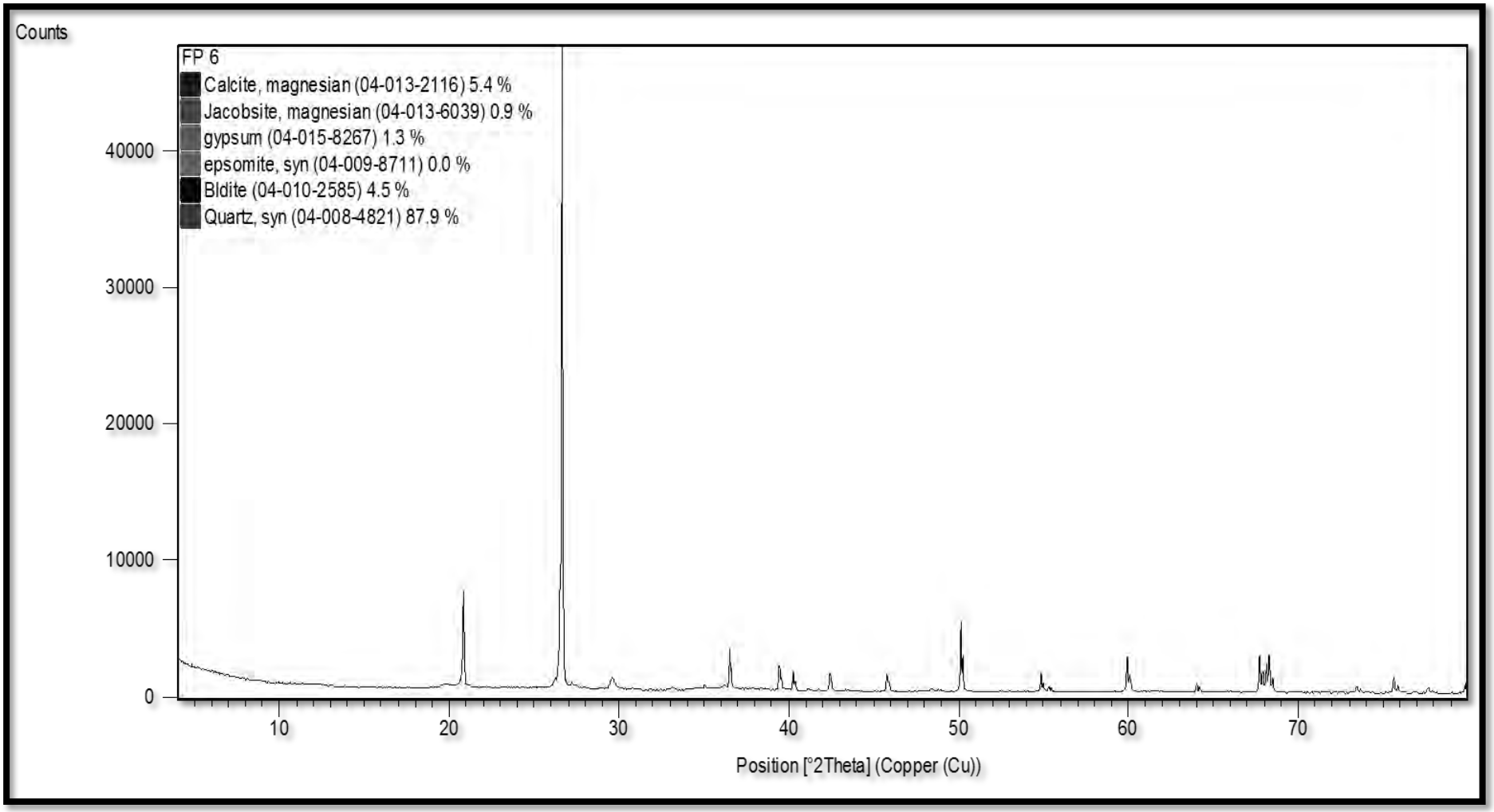

G6: XRD Analysis Diffractogram of FP-6. (Analyst: Belinda Venter, Geo XRD & XRF Laboratory, NWU).

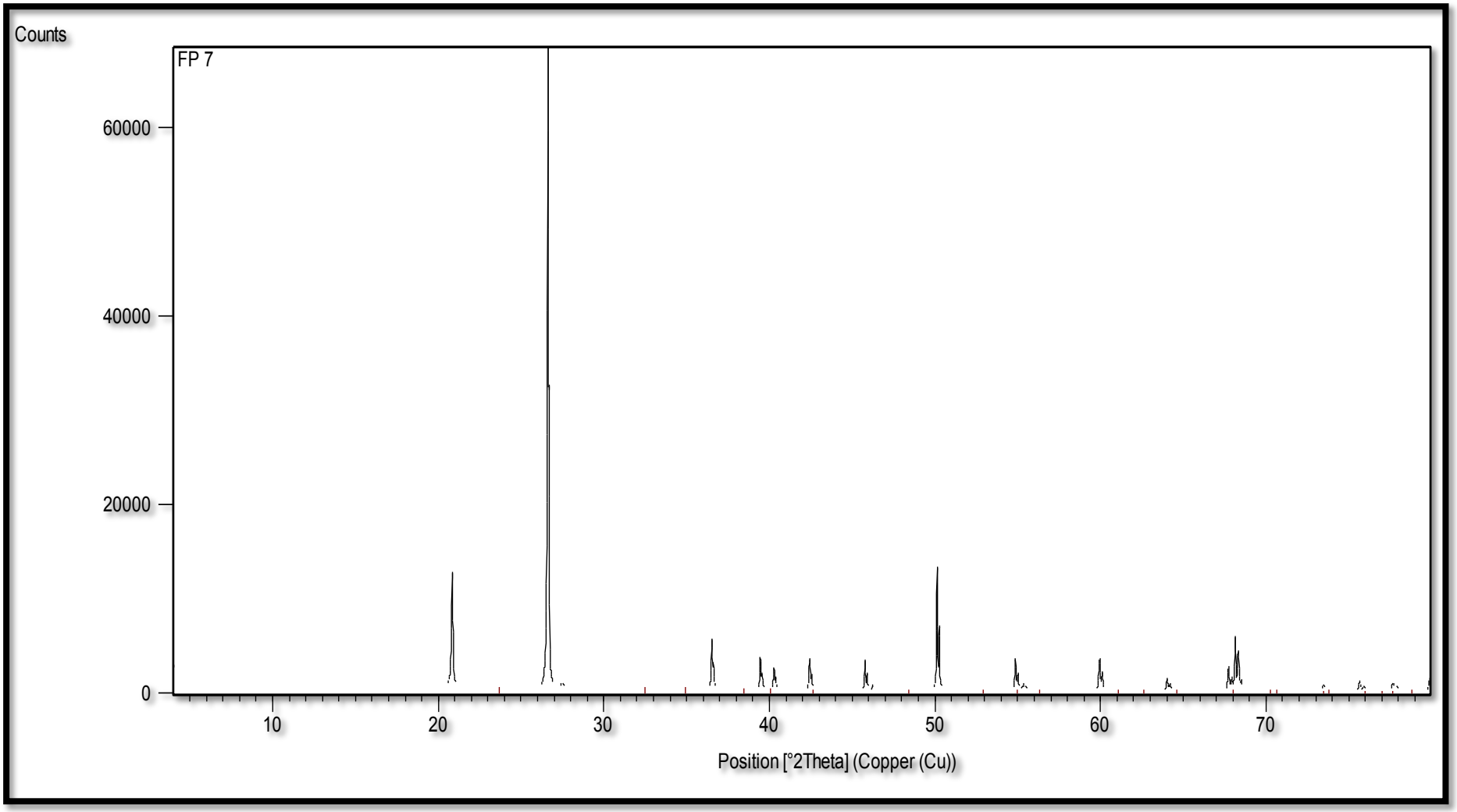

G7: XRD Analysis Diffractogram of FP-7. (Analyst: Belinda Venter, Geo XRD & XRF Laboratory, NWU).

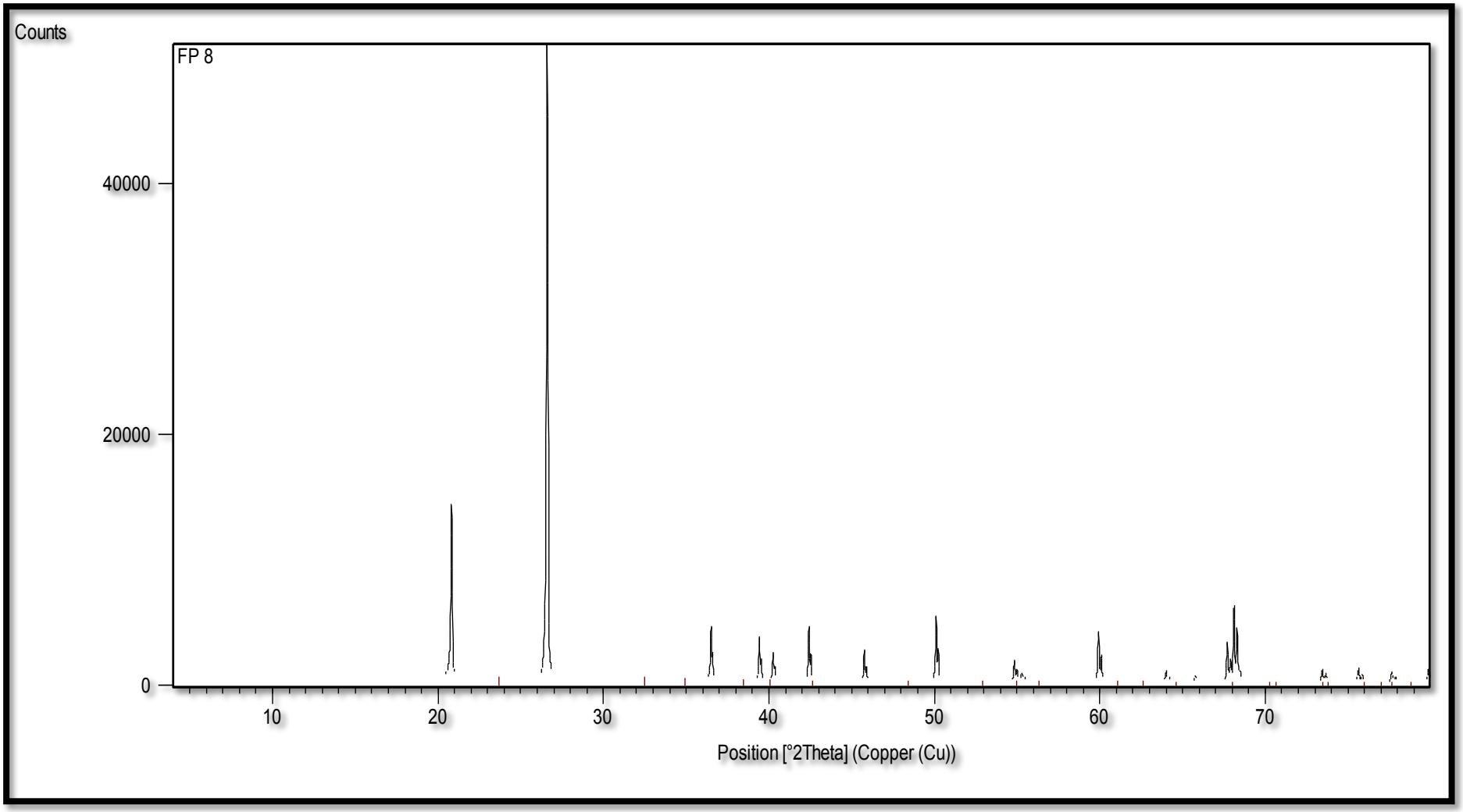

G8: XRD Analysis Diffractogram of FP-8. (Analyst: Belinda Venter, Geo XRD & XRF Laboratory, NWU).

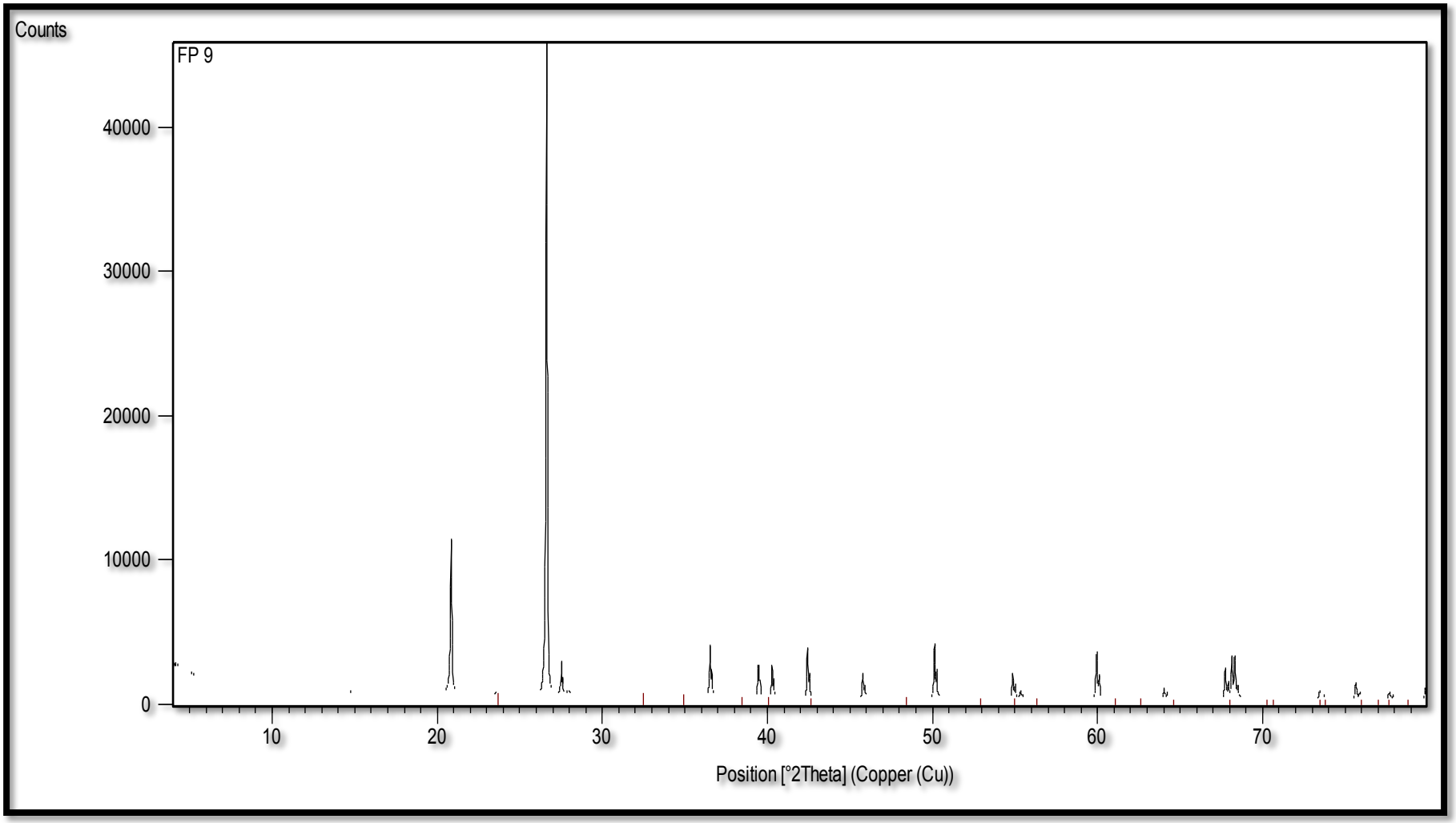

G9: XRD Analysis Diffractogram of FP-9. (Analyst: Belinda Venter, Geo XRD & XRF Laboratory, NWU).

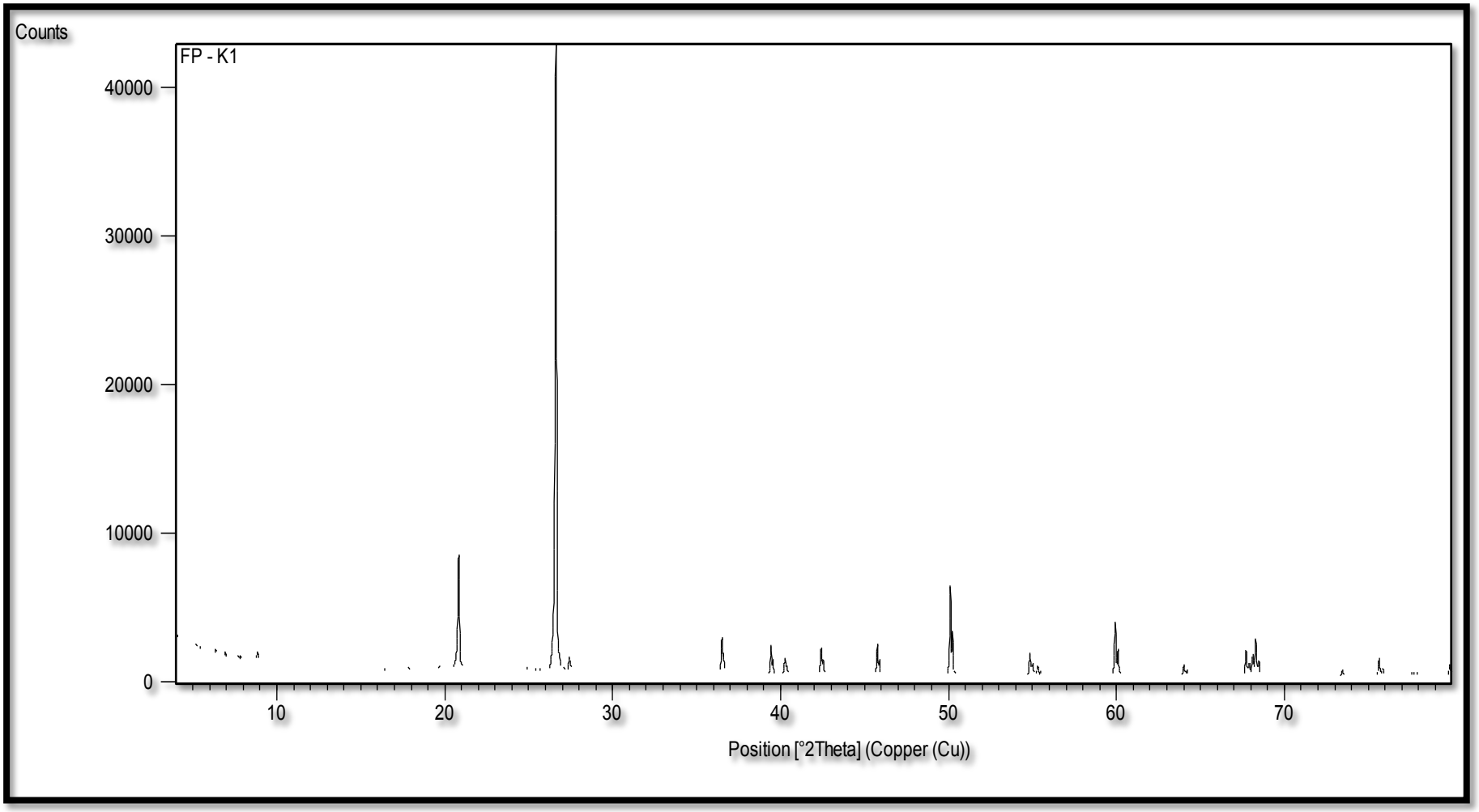

G10: XRD Analysis Diffractogram of FP-K1. (Analyst: Belinda Venter, Geo XRD & XRF Laboratory, NWU).

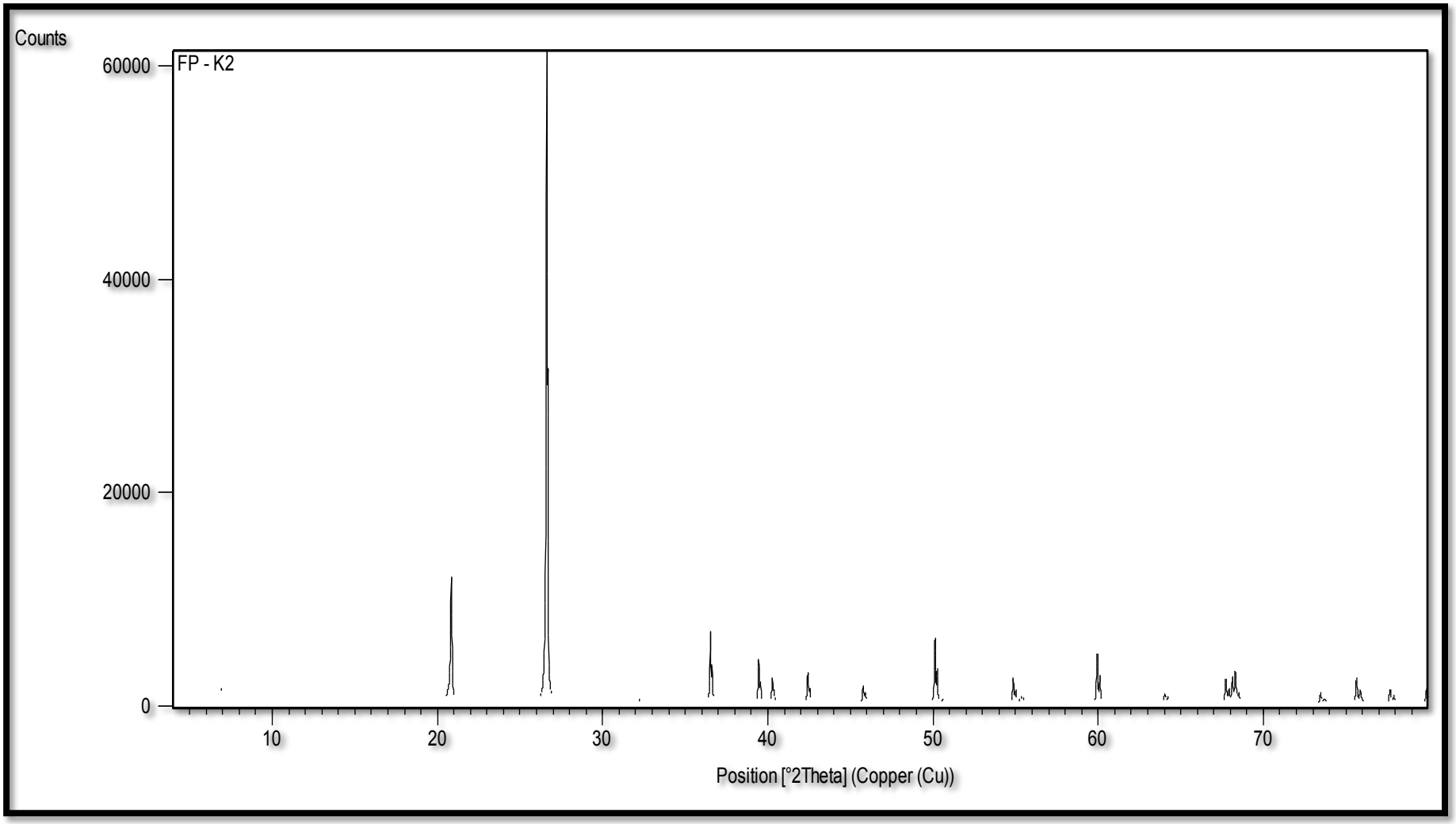

G11: XRD Analysis Diffractogram of FP-K2. (Analyst: Belinda Venter, Geo XRD & XRF Laboratory, NWU).

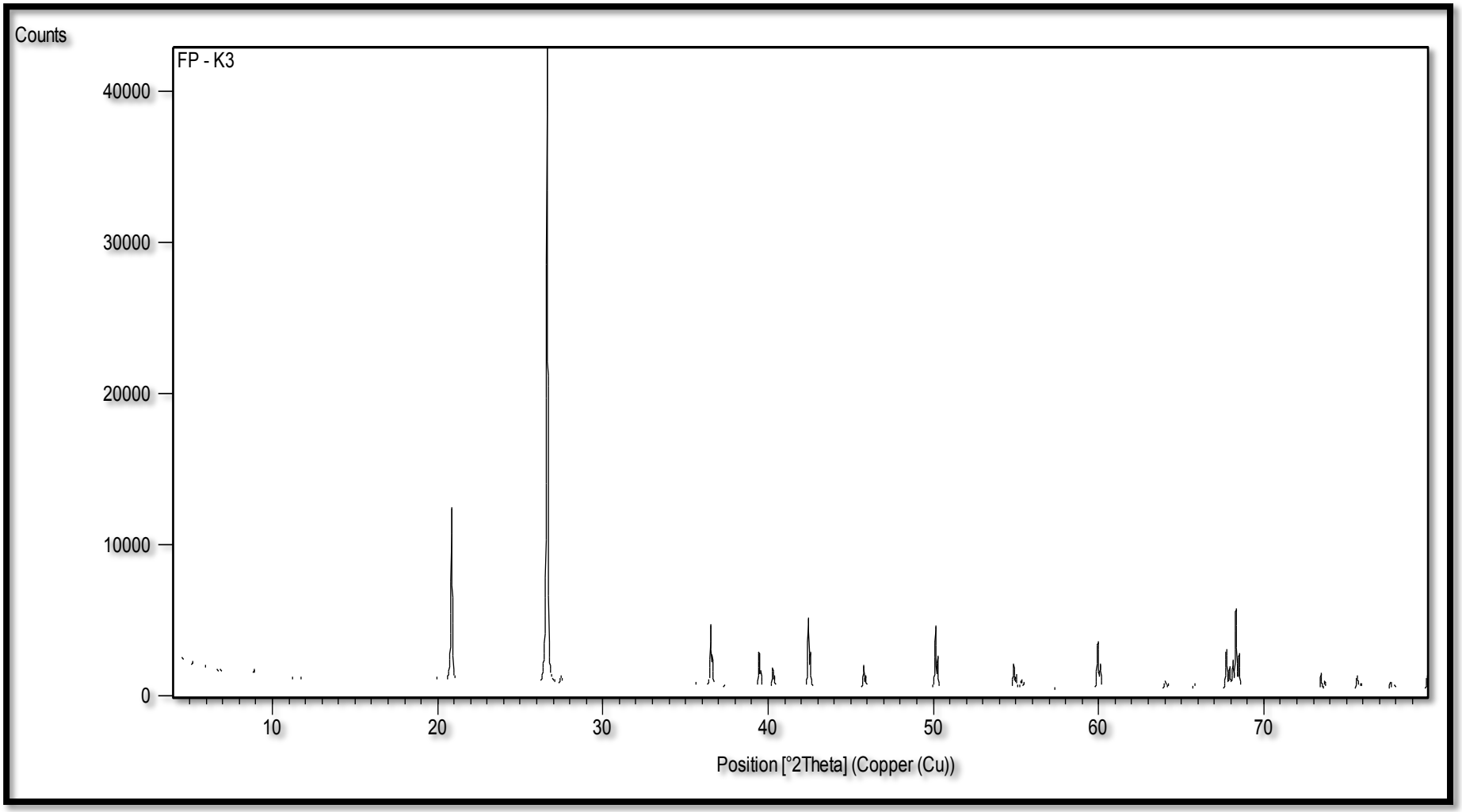

G12: XRD Analysis Diffractogram of FP-K3. (Analyst: Belinda Venter, Geo XRD & XRF Laboratory, NWU).

Appendix H: Representation of the water chemistry data of the sampled boreholes in the study area.

H1: HCO_3^-- $2(SO_4^{2-})$- Cl^- Ternary Diagrams.

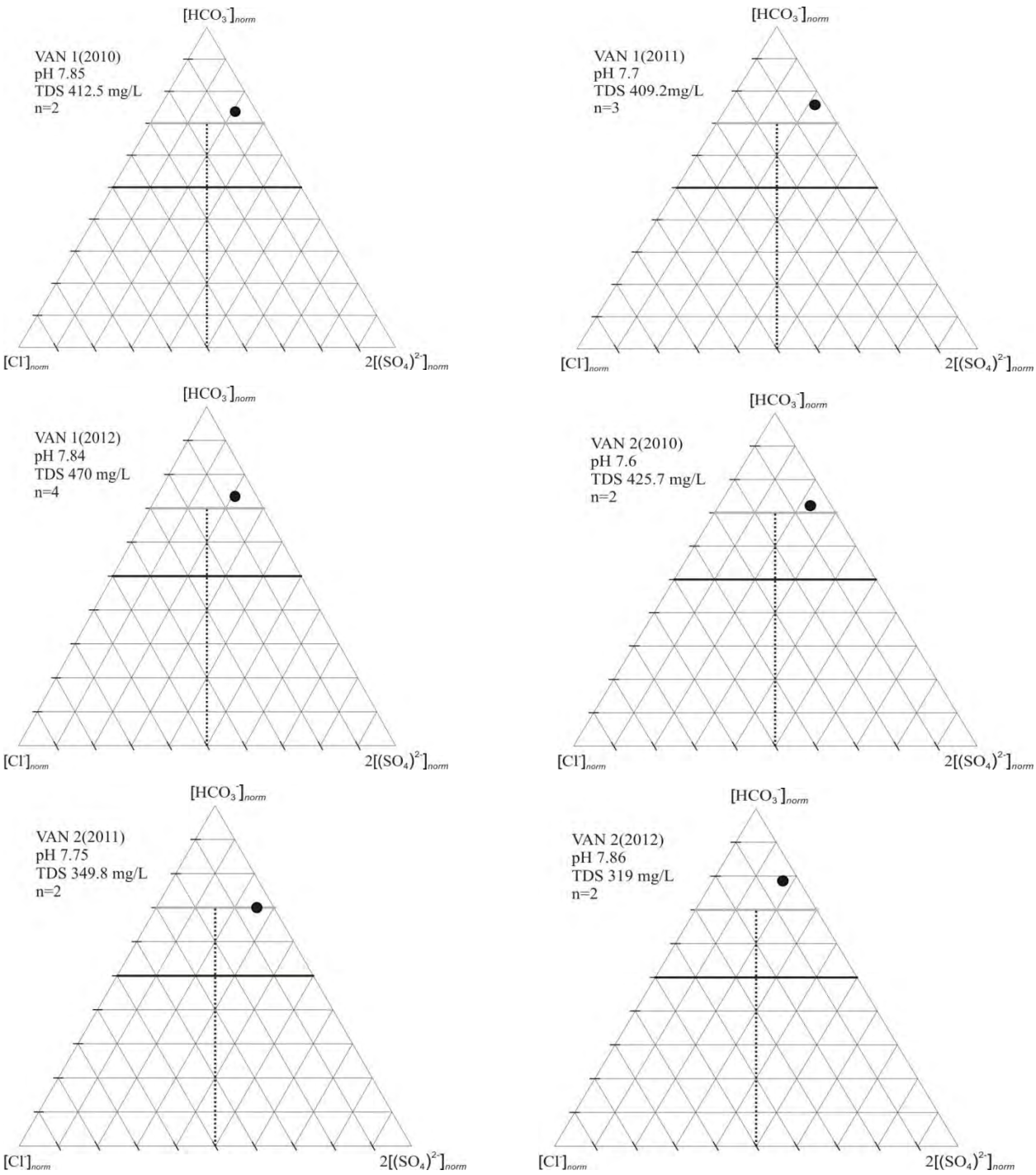

H1.1: HCO_3^-- $2(SO_4^{2-})$- Cl^- Ternary Diagrams showing annual variation of the different boreholes water chemistry.

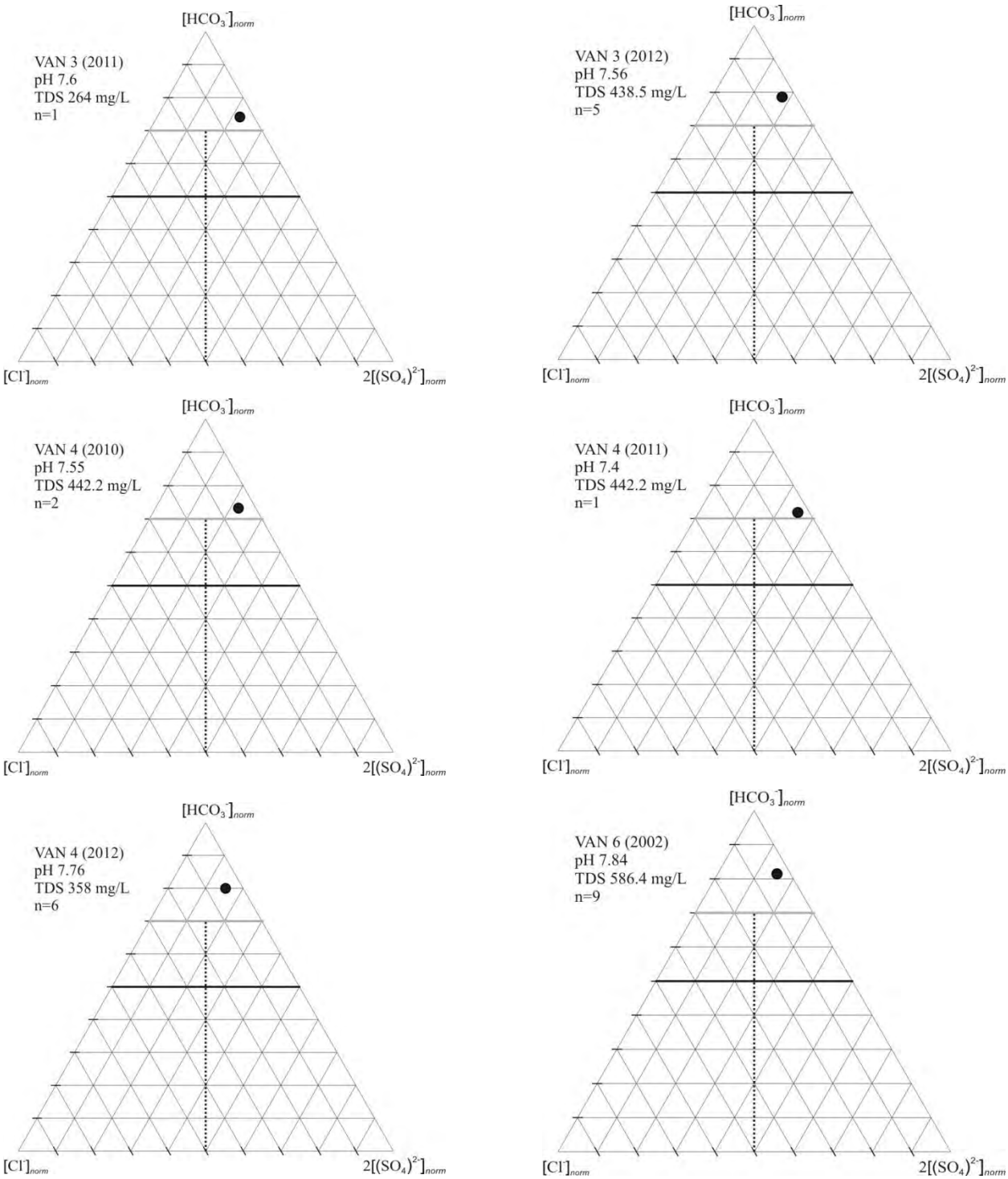

H1.1: HCO_3^-- $2(SO_4^{2-})$- Cl^- Ternary Diagrams showing annual variation of the different boreholes water chemistry.

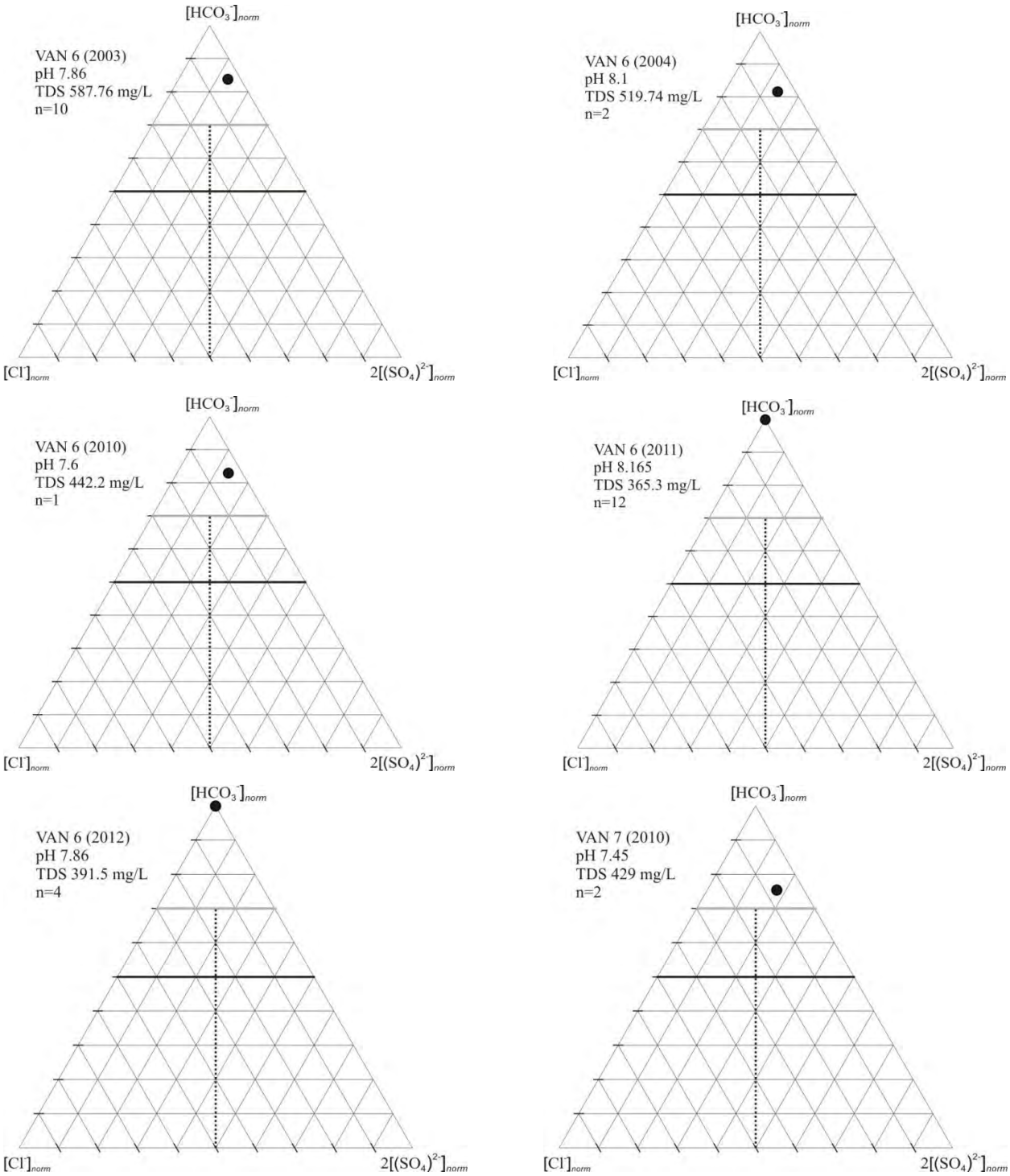

H1.1: HCO_3^-- $2(SO_4^{2-})$- Cl^- Ternary Diagrams showing annual variation of the different boreholes water chemistry.

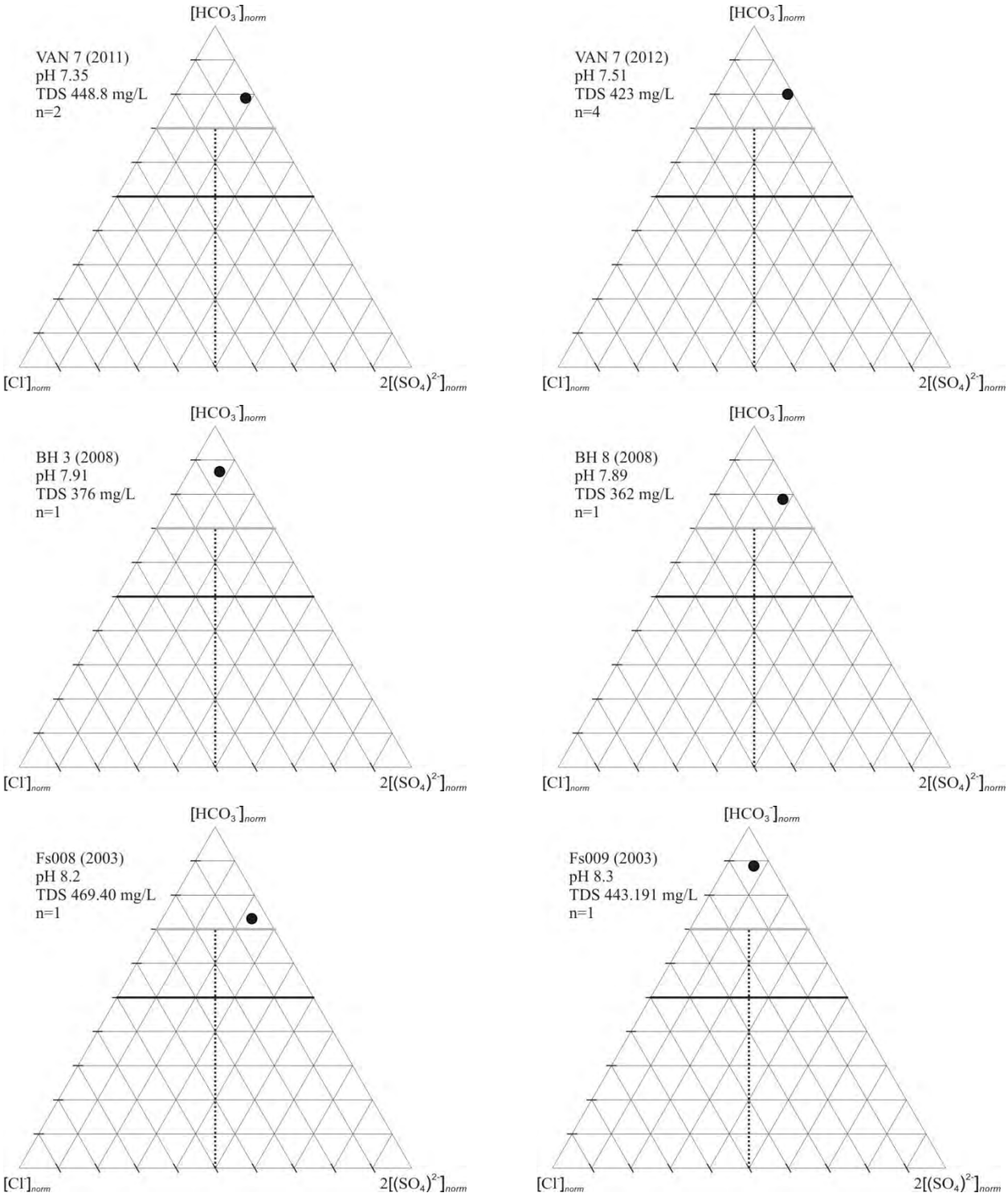

H1.1: HCO_3^-- $2(SO_4^{2-})$- Cl^- Ternary Diagrams showing annual variation of the different boreholes water chemistry.

H2: Piper Diagrams of the major cations and anions present in the borehole water samples collected in the study area.

The Piper diagrams show the relative composition of the major cations and anions for all the calculated water data of the boreholes.

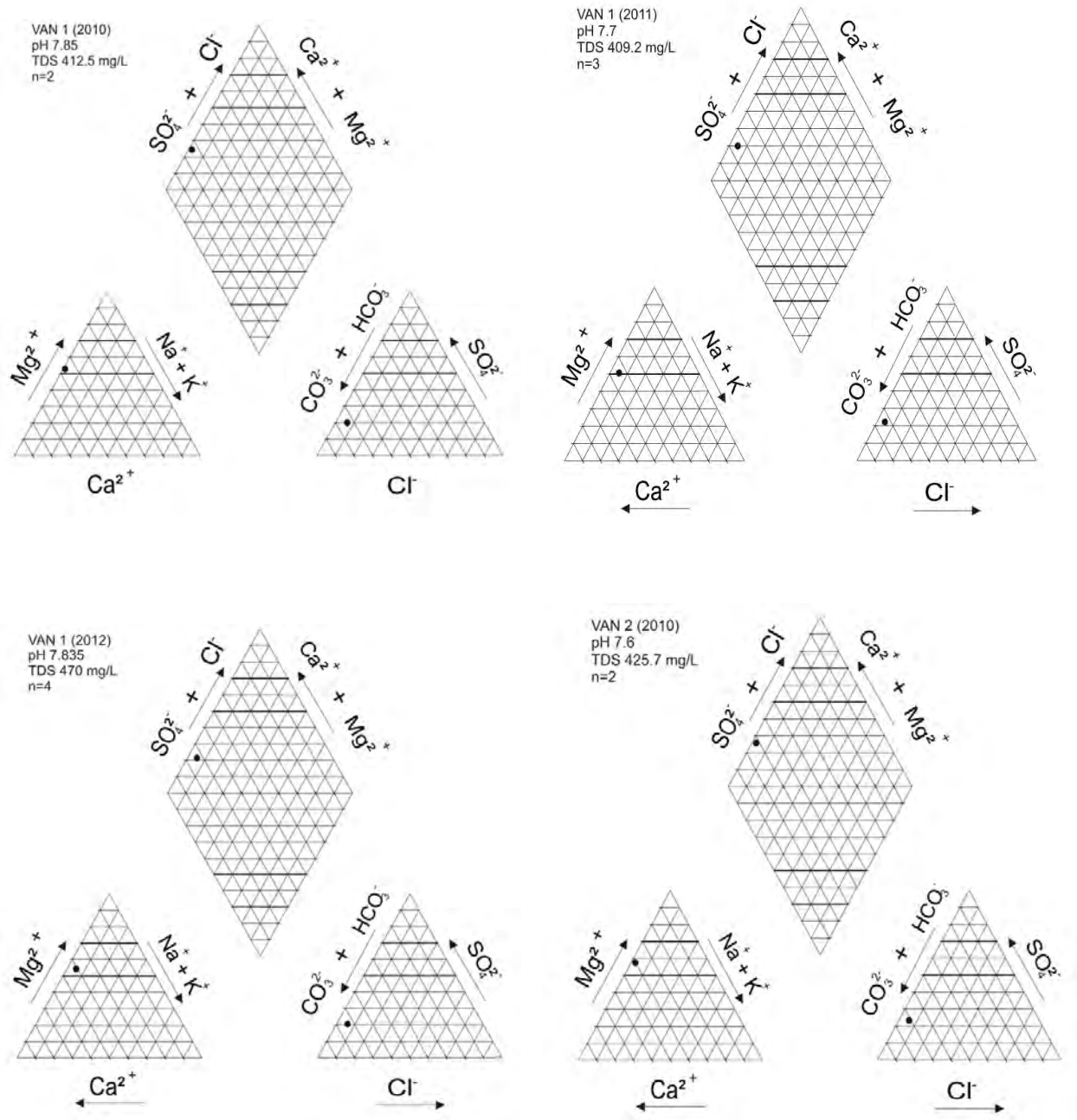

H2.1: Piper Diagrams created for each borehole in the study area.

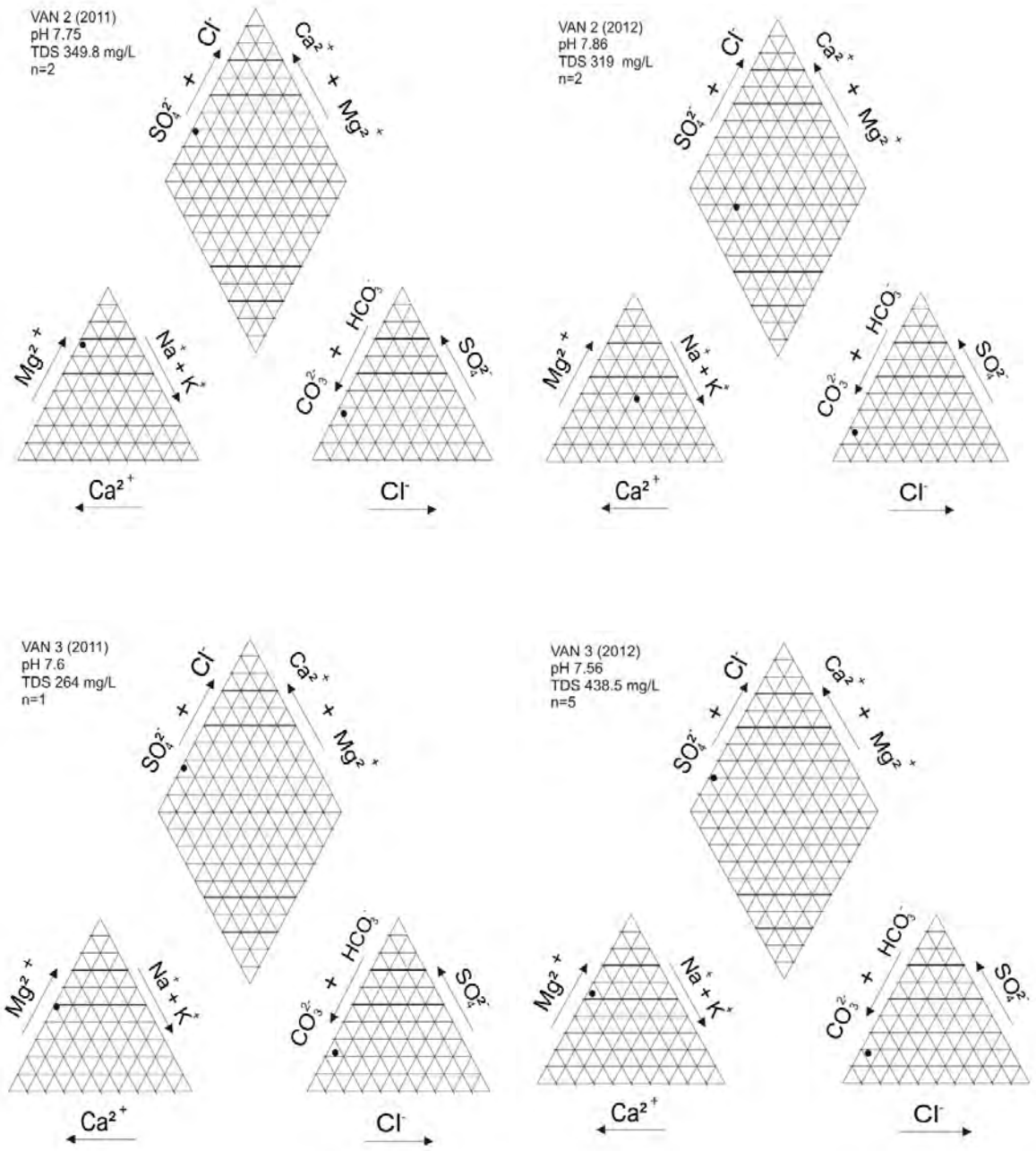

H2.1: Piper Diagrams created for each borehole in the study area.

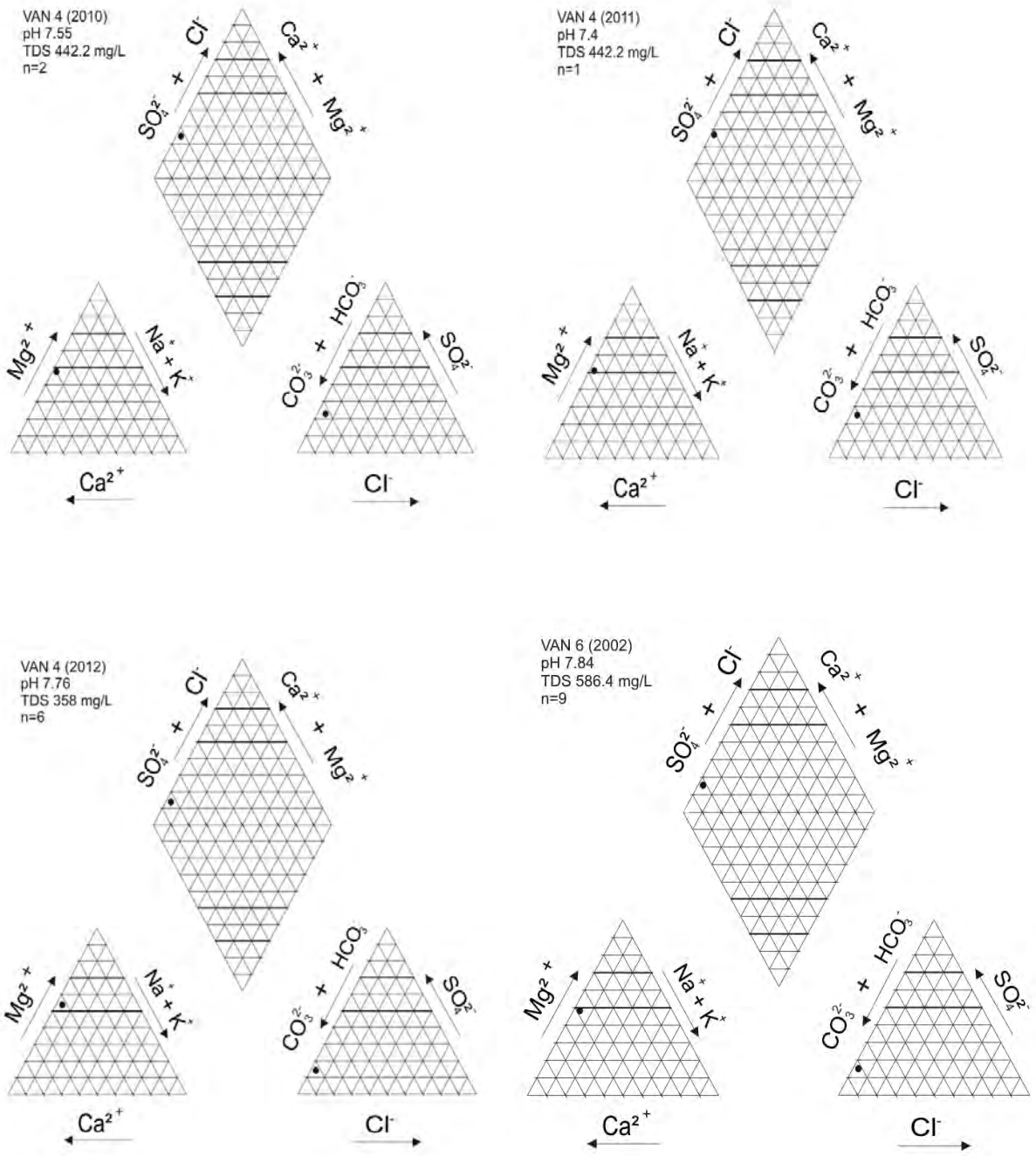

H2.1: Piper Diagrams created for each borehole in the study area.

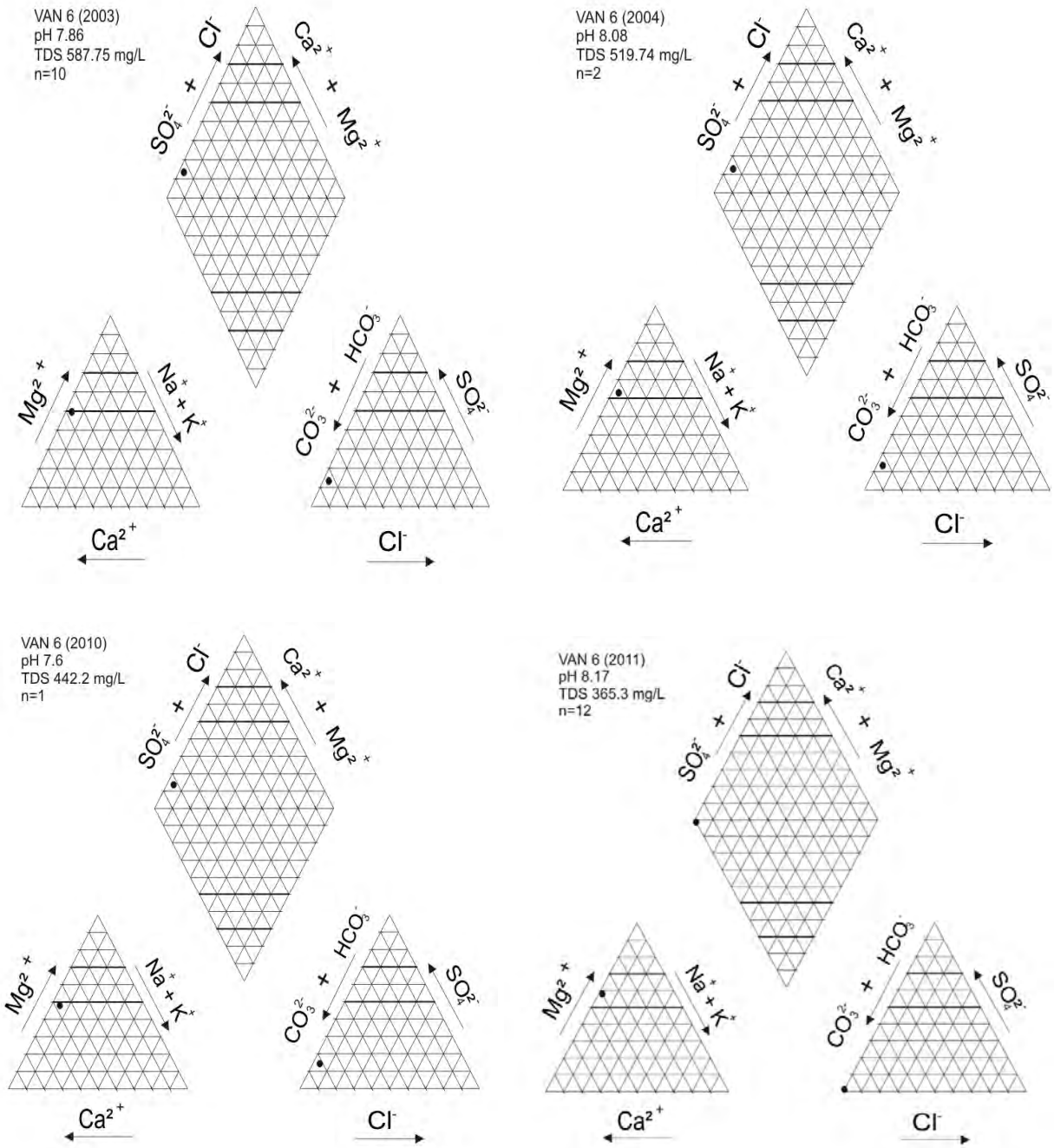

H2.1: Piper Diagrams created for each borehole in the study area.

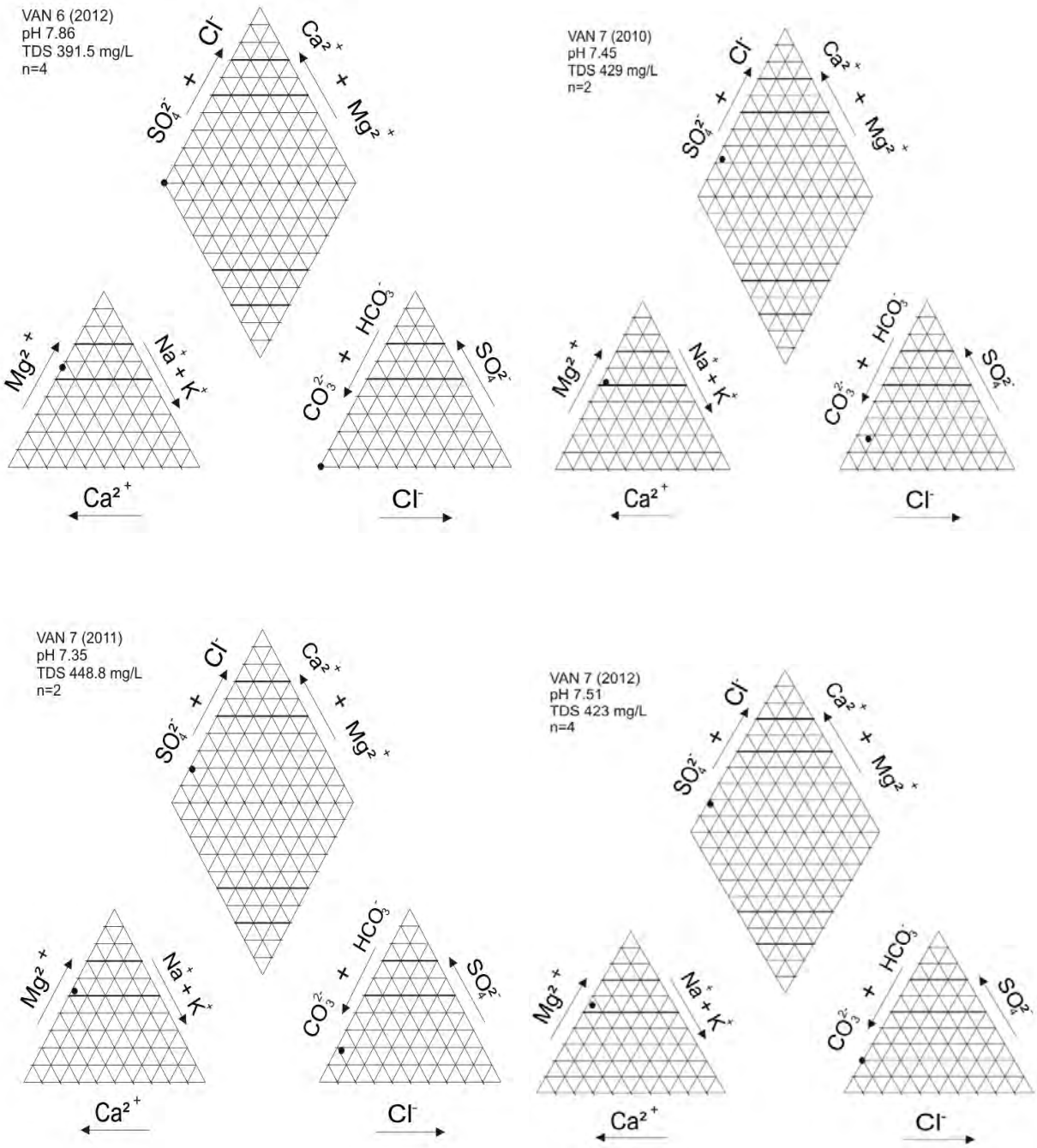

H2.1: Piper Diagrams created for each borehole in the study area.

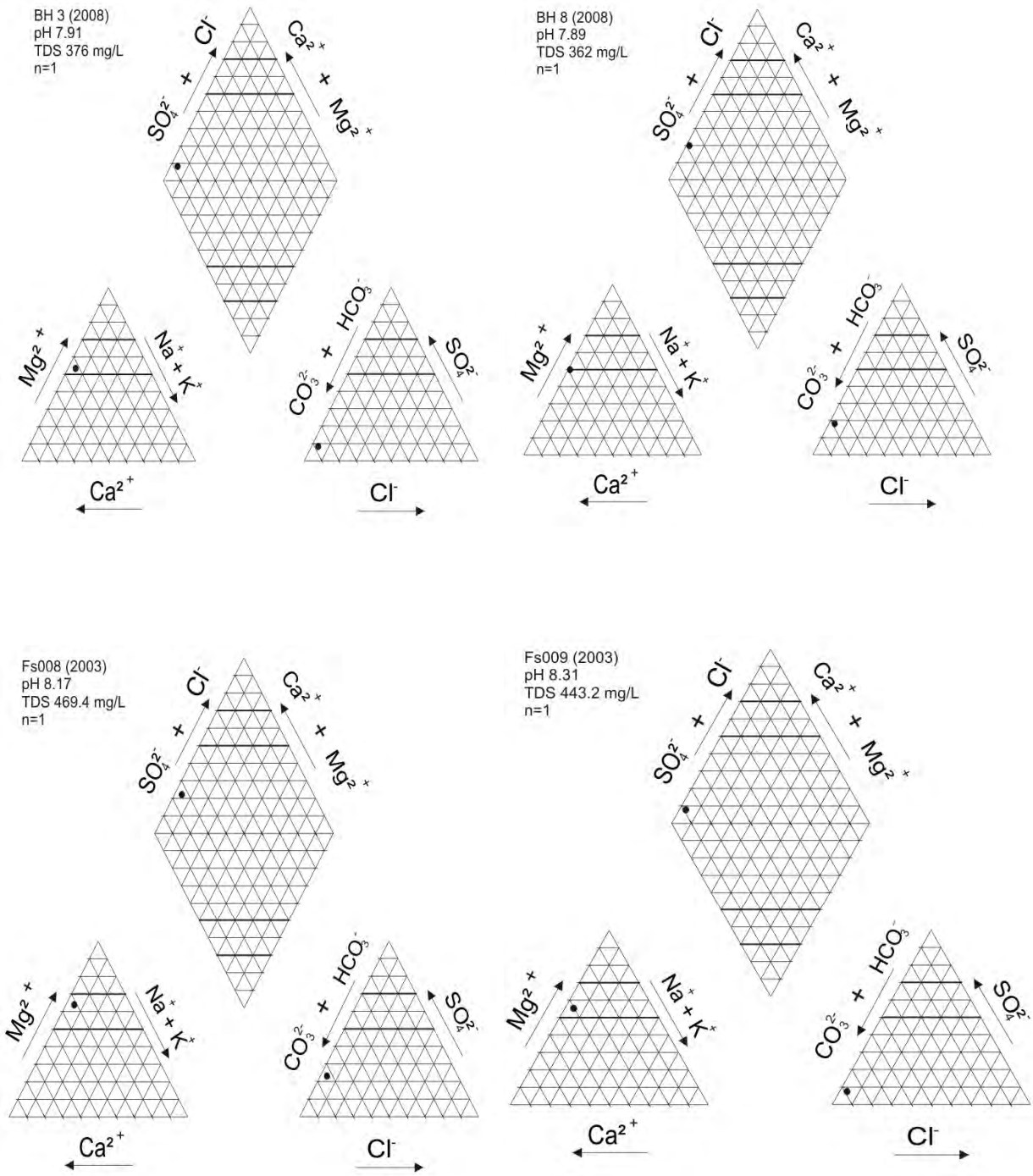

H2.1: Piper Diagrams created for each borehole in the study area.

H3: Stiff Diagrams of the major cations and anions present in the borehole water samples collected in the study area.

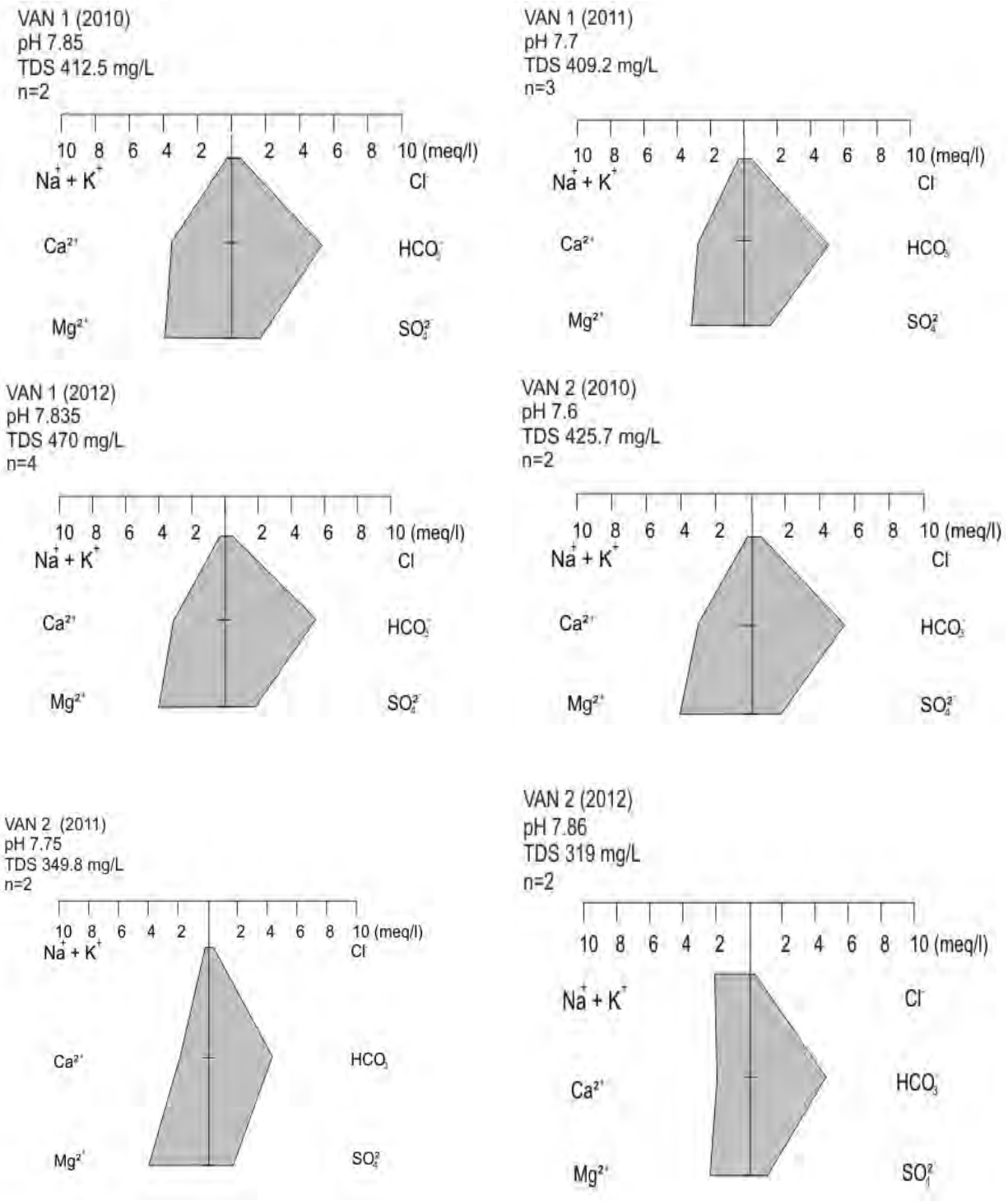

H3.1: Stiff Diagrams created for the water chemisrty of the boreholes sampled in the study area showing the overall ion composition.

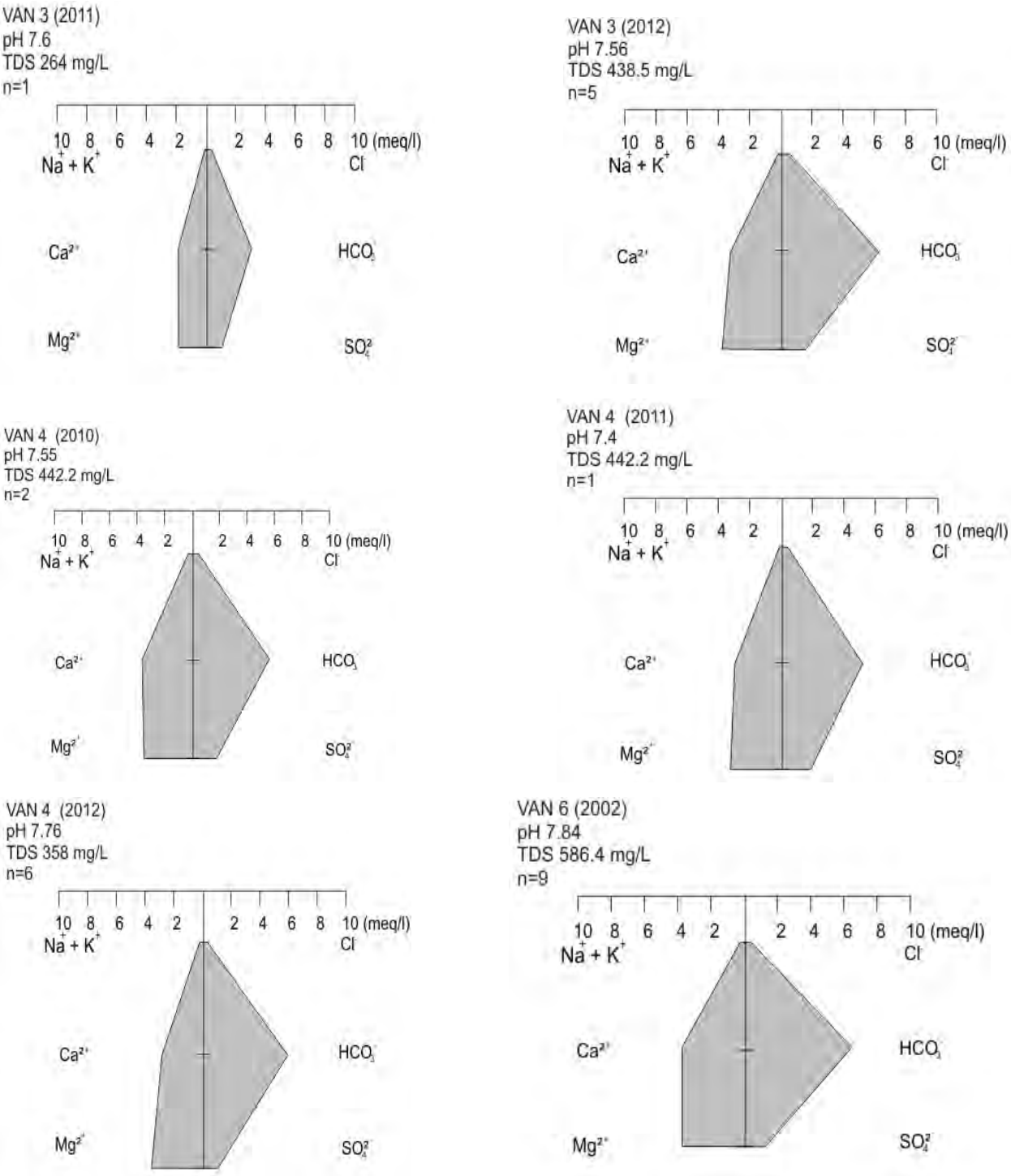

H3.1: Stiff Diagrams created for the water chemisrty of the boreholes sampled in the study area showing the overall ion composition.

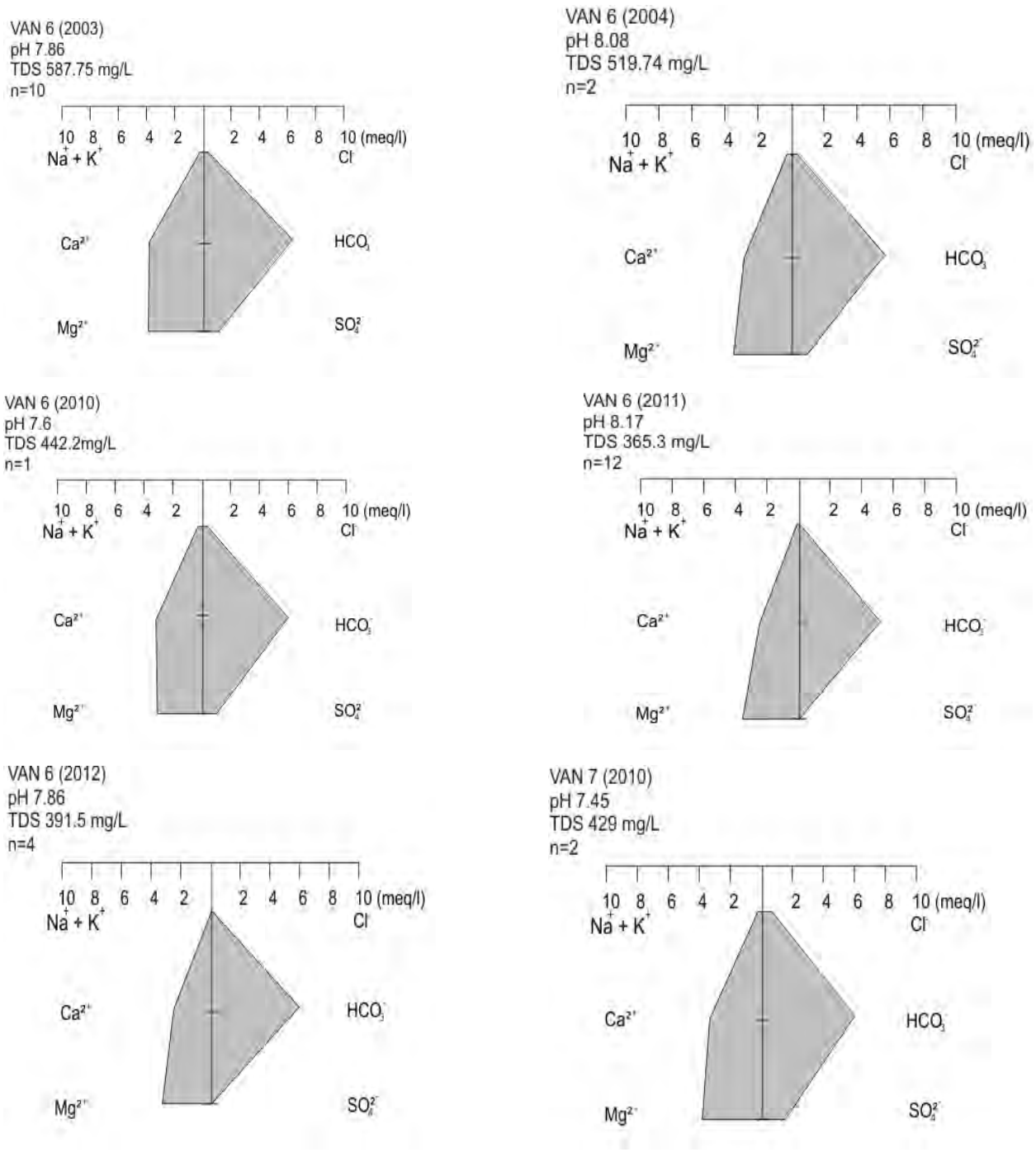

H3.1: Stiff Diagrams created for the water chemisrty of the boreholes sampled in the study area showing the overall ion composition.

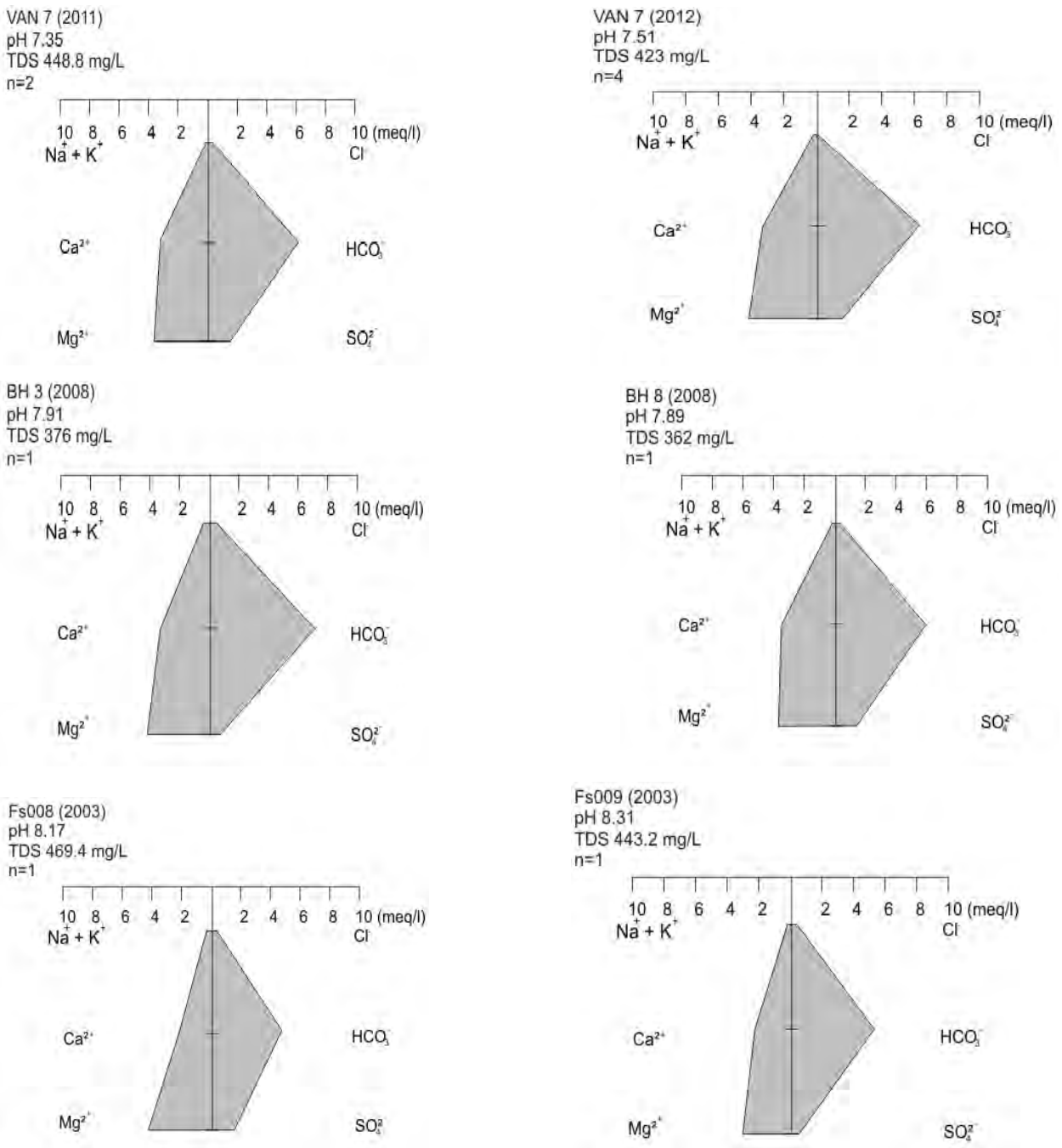

H3.1: Stiff Diagrams created for the water chemisrty of the boreholes sampled in the study area showing the overall ion composition.

Appendix I: Geo-Magnetic survey conducted in the study area.

I1: Magnetometer Survey East-West Line 1 (see Figure 80):

Start GPS: S: 26.79060 E: 26.8080

End GPS: S: 26.79204 E: 26.7790

From East to West

Distance from start (m)	Geo-magnetics (nT)	Distance from start (m)	Geo-magnetics (nT)	Distance from start (m)	Geo-magnetics (nT)	Distance from start (m)	Geo-magnetics (nT)	Distance from start (m)	Geo-magnetics (nT)
0	27976.30	**560**	27986.02	**1120**	27981.85	**1680**	27956.00	**2240**	27955.70
20	27976.79	**580**	27985.31	**1140**	27977.14	**1700**	27969.30	**2260**	27965.40
40	27978.87	**600**	27985.80	**1160**	27978.42	**1720**	27973.70	**2280**	27963.60
60	27978.36	**620**	27980.38	**1180**	27976.61	**1740**	27960.00	**2300**	27962.20
80	27982.05	**640**	27981.87	**1200**	27974.90	**1760**	27961.40	**2320**	27962.80
100	27984.43	**660**	27978.96	**1220**	27973.58	**1780**	27960.40	**2340**	27961.00
120	27981.52	**680**	27980.14	**1240**	27975.97	**1800**	27961.30	**2360**	27968.90
140	27982.71	**700**	27983.53	**1260**	27975.76	**1820**	27958.90	**2380**	27965.30
160	27979.39	**720**	27988.52	**1280**	27973.54	**1840**	27962.00	**2400**	27963.40
180	27979.38	**740**	27983.30	**1300**	27973.73	**1860**	27962.10	**2420**	27961.80
200	27981.97	**760**	27981.69	**1320**	27968.60	**1880**	27961.00	**2440**	27962.60
220	27982.05	**780**	27983.98	**1340**	27945.40	**1900**	27959.70	**2460**	27962.10
240	27980.94	**800**	27981.06	**1360**	27953.50	**1920**	27962.70	**2480**	27959.80
260	27982.83	**820**	27977.55	**1380**	27929.60	**1940**	27959.70	**2500**	27960.20
280	27979.91	**840**	27980.24	**1400**	27932.00	**1960**	27959.90	**2520**	27960.70
300	27979.10	**860**	27979.62	**1420**	27993.60	**1980**	27960.20	**2540**	27958.10
320	27984.99	**880**	27980.51	**1440**	27982.50	**2000**	27957.50	**2560**	27960.30
340	27985.17	**900**	27982.60	**1460**	27975.60	**2020**	27971.30	**2580**	27954.30
360	27983.66	**920**	27980.28	**1480**	27970.70	**2040**	27961.40	**2600**	27958.60
380	27983.35	**940**	27980.17	**1500**	27975.60	**2060**	27959.50	**2620**	27964.80
400	27984.13	**960**	27977.46	**1520**	27970.90	**2080**	27956.40	**2640**	27956.20
420	28000.32	**980**	27978.24	**1540**	27971.60	**2100**	27957.40	**2660**	27956.20
440	27987.11	**1000**	27980.63	**1560**	27972.30	**2120**	27954.10	**2680**	27960.20
460	27984.99	**1020**	27979.62	**1580**	27972.50	**2140**	27956.90	**2700**	27966.50
480	27981.78	**1040**	27979.10	**1600**	27972.40	**2160**	27957.40	**2720**	27960.90
500	27983.07	**1060**	27976.29	**1620**	27969.00	**2180**	27958.50	**2740**	27964.20
520	27981.75	**1080**	27976.08	**1640**	27964.30	**2200**	27963.10	**2760**	27966.70
540	27985.44	**1100**	27977.06	**1660**	27964.50	**2220**	27959.60	**2780**	27969.20

I1: Magnetometer Survey East-West Line 1 (see Figure 80):

Distance from start (m)	Geo-magnetics (nT)
2800	27964.40
2820	27973.70
2840	27978.50
2860	27974.70
2880	27978.80
2900	27969.37

I2: Magnetometer Survey East-West Line 2 (see Figure 80):

Start GPS: S: 26.80673 E: 26.79280

End GPS: S: 26.80767 E: 26.78300

From East to West

Distance from start (m)	Geo-magnetics (nT)	Distance from start (m)	Geo-magnetics (nT)
0	27953.2	**400**	27956.5
20	27957.1	**420**	27963.1
40	27953.0	**440**	27960.3
60	27955.8	**460**	27959.8
80	27951.0	**480**	27964.9
100	27954.0	**500**	27973.0
120	27957.1	**520**	27963.2
140	27961.9	**540**	27959.0
160	27958.5	**560**	27965.7
180	27953.9	**580**	27961.5
200	27957.3	**600**	27962.1
220	27956.9	**620**	27964.9
240	27959.2	**640**	27967.3
260	27960.2	**660**	27968.7
280	27959.8	**680**	27964.2
300	27959.1	**660**	27968.7
320	27957.9	**680**	27964.2
340	27956.7	**700**	27962.9
360	27960.4	**720**	27962.1
380	27962.1	**740**	27966.0

I2: Magnetometer Survey East-West Line 2 (see Figure 80):

Distance from start (m)	Geo-magnetics (nT)	Distance from start (m)	Geo-magnetics (nT)
760	27965.4	**860**	27964.5
780	27966.6	**880**	27962.4
800	27961.6	**900**	27964.8
820	27964.3	**920**	27964.6
840	27965.6	**940**	27967.5

I3: Magnetometer Survey East-West Line 3 (see Figure 80):

Start GPS: S: 26.80401 E: 26.77840

End GPS: S: 26.80052 E: 26.79860

From East to West

Distance from start (m)	Geo-magnetics (nT)	Distance from start (m)	Geo-magnetics (nT)	Distance from start (m)	Geo-magnetics (nT)
0	27945.7	**480**	27947.4	**960**	27942.2
20	27947.4	**500**	27947.3	**980**	27942.5
40	27946.6	**520**	27948.9	**1000**	27944.5
60	27946.6	**540**	27948.7	**1020**	27949.2
80	27951.2	**560**	27948.9	**1040**	27941.1
100	27949.3	**580**	27949.8	**1060**	27946.2
120	27944.2	**600**	27948.4	**1080**	27942.6
140	27945.7	**620**	27925.3	**1100**	27946.9
160	27945.8	**640**	27951.1	**1120**	27945.4
180	27950.5	**660**	27949.5	**1140**	27945.2
200	27949.8	**680**	27948.0	**1160**	27945.5
220	27949.4	**700**	27949.6	**1180**	27947.0
240	27944.6	**720**	27951.0	**1200**	27945.5
260	27950.7	**740**	27947.9	**1220**	27944.9
280	27950.5	**760**	27949.7	**1240**	27945.9
300	27950.8	**780**	27951.2	**1260**	27945.5
320	27949.7	**800**	27943.0	**1280**	27943.3
340	27949.9	**820**	27948.9	**1300**	27942.1
360	27948.9	**840**	27951.0	**1320**	27944.6
380	27946.4	**860**	27950.9	**1340**	27947.0
400	27947.2	**880**	27949.2	**1360**	27948.1
420	27949.7	**900**	27946.9	**1380**	27949.7
440	27947.2	**920**	27948.0	**1400**	27945.8
460	27952.5	**940**	28141.3	**1420**	27948.8

I3: Magnetometer Survey East-West Line 3 (see Figure 80):

Distance from start (m)	Geo-magnetics (nT)	Distance from start (m)	Geo-magnetics (nT)	Distance from start (m)	Geo-magnetics (nT)
1440	27948.7	**1660**	27955.5	**1880**	27943.0
1460	27948.5	**1680**	27950.8	**1900**	27943.1
1480	27949.3	**1700**	27953.1	**1920**	27943.7
1500	27947.7	**1720**	27955.6	**1940**	27940.4
1520	27944.8	**1740**	27971.5	**1960**	27945.2
1540	27945.1	**1760**	28123.8	**1980**	27942.6
1560	27947.7	**1780**	27985.3	**2000**	27949.3
1580	27943.9	**1800**	27930.3	**2020**	27909.2
1600	27948.9	**1820**	27933.2		
1620	27950.6	**1840**	27940.6		
1640	27954.3	**1860**	27941.0		

I4: Magnetometer Survey East-West Line 4 (see Figure 80):

Start GPS: S: 26.80699 E: 26.79280

End GPS: S: 26.80784 E: 26.78300

From East to West

Distance from start (m)	Geo-magnetics (nT)	Distance from start (m)	Geo-magnetics (nT)
0	27939.7	**340**	27933.2
20	27942.6	**360**	27934.2
40	27936.2	**380**	27932.4
60	27941.1	**400**	27932.6
80	27939.8	**420**	27933.2
100	27950.5	**440**	27970.4
120	27941.2	**460**	27937.1
140	27936.0	**480**	27958.2
160	27939.7	**500**	27947.9
180	27942.0	**520**	27946.5
200	27939.5	**540**	27933.6
220	27940.8	**560**	27935.5
240	27938.9	**660**	27937.1
260	27938.4	**680**	27932.7
280	27941.5	**700**	27934.9
300	27935.8	**720**	27935.0
320	27930.5	**740**	27932.5

I4: Magnetometer Survey East-West Line 4 (see Figure 80):

Distance from start (m)	Geo-magnetics (nT)	Distance from start (m)	Geo-magnetics (nT)
760	27928.9	**880**	27936.7
780	27910.1	**900**	27933.3
800	27967.5	**920**	27930.0
820	27932.6	**940**	27935.5
840	27934.3	**960**	27933.8
860	27932.8		

Magnetic survey on the No. 2 tailings disposal facility footprint.

I5: Magnetometer Survey North-South Line 1 (see Figure 80):

Start GPS: S: 26.82908 E: 26.79970

End GPS: S: 26.82202 E: 26.79915

From South to North

Distance from start (m)	Geo-magnetics (nT)
0	27929.7
20	27921.2
40	27931.4
60	27936.7
80	27942.5
100	27940.5
120	27957.3
140	27962.8
160	27956.1
180	27949.5
200	27957.8

I6: Magnetometer Survey North-South Line 2 (see Figure 80):

Start GPS: S: 26.83900 E: 26.78664

End GPS: S: 26.82992 E: 26.78596

From South to North

Distance from start (m)	Geo-magnetics (nT)
0	27964.6
20	27968.5
40	27978.5
60	27985.8
80	27999.3
120	28037.5
140	27997.9

I6: Magnetometer Survey North-South Line 2 (see Figure 80):

Distance from start (m)	Geo-magnetics (nT)
160	28004.7
180	27993.6
200	27991.6

Appendix J: Down-hole Camera Survey videos.

See attached CD.

J1: Summary of the Down-hole Camera Survey Boreholes.

	BH 2	**BH 3**	**BH 7**	**BH 8**	**VAN 1**	**VAN 2**	**VAN3**	**VAN 4**	**MWSBH 8**	**MWSBH 9**
Drilled by:	GCS	GCS	GCS	GCS	Sarel van Rensburg	Sarel van Rensburg	Sarel van Rensburg	Sarel van Rensburg	MWS	MWS
Depth	18 m	50 m	20 m	30 m	8 m	18 m	30 m	20 m	27 m	17 m
Uses	Monitoring	Monitoring	Monitoring	Monitoring	Household	Cattle	Cattle	Cattle	Monitoring	BH collapsed and could not be accessed

Appendix K: Vegetation and Landscape Function Analysis.

K1: Macro– and micronutrients and total trace metals of the vegetation samples collected at the 12 fixed points in the study area (Analyst: Yvonne Visagie, Eco-Analytica, NWU).

K1.1: Macro– and micronutrients and total trace metals of the vegetation samples in 2012.

Sample no.	Species	FP-1	FP-2	FP-3	FP-4	FP-5	FP-6	FP-7	FP-8	FP-9	FP-K1	FP-K2	FP-K3
Major elements *mg/kg*													
Ti	Cd	3.2	-	3.3	3.8	2.5	3.1	-	-	-	2.8	3.0	3.4
	EC	2.3	2.3	1.7	1.8	1.9	-	1.7	-	-	-	2.0	-
	SST	2.1	2.3	2.3	-	2.2	2.4	-	2.1	-	-	-	1.6
Al	Cd	93.9	-	73.0	115.4	43.2	52.0	-	-	-	82.0	91.3	129.0
	EC	36.2	33.8	33.5	37.5	27.9	-	30.6	-	-	-	36.3	-
	SST	36.8	25.2	30.1	-	18.4	25.7	-	65.3	-	-	-	34.1
Fe	Cd	164.7	-	144.1	174.7	99.7	106.3	-	-	-	134.9	148.9	207.7
	EC	84.4	89.5	75.6	77.6	68.5	-	73.2	-	-	-	77.5	-
	SST	81.2	70.8	79.2	-	60.6	65.8	-	103.8	-	-	-	70.0
Mn	Cd	235.0	-	96.1	100.5	38.9	32.9	-	-	-	94.1	174.3	194.0
	EC	51.7	56.4	27.1	35.3	46.6	-	15.8	-	-	-	43.3	-
	SST	50.6	58.9	48.2	-	20.6	25.0	-	27.7	-	-	-	60.1
Mg	Cd	1302.5	-	1411.3	1991.3	1769.0	2260.8	-	-	-	1638.3	1157.5	1421.0
	EC	1103.0	785.0	481.8	693.0	503.8	-	817.5	-	-	-	687.0	-
	SST	1329.8	1347.0	1351.5	-	2142.3	2522.5	-	1387.3	-	-	-	845.3

*CD = ***Cynodon dactylon*** EC = ***Eragrostis chloromelas*** SST = ***Setaria sphacelata* var. *torta***

K1.1: Macro– and micronutrients and total trace metals of the vegetation samples in 2012.

Sample no.	Species	FP-1	FP-2	FP-3	FP-4	FP-5	FP-6	FP-7	FP-8	FP-9	FP-K1	FP-K2	FP-K3
Major elements *mg/kg*													
Ca	Cd	4655.0	-	2660.0	3710.0	3157.5	3742.5	-	-	-	3767.5	2642.5	3532.5
	EC	2962.5	2655.0	1716.0	2022.3	1889.5	-	1886.5	-	-	-	2447.0	-
	SST	2299.8	2535.0	3235.0	-	2950.0	2570.0	-	2682.5	-	-	-	1569.8
Na	Cd	181.5	-	166.5	159.8	135.1	168.6	-	-	-	140.0	109.8	144.8
	EC	152.4	146.2	152.8	150.2	165.0	-	137.1	-	-	-	150.8	-
	SST	171.6	148.0	169.8	-	162.2	162.4	-	144.3	-	-	-	165.5
K	Cd	7267.5	-	8342.5	8970.0	9862.5	12847.5	-	-	-	7852.5	8042.5	8232.5
	EC	7055.0	7545.0	3665.0	4225.0	4877.5	-	3397.5	-	-	-	4132.5	-
	SST	14952.5	15585.0	17002.5	-	32325.0	22170.0	-	7090.0	-	-	-	13577.5
P	Cd	1043.8	-	1328.8	1299.8	1234.5	1401.0	-	-	-	1059.8	1078.8	955.3
	EC	1007.5	1010.3	622.8	693.0	787.3	-	650.0	-	-	-	909.0	-
	SST	939.5	1078.5	1060.3	-	1168.8	1198.5	-	680.8	-	-	-	588.8
B	Cd	4.6	-	3.9	3.1	3.4	3.7	-	-	-	3.2	2.7	4.2
	EC	4.0	3.5	3.2	3.6	3.0	-	3.3	-	-	-	3.0	-
	SST	3.9	4.5	5.1	-	4.2	3.6	-	3.4	-	-	-	3.3
Ba	Cd	2.3	-	2.3	2.0	1.8	1.5	-	-	-	1.5	3.1	2.1
	EC	1.6	1.6	1.6	3.5	3.7	-	1.9	-	-	-	4.4	-
	SST	1.7	1.4	19	-	1.6	1.8	-	2.5	-	-	-	2.7

*CD = ***Cynodon dactylon*** EC = ***Eragrostis chloromelas*** SST = ***Setaria sphacelata* var. *torta***

K1.1: Macro– and micronutrients and total trace metals of the vegetation samples in 2012.

Sample no.	Species	FP-1	FP-2	FP-3	FP-4	FP-5	FP-6	FP-7	FP-8	FP-9	FP-K1	FP-K2	FP-K3
Trace elements *mg/kg*													
Be	Cd	0.01	-	0.01	0.01	0.01	0.01	-	-	-	0.01	0.01	0.01
	EC	0.01	0.01	0.01	0.01	0.01	-	0.01	-	-	-	0.01	-
	SST	0.01	0.01	0.01	-	0.01	0.01	-	0.01	-	-	-	0.01
Co	Cd	0.3	-	0.2	0.2	0.1	0.1	-	-	-	0.1	0.2	0.2
	EC	0.2	0.1	0.1	0.1	0.1	-	0.1	-	-	-	0.1	-
	SST	0.2	0.2	0.1	-	0.1	0.1	-	0.2	-	-	-	0.1
Cr	Cd	4.6	-	4.7	4.7	4.3	4.5	-	-	-	4.1	4.0	4.1
	EC	4.5	4.6	4.3	4.1	4.4	-	4.1	-	-	-	3.9	-
	SST	4.5	4.5	4.4	-	4.5	4.3	-	4.1	-	-	-	4.1
Cu	Cd	6.2	-	4.4	5.1	4.0	5.7	-	-	-	4.1	3.6	3.8
	EC	6.5	5.6	4.8	5.1	9.7	-	3.7	-	-	-	3.9	-
	SST	4.5	4.2	5.6	-	4.7	4.7	-	4.8	-	-	-	3.3
Ni	Cd	2.0	-	1.6	1.2	1.0	0.9	-	-	-	0.8	1.1	1.1
	EC	1.2	1.2	1.0	1.0	0.9	-	0.9	-	-	-	0.9	-
	SST	1.3	1.0	1.1	-	0.8	0.8	-	0.8	-	-	-	0.9
Sr	Cd	2.1	-	2.4	2.4	2.1	1.7	-	-	-	2.3	3.2	3.0
	EC	2.4	3.8	2.6	3.4	6.1	-	2.0	-	-	-	13.3	-
	SST	1.5	3.5	4.6	-	2.8	2.2	-	2.6	-	-	-	2.9
V	Cd	1.1	-	1.1	1.1	1.0	1.0	-	-	-	1.0	1.0	1.1

*CD = ***Cynodon dactylon*** EC = ***Eragrostis chloromelas*** SST = ***Setaria sphacelata* var. *torta***

K1.1: Macro– and micronutrients and total trace metals of the vegetation samples in 2012.

Sample no.	Species	FP-1	FP-2	FP-3	FP-4	FP-5	FP-6	FP-7	FP-8	FP-9	FP-K1	FP-K2	FP-K3
Trace elements *mg/kg*													
V	EC	1.0	1.0	1.0	1.0	1.0	-	1.0	-	-	-	0.9	-
	SST	1.0	1.0	1.0	-	1.0	1.0	-	1.0	-	-	-	1.0
Zn	Cd	49.3	-	23.5	21.7	23.2	20.9	-	-	-	23.1	32.2	29.0
	EC	11.2	12.9	9.9	16.8	21.8	-	9.0	-	-	-	39.1	-
	SST	19.9	16.7	13.2	-	22.6	13.7	-	20.3	-	-	-	17.0
U	Cd	0.2	-	0.1	0.1	0.1	0.1	-	-	-	0.1	0.1	0.1
	EC	0.1	0.1	0.1	0.1	0.1	-	0.1	-	-	-	0.1	-
	SST	0.2	0.1	0.1	-	0.1	0.1	-	0.1	-	-	-	0.1
As	Cd	0.4	-	0.2	0.2	0.2	0.2	-	-	-	0.2	0.2	0.2
	EC	0.2	0.3	0.2	0.2	0.2	-	0.2	-	-	-	0.2	-
	SST	0.2	0.2	0.2	-	0.2	0.2	-	0.2	-	-	-	0.2
Se	Cd	0.4	-	0.2	0.1	0.2	0.1	-	-	-	0.2	0.2	0.2
	EC	0.2	0.2	0.2	0.1	0.1	-	0.2	-	-	-	0.1	-
	SST	0.2	0.2	0.2	-	0.2	0.1	-	0.1	-	-	-	0.1
Mo	Cd	0.7	-	0.2	0.2	0.3	0.2	-	-	-	0.2	0.2	0.2
	EC	0.4	0.2	0.2	0.2	0.2	-	0.2	-	-	-	0.2	-
	SST	0.4	0.2	0.2	-	0.3	0.3	-	0.2	-	-	-	0.2
Pd	Cd	0.3	-	0.2	0.2	0.1	0.1	-	-	-	0.2	0.1	0.1
	EC	0.2	0.2	0.2	0.2	0.2	-	0.2	-	-	-	0.2	-

*CD = ***Cynodon dactylon*** EC = ***Eragrostis chloromelas*** SST = ***Setaria sphacelata* var. *torta***

K1.1: Macro– and micronutrients and total trace metals of the vegetation samples in 2012.

Sample no.	Species	FP-1	FP-2	FP-3	FP-4	FP-5	FP-6	FP-7	FP-8	FP-9	FP-K1	FP-K2	FP-K3
Trace elements *mg/kg*													
Pb	SST	0.2	0.2	0.2	-	0.2	0.1	-	0.1	-	-	-	0.1
Ag	Cd	0.3	-	0.2	0.1	0.001	0.1	-	-	-	0.1	0.1	0.1
	EC	0.1	0.1	0.1	0.1	0.2	-	0.4	-	-	-	0.2	-
	SST	0.1	0.1	1.3	-	0.2	0.1	-	0.1	-	-	-	0.1
Cd	Cd	0.03	-	0.01	0.01	0.01	0.01	-	-	-	0.01	0.01	0.01
	EC	0.01	0.01	0.005	0.005	0.01	-	0.01	-	-	-	0.01	-
	SST	0.02	0.01	0.01	-	0.02	0.01	-	0.01	-	-	-	0.01
Sb	Cd	0.6	-	0.3	0.2	0.3	0.2	-	-	-	0.2	0.2	0.2
	EC	0.3	0.3	0.3	0.2	0.3	-	0.3	-	-	-	0.2	-
	SST	0.3	0.3	0.3	-	0.3	0.2	-	0.2	-	-	-	0.2
Pt	Cd	0.03	-	0.04	0.05	0.04	0.07	-	-	-	0.02	0.02	0.02
	EC	0.03	0.03	0.03	0.05	0.02	-	0.04	-	-	-	0.02	-
	SST	0.03	0.02	0.03	-	0.03	0.03	-	0.03	-	-	-	0.05
Au	Cd	0.6	-	0.3	0.3	0.7	0.3	-	-	-	0.3	0.3	0.3
	EC	0.5	0.4	0.3	0.3	0.4	-	0.3	-	-	-	0.3	-
	SST	0.4	0.4	0.3	-	0.3	0.3	-	0.3	-	-	-	0.3
Hg	Cd	0.02	-	0.01	0.005	0.002	0.005	-	-	-	0.0005	0.002	0.001
	EC	0.01	0.01	0.004	0.002	0.01	-	0.01	-	-	-	0.002	-
	SST	0.1	0.005	0.002	-	0.004	0.001	-	0.0002	-	-	-	0.003

*CD = ***Cynodon dactylon*** EC = ***Eragrostis chloromelas*** SST = ***Setaria sphacelata* var. *torta***

K1.1: Macro– and micronutrients and total trace metals of the vegetation samples in 2012.

Sample no.	**Species**	**FP-1**	**FP-2**	**FP-3**	**FP-4**	**FP-5**	**FP-6**	**FP-7**	**FP-8**	**FP-9**	**FP-K1**	**FP-K2**	**FP-K3**
Trace elements *mg/kg*													
Tl	Cd	0.1	-	0.1	0.1	0.1	0.1	-	-	-	0.1	0.1	0.1
	EC	0.1	0.1	0.1	0.1	0.1	-	0.1	-	-	-	0.1	-
	SST	0.1	0.1	0.1	-	0.1	0.1	-	0.1	-	-	-	0.1
Pb	Cd	0.6	-	0.5	0.5	0.5	0.4	-	-	-	0.5	0.5	0.6
	EC	0.5	0.5	0.5	0.5	0.5	-	0.8	-	-	-	0.5	-
	SST	0.5	0.5	0.5	-	0.5	0.4	-	0.7	-	-	-	0.6

*CD = ***Cynodon dactylon*** EC = ***Eragrostis chloromelas*** SST = ***Setaria sphacelata* var. *torta***

K1.2: Macro– and micronutrients and total trace metals of the vegetation samples in 2013.

Sample no.	Species	FP-1	FP-2	FP-3	FP-4	FP-5	FP-6	FP-7	FP-8	FP-9	FP-K1	FP-K2	FP-K3
Major elements *mg/kg*													
Ti	Cd	2.8	-	-	9.0	3.5	2.6	-	-	-	-	-	-
	EC	2.6	4.4	2.3	3.2	3.5	2.5	-	2.7	-	4.8	-	3.0
	SST	-	4.8	-	-	-	-	-	4.2	-	3.3	-	2.5
Al	Cd	117.8	-	-	414.5	165.1	117.8	-	-	-	-	-	-
	EC	88.8	228.9	96.4	126.1	161.7	109.9	-	116.5	-	232.7	-	129.9
	SST	-	239.0	-	-	-	-	-	186.3	-	136.4	-	96.6
Fe	Cd	216.6	-	-	656.8	241.4	169.5	-	-	-	-	-	-
	EC	167.3	354.5	174.4	220.9	227.9	164.9	-	188.1	-	358.8	-	218.3
	SST	-	347.3	-	-	-	-	-	283.8	-	228.1	-	184.7
Mn	Cd	166.0			233.8	84.7	54.3	-	-	-	-	-	-
	EC	53	62.3	30.9	61.5	35.1	24	-	21.5	-	116.3	-	112.4
	SST	-	141.0	-	-	-	-	-	30.7	-	199.4	-	133.0
Mg	Cd	946.3	-	-	1682.3	1597.8	2116.0	-	-	-	-	-	-
	EC	442.3	314.0	477.0	562.5	1051.3	1343.0	-	690.0	-	425.8	-	449.0
	SST	-	1124.3	-	-	-	-	-	1785.0	-	1184.8	-	1172.8
Ca	Cd	4542.5	-	-	3150.0	2720.0	3835.0	-	-	-	-	-	-
	EC	2149.3	1574.5	1937.5	2620.0	2892.5	2730.0	-	2497.8	-	1807.5	-	2011.0
	SST	-	3370.0	-	-	-	-	-	5075.0	-	3495.0	-	3702.5
Na	Cd	316.8	-	-	358.5	351.0	356.3	-	-	-	-	-	-

*CD = ***Cynodon dactylon*** EC = ***Eragrostis chloromelas*** SST = ***Setaria sphacelata* var. *torta***

K1.2: Macro– and micronutrients and total trace metals of the vegetation samples in 2013.

Sample no.	Species	FP-1	FP-2	FP-3	FP-4	FP-5	FP-6	FP-7	FP-8	FP-9	FP-K1	FP-K2	FP-K3
Major elements *mg/kg*													
Na	EC	348.3	349.0	442.0	345.0	359.0	367.0	-	369.8	-	346.8	-	350.5
	SST	-	320.3	-	-	-	-	-	398.3	-	359.0	-	386.3
K	Cd	3907.5	-	-	5327.5	6677.5	4017.5	-	-	-	-	-	-
	EC	3322.5	1948.0	1920.8	3580.0	4672.5	3417.5	-	2283.3	-	3402.5	-	4235.0
	SST	-	6092.5	-	-	-	-	-	4120.0	-	7010.0	-	7680.0
P	Cd	705.0	-	-	796.8	1009.0	883.0	-	-	-	-	-	-
	EC	690.8	593.0	508.5	838.5	820.3	772.0	-	549.5	-	694.3	-	656.5
	SST	-	686.3	-	-	-	-	-	667.3	-	656.8	-	647.0
B	Cd	6.6	-	-	14.5	6.2	7.5	-	-	-	-	-	-
	EC	6.5	6.4	5.8	7.2	7.1	7.9	-	6.8	-	6.2	-	6.0
	SST	-	4.9	-	-	-	-	-	5.8	-	7.3	-	7.2
Trace elements *mg/kg*													
Ba	Cd	2.4	-	-	7.7	2.6	3.4	-	-	-	-	-	-
	EC	3.2	2.7	3.0	3.3	2.4	2.4	-	4.1	-	4.3	-	6.5
	SST	-	3.5	-	-	-	-	-	4.8	-	4.3	-	4.7
Be	Cd	0.0002	-	-	0.0001	0.0002	0.0003	-	-	-	-	-	-
	EC	0.0002	0.0002	0.0003	0.0002	0.0002	0.0003	-	0.0003	-	0.0002	-	0.0002
Be	SST	-	0.0002	-	-	-	-	-	0.0002	-	0.0002	-	0.0002
Co	Cd	0.1	-	-	0.2	0.1	0.02	-	-	-	-	-	-

*CD = ***Cynodon dactylon*** EC = ***Eragrostis chloromelas*** SST = ***Setaria sphacelata* var. *torta***

K1.2: Macro– and micronutrients and total trace metals of the vegetation samples in 2013.

Sample no.	Species	FP-1	FP-2	FP-3	FP-4	FP-5	FP-6	FP-7	FP-8	FP-9	FP-K1	FP-K2	FP-K3
Trace elements *mg/kg*													
Co	EC	0.1	0.2	0.04	0.1	0.04	0.03	-	0.1	-	0.1	-	0.1
	SST	-	0.2	-	-	-	-	-	0.1	-	0.2	-	0.1
Cr	Cd	1.9	-	-	4.1	3.0	2.0	-	-	-	-	-	-
	EC	2.4	3.3	2.1	2.6	3.2	2.3	-	2.8	-	2.5	-	2.8
	SST	-	2.9	-	-	-	-	-	2.7	-	2.3	-	2.9
Cu	Cd	3.1	-	-	4.1	4.1	3.1	-	-	-	-	-	-
	EC	3.7	3.3	2.6	2.8	3.6	2.8	-	2.7	-	3.5	-	3.7
	SST	-	2.7	-	-	-	-	-	3.4	-	3.2	-	3.3
Ni	Cd	0.5	-	-	0.8	0.7	0.3	-	-	-	-	-	-
	EC	0.6	0.8	0.3	0.3	0.3	0.2	-	0.4	-	0.9	-	0.5
	SST	-	0.5	-	-	-	-	-	0.6	-	0.5	-	0.3
Sr	Cd	2.1	-	-	3.2	2.1	4.4	-	-	-	-	-	-
	EC	1.7	2.5	2.5	4.4	2.8	2.2	-	2.3	-	2.8	-	5.1
	SST	-	3.8	-	-	-	-	-	3.7	-	4.5	-	6.7
V	Cd	0.3	-	-	1.2	0.5	0.2	-	-	-	-	-	-
	EC	0.3	0.7	0.3	0.4	0.4	0.25	-	0.5	-	0.7	-	0.5
	SST	-	0.6	-	-	-	-	-	0.6	-	0.4	-	0.4
Zn	Cd	36.6	-	-	22.8	10.9	21.9	-	-	-	-	-	-
	EC	13.6	12.5	11.6	11.5	9.6	10.7	-	11.1	-	17.3	-	19.6

*CD = ***Cynodon dactylon*** EC = ***Eragrostis chloromelas*** SST = ***Setaria sphacelata* var. *torta***

K1.2: Macro– and micronutrients and total trace metals of the vegetation samples in 2013.

Sample no.	Species	FP-1	FP-2	FP-3	FP-4	FP-5	FP-6	FP-7	FP-8	FP-9	FP-K1	FP-K2	FP-K3
Trace elements *mg/kg*													
Zn	SST	-	14.9	-	-	-	-	-	12.8	-	23.1	-	17.8
U	Cd	0.1	-	-	0.03	0.02	0.01	-	-	-	-	-	-
	EC	0.2	0.2	0.06	0.04	0.02	0.02	-	0.05	-	0.1	-	0.02
	SST	-	0.1	-	-	-	-	-	0.04	-	0.04	-	0.02
As	Cd	0.1	-	-	0.1	0.05	0.0001	-	-	-	-	-	-
	EC	0.1	0.2	0.1	0.1	0.1	0.02	-	0.1	-	0.1	-	0.03
	SST	-	0.1	-	-	-	-	-	0.1	-	0.04	-	0.04
Se	Cd	0.004	-	-	0.003	0.004	0.004	-	-	-	-	-	-
	EC	0.003	0.003	0.004	0.003	0.004	0.004	-	0.004	-	0.004	-	0.004
	SST	-	0.004	-	-	-	-	-	0.004	-	0.004	-	0.004
Mo	Cd	0.2	-	-	0.2	0.3	0.2	-	-	-	-	-	-
	EC	0.4	0.2	0.2	0.2	0.2	0.2	-	0.2	-	0.1	-	0.1
	SST	-	0.1	-	-	-	-	-	0.2	-	0.1	-	0.1
Pd	Cd	0.1	-	--	0.2	0.1	0.1	-	-	-	-	-	-
	EC	0.2	0.2	0.1	0.2	0.1	0.1	-	0.1	-	0.1	-	0.1
	SST	-	0.1	-	-	-	-	-	0.1	-	0.2	-	0.1
Ag	Cd	0.002	-	-	0.002	0.001	0.002	-	-	-	-	-	-
	EC	0.002	0.001	0.002	0.0003	0.001	0.002	-	0.002	-	0.001	-	0.001
	SST	-	0.002	-	-	-	-	-	0.001	-	0.001	-	0.002

*CD = ***Cynodon dactylon*** EC = ***Eragrostis chloromelas*** SST = ***Setaria sphacelata* var. *torta***

K1.2: Macro– and micronutrients and total trace metals of the vegetation samples in 2013.

Sample no.	Species	FP-1	FP-2	FP-3	FP-4	FP-5	FP-6	FP-7	FP-8	FP-9	FP-K1	FP-K2	FP-K3
Trace elements *mg/kg*													
Cd	Cd	0.01	-	-	0.0	0.0001	0.0001	-	-	-	-	-	-
	EC	0.01	0.004	0.00004	0.00002	0.01	0.0001	-	0.004	-	0.003	-	0.002
	SST	-	0.0	-	-	-	-	-	0.01	-	0.01	-	0.0001
Sb	Cd	0.1	-	-	0.1	0.1	0.1	-	-	-	-	-	-
	EC	0.2	0.2	0.1	0.1	0.1	0.1	-	0.1	-	0.1	-	0.1
	SST	-	0.1	-	-	-	-	-	0.1	-	0.1	-	0.1
Pt	Cd	0.00001	-	-	0.0001	0.0001	0.0001	-	-	-	-	-	-
	EC	0.01	0.002	0.0001	0.004	0.0001	0.001	-	0.00005	-	0.0001	-	0.0001
	SST	-	0.0001	-	-	-	-	-	0.0001	-	0.0001	-	0.0001
Au	Cd	0.2	-	-	0.3	0.2	0.2	-	-	-	-	-	-
	EC	0.4	0.3	0.2	0.2	0.3	0.2	-	0.2	-	0.2	-	0.2
	SST	-	0.2	-	-	-	-	-	0.3	-	0.2	-	0.2
Hg	Cd	0.002	-	-	0.007	0.001	0.002	-	-	-	-	-	-
	EC	0.01	0.02	0.005	0.06	0.01	0.003	-	0.006	-	0.004	-	0.001
	SST	-	0.00001	-	-	-	-	-	0.00005	-	0.001	-	0.00001
Tl	Cd	0.0004	-	-	0.0004	0.0004	0.0004	-	-	-	-	-	-
	EC	0.0004	0.0004	0.0004	0.0004	0.0004	0.0004	-	0.0004	-	0.0004	-	0.0004
	SST	-	0.0004	-	-	-	-	-	0.0004	-	0.0004	-	0.0004
Pb	Cd	0.1	-	-	0.2	0.01	0.00002	-	-	-	-	-	-

*CD = ***Cynodon dactylon*** EC = ***Eragrostis chloromelas*** SST = ***Setaria sphacelata* var. *torta***

K1.2: Macro– and micronutrients and total trace metals of the vegetation samples in 2013.

Sample no.	**Species**	**FP-1**	**FP-2**	**FP-3**	**FP-4**	**FP-5**	**FP-6**	**FP-7**	**FP-8**	**FP-9**	**FP-K1**	**FP-K2**	**FP-K3**
Trace elements *mg/kg*													
Pb	EC	0.2	0.5	0.2	0.2	0.05	0.02	-	0.05	-	0.3	-	0.2
	SST	-	0.2	-	-	-	-	-	0.4	-	0.2	-	0.1

*CD = ***Cynodon dactylon*** EC = ***Eragrostis chloromelas*** SST = ***Setaria sphacelata*** **var.** ***torta***

K1.3: Macro– and micronutrients and total trace metals of the vegetation samples in 2014.

Sample no.	Species	FP-1	FP-2	FP-3	FP-4	FP-5	FP-6	FP-7	FP-8	FP-9	FP-K1	FP-K2	FP-K3
Major elements *mg/kg*													
Ti	Cd	2.5	2.8	7.9	11.7	3.6	5.1	2.9	4.0	4.2	4.4	3.8	4.3
	EC	2.3	-	2.9	6.9	2.8	3.1	2.3	2.4	2.7	3.0	2.2	3.9
	SST	-	-	2.3	4.3	-	-	2.1	-	-	2.0	2.1	-
Al	Cd	57.3	62.2	538.5	960.3	208.3	312.8	66.6	228.2	167.0	283.0	179.8	327.8
	EC	88.8	-	159.9	455.3	138.6	165.4	48.1	106.9	101.0	136.5	79.3	197.6
	SST	-	50.3	231.2	-	-	-	25.6	-	-	65.9	86.5	-
Fe	Cd	108.0	174.9	634.8	900.5	191.8	295.0	111.0	224.8	188.8	302.8	214.8	387.0
	EC	142.3	-	171.0	415.3	158.4	178.2	99.1	127.1	119.3	181.3	103.7	262.5
	SST	-	93.2	240.5	-	-	-	73.4	-	-	101.1	121.0	-
Mn	Cd	93.6	88.8	414.3	431.8	45.7	62.2	82.1	60.2	62.0	196.2	175.6	241.6
	EC	43.1	-	43.4	148.4	26.9	27.1	37.8	29.0	31.3	86.8	77.6	119.3
	SST	-	118.7	96.5	-	-	-	70.6	-	-	190.7	120.8	-
Mg	Cd	1273.5	1852.3	1897.8	2507.5	1548.8	2484.5	1743.0	2925.0	1760.3	1258.8	1373.0	1495.8
	EC	566.3	-	691.5	595.5	1259.3	2072.3	805.3	1025.0	938.3	498.8	819.3	757.5
	SST	-	1998.8	1875.0	-	-	-	2927.5	-	-	1202.8	1113.0	-
Ca	Cd	3730.0	5375.0	3462.5	3932.5	2677.5	3277.5	3302.5	3922.5	3637.5	3260.0	2652.5	2820.0
	EC	2592.5	-	1972.5	1584.3	2399.3	2715.0	2790.0	2243.8	2186.3	1859.5	1686.0	2005.3
	SST	-	2512.5	1915.0	-	-	-	2322.3	-	-	1434.8	1117.3	-
Na	Cd	352.3	334.0	385.8	430.8	367.5	396.8	412.0	440.3	407.5	350.5	539.3	374.3

*CD = ***Cynodon dactylon*** EC = ***Eragrostis chloromelas*** SST = ***Setaria sphacelata* var. *torta***

K1.3: Macro– and micronutrients and total trace metals of the vegetation samples in 2014.

Sample no.	Species	FP-1	FP-2	FP-3	FP-4	FP-5	FP-6	FP-7	FP-8	FP-9	FP-K1	FP-K2	FP-K3
Major elements *mg/kg*													
Na	EC	355.0	-	364.5	351.3	361.8	378.0	353.3	316.0	350.5	339.0	348.3	298.5
	SST	-	356.3	292.0	-	-	-	368.8	-	-	307.8	311.3	-
K	Cd	8910.0	12955.0	6567.5	10262.5	8077.5	8412.5	10450.0	7317.5	6647.5	8210.0	9475.0	10547.5
	EC	4592.5	-	4462.5	4670.0	4705.0	4560.0	4365.0	3442.5	4855.0	4317.5	7622.5	4367.5
K	SST	-	16617.5	8670.0	-	-		10185.0	-	-	10652.5	11852.5	-
P	Cd	858.5	1219.5	1221.0	1388.8	881.8	1138.3	1266.0	845.3	1057.3	1150.3	1136.0	1033.3
	EC	680.8	-	692.3	868.0	707.0	849.8	924.5	628.0	649.5	660.0	1013.8	720.3
	SST	-	947.0	698.0	-	-	-	925.5	-	-	636.3	946.0	-
B	Cd	2.5	2.5	0.3	2.4	0.3	0.3	0.3	0.3	0.3	2.1	2.2	2.3
	EC	1.8	-	2.0	2.2	0.3	0.3	0.3	0.3	0.3	2.0	1.7	2.0
	SST	-	1.2	2.1	-	-	-	0.3	-	-	1.0	1.5	-
Trace elements *mg/kg*													
Ba	Cd	1.9	1.7	14.2	8.4	2.5	5.1	4.2	2.3	3.2	2.8	19.0	9.9
	EC	2.3	-	2.3	7.5	2.3	2.2	4.0	2.1	1.7	2.9	4.2	5.6
	SST	-	1.4	2.2	-	-	-	2.2	-	-	2.1	3.8	-
Be	Cd	0.0006	0.0006	0.0004	0.0003	0.0006	0.0005	0.0006	0.0006	0.0006	0.0005	0.0006	0.0005
	EC	0.0006	-	0.0006	0.0005	0.0006	0.0006	0.0006	0.0006	0.0006	0.0006	0.0006	0.0005
	SST	-	0.0006	0.0006	-	-	-	0.0006	-	-	0.0006	0.0006	-
Co	Cd	0.05	0.05	0.33	0.43	0.07	0.10	0.03	0.06	0.06	0.13	0.21	0.17

*CD = ***Cynodon dactylon*** EC = ***Eragrostis chloromelas*** SST = ***Setaria sphacelata* var. *torta***

K1.3: Macro– and micronutrients and total trace metals of the vegetation samples in 2014.

Sample no.	Species	FP-1	FP-2	FP-3	FP-4	FP-5	FP-6	FP-7	FP-8	FP-9	FP-K1	FP-K2	FP-K3
Trace elements *mg/kg*													
Co	EC	0.06	-	0.06	0.19	0.05	0.06	0.05	0.04	0.03	0.07	0.06	0.11
	SST	-	0.02	0.08	-	-	-	0.02	-	-	0.03	0.04	-
Cr	Cd	7.6	5.9	5.1	4.4	3.8	8.3	4.1	2.1	2.1	1.7	3.5	1.4
	EC	2.0	-	1.6	3.9	7.0	2.2	10.3	6.4	5.1	6.1	1.5	5.3
	SST	-	1.4	8.8	-	-	-	7.9	-	-	2.9	0.9	-
Cu	Cd	3.6	6.2	4.8	8.5	4.9	5.9	4.5	5.1	3.7	6.9	5.7	4.9
	EC	3.1	-	3.5	5.5	3.3	3.6	3.3	3.0	3.0	3.4	3.3	3.5
	SST	-	5.1	4.4	-	-	-	4.6	-	-	3.5	3.7	-
Ni	Cd	0.9	0.7	1.4	1.8	0.7	0.6	0.7	0.6	0.5	1.1	1.4	0.8
	EC	0.8	-	0.6	1.0	1.3	0.8	3.0	0.4	0.3	0.5	0.4	0.5
	SST	-	0.5	0.5	-	-	-	0.4	-	-	0.5	0.7	-
Sr	Cd	1.8	4.9	1.9	4.6	2.4	3.1	3.3	2.5	2.5	2.8	3.9	2.7
	EC	1.9	-	2.4	3.9	2.7	2.7	4.0	1.8	2.8	2.7	5.0	3.0
	SST	-	0.5	0.5	-	-	-	3.8	-	-	2.6	3.5	-
V	Cd	0.9	0.6	1.5	1.7	0.5	1.1	0.4	0.3	0.4	0.4	0.5	0.5
	EC	0.2	-	0.3	1.1	0.7	0.3	0.9	0.8	0.7	0.8	0.1	0.8
	SST	-	0.1	1.1	-	-	-	0.9	-	-	0.3	0.1	-
Zn	Cd	28.7	62.4	16.5	40.6	23.3	23.6	32.1	25.8	11.5	58.9	82.5	53.8
	EC	15.0	-	20.4	19.1	14.2	12.3	12.1	16.4	11.9	20.8	25.4	20.2

*CD = ***Cynodon dactylon*** EC = ***Eragrostis chloromelas*** SST = ***Setaria sphacelata* var. *torta***

K1.3: Macro– and micronutrients and total trace metals of the vegetation samples in 2014.

Sample no.	Species	FP-1	FP-2	FP-3	FP-4	FP-5	FP-6	FP-7	FP-8	FP-9	FP-K1	FP-K2	FP-K3
Trace elements *mg/kg*													
Zn	SST	-	17.4	17.5	-	-	-	17.9	-	-	19.7	16.6	-
U	Cd	0.04	0.03	0.04	0.05	0.03	0.03	0.02	0.02	0.02	0.03	0.02	0.02
	EC	0.09	-	0.04	0.07	0.02	0.03	0.02	0.03	0.02	0.06	0.02	0.03
	SST	-	0.02	0.04	-	-	-	0.02	-	-	0.03	0.02	-
As	Cd	0.001	0.001	0.0002	0.0002	0.001	0.0005	0.001	0.002	0.002	0.001	0.002	0.002
	EC	0.001	-	0.001	0.001	0.001	0.002	0.001	0.001	0.001	0.001	0.002	0.001
	SST	-	0.002	0.001	-	-	-	0.001	-	-	0.002	0.002	-
Se	Cd	0.007	0.007	0.007	0.007	0.007	0.007	0.007	0.008	0.007	0.008	0.007	0.008
	EC	0.007	-	0.008	0.007	0.007	0.007	0.007	0.008	0.008	0.007	0.007	0.008
	SST	-	0.007	0.008	-	-	-	0.008	-	-	0.007	0.008	-
Mo	Cd	0.2	0.1	0.1	0.1	0.3	0.1	0.1	0.1	0.1	0.1	0.1	0.1
	EC	0.2	-	0.1	0.1	0.2	0.1	0.3	0.1	0.1	0.1	0.1	0.1
	SST	-	0.1	0.1	-	-	-	0.1	-	-	0.1	0.1	-
Pd	Cd	0.002	0.0001	0.002	0.01	0.0001	0.07	0.0001	0.0001	0.005	0.0001	0.0001	0.0001
	EC	0.0001	-	0.0001	0.006	0.0001	0.0002	0.0001	0.0001	0.0001	0.00004	0.0001	0.05
	SST	-	0.00004	0.03	-	-	-	0.5	-	-	0.00001	0.0001	-
Ag	Cd	0.0004	0.0004	0.0004	0.0004	0.0003	0.0001	0.0005	0.0005	0.0004	0.0003	0.0005	0.0005
	EC	0.0005	-	0.0005	0.0004	0.0004	0.0005	0.0000	0.0004	0.0004	0.0003	0.0005	0.0005

*CD = ***Cynodon dactylon*** EC = ***Eragrostis chloromelas*** SST = ***Setaria sphacelata* var. *torta***

K1.3: Macro– and micronutrients and total trace metals of the vegetation samples in 2014.

Sample no.	Species	FP-1	FP-2	FP-3	FP-4	FP-5	FP-6	FP-7	FP-8	FP-9	FP-K1	FP-K2	FP-K3
Trace elements *mg/kg*													
Ag	SST	-	0.0003	0.0002	-	-	-	0.00003	-	-	0.0005	0.0005	-
Cd	Cd	0.02	0.01	0.06	0.04	0.04	0.05	0.04	0.02	0.01	0.01	0.02	0.06
	EC	0.1	-	0.01	0.1	0.05	0.1	0.06	0.002	0.05	0.08	0.03	0.03
	SST	-	0.01	0.04	-	-	-	0.00	-	-	0.00005	0.01	
Sb	Cd	0.2	0.1	0.2	0.1	0.1	0.1	0.1	0.2	0.1	0.1	0.2	0.1
	EC	0.1	-	0.1	0.2	0.2	0.1	0.2	0.1	0.2	0.1	0.2	0.1
	SST	-	0.1	0.1	-	-	-	0.1	-	--	0.2	0.2	-
Pt	Cd	0.2	0.1	0.2	0.1	0.0003	0.0004	0.0004	0.0004	0.0003	0.0004	0.0004	0.0004
	EC	0.0004		0.0003	0.0003	0.0004	0.0003	0.0003	0.0004	0.0004	0.0004	0.0003	0.0004
	SST	-	0.0003	0.0004	-	-	-	0.0004	-	-	0.0004	0.0003	-
Au	Cd	0.1	0.1	0.1	0.1	0.1	0.3	0.1	0.1	0.1	0.1	0.1	0.1
	EC	0.1	-	0.1	0.1	0.1	0.1	0.1	0.1	0.1	0.1	0.1	0.1
	SST	-	0.1	0.2	-	-	-	0.5	-	-	0.1	0.1	-
Hg	Cd	0.00007	0.00008	0.00008	0.00007	0.00008	0.00008	0.00008	0.00008	0.00007	0.00007	0.00007	0.00007
	EC	0.00006	-	0.00006	0.00006	0.00008	0.00008	0.00008	0.00008	0.00008	0.00007	0.00007	0.00007
	SST	-	0.00005	0.00006	-	-	-	0.00007	-	-	0.00004	0.00005	-
Tl	Cd	0.0002	0.0002	0.0001	0.0001	0.0002	0.0002	0.0002	0.0001	0.0002	0.0002	0.0001	0.0002
	EC	0.0002	-	0.0002	0.0001	0.0002	0.0002	0.0002	0.0002	0.0002	0.0002	0.0002	0.0002
	SST	-	0.0002	0.0001	-	-	-	0.0002	-	-	0.0002	0.0002	-

*CD = ***Cynodon dactylon*** EC = ***Eragrostis chloromelas*** SST = ***Setaria sphacelata* var. *torta***

K1.3: Macro– and micronutrients and total trace metals of the vegetation samples in 2014.

Sample no.	**Species**	**FP-1**	**FP-2**	**FP-3**	**FP-4**	**FP-5**	**FP-6**	**FP-7**	**FP-8**	**FP-9**	**FP-K1**	**FP-K2**	**FP-K3**
Trace elements *mg/kg*													
Pb	Cd	0.2	0.2	0.4	0.5	0.3	0.3	0.2	0.2	0.2	0.2	0.4	0.3
	EC	0.3	-	0.4	0.7	0.3	0.3	0.3	0.3	0.2	0.3	0.4	0.3
	SST	-	0.1	0.3	-	-	-	0.3	-	-	0.2	0.3	-

*CD = ***Cynodon dactylon*** EC = ***Eragrostis chloromelas*** SST = ***Setaria sphacelata* var. *torta***

K2: Landscape Function Analysis Threshold for Potential Concern (TPC) value of landscape function analysis indicators and sites falling below the TPC.

K2.1: TPC 2012.

K2.1.1: TPC for Stability.

Stability				
Reference value (FP K1)	**Min FP value (FP 9)**	**TPC**	**Sites falling below TPC**	
60.3	52.0	56.2	FP 1	FP 7
			FP 2	FP 8
			FP 4	FP 9
			FP 5	FP K2
			FP 6	FP K3

K2.1.2: TPC for Infiltration.

Infiltration				
Reference value (FP K1)	**Min FP value (FP 7)**	**TPC**	**Sites falling below TPC**	
41.0	35.3	38.2	FP 1	FP 7
			FP 2	FP 9
			FP 4	FP K2
			FP 5	FP K3

K2.1.3: TPC for Nutrient Cycling.

Nutrient cycling				
Reference value (FP K1)	**minimum FP value (FP 7)**	**TPC**	**Sites falling below TPC**	
25.5	20.8	23.2	FP 4	FP 9
			FP 5	FP K2
			FP 7	FP K3

K2.2: TPC 2014.

K2.2.1: TPC for Stability.

Stability				
Reference value (FP 1)	**Min FP value (FP 5)**	**TPC**	**Sites falling below TPC**	
64.9	54	59.45	FP 2	FP 7
			FP 3	FP 8
			FP 4	FP 9
			FP 5	FP K1
			FP 6	FP K2
			FP K3	

K2.2.2: TPC for Infiltration.

Infiltration				
Reference value (FP 1)	**Min FP value (FP 5)**	**TPC**	**Sites falling below TPC**	
38.02	29.2	33.61	FP 2	FP 6
			FP 3	FP 7
			FP 4	FP K1
			FP 5	FP K3

K2.2.3: TPC for Nutrient Cycling.

Nutrient cycling				
Reference value (FP 1)	**Min FP value (FP 6)**	**TPC**	**Sites falling below TPC**	
32.03	19.3	25.67	FP 2	FP 7
			FP 3	FP 9
			FP 4	FP K1
			FP 5	FP K2
			FP 6	FP K3